Downloaded from orbit.dtu.dk on: Apr 20, 2024

DTU Library

Annual progress report of the Department of Solid State Physics 1 January - 31 December 1993

Pedersen, J.S.; Almdal, Kristoffer; Feidenhans'l, Robert; Clausen, Kurt Nørgaard; Bechgaard, Klaus

Publication date:
1994

Document Version
Publisher's PDF, also known as Version of record

Link back to DTU Orbit

Citation (APA):
Pedersen, J. S., Almdal, K., Feidenhans'l, R., Clausen, K. N., & Bechgaard, K. (Eds.) (1994). *Annual progress report of the Department of Solid State Physics 1 January - 31 December 1993*. Risø National Laboratory. Denmark. Forskningscenter Risoe. Risoe-R No. 725(EN)

General rights
Copyright and moral rights for the publications made accessible in the public portal are retained by the authors and/or other copyright owners and it is a condition of accessing publications that users recognise and abide by the legal requirements associated with these rights.

- Users may download and print one copy of any publication from the public portal for the purpose of private study or research.
- You may not further distribute the material or use it for any profit-making activity or commercial gain
- You may freely distribute the URL identifying the publication in the public portal

If you believe that this document breaches copyright please contact us providing details, and we will remove access to the work immediately and investigate your claim.

DK9400046

RISØ

Risø-R-725(EN)

Annual Progress Report of the Department of Solid State Physics

1 January – 31 December 1993

edited by J. Skov Pedersen, K. Almdal, R. Feidenhans'l, K.N. Clausen, and K. Bechgaard

Risø National Laboratory, Roskilde, Denmark
January 1994

Annual Progress Report of the Department of Solid State Physics
1 January – 31 December 1993

Risø-R-725(EN)

edited by J. Skov Pedersen, K. Almdal, R. Feidenhans'l, K.N. Clausen, and K. Bechgaard

Risø National Laboratory, Roskilde, Denmark
January 1994

Abstract

Research in the department is concerned with "Materials with Distinct Physical and Chemical Properties". The principal activities of the department in the period from 1 January, to 31 December, 1993, are presented in this Progress Report.

Neutrons and X-ray diffraction techniques are used to study a wide variety of problems in condensed matter physics and include: two- and three-dimensional structures, magnetic ordering, heavy fermions, high T_c superconductivity, phase transitions in model systems, precipitation phenomena, and nano-scale structures in various materials. The research in chemistry includes chemical synthesis and physico-chemical investigations of small molecules and polymers, with emphasis on polymers with new optical properties, block copolymers, surface modified polymers, and supramolecular structures.

This report is organized in 13 categories with the following headings:

- Theory, Monte Carlo simulations, and methods of data analysis
- Magnetic structures, magnetic phase transitions, and spin dynamics
- High T_C superconductivity
- Structures and structural phase transitions
- Inclusions and precipitates in alloys and metals
- Interaction of particles and photons with surfaces
- Surfaces, interfaces, and amorphous structures
- Langmuir films
- Polymers
- Molecular science
- Microemulsions and biological systems
- Instrument developments
- Other activities

This report contains unpublished results and should not be quoted without permission from the authors.

ISBN 87-550-1947-1
ISSN 0106-2840
ISSN 0907-0249

Grafisk Service Risø, 1994

Contents

1 INTRODUCTION 9

THEORY, MONTE CARLO SIMULATIONS, AND METHODS OF DATA ANALYSIS 10

1.1 Numerical Transfer-matrix Study of a Model with Competing Metastable States 10
1.2 Lattice-gas Monte Carlo Simulations on the Connection Machine 11
1.3 Theory and Computer Simulation of Diffuse Scattering 12
1.4 Phase Diagram, Structure Factor, and Oxygen Equilibrium Pressure of $YBa_2Cu_3O_{6+x}$ Studied by Monte Carlo Simulation 13
1.5 Monte Carlo Simulations of Enhanced Lattice Gas Models for the High Temperature Oxygen Ordering Thermodynamics in $YBa_2Cu_3O_{6+x}$ 14
1.6 Calculation of Electronic and Structural Influence on the Thermal Magnetic Properties of Clusters 15
1.7 Calculations of Neutron Magnetic Scattering Cross Section of a Triangular 2D Quantum Antiferromagnet 16
1.8 Asymmetric Lineshapes in Powder Diffraction 17
1.9 The Relation between Kinematical and Dynamical Theories of Neutron and X-Ray reflectivity 18
1.10 Determination of Size Distributions from Small-angle Scattering Data for Systems with Effective Hard-sphere Interactions 19
1.11 Analytical Calculation of the Three-dimensional Resolution Function for Laue Geometries. 20
1.12 Best Geometry to Perform a Given SANS Measurement. A Graphical Approach 21
1.13 Spin-spin Coupling in Cation Stabilised Free Radicals. Molecular and Polymeric Materials 22

MAGNETIC STRUCTURES, MAGNETIC PHASE TRANSITIONS, AND SPIN DYNAMICS 23

1.14 Analysis of the Magnetic Ordering in MnSi 23
1.15 SANS Studies of the Nearly Ferromagnetic Frustrated Antiferromagnet, $Y_2Mn_2O_7$ 24
1.16 Commensurate Magnetic Ordering in dhcp Nd Metal 25
1.17 Studies of Modulated Magnetic Structures under High Pressure 26
1.18 A New Mode of Magnetic Excitation in Praseodymium 27
1.19 Collapsed Cycloidal structures in Erbium 28
1.20 Competing Anisotropies in Ho/Er Superlattices 29
1.21 Metallic Superlattices - X-ray and Neutron Scattering Investigations 30
1.22 The Magnetism of an Epitaxially Grown Fe Layer 31
1.23 The Spin Structure of Na_6CoS_4 32
1.24 Nuclear Magnetism of a ^{13}C diamond 33
1.25 Spin Wave Collapse, Magnetic Divergence, and Incommensurate Fluctuations in URu_2Si_2 34
1.26 Magnetic Response of the fcc Heavy Fermion System YbBiPt 35
1.27 Spin Dynamics of the Kondo Insulator CeNiSn 36

1.28 Magnetic Structures in $PrBa_2Cu_3O_{6+x}$ 37
1.29 Magnetic Fluctuations in the Normal State of $La_{1.86}Sr_{0.14}CuO_4$ 38
1.30 Magnetic Flux Lattice Melting in High Temperature Superconductor $Bi_{2.15}Sr_{1.95}CaCu_2O_{8+x}$ 39
1.31 Magnetic Flux Lattice in Single Crystal 2H-$NbSe_2$ 40

HIGH T_C SUPERCONDUCTIVITY 41
1.32 Interstitial Oxygen Defects in Room Temperature Oxidized $La_{2-x}Sr_xCuO_{4+y}$ $(0 < x < 0.15)$ 41
1.33 Determination of the Crystallographic Parameters in $YBa_2Cu_3O_{6+x}$ Single Crystals 42
1.34 The Lineshape of Ortho-II Superstructure Reflections in $YBa_2Cu_3O_{6.5}$ . . . 43

STRUCTURES AND STRUCTURAL PHASE TRANSITIONS 44
1.35 Crystal Structure of the Commensurately Modulated ζ Phase of PAMC . . 44
1.36 Solution and Refinement of Structures by the Use of Neutron Powder Diffraction Data 45
1.37 Crystal Structures of $SrCeO_3$ Based Electrolyte Materials 46

INCLUSIONS AND PRECIPITATES IN ALLOYS AND METALS 47
1.38 Grazing Incidence Small-Angle X-ray Scattering Study of Krypton Inclusions in Aluminium 47
1.39 Melting and Solidification of Bismuth Inclusions in Aluminium Studied by X-ray Diffraction 48
1.40 Atomic Structure of a Pd Cluster Compound: X-ray-scattering Measurements 49
1.41 Small-angle Neutron Scattering on Ni-11 at.% Ti 50
1.42 Study of Bimodal Size Distributions of γ' Precipitates in Ni-Al-Mo 51
1.43 A SANS Investigation of the Influence of Hydrogen on the Age-hardening of Commercial Aluminimum-Lithium Alloys 52

INTERACTION OF PARTICLES AND PHOTONS WITH SURFACES 53
1.44 Sputtering of Solid Deuterium by keV Electrons 53
1.45 Fundamental Laser Ablation of Simple Materials 54

SURFACES, INTERFACES, AND AMORPHOUS STRUCTURES 55
1.46 X-ray Scattering from Free-standing Amorphous Diamond-like Carbon Films 55
1.47 Material Properties and Production Parameters of Diamond-like Carbon Thin Films 56
1.48 Order-disorder Transition in Sandwiched Cu_3Au Films 57
1.49 Investigation of the (1×2)-phases of Bi/GaSb(110) 58
1.50 Investigations of Surface Structures at Beamline BW2 59
1.51 The Specular Reflectivity as a Structural Probe 60
1.52 X-ray Scattering Investigations of the Discommensurate Structures of Ga on Ge(111) 61
1.53 Metal on Metal Growth: Au on Ni(110) 62
1.54 Metal on Metal Growth: Au on Ni(111) 63

1.55 The Ni(111)($5\sqrt{3}$×2)-S Reconstruction Examined by Surface X-ray Diffraction . . . 64
1.56 The Cu(111)-S "Zig-zag" Structure Examined by Surface X-ray Diffraction 65

LANGMUIR FILMS 66
1.57 Phase Transitions in Di-glyceride Monolayers Studied by Molecular Dynamics Simulation and Synchrotron X-ray Diffraction . . . 66
1.58 Langmuir and Langmuir-Blodgett Films of Functionalized Molecules with Cross-sectional Mismatch between Head and Tail . . . 67
1.59 Structure of Relaxed Monolayers of Shorter-chain Alcohols on Water . . . 68
1.60 Grazing Incidence X-Ray Diffraction (GID) Studies of Monolayers of Mixed Amphiphilic Alcohols . . . 69
1.61 Two-dimensional Crystal Structure of a Long-chain Amino Acid . . . 70
1.62 Controlled Formation of Amphiphilic Amide Multilayers and Monolayers at the Air-liquid Interface . . . 71
1.63 Spontaneous Formation of Crystalline Multilayers of HO-$C_{22}H_{44}$-OH at the Air/Water Interface Studied by Grazing Incidence X-ray Diffraction . . . 72
1.64 Phase-separated Two-component Monolayer Systems . . . 73
1.65 The Adsorption of Molecular Polymer Layers to Lipid Monolayers . . . 74
1.66 Influence of Chirality on the Structure of a Diol Monolayer . . . 75
1.67 Condensed Phases in Monolayers of Double-chain Lecithins on Water . . . 76
1.68 Influence of Changes in the Hydrophobic Region on the Monolayer Structure of Lecithins . . . 77
1.69 A New Phase Transition in a Fatty Acid Monolayer on Water . . . 78
1.70 Tilted Structures in Monolayers of Fluorinated Molecules . . . 79
1.71 Microscopic Structure of a Polymerizable Langmuir Monolayer . . . 80
1.72 Internal Structure of Electrostatically Adsorbed Polyelectrolyte Films . . . 81
1.73 Interfacial Melting (?) at an Ice/Silicon Interface . . . 82

POLYMERS 83
1.74 Confined Motion in the Amorphous Regions of Partially Crystalline Polyethylene . . . 83
1.75 Towards a Phenomenological Definition of the Term 'Gel' . . . 84
1.76 Structural Characterization of a Bis-arborol-tetrathiafulvalene Gel . . . 85
1.77 SANS Investigation of Tube Constraints in Polymer Networks . . . 86
1.78 On the Cross-over from Ising to Mean-field Behaviour in Binary Polymer Blends. . . . 87
1.79 Pressure Dependent SANS on Polymer Blends and a Comparison to the Lattice Cluster Theory. . . . 88
1.80 Pressure Dependence of Spinodal Temperature in DPB-HPI Block Copolymer with LCST-type Phase Behavior . . . 89
1.81 Mesophase Formation in a Symmetric Poly(styrene-b-paramethylstyrene) Diblock Copolymer . . . 90
1.82 Diblock Copolymers as Compatibilisers for Rubber Toughened Blends . . . 91
1.83 Microstructural Characteristics of Microhpase-separated Tapered Block Copolymers . . . 92
1.84 Structural Studies of ABA-triblock Copolymer Gels . . . 93

1.85 Pressure Induced Melting of Poly(ethylene Oxide)-poly(propylene oxide)-poly(ethylene oxide) Triblock Copolymer Micellar Crystal 94
1.86 Structural Investigations of PEP, Poly(propylene oxide)-poly(ethylene oxide)-poly(propylene oxide), Triblock Copolymers in Aqueous Solution 95
1.87 Shear-induced Order in a Diblock Copolymer Solution 96
1.88 Lamellae Orientation in Dynamically Sheared Diblock Copolymer Melts . . 97
1.89 Dynamically Sheared bcc Ordered Diblock Copolymer Melts 98
1.90 Orientational Ordering in Nematic Liquid Crystals: Isotope Labelling Neutron Diffraction Experiments 99
1.91 Side-chain Liquid Crystalline Polyesters for Optical Information Processing 100
1.92 Characterization of the Segmental Mobility of Side-chain Liquid Crystalline Polyesters by FTIR Spectroscopy and Optical Anisotropy 101
1.93 New Polymer Materials for Optical Storage 102

MOLECULAR SCIENCE 103
1.94 Layered Materials Derived from Calixarenes 103
1.95 Peptide Nucleic Acids (PNA) 104
1.96 Film-based Solid-phase Synthesis 105

MICROEMULSIONS AND BIOLOGICAL SYSTEMS 106
1.97 Flexibility and Local Structure of Polymer-like Reverse Micelles 106
1.98 Shear Melting and Orientation of a Lyotropic Cubic Phase 107
1.99 Structural Studies of the Sodium Deoxycholate Surfactant System both with and without Lipopolysaccharide 108
1.100 Bending Rigidity of Sodium Octyl Sulfate/Water/Decanol Lamellae 109
1.101 Observation of a Rod-to-sphere-to-rod Transition in SDS Micelles upon Addition of Cosurfactants 110
1.102 Studies of 1-C_{16}-2-C_6-PC Rod-like Micelles by Small-angle Neutron Scattering 111
1.103 Swelling of Multi-lammellar Membrane Systems Induced by the Main Phase Transition 112
1.104 The Conformation of the Inositol Headgroup in Biological Membranes . . 113
1.105 Structural Changes in Casein Micelles Studied by SANS 114
1.106 Structure of the 50S Subunit of E. Coli Ribosomes from X-ray and Neutron Contrast Variation 115
1.107 Investigation of Moderately or Highly Concentrated Solutions of Colloidal Particles 116
1.108 Structure and Reactions of the Humic Acids 117
1.109 Solution Conformation of a Coiled-coil Protein from Salmonella Typhimurium 118

INSTRUMENT DEVELOPMENTS 119
1.110 New Stretching Cell for Structural Studies of Elastomers and Swollen Gels 119
1.111 Polarized Neutrons for Reflectometry 120
1.112 Software for Analyzing Image-plate Data 121
1.113 An Image-plate Camera for X-ray-Scattering Measurements of Freely Suspended Clusters 122

1.114 Double Focussing Laue-Bragg Monochromator at Troika Beamline in ESRF 123

OTHER ACTIVITIES 124
1.115 LIP - CEC Large Installation Programme at Risø 125

2 PARTICIPANTS IN THE WORK IN THE DEPARTMENT 128

3 PUBLICATIONS AND EDUCATIONAL ACTIVITIES IN THE DEPARTMENT 136
3.1 Publications 136
3.2 Conferences 145
3.3 Lectures 154
3.4 Organizations of Conferences, Schools 157
3.5 Seminars at Risø, 1993 161

1 INTRODUCTION

The research activities of the department of Solid State Physics underwent an expansion in 1993 to include a program in synthesis and characterization of macromolecular materials. This new research area accords well with the department's strategy of analysing advanced materials using the unique access to neutron and X-ray scattering facilities at DR3, ESRF and Hasylab. In this way the department will be able to fulfill its objectives in the program on "Materials with Distinct Physical and Chemical Properties" as part of Risø National Laboratory's long term planning.

The following may serve as examples of the departments achievements in 1993.

- First experiments at the ESRF were performed in the fields of grazing incidence X-ray diffraction from liquid surfaces, scattering from clusters and amorphous films, and magnetic X-ray scattering. All experiments utilized the Troika beamline.
- The status of the experimental stations at Hasylab has improved considerably. The DORIS III storage ring has been running very reliable, and successful experiments were performed in the autumn investigating structures of metal and semiconductor surfaces and monolayers on the surface of water.
- The high standard of the experiments under the Large Facility Programme has continued in 1993. One of the most noteworthy experiments was the observation of magnetic flux lattice melting in the BSCCO high temperature superconductor.
- The phase behavior of block copolymer melts has proved to be very exotic. It has been found that application of an external oscillatory shear field on a di-block copolymer system acts in an analogous way to a magnetic field on a ferromagnetic system and that crystallization in tri-block copolymer systems can be entropy driven, with a gain in entropy going from the liquid to the crystalline phase.
- Magnetic clusters have been investigated theoretically, showing that even large electronic modifications only have negligible effect on the thermodynamic properties.
- As a benefit from the increase in flux in connection with the neutron guide installed in 1992, a novel propagating mode of magnetic excitations associated with the dynamics of the conduction electrons has been observed in Pr.
- Observation of novel biphotonic processes in side-chain liquid crystalline polyesters with pendant azobenzene moieties. Gratings generated through the interference of a blue-green argon ion laser beam can be "fixed" in the film by light from a red laser, at about 650 nm. This point to new photophysics in azobenzenes not reported at such long wavelengths.

1.1 Numerical Transfer-matrix Study of a Model with Competing Metastable States

T. Fiig, *Department of Solid State Physics, Risø National Laboratory, Denmark*, B. M. Gorman, P. A. Rikvold, and M. A. Novotny, *Supercomputer Computations Research Institute, Florida State University, USA*

We have applied a recently developed constrained-transfer-matrix (CTM) formalism[1] to study the stationary properties of metastability in a system with competing metastable states. Langer[2] related the imaginary part of the analytic continuation of the free energy $\mathrm{Im}\bar{F}$ into the region of metastability, to the decay rate Γ of the metastable states as $\Gamma \sim |\mathrm{Im}\bar{F}|$. We have studied a variant of the Blume-Capel model with weak, long-range interactions with the Hamiltonian

$$\mathcal{H} = -JN\sum_{i=1}^{L} m_i m_{i+1} + DN\sum_{i=1}^{L} q_i - HN\sum_{i=1}^{L} m_i ,$$

where m_i and q_i are the magnetization density and the density of nonzero spins at layer i. The spin-spin interaction is ferromagnetic ($J>0$), D is an applied field that either favors ($D>0$) or disfavors ($D<0$) $q_i=0$, and H is an applied magnetic field. There are three stable states $(m,q) = (0,0)$, $(m,q) = (-1,1)$, and $(m,q) = (1,1)$, which are denoted by (0), (−), and (+) in Fig. 1. The CTM formalism produces a complex constrained free-energy density. This is obtained by reweighting the eigenvalues from the transfer matrix of the equilibrium system. The results for the real part of the constrained free-energy density $\mathrm{Re}f_a$ are in excellent agreement with those from mean-field theory. The imaginary part $|\mathrm{Im}f_a|$ (Fig. 1) is extremely small, showing exponential dependence on the interaction range away from the classical spinodal line. The lobe structure correspond to different metastable states. The diamonds are data points obtained using extended numerical precision (128 bit) on the Cray YMP supercomputer. In the region of competing metastability it was found that $\mathrm{Im}f_a$ for a metastable state is closely related to the activation barrier involved in the transition, which, according to the Arrhenius formula of chemical reaction theory, is related to the decay rate.

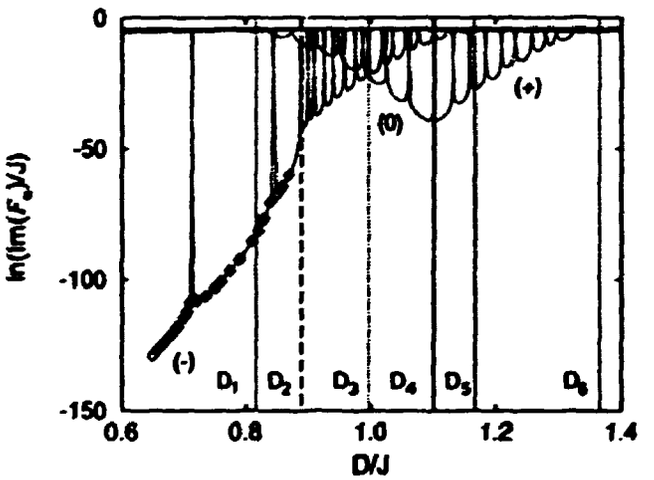

Fig. 1. Imaginary parts of the constrained free-energy densities for $N = 18$, $H/J = 0.1$, and $T/J = 0.25$, shown as functions of D/J. Vertical lines indicate the (0)-spinodal point at D_1, the exchange of metastable states at D_2, the point of equal barrier heights at D_3, the equilibrium transition at D_4, the (−)-spinodal point at D_5, and the (+)-spinodal point at D_6.

[1] P.A. Rikvold, (1989). Prog. Theor. Phys. **99**, 95.
[2] J.S. Langer, (1967). Ann. Phys. **41**, 108, and (1968). Phys. Rev. Lett. **21**, 973.

1.2 Lattice-gas Monte Carlo Simulations on the Connection Machine

S. Mannstaedt, O.G. Mouritsen, *Department of Physical Chemistry, The Technical University of Denmark*, T. Fiig, N.H. Andersen, and P.-A. Lindgård, *Department of Solid State Physics, Risø National Laboratory, Denmark*

In order to determine the effect on the material properties of the interplay between oxygen ordering and the diffusive motion of metal-ion dopants in $YBa_2Cu_{3-y}M_yO_{6+x}$, (M = Co, Fe, Al), we have developed a Monte Carlo computer-simulation program. The program is written in optimized C* for a lattice-gas model and implemented on a CM200 connection machine (CM). Interacting neighboring sites in the lattice-gas model cannot be updated simultaneously, since it is not possible to satisfy detailed balance. We have therefore developed a program, which takes full advantage over all single-bit processors available on the CM200, by updating several independent systems at the same time. The statistical mechanical lattice-gas model we have used to study the effect of metal-ion doping in $YBa_2Cu_{3-y}M_yO_{6+x}$ is a modified version[1] of the 2D ASYNNNI model which is known, to account quantitatively for the structural properties of $YBa_2Cu_3O_{6+x}$[2]. The objective is to determine if a suitable choice of the effective nearest neighbor interaction parameter for an oxygen pair around metal ion (V_1^M) may lead to M-dopant clustering as observed experimentally[3]. The equilibrium is reached very slowly in the case of parallel updating, probably because the formation of the clustering is hampered by the limitations in the parallel-movement algorithm. The results of the simulations (Fig. 1) show that for systems with low oxygen content the M-dopants will start to cluster in large formations when the V_1^M parameter is sufficiently attractive ($V_1^M > 0.3$). For systems with a high oxygen content the M-dopant clustering is not observed. These observations are in agreement with experimental observations. The results may be used to gain a better understanding of the superconducting properties of $YBa_2Cu_{3-y}M_yO_{6+x}$.

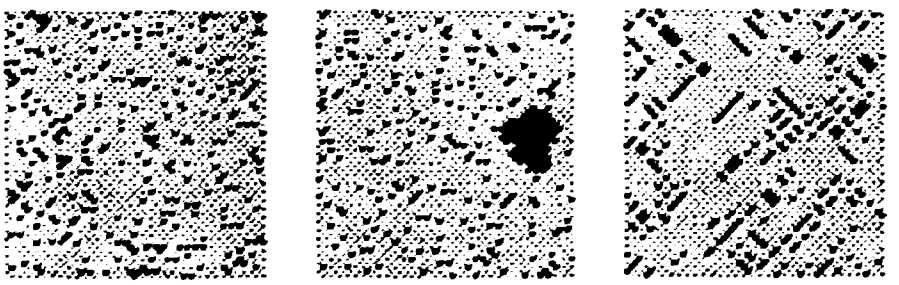

Fig. 1. M-dopant clustering for a 64 x 64 system at T = 800 K with metal concentration 7.5%. (a) V_1^M=0.20 and 5% oxygen, (b) V_1^M=0.33 and 5% oxygen, (c) V_1^M=0.33 and 50% oxygen.

[1] J. V. Andersen, N. H. Andersen, O. G. Mouritsen, and H. F. Poulsen (1993). Physica C 214, 142.
[2] T. Fiig, J. V. Andersen, N. H. Andersen, P. A. Lindgaard, O. G. Mouritsen, and H. F. Poulsen (1993). Physica C 217, 34.
[3] S. Katsuyama, Y. Ueda, and K. Kosuge (1990). Physica C 165, 404.

1.3 Theory and Computer Simulation of Diffuse Scattering

T. Fiig, P.A. Lindgård, N.H. Andersen, *Department of Solid State Physics, Risø National Laboratory, Denmark*, J. Berlin, *Supercomputer Computations Research Institute Florida State University, USA*, and O.G. Mouritsen, *Department of Physical Chemistry, The Technical University of Denmark*

The analysis of the diffuse scattering of neutrons or X-rays is an important tool in the disentangling of the properties of complex systems. Computer simulations are important since they allow a direct comparison between models and experiments. With modern technique and powerful computers it is at present possible to study systems of the same size over which the studied crystals are perfect. In order to obtain a simple understanding of the diffuse scattering we have analytically investigated the results for a number of mathematical distributions of domains in one dimensions with the purpose to see the effect of the excluded volume, a preferred domain size *etc.* It is found that the line shapes for an exponential distribution ($\propto e^{-\kappa r}$) is quite close to a Lorentzian, however the FWHM is strongly dependent on the volume fraction x of the domains yielding an effective inverse correlation length $\kappa_{eff} = \kappa/(1-x)$. For distributions with a characteristic length ℓ, (for example a Poisson distribution) the line shape becomes for small x more like a Lorentzian squared and for large x a satellite peak occurs at a wave vector with no simple relation to ℓ. Various line shapes are shown in Fig. 1. These results are difficult to generalize to higher dimensions and we have therefore performed computer simulations after a large scale implementation on the connection machine. The advantage of using this machine as compared to work stations is in particular evident for very large systems. Figure 2 shows a contour plot of the simulated diffuse scattering for the high T_c material $YBa_2Cu_3O_{6.5}$ using a 256 x 256 x 162 lattice. We have used the ASYNNNI model which quantitatively accounts for the structural properties of this system, as was recently demonstrated[1].

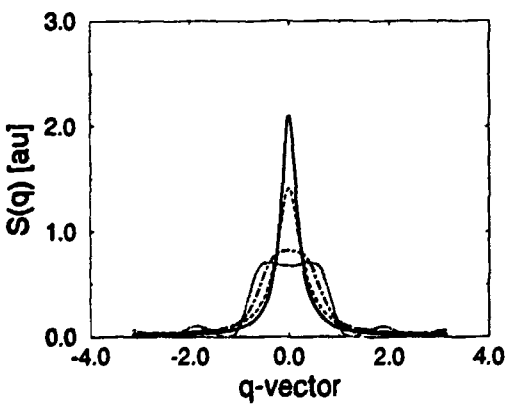

Fig. 1. Calculated lineshapes for the diffuse scattering for various cluster distribution functions in a one-dimensional chain when taking into account the 'excluded' volume effect.

Fig. 2. Simulated diffuse scattering for $YBa_2Cu_3O_{6.4}$ at 800 K using a 256 x 256 x 16 lattice.

[1] T. Fiig, J. V. Andersen, N. H. Andersen, P.-A. Lindgård, O. G. Mouritsen, and H. F. Poulsen, (1993). Physica **C217**, 34.

1.4 Phase Diagram, Structure Factor, and Oxygen Equilibrium Pressure of $YBa_2Cu_3O_{6+x}$ Studied by Monte Carlo Simulation[1)]

T. Fiig, N.H. Andersen, P.-A. Lindgård, *Department of Solid State Physics, Risø National Laboratory, Denmark*, J.V. Andersen, *Department of Physics, McGill University, Montreal, Canada*, O.G. Mouritsen, *Department of Physical Chemistry, The Technical University of Denmark*, and H.F. Poulsen, *HASYLAB, Hamburg, Germany*

The structural order and the oxygen equilibrium pressure related to the variable oxygen content in the basal CuO_x plane of the high temperature superconductor $YBa_2Cu_3O_{6+x}$, $(0 < x < 1)$, have been studied by Monte Carlo simulations with the two-dimensional ASYNNNI lattice gas model. The interaction parameters in the ASYNNNI model include the nearest-neighbor repulsive interaction, V_1, and the anisotropic next-nearest-interaction parameters, which are atttractive, (V_2), and repulsive, (V_3), depending on whether or not the two oxygen atoms are bridged by a Cu atom. The structural phase diagram has been calculated for the interaction parameters, $V_1 = -V_0, V_2 = 0.36\ V_0$ and V_3 = -0.12 V_0, and good agreement with experimental data for the phase line separating the tetragonal disordered and the two orthorhombic ordered structures, ortho-I and ortho-II has been etablished by the choice: $V_0/k_B = 5430$ K (see Fig. 1). The calculated phase diagram was determined from an investigation of the order parameters and their fluctuations as well as by use of an improved version of the Ferrenberg-Swendsen method. The structure factors have been calculated as function of temperature and wave vector for the oxygen stoichiometry, $x = 0.4$, for which the double cell ortho-II phase is predicted to be thermodynamic stable at room temperature, but only short range correlations of this structural phase has been observed experimentally. However, excellent agreement is found between measured room temperature neutron diffraction data and the structure factors calculated just above the structural phase line. We suggest that the observation of an orthorhombic distortion, simultaneously with only short range ortho-II oxygen order at room temperature is due to freezing-in of an ortho-II domain state with a preferred oxygen chain direction and accordingly only two types of domains. Using thermodynamic relations the chemical potential determined from the ASYNNNI model has been related to the oxygen equilibrium pressure. Characteristic features observed in available experimental data are predicted but quantitative agreement is not established (see ref. 1).

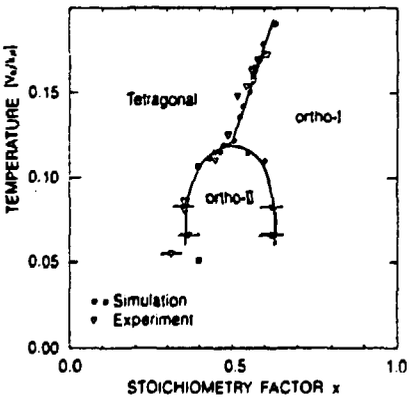

Fig. 1. The structural phase diagram of $YBa_2Cu_3O_{6+x}$ in the $x-T$ plane obtained by Monte Carlo simulations. Solid circles represent data obtained by Glauber dynamics, while the diamonds represents results obtained with Kawasaki dynamics. The triangles are experimental data points. The location of the points were obtained from the position of the peak in the fluctuation of the relevant order parameter. The (*) indicates the position in phase space where the neutron diffraction data, that have been analysed within the context of the ASYNNNI model, were recorded.

1) T. Fiig, J.V. Andersen, N.H. Andersen, P.A. Lindgård, O.G. Mouritsen, and H.F. Poulsen, (1993). Physica C **217**, 34.

1.5 Monte Carlo Simulations of Enhanced Lattice Gas Models for the High Temperature Oxygen Ordering Thermodynamics in $YBa_2Cu_3O_{6+x}$

P. Schleger and N.H. Andersen, *Risø National Laboratory, Department of Solid State Physics, Roskilde, Denmark*

We have studied by Monte Carlo simulation two modifications to the 2D asymmetric next-nearest neighbour interaction (ASYNNNI) lattice gas model describing the oxygen ordering thermodynamics in the basal plane of $YBa_2Cu_3O_{6+x}$. Although the ASYNNNI model is able to qualitatively describe the basic structural oxygen ordering phenomena[1], it fails to reproduce the behaviour of the chemical potential (see Fig. 1). Two models have been put forward recently, which go beyond the ASYNNNI model, utilizing different approaches to take into account additional intrinsic electronic degrees of freedom. In the model of Uimin *et al.*[2], an expression is derived for the free energy of finite chain fragments, based upon ground state energy calculations for the 1D Kondo-lattice approximation for the chain fragment electronic structure. The other approach[3], consists of assuming a narrow band limit for the motion of the charge carriers, reducing the thermodynamic description of the electronic states to seperate configurational entropies for the electropn spin and charge.

In Fig. 1, we show the results for the calculation of the non-ordering susceptibitity, $kT(\partial x/\partial \mu)_T$, for the pure ASYNNNI, as well as the two alternate models. The non-ordering susceptibility is a thermodynamic response function, analogous to the specific heat and compressibility. It is sensitive to the details of the oxygen chemical potential, and represents a stringent test for oxygen ordering models in $YBa_2Cu_3O_{6+x}$ for temperatures above 450° C. One sees that the ASYNNNI model differs drastically from experiment.

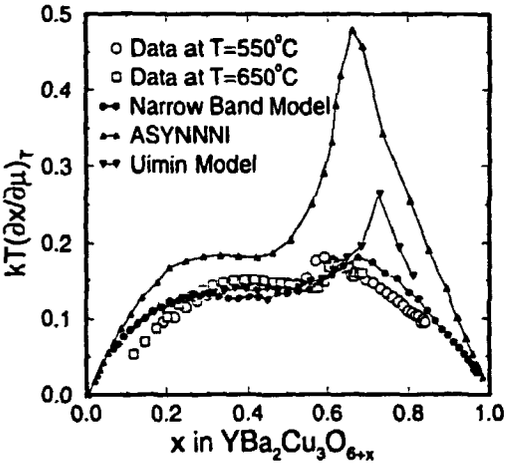

Fig. 1. Plot of $kT(\partial x/\partial \mu)_T$ vs. x (μ is the chemical potential).

The model of Uimin shows some slight improvements. The narrow band hopping model, however, improves the agreement to experiment drastically. It clearly shows the importance of the underlying spin and charge degrees of freedom upon the behaviour of the oxygen chemical potential. The narrow band hopping model also agrees quantitatively with measurements of the fractional site occupancies as well as the shape of the Cu^{1+} count vs. x[1]. We are currently investigating how the additional electronic terms modify the structural phase diagram.

[1] T. Fiig, J.V. Andersen, N.H. Andersen, P.-A. Lindgård, O.G. Mouritsen, and H.F. Poulsen, (1993). Physica C **217**, 34.
[2] G. Uimin and J. Rossat-Mignod, (1991). Physica C **182**, 11.
[3] P. Schleger, W.N. Hardy, and H. Casalta, Phys. Rev B **48**, *in press.*

1.6 Calculation of Electronic and Structural Influence on the Thermal Magnetic Properties of Clusters

P. A. Lindgård, *Department of Solid State Physics, Risø National Laboratory, Denmark*, and P. V. Hendriksen, *Materials Department, Risø National Laboratory, Denmark*

The magnetic properties of clusters of transition metal atoms have recently been studied in order to elucidate how ferro magnetism evolves from the atom to the bulk. In particular the 3*d* electrons are of importance in the potential applications of the clusters in recording materials and in catalysts. Free molecular beam experiments[1] have revealed larger magnetic moments per atom in small iron clusters, than expected in the bulk. Neutron scattering experiments have been performed on clusters supported in a matrix[2]. Calculations for nano-sized particles by Pastor et al[3] have shown that the magnetization at zero temperature has a non-uniform profile with larger moments at the surface. We have previously discussed the intrinsic thermodynamic magnetic properties of clusters using spin wave theory[4] for a Heisenberg model, where a fixed magnitude of the spins $S_i = S$ and site-independent nearest-neighbour exchange interaction were assumed. We have extended this to include a discussion of the consequences of the more realistic model in which we allow for a magnetization profile at $T = 0$ and a structural relaxation, which in turn will give rise to a site-dependent exchange interaction. Also longer range interactions and effects of possible enhanced surface anisotropy has been considered. In Fig.1. is shown the schematic effect of surface anisotropy, which will be enhanced both due to a surface contraction and to the lowering of the symmetry at the surface. In general the considered effects have a very small influence on the thermal properties as described by the simple Heisenberg model. The reason is that the perturbations of the magnetic interactions are too small to significantly alter the spin wave spectrum and the wave functions. This is contrary to the case for the electrons, where large changes occur in order to assure lack of charge transfer between the atoms in the cluster. Our previous results[4] for the Heisenberg model therefore remain valid with high accuracy.

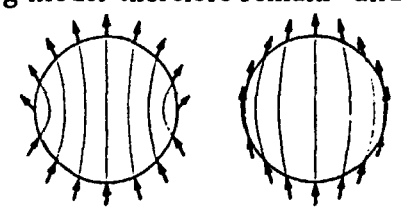

Fig. 1. Influence of an enhanced surface crystal field anisotropy term DS_ξ^2 on the magnetic ground state of the cluster (schematic) for $D < 0$ (radial) and $D > 0$ (tangential).

[1] W.A. de Heer, P. Milani, and A. Châtelain, (1990). Phys. Rev. Lett. **65**, 488.
[2] I. Mirebeau, C. Bellouard, M. Hennion, J.L. Dormann, C. Djega-Mariadassou, and M. Tessier, (1992). J. Magn. Magn. Mater., **104-107**, 1560, and J.R. Childress, C.L. Chien, J.J. Rhyne, and R.W. Erwin, (1992). ibid., 1585.
[3] G.M. Pastor, J. Dorantes-Dávila, and K.A. Bennemann, (1989). Phys. Rev. **B 40**, 7642, J. Dorantes-Dávila, H. Dreyssé, and G.M. Pastor, (1992). Phys. Rev. **B 46**, 10432, and A. Vega, J. Dorantes-Dávila, L.C. Balbás, and G. M. Pastor, (1993). Phys. Rev. **B 47**, 4742.
[4] P.V. Hendriksen, S. Linderoth, and P.-A. Lindgård, (1993). J. Phys. C. **31**, 5675, P.V. Hendriksen, S. Linderoth, and P.-A. Lindgård, (1993). Phys. Rev. **B48**, 7259.

1.7 Calculations of Neutron Magnetic Scattering Cross Section of a Triangular 2D Quantum Antiferromagnet

K. Lefmann, *Department of Solid State Physics, Risø National Laboratory, Denmark,* and P. Hedegård, *Ørsted Laboratory, Niels Bohr Institute, University of Copenhagen, Denmark*

The earlier work[1] about the magnetic structure and dynamics of the $S = 1/2$ triangular Heisenberg antiferromagnet has been extended, and a detailed calculation of the neutron scattering cross section from both single crystal and powder sample has been made[2].

A Schwinger boson formalism has been used to express the Heisenberg Hamiltonian $H = J \sum_{\langle i,j \rangle} \mathrm{S}_i \cdot \mathrm{S}_j$, which in turn is diagonalized by Hartree-Fock and BCS factorization. Two mean fields are introduced: Δ, which gives the strength of the antiferromagnetic singlet bonds, and ρ, which is a measure of the ferromagnetic correlations. We find two candidates for the ground state: State A with long range order corresponding to the classical Néel state, and a disordered state B resembling Andersons resonating valence bond state. The elementary excitations (*spinons*) of the B state shows an energy gap, while the A state is gapless. The thermodynamic properties of these states has earlier been discussed[3].

The $T = 0$ scattering function $S^{\alpha\beta}(\kappa,\omega)$ for polarized neutron scattering has been calculated. For both the A and B state $S^{\alpha\beta}(\kappa,\omega) = \delta_{\alpha,\beta} S^{zz}(\kappa,\omega)$, giving this model the same polarization dependence as that of a paramagnet. The A state shows elastic peaks at (1/3 1/3) with spin-wave-like excitations, as for the three-sublattice Néel state. The B state shows no elastic, but a broad inelastic signal peaking around (1/2 0) and (1/3 1/3) for $\omega \approx 0.5\ J$. The powder average of the scattering function is shown as Fig. 1.

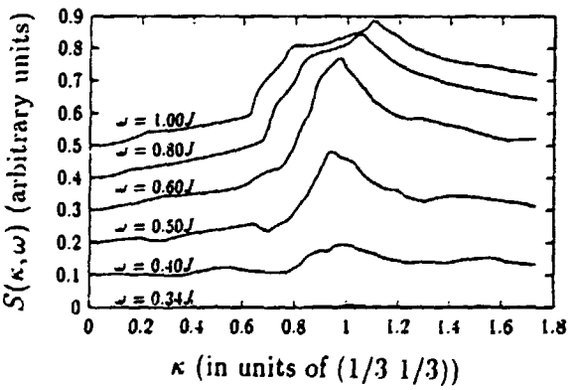

Fig. 1. Powder averaged scattering function $S(\kappa,\omega)$ for the RVB state at $T = 0$. The curves display the result of q-scans for different values of the energy transfer, ω.

Recent neutron experiments at TAS8 and at E4/E7 at HMI, Berlin has neither found any evidence of the A nor of the B state in a powder sample of $YCuO_{2.5}$, which is believed to be a physical realization of the model.

[1] K. Lefmann and P. Hedegård, (1992). *Contribution* 1.2 in Risø-R-660(EN).
[2] K. Lefmann and P. Hedegård, Phys. Rev. B, *submitted.*
[3] D. Yoshioka and J. Miyazaki, (1991). J. Phys. Soc. Jpn. **60**, 614.

1.8 Asymmetric Lineshapes in Powder Diffraction

W. Montfrooij, R. Hadfield* and N.H. Andersen, *Department of Solid State Physics, Risø National Laboratory, Denmark*

The information derived from neutron powder diffraction studies relies heavily upon the assumption that the lineshapes corresponding to Bragg peaks can be approximated by Gaussian functions. For most practical purposes, this assumption is adequate. However, at small scattering angles 2θ, one encounters distinctly asymmetric lineshapes due to the curvature of the Debye-Scherrer cone combined with the finite sample and detector heights. On doing a Rietveldt refinement of the powder pattern, this invariably results in a discrepancy between fitted and observed lineshapes. There will be a small shift in observed peak position, and a considerable difference between observed and calculated intensities (see Fig. 1). Since the latter plays a crucial role in determining the positions and occupancies of the atoms within the unit cell, we are developing a code which accounts for the asymmetric lineshapes. The lineshape is simply given by the intersection of the Debye-Scherrer cone with the detector bank (convoluted with the in-plane resolution function) as

$$I(2\theta) = S_f(\theta_B) \int \frac{1+\tan^2(2\theta)}{\sqrt{\tan^2(2\theta_B)-\tan^2(2\theta)}} F(2\theta') e^{-(2\theta-2\theta')^2 \ln 2/\sigma^2} d(2\theta') \qquad (1)$$

$$F(2\theta) = \begin{cases} G(2\theta) = \frac{d+s-2r\cos(2\theta)\sqrt{\tan^2(2\theta_B)-\tan^2(2\theta)}}{s/2} & \text{if } 0 < G(2\theta) < 1 \\ 0 & \text{if } G(2\theta) \leq 0 \\ 1 & \text{if } G(2\theta) \geq 1\,, \end{cases} \qquad (2)$$

where d and s are the detector and sample heights respectively, r is the distance between sample and detector, σ is the resolution halfwidth and $S_f(\theta_B)$ is the structure factor squared at the Bragg scattering angle θ_B. So far, we have incorporated this lineshape in a Reverse Monte Carlo (RMC) fitting routine for powders, and we do indeed find a better agreement between fit and experiment at the low angles (*cf.* Fig. 1). In particular, one observes a drastic change in fitted intensity at these angles (the Rietveldt intensity being too small) and a change in fitted $2\theta_B$ (10°.97 *vs.* 10°.84 of the Rietveldt refinement).

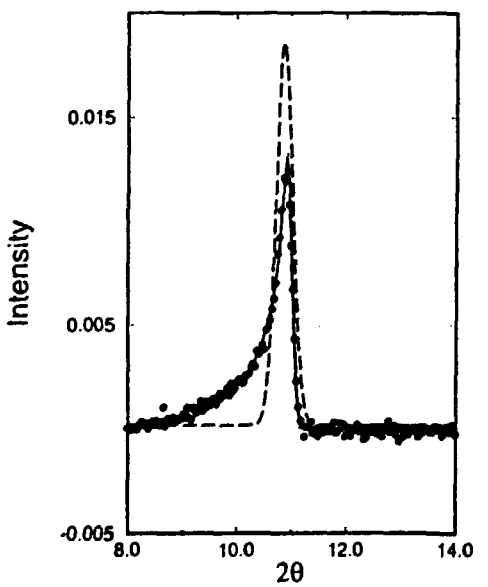

Fig. 1. Low-angle scattering intensity of a powder sample for a typical diffractometer setting. The solid line is the RMC fit (*cf.* eqs. (1) and (2)) while the dashed curve is the Gaussian produced by a standard Rietveldt refinement.

* On leave from Clarendon Laboratory, Oxford, UK and AEA Technology, Harwell, UK

1.9 The Relation between Kinematical and Dynamical Theories of Neutron and X-Ray reflectivity

I.W. Hamley, *Department of Physics, University of Durham, UK*, and J. Skov Pedersen, *Department of Solid State Physics, Risø National Laboratory, Denmark*

The determination of a scattering density profile from X-ray and neutron reflectivity data is non-trivial. It always involves optimization of parameters in non-linear expressions. Techniques based on the full dynamical theory are rather cumbersome and it is consequently helpful to introduce various approximations. In dynamical theory, the reflectance is calculated at each interface in a film supposed to consist of a discrete number of slices, using methods from optics. The simplest approximation to apply is the kinematical theory, which can be expressed in terms of a Fourier transform, with resulting simplification of the data analysis. We have carefully discussed the intermediate approximations between dynamical and kinematical theory[1]. These involve: (i) The neglect of multiple scattering, (ii) the replacement of the pathlength corrected for refraction in each slice by an approximate pathlength for the entire film and bulk, and (iii) the assumption that the reflectance at an interface is proportional to the change in the scattering density at that interface. All these approximations break down near the critical scattering vector, as demontrated by calculations for model profiles. Figure 1 shows the reflectivity calculated by four different approaches for a single layer on a substrate. The layer thickness is 1000 Å and the scattering length density of the layer is five times larger than that of the substrate ($\rho_\infty = 1 \times 10^{-6}$ Å^{-2}).

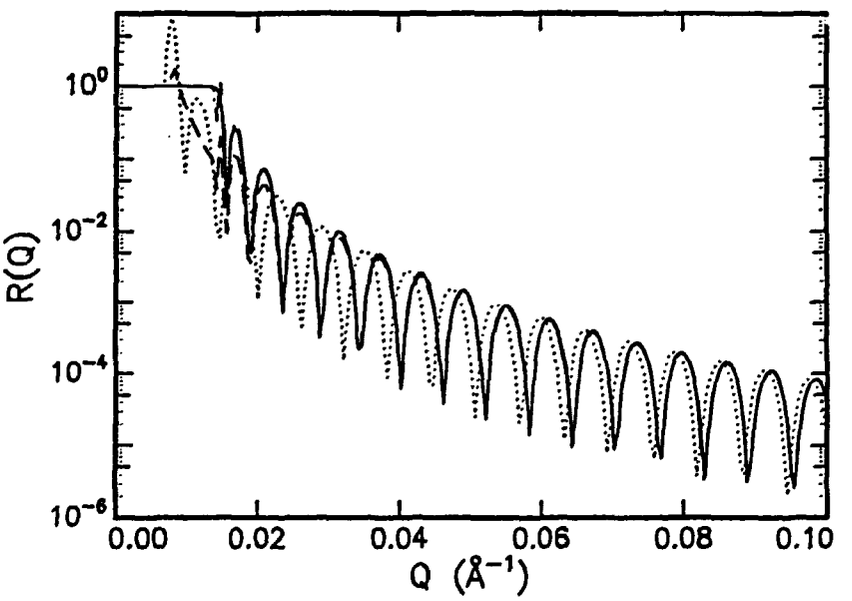

Fig. 1. Reflectivities calculated by different approaches: Full dynamical calculation: solid line; single scattering theory: dashed-dotted line; kinematical theory with optical pathlength correction: dashed line; kinematical theory with refraction corrections: dotted line.

[1] I.W. Hamley and J. Skov Pedersen (1994). J. Appl. Cryst. *in press.*

1.10 Determination of Size Distributions from Small-angle Scattering Data for Systems with Effective Hard-sphere Interactions

J. Skov Pedersen, *Department of Solid State Physics, Risø National Laboratory, Denmark*

Two new methods for free-form determination of size distributions for systems with hard-sphere interactions have been introduced[1]. In order to have a simple approach for calculating the scattering from a system of hard-spheres an approximation, called the local monodisperse approximation, was introduced. Model calculations shows that this approximation gives relatively small errors even at relatively high polydispersities and large volume fraction. In the first method the determination of size distributions was done by least-squares methods with a smoothness and a non-negativity constraint and the local monodisperse approximation was applied. It leads to normal equations which are linear in the amplitude of the size distribution. This was used when solving the least-squares problem: Only the two effective parameters describing the interference effects were treated as non-linear parameters in an external optimization routine. The parameters describing the size distribution were determined by a linear least-squares method. In the second method determination of the size distribution was done using the non-linear equations from the calculation of the scattering intensity in the Percus-Yevick approximation[2]. For this a non-linear least-squares routine with a smoothness and a non-negativity constraint was used. Both approaches have been tested by analyzing simulated examples calculated by the analytical expressions in the Percus-Yevick approximation. The methods have also been applied on two sets of experimental data from silica particles and from δ' precipitates in an Al-Li alloy. For the simulated examples good agreement was found with the input distributions (Fig. 1). For the experimental examples the results agreed with the expected and known properties of the samples.

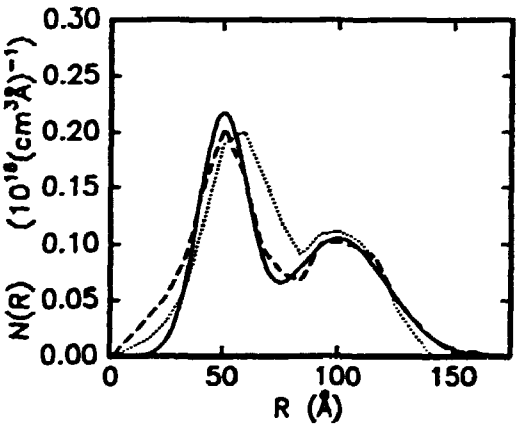

Fig. 1. Size distributions from analyzing simulated scattering data. Full curve: original distribution. Dotted curve: distribution from the local monodisperse approximation. Broken curve: Distribution from the analytical model.

[1] J. Skov Pedersen, (1994). J. Appl. Cryst. *in press.*
[2] A. Vrij, (1979). J. Chem. Phys. 71, 3267.

1.11 Analytical Calculation of the Three-dimensional Resolution Function for Laue Geometries

P. Harris, B. Lebech, and J. Skov Pedersen *Department of Solid State Physics, Risø National Laboratory, Denmark*

Within the last decade several single crystal measurements using traditional SANS geometries have made a demand for methods for calculating the three-dimensional resolution function. Knowledge of the resolution function is crucial for analyzing and understanding these experiments, and analytical expressions for the resolution function are desirable because these will decrease the computational time spend on data analysis.

The first component in the experimental geometry is a mechanical velocity selector that makes it possible to select the wavelength, $\langle\lambda\rangle$, and the wavelength spread $\delta\lambda$. The beam is defined by two circular or rectangular pin-holes separated by a distance l_1, and the sample is placed just after the second pin-hole. Finally a position sensitive detector is plared at a distance l_2 from the detector. To describe the performance of the experimental set-up we have employed the analytical beamline analysis[1] outlined in the following. The distribution of the incoming neutrons is described as a function of two position parameters, x, y, which gives the position relative to the beam center in the plane perpendicular to the beam direction (the z direction), the corresponding angles relative to the direction of the nominal neutron, x', y', and the relative wavelength deviation, $\Delta\lambda/\lambda$, $(\Delta\lambda = \lambda - \langle\lambda\rangle)$. By applying Gaussian approximations for the neutron distribution and the transmission functions of the apertures one may analytically calculate the neutron distribution at the sample position as a function of x, y, x', y', and $\Delta\lambda/\lambda$. After finding $\mathbf{\Delta q}(x, x', y, y', \Delta\lambda/\lambda)$, the resolution function may be calculated as the integral over the five parameters $x, x', y, y', \Delta\lambda/\lambda$ of the neutron distribution multiplied by three δ function conditions given by $\mathbf{\Delta q}(x, x', y, y', \Delta\lambda/\lambda)$.

Most real crystals have Bragg reflections with a finite width, usually due to mosaic spread, finite correlation lengths, or both. Therefore, it is necessary to introduce Bragg reflections of finite width and perform the convolution of these by the resolution function. The use of Gaussian functions to describe the reflections of finite widths has allowed this to be performed analytically.

The final equations for the resolution function convoluted with the scattering cross section from a crystal with Bragg reflections broadened by mosaic spread as well as finite correlation effects, have been implemented in a least squares programme. Until now, we have performed data analysis on the magnetic ordering on MnSi[2].

For applications in the future, it should be noted, that the equations easily may be extended to the case with a monochromator crystal, as one, for example, has for small angle X-ray scattering. In addition, we have not used the small-angle approximation of 2θ, and the model is generally valid for experiments using Laue geometries.

[1] J. Skov Pedersen and C. Riekel, (1991). J. Appl. Cryst. 24, 893.
[2] Contribution 1.14 in this report.

1.12 Best Geometry to Perform a Given SANS Measurement. A Graphical Approach

A.N. Falcão, J. Skov Pedersen, and K. Mortensen, *Department of Solid State Physics, Risø National Laboratory, Denmark*

In a SANS experiment a range of scattering vectors, q, is measured with a certain resolution. Both range and resolution are imposed by the physics of the sample to be studied, and by the specifications of the instrument to be used. Very often, different sets of the geometric parameters of the spectrometer can fulfill the requirements of the experiment, and the user can gain considerably by making a careful choice of the geometry. To solve the problem of determining the set of geometric parameters that optimize the detector count rate, C_D, for fixed resolution, a simple graphical approach was developed. It is based on the following: (1) By optimizing C_D with only the restriction of fixed resolution the solution is not determined due to the number of parameters involved, and additional constraints are needed. (2) At constant resolution, C_D is an increasing function of each one of the geometric parameters (distances source-sample, L_1, and sample-detector, L_2, neutron source and sample radius, R_{NS} and R_S, respectively, and detector resolution Δl). In particular it can be written as a function of L_1 and L_2 as: $C_D = c\ (\Delta\theta_0)^6[L_1L_2/(L_1+L_2)]^2$ where $\Delta\theta_0$ is the constant geometric contribution to the resolution and c is a constant (see Fig. 1.a). (3) The proper constraints to introduce are those that result both from the requirements of the experiment (q range and resolution), and from the physical limits of the geometrical parameters. (4) All the constraints can be written as constraints on L_1 and L_2. Then, using the contour plot of C_D, the sub-space where the solution has to be searched is defined by the inequalities that represent the restrictions, and the optimal solution is easily determined (see Fig. 1.b).

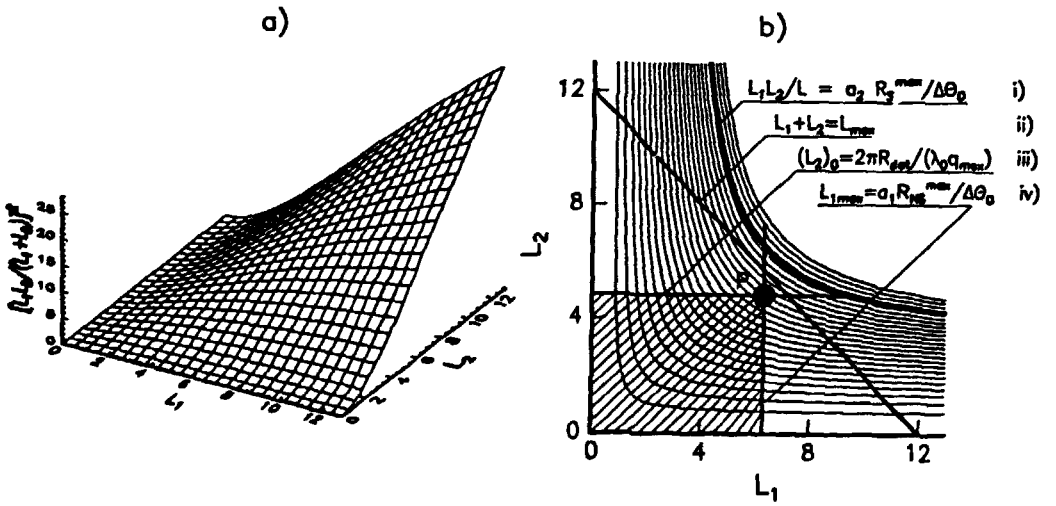

Fig. 1. (a) Plot of $C_D/c(\Delta\theta_0)^6$ as a function of L_1 and L_2. (b) Contour plot of $C_D/c(\Delta\theta_0)^6$ and combined effect of the restrictions on: (i) the size of the sample available. (ii) the space available. (iii) the q range required and (iv)- the size of the neutron source available. Each restriction defines a sub-space to which the solution has to belong. The optimal geometry has to be searched in the intersection of all the sub-spaces (shaded area). Point P represents the optimal geometry. In the figure, R_{det} is the radius of the detector, λ_0 is the wavelength, and max refers to the maximum possible value of the respective parameter.

1.13 Spin-spin Coupling in Cation Stabilised Free Radicals. Molecular and Polymeric Materials

K. Bechgaard, *Department of Solid State Physics, Risø National Laboratory, Denmark*

Chemically stable biradicals have been identified in a series of compounds; bis complexes of zinc cations and azothioformamide anion radicals (see Fig. 1). These complexes exhibit a magnetic behaviour mimicing two weakly coupled spins. EPR analysis of frozen dilute glasses indicate an average distance between the spins of about 8 Å [1]. The magnetic properties of the molecular material, as investigated by the Faraday method, indicate singlet-triplet equilibria with the singlet as the ground state. An efficient J/k of about 15-17 K was observed. It is presently not known whether this efficient J/k originates from intra- or intermolecular interactions.

It has been found that the analogous (doublet) copper and (singlet) nickel materials are isomorphous with the zinc compound. Therefore, investigations of dilute samples of the Zinc compounds in copper and nickel matrices should clarify the situation.

Also a polymer version of the zinc biradical has been prepared. Particular attention was given to the "linker" which interconnects the spin bearing fragments. The fragment chosen (a two carbon chain) should according to theoretical models enhance the "antiferromagnetic" intermolecular interaction, but in spite of this, it was found that the efficient J of the polymeric biradical dropped to about 9 K (J/k = 9.3 K). Further experiments with materials designed to promote "ferromagnetic" intermolecular interaction are in progress.

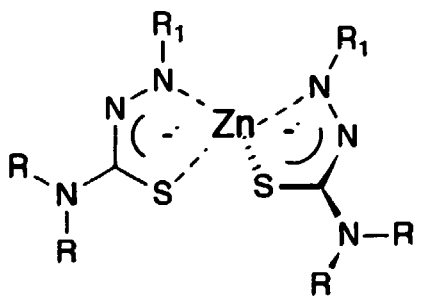

Fig. 1. Molecular structure of the biradical zinc-bis-N,N-dialkyl-phenylazothioformamide.

[1] K.A. Jensen, K. Bechgaard, and C.Th. Pedersen, (1972). Acta Chem. Scan. **26**, 2271.

1.14 Analysis of the Magnetic Ordering in MnSi

P. Harris, B. Lebech, J. Skov Pedersen, K. Mortensen *Department of Solid State Physics, Risø National Laboratory, Denmark*, and M. Jermy, *Physics Laboratory, The University Canterbury, Kent, UK*

The intermetallic compound MnSi crystallizes in the cubic non-centrosymmetric space group $P2_13$, and has therefore the possibility to support magnetic helical structures of a very long repetition length[1]. This is indeed the case below 29 K, where MnSi orders into a magnetic structure with propagation vectors along equivalent ⟨111⟩ directions. We have investigated the magnetic phase diagram of MnSi on the Risø SANS spectrometer[2]. Our measurements show, that when a magnetic field is applied along the [001] direction, the propagation vectors turn gradually into equivalent ⟨100⟩ directions. Further increase of the field induces domain growth of the domains with q||H and finally the structure becomes ferromagnetic.

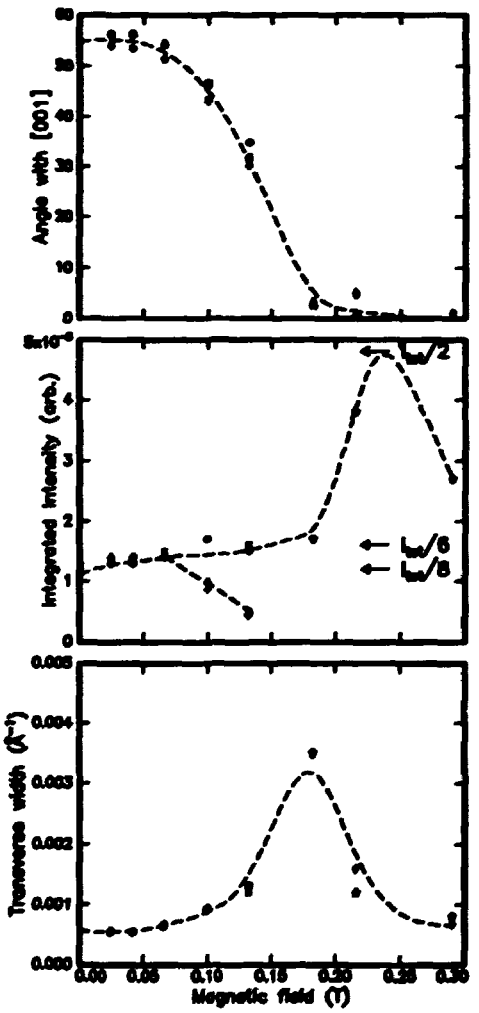

Data analysis was done to find the detailed peak shapes[3]. In Fig. 1 the angle between the peaks and the field direction, the integrated peak intensities, and the transverse widths are given as a function of field. Due to the relaxed resolution, it was not possible to determine the width along q. When a lower field limit of $H_1 = 0.07$ T is reached, the peaks turn away from the ⟨111⟩ directions towards the ⟨100⟩ directions. This second order phase transition at $H_2 \approx 0.18$ T, is associated with diverging peak widths, and the eight reflections along equivalent ⟨111⟩ directions are reduced to six reflections along equivalent ⟨100⟩ directions. Above H_2, a domain reorientation regime occurs, where the ⟨100⟩ domain having q||H is prefered. The six reflections are then reduced to two. Finally the satellite intensity is seen to decline, as the structure becomes conical and eventually ferromagnetic. There is a lack of data points above 0.15 T, and another experiment has to be performed before a more detailed description of the ordering can be made.

[1] P. Bak and M.H. Jensen, (1980). J. Phys. C **13**, L881.
[2] C. M. Gregory, (1992). Ph. D. Thesis, University of Durham, U.K.
[3] Contribution 1.11 in this report.

1.15 SANS Studies of the Nearly Ferromagnetic Frustrated Antiferromagnet, $Y_2Mn_2O_7$

J.E. Greedan, *Institute for Materials Research, McMaster University, Hamilton, Canada*, J. Skov Pedersen, *Department of Solid State Physics, Risø National Laboratory, Denmark*, and M.A. Subramanian, *CR and D, E.I. DuPont, Wilmington, Delaware, USA*

$Y_2Mn_2O_7$ is nearly ferromagnetic with Curie-Weiss behaviour with θ_c = +41 K and an apparent T_c in d.c. and a.c. susceptibility near 17 K. Yet, no long range order is seen down to 2 K in the heat capacity. Diffuse neutron scattering from wide angle studies is consistent with nearest-neighbour antiferromagnetic interactions competing with longer range ferromagnetic interactions. Antiferromagnetic near-neighbour exchange is a necessary condition for frustration on the Mn^{4+} sublattice which consists of a three-dimensional array of corner shared tetrahedra.

Strong SANS intensity is seen from $Y_2Mn_2O_7$ and the isostructural $Lu_2Mn_2O_7$ over the temperature range 25 K to 5 K and the scattered intensities can be fit to a cross section consisting of both a Lorentzian (LOR) and a Lorentzian-squared (LORSQ) term:

$$I(q) = A/(q^2 + 1/\xi_1^2) + B/(q^2 + 1/\xi_2^2)^2,$$

where ξ_1 and ξ_2 are correlation lengths, and q is the scattering vector. The most straightforward interpretation of the two terms is that the LOR term measures spin correlations of subcritical ferromagnetic clusters and the LORSQ term is due to random field effects. Previous SANS measurements at Risø established that $\xi_2 \gg \xi_1$ at all temperatures and that their temperature dependencies were different in the range 20 K to 15 K. ξ_1 saturated at 25 Å near 15 K while ξ_2 became resolution limited > 300 Å in the some range.

Data from February 1993 determine with much better thermal resolution the temperature dependence of all four parameters in the cross section as shown in the figures below:

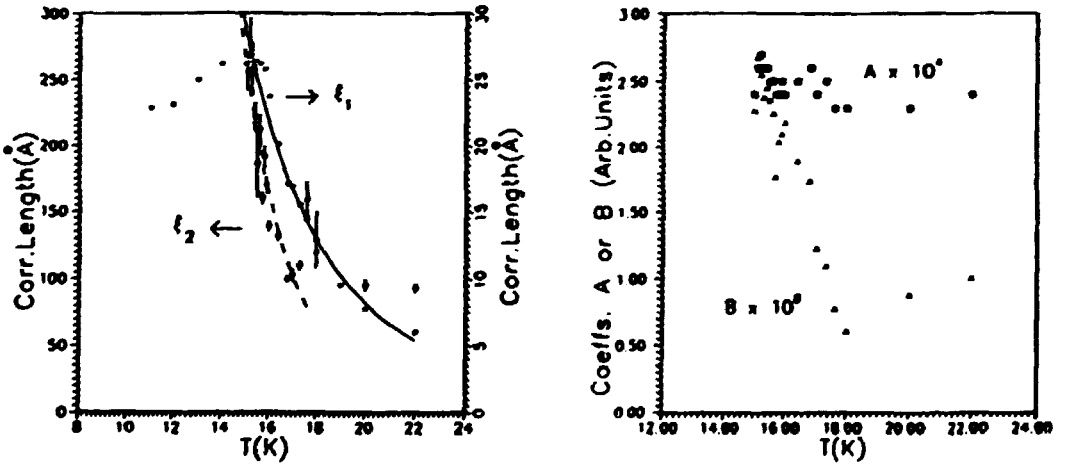

These results show in dramatic fashion the competition between the ferromagnetic and random field tendencies.

1.16 Commensurate Magnetic Ordering in dhcp Nd Metal

B. Lebech, *Department of Solid State Physics, Risø National Laboratory, Denmark*, J. Wolny, *Institute of Physics and Nuclear Techniques, Academy of Mining and Metallurgy, Cracow, Poland*, and R. M. Moon, *Solid State Division, Oak Ridge National Laboratory, Tennessee, USA*

Below T_N = 19.9 K the magnetic ordering in *dhcp* Nd metal consists of a series of at least four different multi-q modulated magnetic structures. The modulation vectors are temperature dependent and lie predominantly in the basal plane close to the equivalent (100) (a^*) reciprocal lattice vectors. This means that they may be described by symmetry related basal plane vectors given by cartesian components (q_x, q_y). Figure 1 shows q_y versus q_x (filled circles) with temperature as an implicit parameter. Although the length of q and the components (q_x, q_y) in general are incommensurate, the dependence shown in Fig. 1 may, within a phenomenological model having similarties to rotational epitaxy, be represented by two-dimensional higher order commensurate structures. The corresponding magnetic cell is much larger and turned further away from the (100) directions than implied by (q_x, q_y)[1]. The model is based on the following idea: Within each hexagonal layer the Nd atoms lie on a regular lattice consisting of equilateral triangles with sides of unit lengths. Equivalently the spin system forms a magnetic lattice of equilateral triangles (three-q structure) or isosceles triangles (single-q or two-q structures) which decorate the crystal lattice. Depending on the misfit between q and a^*, the lattice of the spin system may at some points coincide with the crystal lattice. We call this a two-dimensional higher order commensurate structure. The stars shown in Fig. 1 fulfill this condition. There is a discret, but infinite number of higher order commensurate structures and the actually commensurate magnetic cell presumeably depends on the balance between for instance the magneto-elastic and the anisotropy energies.

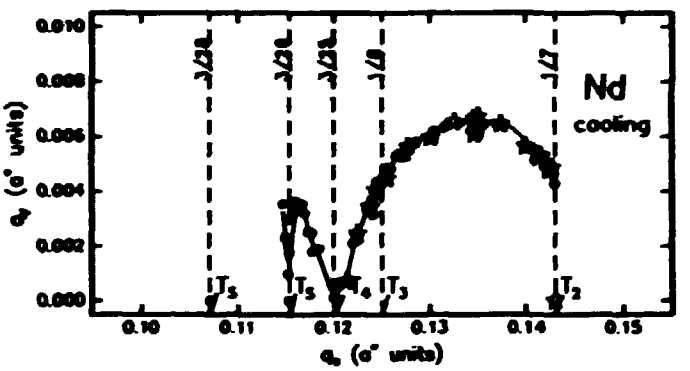

Fig. 1. Basal plane components of the modulation vector describing the magnetic structure in pure Nd metal with temperature as an implicit parameter. The numbers at the dashed lines indicate the commensurate values of q_x. The transition temperatures T_N, T_2 to T_5 correspond to 19.1, 17.9, 8.7, 6.8 and 5.6 K on cooling.

[1] B. Lebech, J. Wolny, and R.M. Moon, (1994). Commensurate-incommensurate magnetic phase transitions in *dhcp* Nd metal. J. Phys. Cond. Matter, *submitted*.

1.17 Studies of Modulated Magnetic Structures under High Pressure

S.A. Sørensen and B. Lebech, *Department of Solid State Physics, Risø National Laboratory, Denmark*

The well known magnetic structures observed in, for instance the rare earth metals, are the results of competition between different types of magnetic interactions. Magnetic structures and phase transitions associated with these have been extensively investigated by scattering of thermal neutrons under variation of temperature and external magnetic field. As the application of an external pressure will change the interatomic distances in the material concerned, neutron scattering measurements on magnetic materials under variation of pressure will contain important information about the distance dependence of the magnetic interactions.

Until recently, the posibilities of neutron scattering on single crystals with pressures in the kbar range have been very limited. An improved McWhan type of pressure cell, HPCNS, has become commercially avaiable[1]. The sample is mounted in a micro cell filled with a pressure transmitting fluid. The micro cell is pressed between two clamped pistons and supported by a cylinder of hot pressed Al_2O_3. By pre-stressing the supporting cylinder it is possible to have a 10 mm high window without any heavy neutron absorbers in the beam path and a maximum pressure of 25 kBar in the sample cell. One of the developers of HPCNS used the cell in 1990 at Risø for an experiment on Er at 4.2 K and 11.5 kbar[2]. In this experiment it was shown, that the ferromagnetic phase observed at ambient pressure below 17 K is suppressed by 11.5 kbar.

After two and a half year under pressure the Er sample was taken out of the cell. It was observed, that the pressure in the cell and the orientation of the crystal had been kept stable during the period. A neutron scattering experiment on the sample at ambient pressure showed, that the virgin properties[3] of the sample were restored after releasing the pressure. The pressure was then raised to 15 kbar to search for suppresion of the basal plane magnetic ordering, observed between 52 and 17 K at ambient pressure. Within the experimental uncertainties the results at 15 kbar could not be distiguised from those obtained at 11.5 kbar.

The technique of operating HPCNS has now become well established and further experiments will be done to determine the PT-phase diagram of Er. It is planned to extend the pressure measurements to several other materials in the near future.

[1] A. Onodera, Y. Nakai, N. Kunitomi, O. Pringle, H. Smith, R. Nicklow, R. Moon, F. Amita, N. Yamamoto, S. Kawano, N. Achiwa, and Y. Endoh, (1987). Jap. Jour. App. Phys. **26**, 152.
[2] S. Kawano, B. Lebech and N. Achiwa, (1993). J. Phys. Cond. Mat. **5**, 1535.
[3] M. Habenschuss, C. Stassis, S.K. Sinha, H. W. Deckman, and F.H. Spedding, (1974). Phys. Rev. B **10**, 1020.

1.18 A New Mode of Magnetic Excitation in Praseodymium

K.N. Clausen, *Department of Solid State Physics, Risø National Laboratory, Denmark*, K.A. McEwen, *Department of Physics, Birckbeck College, London, UK*, J. Jensen, and A.R. Mackintosh, *Niels Bohr Institute, Ørsted Laboratory, Denmark.*

A novel propagating mode of magnetic excitation has been observed in Pr. It takes the form of low-energy satellites to the crystal-field excitations on both the hexagonal and cubic sites. In each case, the crystal-field excitation hybridizes strongly with a low-energy satellite excitation, whose energy increases rapidly with q, and which disappears rapidly beyond the nominal crossing point of the two modes (see Fig. 1). The excitations are resolution limited at large q, but broadens rapidly as q approaches 0. The broadening may be abruptly quenched by a magnetic field.

The satellite excitations are believed to be associated with the interaction with the electron-hole-pair excitations of the conduction electron gas. The explanation of the mode requires a detailed understanding of the mixing of the *4f* states and the conduction band, taking into account the dynamical response of the conduction electrons. This effect is not included in the so-called standard model[1].

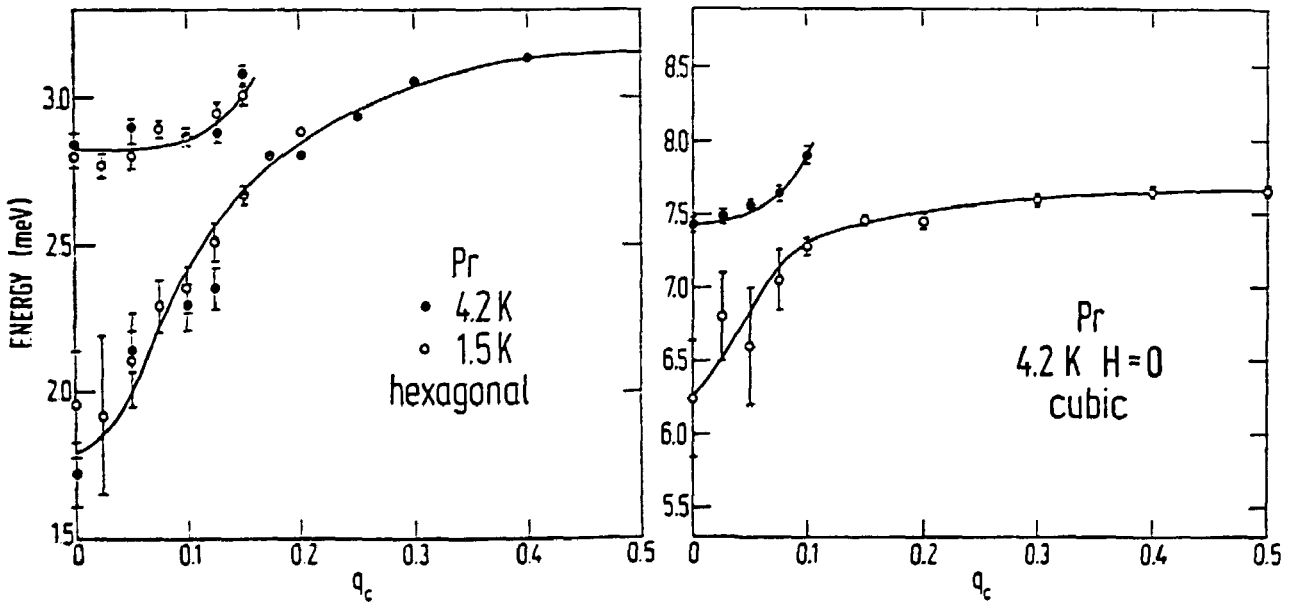

Fig. 1. The dispersion of the magnetic excitations propagating in the *c*-direction on the hexagonal and cubic sites in Pr in zero field. The full lines are guides to the eye.

[1] J. Jensen and A.R. Mackintosh, Rare Earth Magnetism; Structure and Excitations (Oxford University Press, Oxford, 1991).

1.19 Collapsed Cycloidal structures in Erbium

D.A. Jehan, D.F. McMorrow, R.A. Cowley, P.P. Swaddling, *Clarendon Laboratory, University of Oxford, UK*, and K.N. Clausen, *Department of Solid State Physics, Risø National Laboratory, Denmark*

The application of a magnetic field to the heavy rare-earth metals gives rise to a range of interesting phenomena, such as the devil's Staircase[1] and helifans[2] structures seen in Ho. We have performed an investigation of Er in an basal-plane (a-axis) magnetic field, with particular emphasis on the structure of the long-period cycloidal phases.

Two studies were made using TAS1. From the first, we were able to map out the phase diagram, shown in Fig. 1. At low temperatures, there is a first-order transition from a cone structure to a q =1/4c* fan structure. At higher temperatures, there is enhanced stability of commensurate phases that have a net c-axis moment, with the q=2/7c* cycloidal structure being particularly stable.

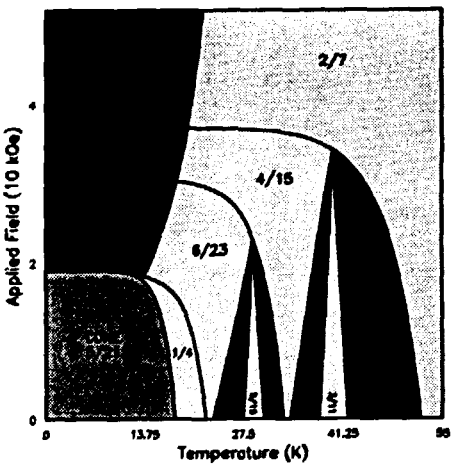

Fig. 1. Phase diagram of Er in an a-axis magnetic field. The wavevectors are in units of c* and have been determined from the position of the first magnetic satellite. The dark regions between the commensurate cycloidal phases have an incommensurate wavevector.

In the second study, the q=2/7c* phase was investigated in detail. From a combination of the neutron scattering results and mean-field calculations, we have determined how the zero-field cycloidal structure distorts in an applied field. At $\approx$ 1 T the plane of the cycloid rotates out of the $a-c$ plane to become normal to the field. At higher fields, the structure may be thought of as a highly irregular cone with the cone axis along a and different components of the moment along the b and c directions. On further increasing the field, the moments along the b direction become very small and the structure is almost a fan in the a-c plane. There is some evidence in the neutron scattering results at high temperatures and fields for the formation of a long-period structure, analogous to the helifans seen in Ho. Further investigations are planned to study this phase.

[1] R.A. Cowley, D.A. Jehan, D.F. McMorrow, and G.J. McIntyre, (1991). Phys. Rev. Lett. **11**, 1521.
[2] J. Jensen and A.R. Mackintosh, (1990). Phys. Rev. Lett. **64**, 22.

1.20 Competing Anisotropies in Ho/Er Superlattices

J.A. Simpson, D.F. McMorrow, R.A. Cowley, D.A. Jehan, R.C.C. Ward, M.R. Wells, *Clarendon Laboratory, University of Oxford, UK*, and K.N. Clausen, *Department of Solid State Physics, Risø National Laboratory, Denmark*

Most work on rare-earth superlattices has focussed on systems with magnetic materials separated by a non-magnetic spacer, and the magnetic structures have been strongly modified by the epitaxial strain[1,2]. We have studied the magnetic structure of three Ho/Er superlattices in order to investigate another effect, that of competing anisotropy.

Scans were performed with the wavevector transfer along $[00\ell]$ and $[10\ell]$ using TAS6 at a series of temperatures between 100 K and 8 K. Above the Er ordering temperature, the magnetic structure is similar to that of Ho/Y [2]: the Ho moments form a basal-plane spiral, which is coherent across approximately four bilayers (500 Å), with a "phantom" turn angle of 51° per plane in the Er.

Below the Er ordering temperature, Ho moments in successive blocks still form a coherent basal-plane spiral, with a turn angle that reduces with temperature. The Er moments form a cycloidal structure with its major axis in the *c* direction. Although the cycloid is coherent in the basal plane, there is no long range order of the *c*-axis components. This manifests in the $[10\ell]$ data by the presence of a broad peak with a coherence length of one Er block length, as shown in Fig. 1. Interestingly, the coherence length of the basal plane component decreases with temperature, by up to a factor of two. This may be linked to commensurate lock-ins and work is in progress to investigate this.

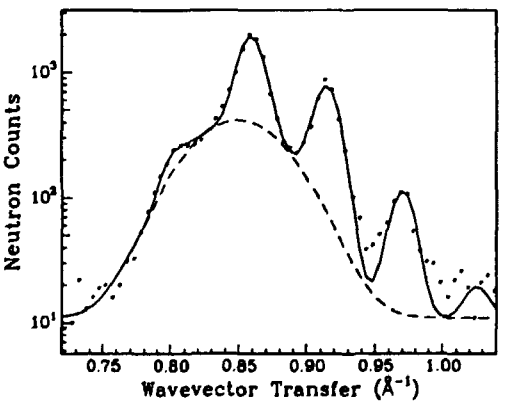

Fig. 1. $[10\ell]$ scattering from the Ho_{20}/Er_{20} sample at 8 K. The dashed line shows scattering from the Er *c*-axis moments. The solid line is a fit including the coherent basal-plane order of the Ho and Er.

[1]C.F. Majkrzak, J. Kwo, M. Hong, Y. Yafet, Doon Gibbs, C.L. Chien, and J. Bohr, (1991) Advances in Physics **40**, 99.
[2]D.A. Jehan, D.. McMorrow, R.A. Cowley, R. Ward, M.R. Wells, N. Hagmann, and K.N. Clausen, (1993) Phys. Rev. B **48**, 5594.

1.21 Metallic Superlattices - X-ray and Neutron Scattering Investigations

M. Christensen, R. Feidenhans'l, K. N. Clausen, and M. Nielsen, *Department of Solid State Physics, Risø National Laboratory, Denmark*

Metallic superlattices and multilayers have applications as polarising devices for neutrons, as X-ray optics, and as magnetic storage devices and sensors. With Molecular Beam Epitaxy (MBE), we have produced metallic superlattices consisting of Ag/Au, Fe/Au, and Fe/V. These superlattices have been investigated by means of X-ray diffraction.

Special attention has been paid to Fe/V superlattices, where X-ray measurements have revealed a tilt of the Fe/V-superlattice with respect to the substrate of up to 1.55°. Superlattices grown at different temperatures have been compared, and we are close to determining the optimal growth temperature. The Fe/V system has also been examined for magnetic ordering with neutron diffraction.

Figure 1 shows X-ray and neutron data for 200 Å $V[Fe_{20}V_{30}]_{20}$. The short notation means that there is a buffer layer of 200 Å V then a superlattice with 20 bi-layers, each consisting of 20 Å Fe and 30 Å V. The neutron data is from the low$-q$ range. The X-ray data is a rod scan at higher q values, where we measure in-plane as well as perpendicular components. Both scans show a periodicity of 0.12 $Å^{-1}$ corresponding to a 52 Å bi-layer in good agreement with the desired 50 Å. The neutron data also shows that the iron orders ferromagnetically in the superlattice.

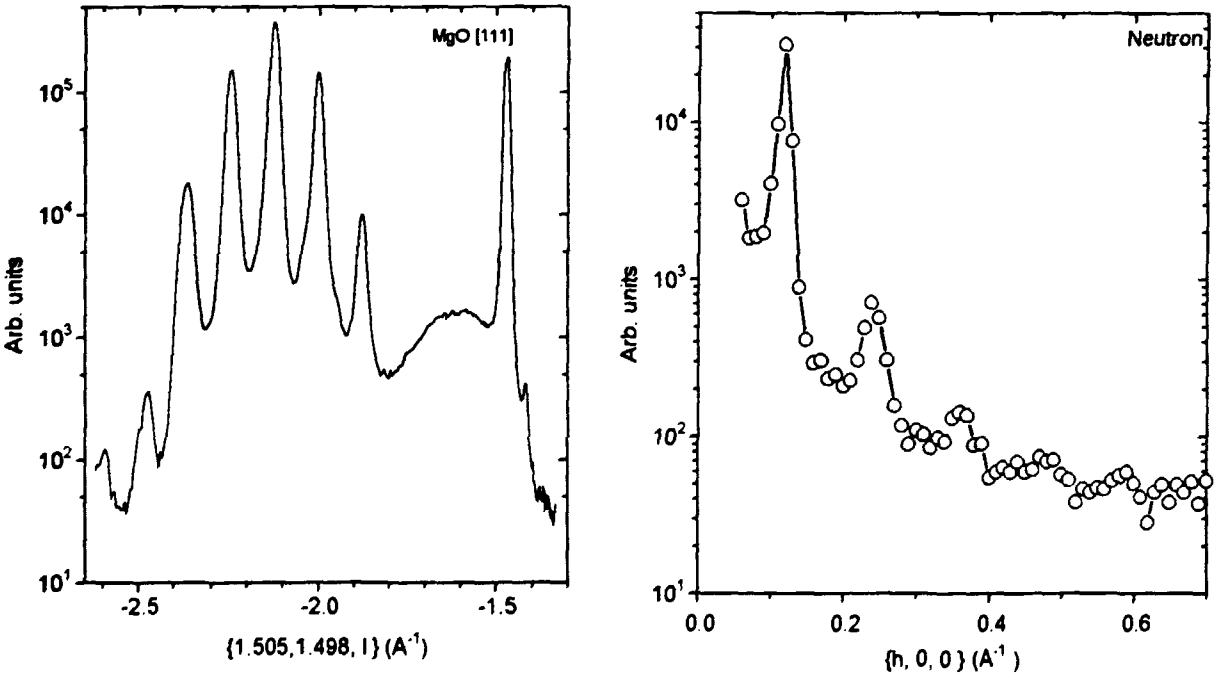

Fig. 1. Left: X-ray data from HASYLAB. The figure shows a scan along the $[1.5\ 1.5\ l]_{MgO}$ direction. It shows that the $[110]_{MgO}$ is parallel to the [100] direction of the superlattice. Right: Neutron diffraction from TAS1 at Risø. The scan is along $[100]_{MgO}$.

1.22 The Magnetism of an Epitaxially Grown Fe Layer

M.C. Gerstenberg, M.J. Christensen, and K.N. Clausen *Department of Solid State Physics, Risø National Laboratory, Denmark*

To test the polarized reflectometer, a sample consisting of 202 Å MgO/402 Å Fe/(100) on a MgO substrate, was grown by Molecular Beam Epitaxy (MBE).

In a ferromagnetic material the critical momentum transfer, Q_c, is dependent on the initial neutron spin direction in the following way:

$$Q_c = 4\sqrt{\pi N(b \pm p)}, \tag{3}$$

where N is the density of scatterers, b and p the nuclear and magnetic scattering length, respectively. The sign of p correspond to parallel and anti-parallel orientation of the field with respect to the incident neutron spin. From a determination of p, the component of the effective magnetic moment perpendicular to the scattering vector can be determined.

The polarization of the incident beam was determined by a Heusler alloy placed at the sample table. The flipping ratio, which is the ratio of the intensity of the two spin states measured with the Heusler alloy, was found to be 20±1. No analysis of the polarization of the scattered been was performed. In the reflectivity measurements the sample was placed in a field of 7 Gauss, which should be sufficient to align the Fe magnetic dipole moments in the sample. The obtained results are shown in Fig. 1, where the data has been corrected for geometrical effects and the finite polarization of the incident beam. The two different momentum transfers (1) and (2) for the different spin directions are clearly visible.

To reach a consistent result of the effective moment of the Fe-layer the two curves have to fitted simultaneously. A consistent physical model has not yet been found. Future X-ray studies will reveal more structural information, which in effect will reduce the number of parameters in the problem.

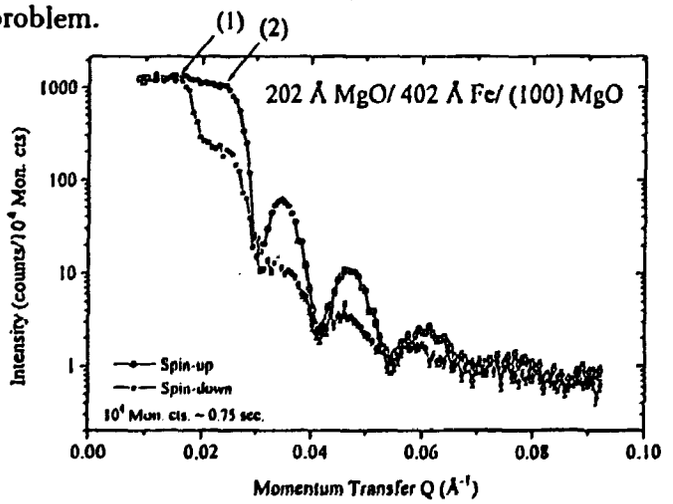

Fig. 1. The corrected scans for the "spin-up" and "spin-down" of a 202 Å MgO/402 Å Fe/(100)Mg epitaxially grown film. (1) and (2) are the two different critical momentum transfers of the different neutron spin states.

1.23 The Spin Structure of Na_6CoS_4

W. Bronger, W. Koelman, P. Müller, *Institut für Anorganische Chemie der RWTH, Aachen, Germany*, and Kurt N. Clausen, *Department of Solid State Physics, Risø National Laboratory, Denmark*

The hitherto known ternary alkali-metal-cobalt-chalcogenides are characterized by edge-linked chalcogen tetrahedra, centered by cobalt ions. We succeeded in preparing Na_6CoS_4, the first compound with isolated cobalt-chalcogen tetrahedra[1]. The atomic arrangement is show below. Measurements of the magnetic susceptibilities revealed Curie-Weiss-paramagnetism down to 6.1 K, where a maximum in the susceptibility is observed. This points to antiferromagnetic interactions of the cobalt ions, which are separated by 6.18 Å. To determine the spin structure and the magnetic moment of the cobalt ion, neutron diffraction experiments were performed at TAS1 at room temperature and at 1.9 K. The additional Bragg reflections at low temperature could be indexed by assuming a fourfold orthorhombic unit cell.

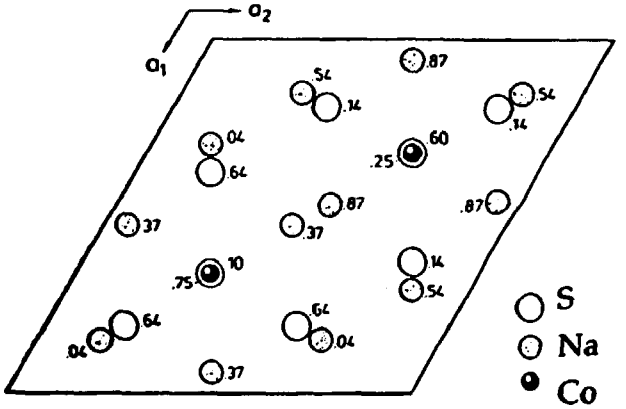

Fig. 1. Na_6CoS_4, projection of the atomic arrangement along [001].

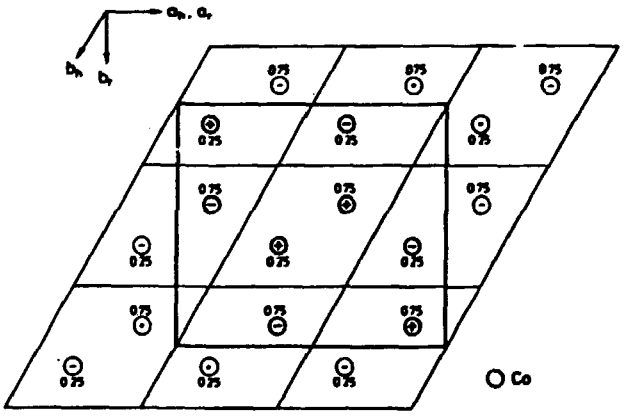

Fig. 2. Na_6CoS_4, projection of the crystallographic and magnetic cell along [001].

The profile analysis with Rietveld's program led to the values given in the following table.

Temperature	298 K	1.9 K	
Space group	$P6_3mc$	$P_{2a}bc2_1$	
Lattice constants	$a = 8.918(3)$ Å	$a = 17.705(11)$ Å	$b = 15.374(10)$ Å
	$c = 6.895(3)$ Å	$c = 6.850(2)$ Å	
Magnetic moment		$\mu = 3.04(6)\mu_B$	
$R_{nuc.}(R_{mag.})$	0.064	0.06	(0.14)

The refinement revealed that the magnetic moments are directed along the *c*-axis. the magnetic moment is in accordance with three unpaired electrons[2].

[1] K. Klepp and W. Bronger, (1983). Z. Naturforsch. **38b**, 12
[2] W. Koelman, (1994). Part of the thesis, RWTH Aachen, Germany.

1.24 Nuclear Magnetism of a ^{13}C diamond

B. Buras, K. Lefmann, M. Vigild, *Department of Solid State Physics, Risø National Laboratory, Denmark*, F.B. Rasmussen, *Ørsted Laboratory, Niels Bohr Institute, University of Copenhagen, Denmark*, E.J. Pedersen, P.A. Thorsen, *Institute of Chemistry, University of Copenhagen Denmark*, and J.P.F. Sellschop, *University of the Witwatersrand, Johannesburg, South Africa*

Recently produced artificial diamonds of ^{13}C enable studies of nuclear magnetism in a diamond lattice insulator with pure dipole-dipole interactions for spins $I = 1/2$. Our aim is to study the ordering of the magnetic moments at extremely low nuclear temperatures. Our six samples of roughly 30 mg each have been produced from very pure (more than 99 %) ^{13}C[1]. They all show well developed (001) and (111) faces. Optical microscopy has revealed the presence of metallic inclusions. All crystals are greenish transparent, indicating N impurities as colour centers. The crystals were tested by means of X-rays, and no irregularities has been revealed. A series of NMR measurements has been made at room temperature varying the orientation of the crystal axes with respect to the magnetic field. The spectral line shape has a strong dependence on the crystal orientation, displaying a line splitting of 8.4 kHz at the [111] direction. This behaviour may be understood from dipolar broadening combined with the Pake's doublet mechanism[2] along the [111] direction. However, both broadening and line splitting are 25 % larger than expected from pure dipolar interaction, suggesting that some indirect interaction between the ^{13}C nuclei is present. The spin-lattice relaxation does not show a simple exponential behaviour, suggesting that relaxation is due to paramagnetic impurities in connection with spin diffusion. The average value of the relaxation time T_1 was found to be 15 s at room temperature, and it shows a T^{-3} dependence, extrapolating T_1 to around 100 days at 4 K, effectively preventing 'brute force' nuclear cooling. The only way to achieve nuclear ordering seems to be dynamic nuclear polarization followed by adiabatic demagnetization in the rotating frame[3].

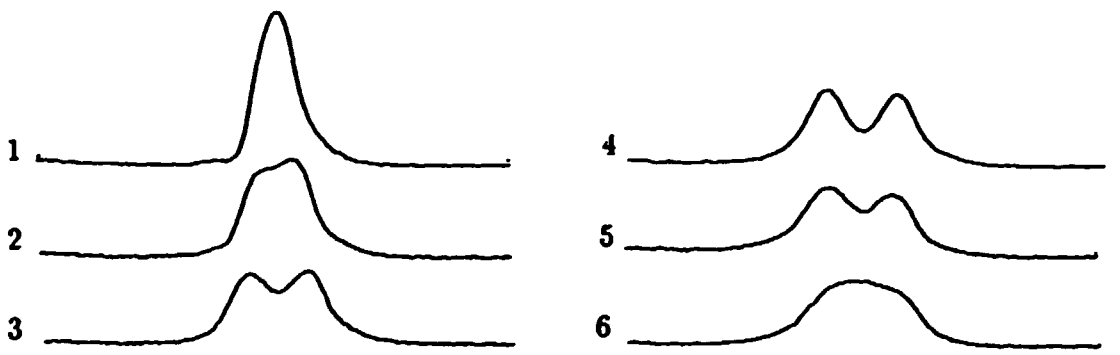

Fig. 1. NMR spectra of a ^{13}C diamond for various orientations of the crystal in the magnetic field. In (1) the [001] direction is along the field, then the crystal is turned gradually so that in (4) the [111] axis is along the field and in (6) the [110] direction.

[1] H. Kanda, *private communication.*
[2] G.E. Pake, (1948). J. Chem. Phys. **16**, 327.
[3] A. Abragam and M. Goldman, (1982). Nuclear Magnetism: Order and Disorder (Oxford Univ. Press), ch. 8.

1.25 Spin Wave Collapse, Magnetic Divergence, and Incommensurate Fluctuations in URu_2Si_2

T. Petersen, T. Mason, *Department of Solid State Physics, Risø National Laboratory, Denmark, and Department of Physics, University of Toronto, Canada*, W.J.L. Buyers, *AECL Research, Chalk River, Canada*, and A.A. Menovsky, *University of Amsterdam, Netherlands*

The phase transition at T_N = 17.5 K in the heavy fermion superconductor URu_2Si_2 has generally been believed to be antiferromagnetic, but the smallness of the apparently magnetic staggered moments $M = 0.04\ \mu_B$ has led to doubts about the nature of the ordering. To settle this issue we performed a high resolution neutron scattering study of the magnetic excitations near the ordering wave vector $q = (100)$ at the new beam-guide at TAS7 with a scattered energy of 5 meV.

By convoluting the spectrometer resolution with a model of coupled damped harmonic oscillators and fitting to constant q scans taken at the ordering wave vector we extracted the energy gap, damping and susceptibility as function of temperature shown in Fig. 1. A softening of the magnetic mode is seen as $T \rightarrow T_N$ from below while the damping grows rapidly and there is a sharp peak in the susceptibility. All of these features are consistent with a magnetic singlet-singlet transition and are not readily explainable in non-magnetic scenarios. At temperatures above T_N we find that the susceptibility of the inelastic response is weakened and transferred to a central peak[1]. Surprisingly this peak coexists with the ring of incommensurate fluctuations reported in[1]. Figure 2 shows the temperature dependence of scattering at a constant energy transfer $\hbar\omega = 0.3$ meV at $q = (1, \eta, 0)$ where the scattering of the ring is visible at $q = (1, 0.4, 0)$. At temperatures above 20 K the incommensurate scattering even dominates, hinting that the explanation for the small ordered moment may be found in the competing fluctuations.

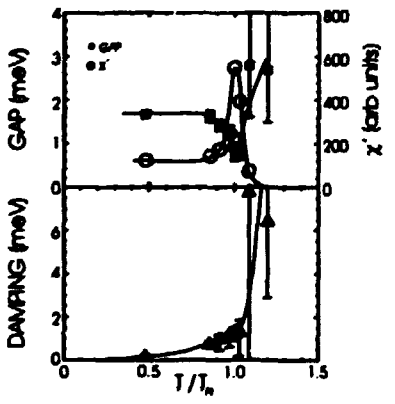

Fig. 1. For $q = (100)$ the spin gap (squares), the susceptibility, and the damping (triangles).

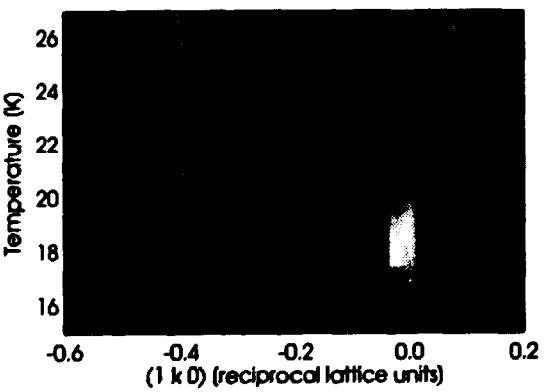

Fig. 2. Contours of intensity at 0.3 meV in the temperature (vertical axis) – wavevector (horizontal axis) plane.

[1] C. Broholm, H. Lin, P.T. Matthews, T.E. Mason, W.J.L. Buyers, M.F. Collins, A.A. Menovsky, J.A. Mydosh, and J.K. Kjems, (1991). Phys. Rev. B 43, 12809.

1.26 Magnetic Response of the fcc Heavy Fermion System YbBiPt

C. Broholm, *Department of Physics and Astronomy, The Johns Hopkins University, USA*, G. Aeppli, D.J. Bishop, *AT&T Bell Laboratories, Murray Hill, New Jersey, USA*, T.E. Mason, *Department of Physics, University of Toronto, Canada*, P.C. Canfield, *Ames Laboratory, USA*, and Z. Fisk, *Los Alamos National Laboratory, USA.*

The cubic heavy fermion compound YbBiPt has one of the largest linear specific heat coefficients observed to date, 8 J $mol^{-1}K^{-2}$ [1]. An anomaly in the susceptibility at 0.4 K has been attributed to antiferromagnetic ordering however neutron powder diffraction measurements have failed to reveal any magnetic Bragg peaks. Because the fcc structure of this material is three dimensionally frustrated for nearest-neighbour antiferromagnetic interactions there is the possibility that YbBiPt is exhibiting a novel frustrated heavy fermion ground state.

Measurements of the inelastic magnetic response of YbBiPt, along with a search for antiferromagnetic order at low temperatures, have been carried out on the TAS7 cold neutron spectrometer using the AT&T dilution refrigerator. The sample consisted of three aligned single crystals of YbBiPt mounted in the (*hhl*) zone. These preliminary measurements revealed several new features. In particular, the crystal field excitation at 5 meV , previously seen in powder measurements[2] has an asymmetric lineshape that cannot be accounted for by a conventional relaxation response function. The apparent transition at 0.4 K is preceded by a marked increase in the low frequency response near (001) followed by a suppression below 0.5 K. No Bragg peaks are observed near (001) however. Clearly additional measurements in the (*h0l*) zone are needed to fully characterize this novel system.

[1] P.C. Canfield, J. Thompson, W.P. Beyerman, A. Lacerda, M.F. Hundley, E. Peterson, Z. Fisk, and H.R. Ott, (1991). J. Appl. Phys. **70**, 5800.
[2] R.A. Robinson, M. Kohgi, T. Osakabe, P.C. Canfield, T. Kamiyama, T. Nakane, Z. Fisk, and J.D. Thompson, (1993). Physica B, *in press.*

1.27 Spin Dynamics of the Kondo Insulator CeNiSn

T.E. Mason, *Risø National Laboratory, Denmark*, G. Aeppli, and E. Bucher, *AT&T Bell Laboratories, Murray Hill, New Jersey, USA*

Measurements of the spin dynamics of the Kondo insulator, CeNiSn, have shown that the crossover to a semiconducting state below 10 K is accompanied by the development of a gap in the spin excitations[1]. The lineshape of the response above the spin gap is qualitatively similar to that expected for excitations across a band gap and has the peculiar property that the real part of the susceptiblity (computed from the Kramers-Kronig transform of the neutron data) has no **Q**-dependence at zero frequency in the $(h0l)$ plane; despite a strong variation of χ'' at finite frequency.

We have extended these measurements to the $(hk0)$ plane on the TAS7 cold neutron spectrometer where the additional intensity available with the new guide has permitted a comprehensive mapping of the **Q** and T dependence of the inelastic scattering. The resonance observed at 2 meV in the $(h0l)$ plane shifts to 4 meV at $(1k\ 0)$, increasing in intensity as the frequency increases (see Fig. 1). The lineshape preserves the characteristically sharp onset and also appears to have the same absence of **Q** dependence of the correlations in the zero frequency limit (at least to the extent this can be determined with the range of energies accessed). The fact that this 4 meV transition is destroyed by warming to 15 K is an indication of the strong interactions responsible for its formation.

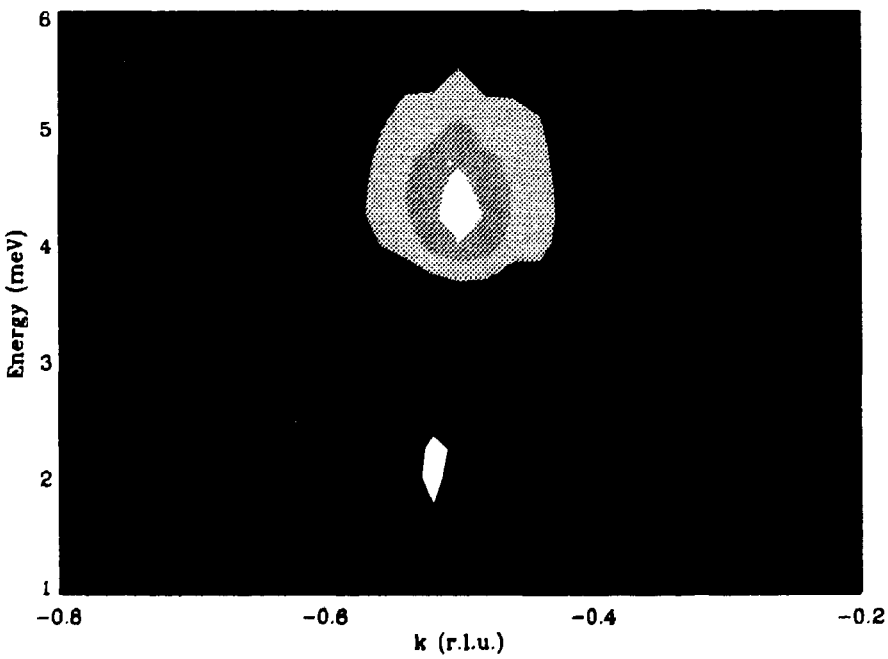

original contains color illustrations

Fig. 1. The energy dependence of the inelastic magnetic scattering from CeNiSn at $T = 4.2$ K along the $(1k0)$ direction.

[1] T.E. Mason, G. Aeppli, A.P. Ramirez, K.N. Clausen, C. Broholm, N. Stücheli, E. Bucher, and T.T.M. Palstra, (1992). Phys. Rev. Lett. **69**, 490.

1.28 Magnetic Structures in $PrBa_2Cu_3O_{6+x}$

M.P. Nutley, *Institut Laue-Langevin, Grenoble, France*, A.T. Boothroyd, A. Longmore, *Oxford University, UK*, N.H. Andersen, H. Casalta, and P. Schleger, *Department of Solid State Physics, Risø National Laboratory, Denmark*

$PrBa_2Cu_3O_{6+x}$ is an interesting member of the iso-structural family $LnBa_2Cu_3O_{6+x}$ (Ln = lanthanide ion) because it is the only one that is not a high-temperature superconductor. As the magnetism in the cuprate superconductors appears to be competing with superconductivity the knowledge of the changes in the magnetic properties related to the Pr ions may provide important information on the superconducting state itself. From single crystal neutron diffraction studies carried out on samples prepared under different oxidation conditions a rather complicated behaviour has emerged. It involves both the Cu and Pr ions, and it depends on the oxygen stoichiometry and temperature. Magnetic Bragg reflections were observed with indices of the types $(\frac{h}{2}, \frac{h}{2}, l)$ and $(\frac{h}{2}, \frac{h}{2}, \frac{l}{2})$, h and l being integers. The former type of reflection (except $l = 0$) were present at all temperatures measured (2 K to 300 K), and arise from an antiferromagtic arrangement of the Cu spins in the CuO_2 planes, with the spins in the basal CuO_x planes of the structure disordered. This magnetic structure also occurs in $YBa_2Cu_3O_{6+x}$ when x is less than 0.5, and is referred to as the AM1 phase. The $(\frac{h}{2}, \frac{h}{2}, \frac{l}{2})$ reflections appear at a temperature well below 300 K (depending on the level of oxygenation) and correspond to the formation of a new antiferromagnetic structure, the AM2 phase, in which the Cu spins in the basal CuO_x planes begin to order weakly while the Cu spins in adjacent CuO_2 planes rotate in unison such that they are set at an angle relative to one another. Figure 1 shows the temperature variation of the intensities of the $(\frac{1}{2}, \frac{1}{2}, 2)$, $(\frac{1}{2}, \frac{1}{2}, \frac{3}{2})$, and $(\frac{1}{2}, \frac{1}{2}, 0)$ reflections measured from a crystal with highest oxygen content. The transition from the AM1 to the AM2 phase is seen to occur at about 10 K. According to the Cu ordering models described above the $(\frac{1}{2}, \frac{1}{2}, 0)$ reflection is predicted to be zero in both phases. This peak is interpreted to result from the Pr ordering. It is highly extended along the z direction indicating that the Pr ordering is relatively two-dimensional with a correlation length along the z axis of 50 Å (see Fig. 2). The magnetic ordering temperature of Pr is unusually high, which indicates that the $4f$-electrons of Pr hybridize with the charge carriers in the CuO_2 planes.

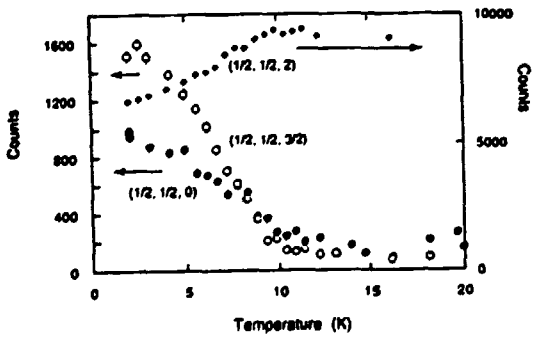

Fig. 1. The temperature variation of the $(\frac{1}{2}, \frac{1}{2}, 2)$, $(\frac{1}{2}, \frac{1}{2}, \frac{3}{2})$ and $(\frac{1}{2}, \frac{1}{2}, 0)$ magnetic reflections measured by neutron diffraction from a single crystal of $PrBa_2Cu_3O_{6+x}$.

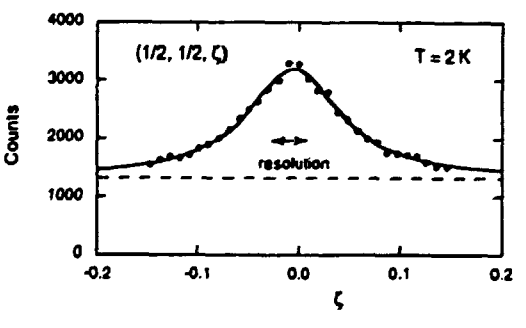

Fig. 2. Scan in the z direction through the $(\frac{1}{2}, \frac{1}{2}, 0)$ magnetic reflection indicating two-dimensional Pr ordering. The line is a fit to a Lorentzian function.

1.29 Magnetic Fluctuations in the Normal State of $La_{1.86}Sr_{0.14}CuO_4$

T.E. Mason, *Risø National Laboratory, Denmark, and Department of Physics, University of Toronto, Canada*, G. Aeppli, *AT&T Bell Laboratories, USA*, S.M. Hayden, *H.H. Wills Physics Laboratory, Bristol University, UK*, and H.A. Mook, *Oak Ridge National Laboratory, USA*

The performance of TAS6 for measurements of low energy magnetic excitations in high temperature superconductors has been improved substantially during the course of measurements of the momentum dependence of the superconducting gap[1]. The increased sensitivity to small cross-sections has been used to study, in greater detail than previously possible, the temperature dependence of the magnetic fluctuations that characterize the normal state of $La_{1.86}Sr_{0.14}CuO_4$. This incommensurate response is associated with the proximity of the two-dimensional Fermi surface to a nesting instability. Studies of its temperature dependence can therefore provide valuable information about how close the system is to a magnetic instability and may shed light on the anomalous normal state transport properties.

Figure 1 shows a constant energy scan at 9 meV energy transfer through the incommensurate positions for $T = 295$ K. The sharp peaks present at lower temperatures[1] are no longer well defined although the overall square symmetry near (π, π) is preserved.

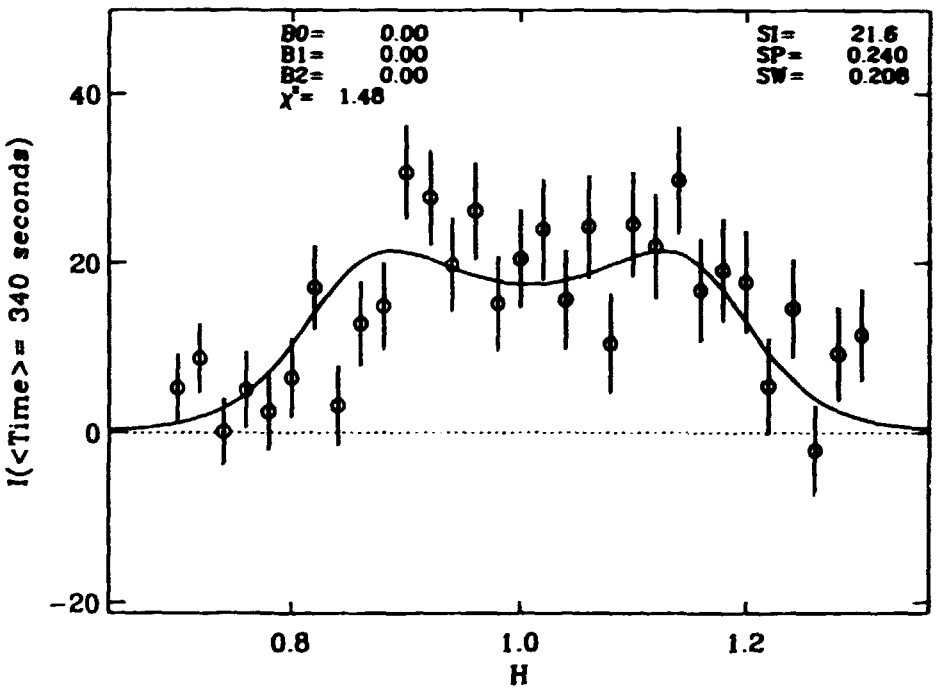

Fig. 1. A constant energy scan for $\hbar\omega = 9$ meV along (H,K,0.12) at $T = 295$ K.

[1] T.E. Mason, G. Aeppli, S.M. Hayden, A.P. Ramirez, and H.A. Mook, (1993). Phys. Rev. Lett. 71, 919.

1.30 Magnetic Flux Lattice Melting in High Temperature Superconductor $Bi_{2.15}Sr_{1.95}CaCu_2O_{8+x}$

E.M. Forgan, R. Cubitt, G. Yang, S.L. Lee, *University of Birmingham, UK*, D. McK Paul *University of Warwick, UK*, H.A. Mook, M. Yethiraj *Oak Ridge National Laboratory, Tennessee, USA*, P.H. Kes, T.W. Li, *Leiden University, The Netherlands*, Z. Tarnawski *University of Amsterdam, The Netherlands*, and K. Mortensen, *Department of Solid State Physics, Risø National Laboratory, Denmark*

The properties of the high-temperature superconductors in various ceramics containing CuO_2 planes are in several aspects different from conventional superconductors. The high transition temperature means that thermal fluctuations are far more important than in conventional low T_c superconductors. Magnetization and a.c. electric response measurements have shown an 'irreversibility' line in the $B-T$ plane. Above this line, the magnetic flux lines move in response to external forces, giving reversible magnetization curves and a finite electrical resistivity, even though the temperature may be well below T_c. It has been speculated that this irreversibility line dividing pinned from unpinned flux lines, is associated with melting of the vortex lattice[1]. Using small-angle neutron diffraction measurements on a single crystal of BSCCO, $Bi_{2.15}Sr_{1.95}CaCu_2O_{8+x}$, we have directly probed the bulk properties of the magnetic flux line lattice[2]. The intensity diffracted from the vortex lattice goes rapidly to zero at a magnetic-field-dependent flux lattice melting temperature, which coincides with the appearance of the finite resistance within the superconducting state, thus giving good evidence of a vortex liquid. The flux lattice signal can also be made to disappear at low temperatures, by applying a sufficiently high field, probably because of the decomposition into two dimensional pancake vortices. In Fig. 1 is shown the experimentally obtained $B-T$ plane. Figure 2 shows an example of a flux line scattering pattern, as observed on the vortex solid.

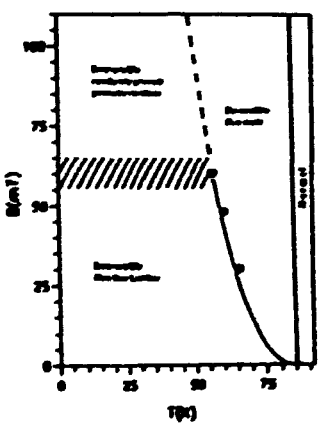

Fig. 1. $B-T$ phase diagram showing the vortex melting line.

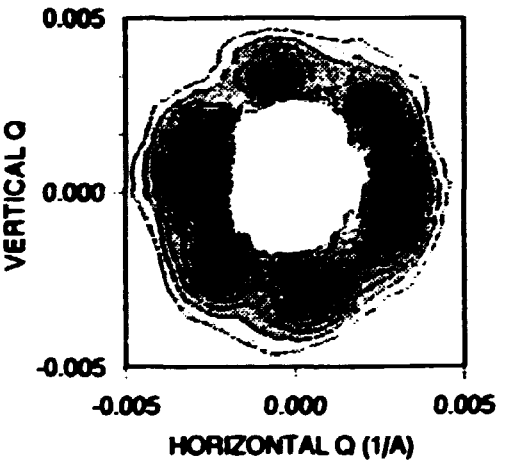

Fig. 2. Diffraction pattern from the flux lattice in BSCCO at obtained at T = 1.5 K and B = 50 mT.

[1] P.L. Gammel, et al. L.F. Schneemeyer, J.V. Warszczak, and D.J. Bishop, (1988) Phys. Rev. Lett. 61, 1666.
[2] R. Cubitt, E.M. Forgan, G. Yang, S.L. Lee, D. McK Paul, H.A. Mook, M. Yethiraj, P.H. Kes, T.W. Li, Z. Tarnawski, and K. Mortensen, (1993). Nature 365, 407.

1.31 Magnetic Flux Lattice in Single Crystal 2H-$NbSe_2$

P.L. Gammel, D.A. Huse, R.N. Kleiman, B. Batloff, C.S. Oglesby, E. Bucher, D.J. Bishop, *AT&T Bell Laboratories, Murray Hill, New Jersey, USA*, K. Mortensen, and T.E. Mason, *Department of Solid State Physics, Risø National Laboratory, Denmark*

The flux-line lattice in anisotropic superconductors has been reported to possess remarkable properties, which disagree with the predictions of either uniaxial London or Ginzburg-Landau theories which was expected to be applicable. This concerns in particular the lattice response to the magnetic field turned away from the principal crystal directions, when measured by Bitter decoration and STM. Using small-angle neutron scattering we have measured[1] the bulk flux line lattice on a large, high quality single crystal of 2H-$NbSe_2$ with dimensions 4×8×1 mm^3. The scattering function was measured with λ=10 Å neutrons and neutron bandwidth $\Delta\lambda/\lambda$=0.18. The sample to detector distance was 6 meter. The magnetic field was applied along the beam direction, and the sample was mounted on a special rotation stage allowing us to rotate the sample with respect to applied magnetic field *in situ*.

With the magnetic field parallel to the c axis, the diffraction pattern shows six peaks, with an intensity which follows the Ginzburg-Landau mean field theory $I \propto (T - T_c(H))^2$. For magnetic fields applied in an angle, θ, to the c axis, the lattice distorts, but remains pinned to to the underlying crystalline a axis, in contrast to both London theory and Ginzburg-Landau theory estimates of minimum free energy. The intensity of the flux lattice Bragg peaks, on the other hand, are in good agreement with theory. In general, the flux lattice Bragg peaks lie on an ellipse. Defining the distortion, Δ, as the ratio between the major and the minor axis of this ellipse, the London theory predicts a relationship $\Delta^2 = (1 - 1/\Gamma)\cos^2\theta + 1/\Gamma$, where Γ is the mass anisotropy. In Fig. 1 is shown the experimental data, which shows that the bulk of the flux lattice follows the London theory very well.

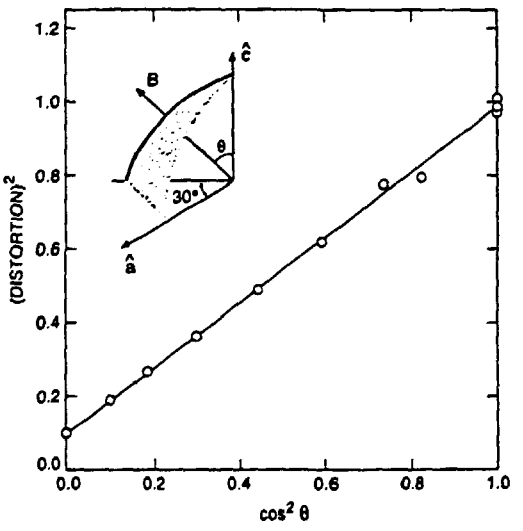

Fig. 1. Distortion of the hexagonal flux lattice as the magnetic field is turned from the crystalline c axis. The solid line is the London prediction, with m_c/m_a=10.1.

[1] P.L. Gammel, D.A. Huse, R.N. Kleiman, B. Batloff, C.S. Oglesby, E. Bucher, D.J. Bishop, T.E. Mason, and K. Mortensen, (1993). Phys. Rev. Lett., *in press.*

1.32 Interstitial Oxygen Defects in Room Temperature Oxidized $La_{2-x}Sr_xCuO_{4+y}$ $(0 < x < 0.15)$

C. Rial, U. Amador, E. Morán and M.A. Alario-Franco, *Departamento de Química Inorganica, Facultad Ciencias Quimicas, Universidad Complutense, Madrid, Spain*, and N.H. Andersen, *Department of Solid State Physics, Risø National Laboratory, Denmark*

Oxygen non-stoichiometry influences the superconducting properties of $La_2CuO_{4\pm y}$ and the related Sr-doped $La_{2-x}Sr_xCuO_{4+y}$. Oxygen deficiencies reduce the hole density and induce some disorder in the CuO_2 planes which destroy superconductivity. Excess oxygen seems to increase the positive charge carrier density and improves the superconducting properties. However, above a certain limit of hole doping, referred to as over-doping, superconductivity is deteriorated or even suppressed. In superconducting $La_{2-x}Sr_xCuO_4$, T_c increases with Sr content until $x = 0.15$, where the maximum value (35 – 40 K) is reached, and then decreases with x. This behaviour of T_c could be related to the mechanism of over-doping. The existence of oxygen vacancies in the structure of these compounds have been widely discussed, and evidence for excess interstitial oxygen defects at the site $(1/4, z, 1/4; z \approx 1/4)$ has been reported in $LaCuO_{4+y}$, but, to our knowledge, not in $La_{2-x}Sr_xCuO_{4+y}$ [1,2]. We have studied the crystal structure, superconducting properties and oxygen stoichiometry of room temperature chemically oxidized $La_{2-x}Sr_xCuO_{4+y}$ by means of powder neutron diffraction, magnetic ac-susceptibility and thermogravimetric (TG) analysis. We expected that the superconducting properties of low Sr-doped $La_{2-x}Sr_xCuO_4$ $(x < 0.15)$ could be improved by insertion of oxygen into the structure until the limit of over-doping is reached. As shown in Table I the effect of chemically oxidation is in all cases an increase of T_c. The presence of interstitial oxygen defects located at the $(1/4, z, 1/4; z \approx 1/4)$ site, as in oxygen rich La_2CuO_{4+y}, is proposed from the neutron diffraction data, and supported by the excess weight loss detected by TG for the oxidized material relative to the starting ones. The lattice parameters and the amount of excess interstitial oxygen (O_{int}) determined from refinement of the neutron diffraction data and from TG are also given in Table I.

x	a (A) starting	b (A) starting	c (A) starting	a (A) oxidized	b (A) oxidized	c (A) oxidized	Oint TGA	Oint neutron	Tcs (K)	Tcox (K)
0.05*	5.3522(2)	13.175(1)	5.3824(2)	5.3445(4)	13.232(1)	5.3856(5)		0.13(2)	n.s.	39
0.09*	5.3497(8)	13.206(2)	5.3695(5)	5.3468(5)	13.238(1)	5.3663(5)	0.11	0.12(2)	31.5	39.5
0.12•	5.3486(5)	5.3486(5)	13.217(2)	5.3495(3)	5.3495(3)	13.237(1)	0.10	0.11(2)	34.5	39.5
0.125•	5.3484(1)	5.3484(1)	13.223(1)	5.3497(3)	5.3497(3)	13.239(1)	0.08	0.12(2)	32	39.5
0.13•	5.3469(5)	5.3469(5)	13.219(2)	5.3486(3)	5.3486(3)	13.236(1)	0.08	0.12(2)	35	39

Table I. Structural and physical features of starting and oxidized $La_{2-x}Sr_xCuO_{4+y}$ $(0 < x < 0.15)$
* Cmca • F4/mmm

[1] T. Kamayama, F. Izumi, H. Asano, H. Takagi, S. Uchida, Y. Tokura, E. Takayama-Muromachi, M. Matsuda, K. Yamada, Y. Endoh, and Y. Hikada, (1990). Physica C **172**, 120.
[2] Y. Ueda, Y. Fujiwara, A. Hayashi, K. Shibutani, and R. Ogawa, (1992). Physica C **198**, 237.

1.33 Determination of the Crystallographic Parameters in $YBa_2Cu_3O_{6+x}$ Single Crystals

H. Casalta, P. Harris, P. Schleger, B. Lebech, and N.H. Andersen, *Department of Solid State Physics, Risø National Laboratory, Denmark*

Recently, there has been an increased interest and demand for quantitative structural information on $YBa_2Cu_3O_{6+x}$. This demand is partly motivated by the desire to investigate the electron-lattice coupling, and to determine which ions in the structure might be moving in a double well potential, leading to an enhancement of the electron-phonon coupling strength λ [1]. Another motivation comes from studies of structural long range order like the Ortho-II phase which requires a good set of crystallographic parameters to be analysed properly. Until recently, many experimental investigations have relied on crystallographic parameters obtained from powder diffraction, most notably by Jorgensen *et al.*[2]. One of the problems encountered in determining these crystallographic parameters for orthorhombic $YBa_2Cu_3O_{6+x}$ is the twinning, which results in a mixing of the intensities I_{hkl} and I_{khl} (*cf.* Fig. 1). To obtain twin domain information and optimize the fit to the structure factors, we have combined experiments on both TAS1 and TAS2 (4-circle): TAS1 provides information about the relative weight of the two twin domains, $2(a-b)/(a+b)$, and the angle α (*cf* Figs. 1,2), and TAS2 provides data for a very large range of Q values, which allows an accurate determination of the Debye-Waller factors (DWF). Combining this information and accounting for the mixed peaks is crucial for the oxygen content determination, because the site occupancies are highly correlated with the DWF. Using this method, we have investigated samples with different oxygen contents, and found good agreement with recent publications[1]. Furthermore, any samples grown in alumina crucibles show major modifications of the DWF and the site occupancies in the vicinity of the Cu(1) site (contaminated by Al). This last point could easily explain many disparities in existing publications.

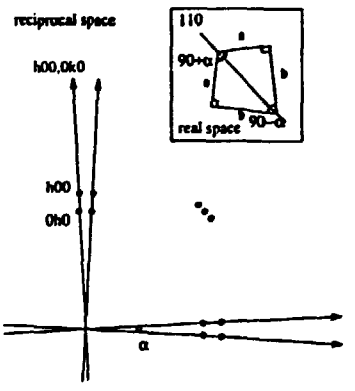

Fig. 1. Superposition and splitting of the peaks due to the twinning.

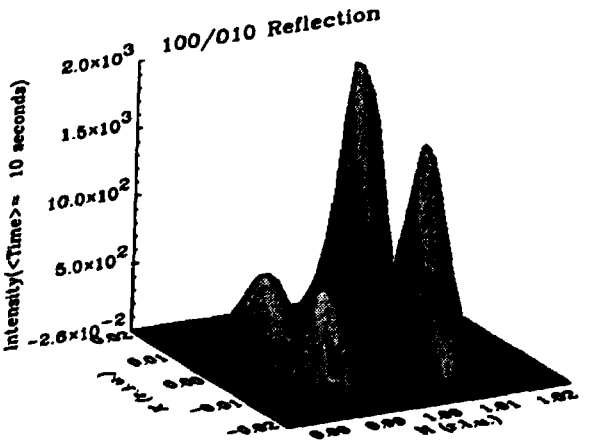

Fig. 2. Data obtained at TAS1 for the 100/010 reflection for a $YBa_2Cu_3O_{6.95}$ crystal.

[1] N. Pyka, W. Reichardt, L. Pintschovius, S.L. Chaplot, P. Schweiss, A. Erb, and G. Muller-Vogt, (1993). Phys. Rev. B **48**, 7746.

[2] J.D. Jorgensen, M.A. Beno, D.G. Hinks, L. Soderholm, K.J. Volin, R.L. Hitterman, J.D. Grace, Ivan K. Schuller, C.U. Segre, K. Zhang, and M.S. Kleefisch, (1987). Phys. Rev. B **36**, 3608.

1.34 The Lineshape of Ortho-II Superstructure Reflections in $YBa_2Cu_3O_{6.5}$

P. Schleger, R.A. Hadfield[1], N.H. Andersen, H. Casalta, *Department of Solid State Physics, Risø National Laboratory, Denmark*, H.F. Poulsen, M. von Zimmermann, J. Schneider, *HASYLAB, Hamburg, Germany*, and R. Liang, P. Dosanjh and W.N. Hardy, *Department of Physics, University of British Columbia, Vancouver, Canada*

For the first time, clear Lorentzian-type lineshapes for the Ortho-II superstructure reflections in $YBa_2Cu_3O_{6.5}$ have been observed by neutron diffraction. Existing neutron diffraction measurements have only seen either vague Gaussian peaks along h and k, or at best Lorentzians which are strongly overlapping along l[1]. Figure 1 shows our results for a scan along $(1.5, 0, \ell)$ measured on TAS6 and an insert showing the lineshape along l for the $(0.5, 0, \ell)$ reflection measured on TAS1. The HWHM of the fitted Lorentzians give Δh=0.0118 and Δl=0.0720, implying Ornstein-Zernicke type correlation lengths of ξ_h=52 Å, and ξ_l=26 Å (note: $\xi_h = a/(2\pi\Delta h)$).

Due to twinning of the orthorhombic structure, scans in the chain direction along k give rise to split peaks which cannot be fully resolved at TAS1 or TAS6. Thus, the crystal was also measured at HASYLAB, Hamburg on BW7, 101.3 keV X-rays. The left insert in Fig. 1 shows a scan along k for the (2.5,0,0). (The resolution along h and k is about ten times less than the size of the data points.) The split peaks are well resolved, with a HWHM of Δk=0.00487 (implying ξ_k = 127 Å). This high resolution scan also reveals that most likely, the line shapes are in fact Lorentzian-squared. Reminiscent of ordering kinetics of Cu_3Au[2], this suggests that perhaps the system is in a state of late-stage domain coarsening, with well defined, sharp domain walls. Alternatively, such lineshapes are seen in random-field Ising systems[3], where domain walls are pinned at defects. In $YBa_2Cu_3O_{6+x}$ the pinning might be due to twin-domain boundaries and/or defects.

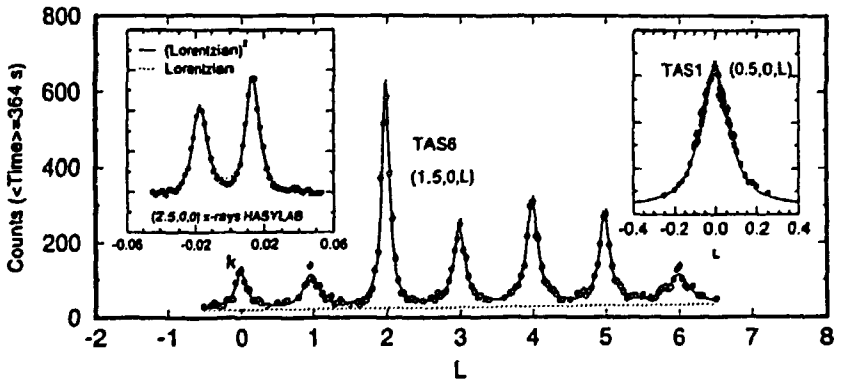

Fig. 1. Plot of Ortho-II superstructure reflections measured on TAS1, TAS6 and HASYLAB. All lines are Lorentzian or Lorentzian-squared fits.

[1] D. Hohlwein, in *Proc. Int. School of Crystallography*, Erice, May 1993, (Kluver Press).
[2] R.F. Shannon, Jr., S.E. Nagler, C.R. Harkless, and R.M. Nicklow, (1992). Phys. Rev. B **46**, 40.
[3] R.J. Birgeneau, H. Yoshizawa, R.A. Cowley, G. Shirane, and H. Ikeda, (1983). Phys. Rev. B **28**, 1438.

[1] On leave from: Clarendon Laboratory, Oxford, UK and AEA Technology, Harwell, UK

1.35 Crystal Structure of the Commensurately Modulated ζ Phase of PAMC

P. Harris, B. Lebech, *Department of Solid State Physics, Risø National Laboratory, Denmark*, F.K. Larsen, *Department of Chemistry, Aarhus University, Denmark*, and N. Achiwa, *Department of Physics, Kyushu University, Higashi-ku, Fukuoka, Japan*

The layered perovskite PAMC bis(propylammonium)tetrachloromanganat(II) belongs to a structural family of compounds of general formula $(C_nH_{2n+1}NH_3)_2MX_4$ with $M = Mn^{2+}$, Cd^{2+}, Fe^{2+}, Cu^{2+}, Cr^{2+}, Pd^{2+}, $X = Cl^-$, Br^-. All compounds consist of (MX_6) octahedra sandwiched between the alkylammonium chains. The compounds having $n = 3$ are unique as they exhibit the largest sequence of phase transitions[1,2]. The phase transitions are due to a gradual selection and ordering of the possible hydrogen bondings between the NH_3^+ groups and the Cl^--ions followed by a reorientation of the propylammonium chains. In the high temperature α phase the time-averaged symmetry of the structure is tetragonal, in the $\beta - \epsilon$ phases it is orthorhombic, and in the low-temperature ζ phase no dynamical disorder persists, and the symmetry becomes monoclinic.

At 112 K the chains order, and the crystal undergoes a phase transition from orthorhombic to monoclinic symmetry. At the same temperature the modulation vector locks in from an incommensurate value of $(\frac{1}{3} + \delta)\mathbf{b}_o^*$ to a commensurate value of $\frac{1}{3}\mathbf{b}_m^*$. These directions are not parallel which means that the modulation vector turns at the lock-in transition - a very unusual behavior.

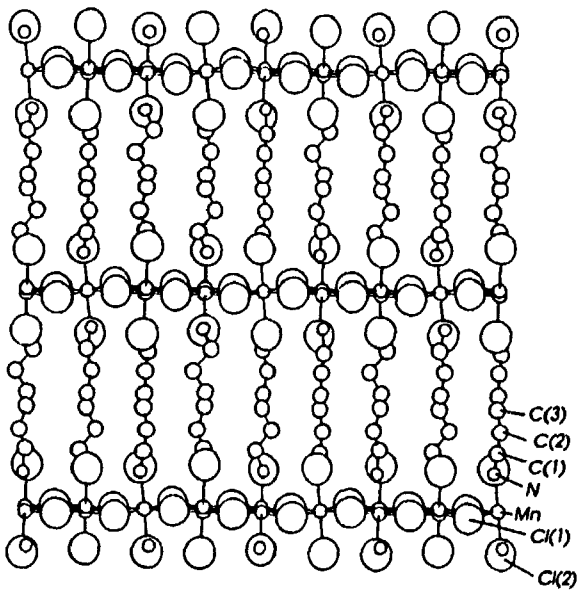

Fig. 1. Crystal structure (without perspective) of the ζ phase of PAMC. The atoms radii are proportional to their atomic or ionic radius.

Analysis of four-circle X-ray data performed at 8 K shows that the modulational wave in ζ PAMC indeed looks like a lock-in of the ϵ phase. Qualitatively, there are very little changes in the displacive modulation of the individual atoms. Therefore the turn of the modulation vector at the phase transition is indicating a phase shift of the modulation wave across adjacent layers. In the layers, the relative movement is almost unchanged.

[1] W. Depmeier, J. Felsche, and G. Wildermuth, (1977). J. Solid State Chem. **21**, 57.
[2] W. Depmeier (1979). J. Solid State Chem. **29**, 15.
[3] W. Steurer and W. Depmeier (1989). Acta Cryst. **B45**, 555.

1.36 Solution and Refinement of Structures by the Use of Neutron Powder Diffraction Data

A. Nørlund Christensen, *Department of Chemistry, Aarhus University, Denmark*, and B. Lebech, *Department of Solid State Physics, Risø National Laboratory, Denmark*

The procedure for a crystal structure determination from powder diffraction data is first to index the powder pattern and determine the space group, then to decompose the pattern by a profile fitting procedure to obtain a set of structure factors, and finally to use these in a structure solution by direct methods or by Patterson methods. The model of the structure can then be refined in a least-squares profile refinement using the Rietveld method. It is often an advantage to combine information from X-ray and neutron powder diffraction patterns, so that the X-ray data may give the unit cell, space group and positions of the heavy atoms, and the neutron data may give the positions of the remaining atoms. The results from both data sets are then used in the profile refinement.

Neutron diffraction powder patterns were measured of mercury oxalate, HgC_2O_4, and of the high temperature modifications of the rare earth disilicates $RE_2Si_2O_7$, RE = La, Ce, Ho, Y, Er, and Yb. The powdered sample of mercury oxalate was precipitated from aqueous solutions, and the silicates were made in high temperature synthesis. The structures of the rare earth disilicates were known from previous X-ray investigations. The structure of HgC_2O_4 was solved by direct methods using the program SIRPOW92[1]. All structures were refined by the Rietveld method using the program DBW3.2S[2]. Figure 1 shows as an example the observed and calculated neutron diffraction powder patterns of mercury oxalate. The standard deviation on the atomic coordinates and the interatomic distances in these seven structure analysis had typical values of 1 to 2% of the respective atomic coordinates and interatomic distances.

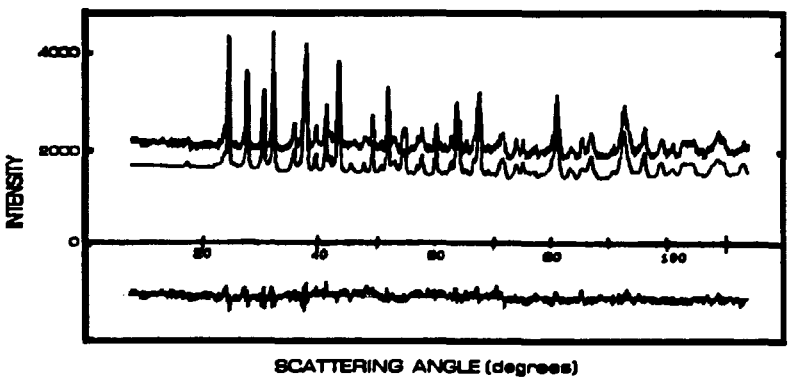

Fig. 1. Neutron diffraction powder pattern of mercury oxalate. The upper and lower curves represent the observed and calculated profiles, respectively, with the difference shown in the lower part of the figure.

[1] A. Altomare, M.C. Burla, M. Camalli, G. Cascarano, C. Giacovazzo, A. Guigliardi, and G. Polidori, (1994). SIRPOW92. J. Appl. Crystallogr., *to be submitted*
[2] D. B. Wiles, A. Sakthivel, and R.A. Young, (1988). Program DBW3.2S for Rietveld Analysis of X-Ray and Neutron Powder Diffraction Patterns. School of Physics, Georgia Institute of Technology, Atlanta, Georgia, USA.

1.37 Crystal Structures of $SrCeO_3$ Based Electrolyte Materials

J. Ranløv, *Materials Department, Risø National Laboratory, Denmark*, and B. Lebech, *Department of Solid State Physics, Risø National Laboratory, Denmark*

The perovskite-type oxides $SrCeO_3$ and $BaCeO_3$, where Ce is partially substituted by aliovalent cations, are host to a variety of point defects and give rise to simultaneous occurrence of *p*-type electronic, oxygen ion, and an appreciable protonic conductivity. The electrical properties of these compounds are determined by aliovalent dopant concentration, temperature, and oxygen fugacity in the atmosphere. Reactions with the gas phase generates electron holes, the concentration of which is a function of oxygen fugacity. In order to improve the understanding of the transport properties in these compounds and to be able to link their electrical behaviour to structural transformations we have carried out crystal structure investigations of pure and doped $SrCeO_3$ as a function of temperature.

Neutron powder diffraction was carried out at fixed temperatures (ambient temperature, 300, 500, 750, 900, and 1200°C) on the multi-detector powder diffractometer at Risø National Laboratory. The crystal structure was refined by whole pattern least-squares refinement of a structural model obtained from room temperature crystal structure analysis[1] to the powder neutron data by use of the Rietveld program DBWS-9006[2]. An example of a plot of observed, calculated, and difference profiles is shown in Fig. 1. Analysis of the powder neutron data showed that, on heating, $SrCeO_3$ retains a primitive orthorhombic symmetry up to at least 1200°C. The oxygen coordination around Ce remains almost perfectly octahedral whereas the SrO_{12} polyhedra, which are considerably distorted at room temperature, steadily becomes more regular as the temperature increases. Correlation of high temperature structural and electrical behaviour of the cerate oxides is in progress and the tentative data indicate that the structure, transport properties, and electrochemistry of the perovskite ionic conductors may be linked in a tangible way.

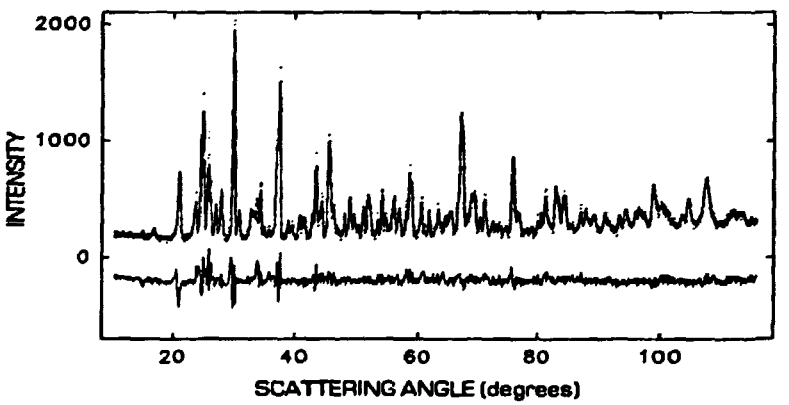

FIG. 1. Observed (dots), calculated (line) and difference plot for the fitted powder neutron diffraction profile

[1] J. Ranløv and K. Nielsen, (1993). The crystal structure of $SrCeO_3$. J. Mater. Chem., *submitted.*

[2] A. Sakthivel and R.A. Young, (1992). Users guide to programs DBWS-9006 and DBWS-9006PC for Rietveld analysis of x-ray and neutron powder diffraction patterns. School of Physics, Georgia Institute of Technology, Atlanta, Georgia, USA.

1.38 Grazing Incidence Small-Angle X-ray Scattering Study of Krypton Inclusions in Aluminium

N.B. Thoft, J. Bohr, *Department of Solid State Physics, Risø National Laboratory, Denmark*, A. Naudon, and T. Slimani, *Laboratoire de Métallurgie Physique, Université de Poitiers, France*

Rare gas inclusions in metals have previously been studied using electron microscopy and X-ray diffraction. Grazing incidence small-angle X-ray scattering (GISAXS) yields information on average size of the inclusions and of the spatial distance between the inclusions. When a narrow and parallel beam impinges on the surface of the sample with a small-angle of incidence that is above the critical angle, the refracted beam propagating immediately below the surface can give rise to small angle scattering due to encountered particles. GISAXS can be observed when the inclusions are small and the surface of the sample sufficiently flat. The experiments described below were performed using a position sensitive detector at a rotating anode X-ray source.

Figure 1 shows the GISAXS curve from a (100) aluminium single crystal implanted with 200 KeV krypton ions to a fluence of 2×10^{16} at/cm^2. The angle of incidence is $\theta_i = 0.6°$. The maximum at $2\theta = 2.95°$ corresponds to an average distance between the inclusions of $\Lambda = 30$ Å. The radius of gyration for the inclusions obtained from this curve, after subtraction of a background spectrum, is $R_g = 13$ Å. The presence of crystalline krypton inclusions was confirmed by measuring their diffraction signal.

It should be noted that the radius of gyration overestimates the value of the average inclusion size, and should only be considered as an indication of the size when studying the change of the inclusion size. Additional experiments on a similar sample indicated growth of the inclusion size and of the average distance between the inclusions upon annealing.

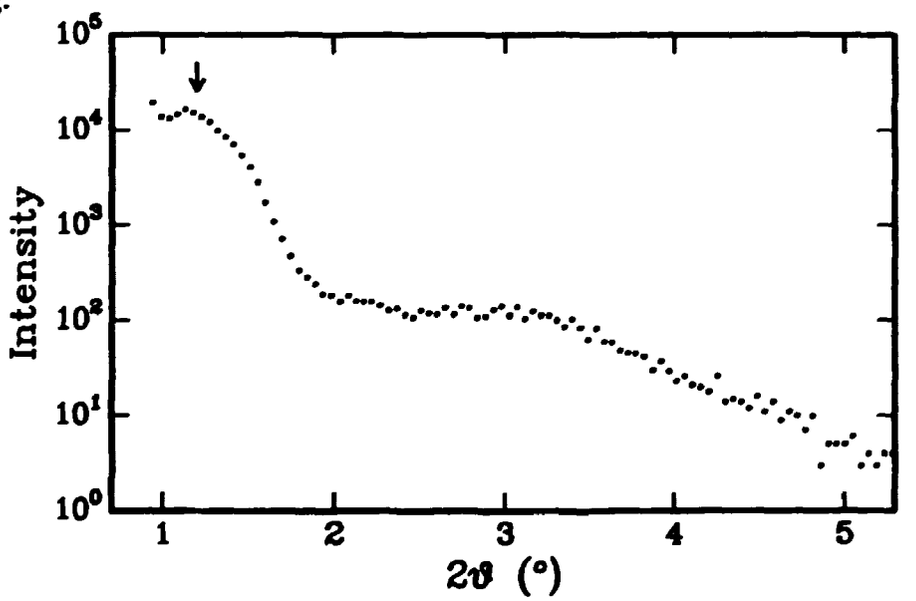

Fig. 1. GISAXS curve of an (100) Al single crystal implanted with Kr. The arrow marks the residual reflected beam at $2\theta_i = 1.2°$.

1.39 Melting and Solidification of Bismuth Inclusions in Aluminium Studied by X-ray Diffraction

N.B. Thoft, J. Bohr, B. Buras, *Department of Solid State Physics, Risø National Laboratory, Denmark*, E. Johnson, A. Johansen, H. H. Andersen, and K. K. Bourdelle, *Ørsted Laboratory, Niels Bohr Institute, University of Copenhagen, Denmark*

The melting and solidification of bismuth inclusions in aluminium single crystals have been studied by X-ray diffraction. Bi and Al are immiscible. Bi inclusions were formed by ion implantation of Bi into an Al single crystal. Bismuth has the property that it contracts upon melting, and that the coefficient of linear expansion of Bi is only half of that of Al. Previous measurements on an annealed Al (111) single crystal implanted with Bi showed that the inclusions (having a mean size of 200 Å) melted in the temperature range 450-544 K and solidified in the range 450-370 K.

Figure 1 shows the intensity of the Bi (011) diffraction peak when heating an as-implanted sample to 570 K (Fig. 1a) and subsequently cooling the sample to room temperature (Fig. 1b). The inclusions melt over a wide temperature range (from 420 K to 520 K). At 20 K below the bulk melting point ($T_B = 544$ K) all the inclusions have melted. Very large supercooling (about 150 K) is seen. As deduced from the FWHM, the mean size of the inclusions in this sample is ≈ 70 Å. A supercooling of $\Delta T = 150$ K corresponds to a critical size of nucleation of 16 Å, much smaller than the measured mean size, so this effect alone cannot explain the observed supercooling. This fact stresses the importance of the influence of the confining aluminium lattice on the solidification of the bismuth inclusions. The differences between the as-implanted and the annealed sample are probably caused by the different mean sizes of the inclusions.

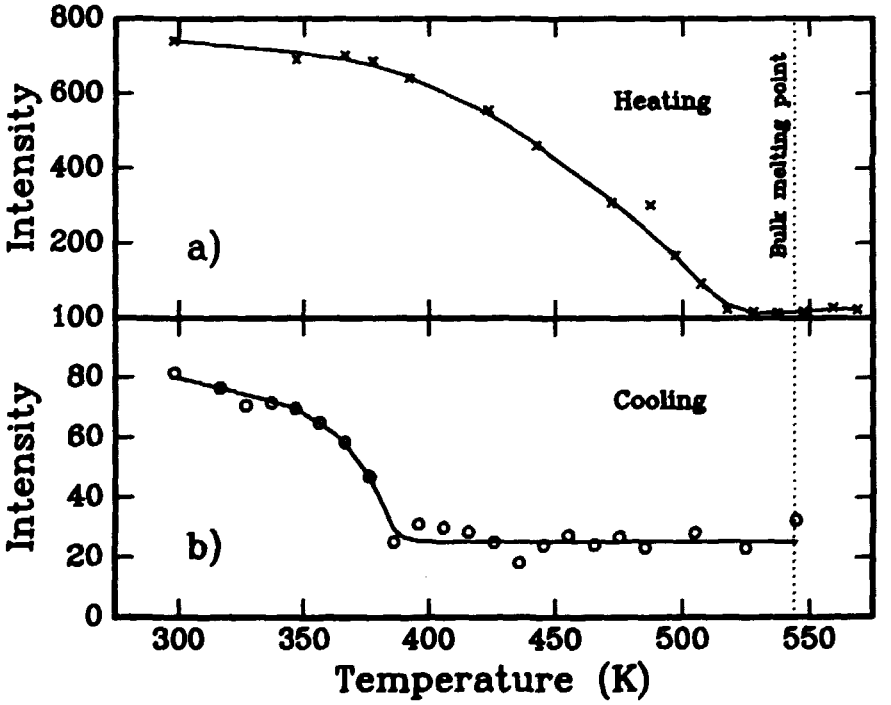

Fig. 1. Intensity of the Bi (011) diffraction peak. a) heating data, b) cooling data. The dotted line marks the bulk melting temperature. The solid curves ar guides to the eye.

1.40 Atomic Structure of a Pd Cluster Compound: X-ray-scattering Measurements

A.R. Sandy, D.B. Pengra, N.B. Thoft, J. Bohr, *Department of Solid State Physics, Risø National Laboratory, Denmark*, and V. V. Volkov, I. Moiseev, *Kurnakov Institute of General and Inorganic Chemistry, Moscow, Russian Federation*

Cluster compounds are molecules composed of an inner metal core (the cluster) surrounded by stabilizing ligands and molecular anions. On the practical side, cluster molecules can be used as large surface area catalysts in solution and are likely building blocks for novel new nanophase materials[1]. On the fundamental side, the physical characteristics of such unique nanoscale materials deserve exploration. Motivated by these considerations we performed an X-ray-scattering study of the atomic structure of the cluster molecule $Pd_{570\pm30}L_{60\pm3}(OAc^-)_{180\pm10}$, where L = 1,10-phen[2]. The number of atoms in the Pd core is approximately that for a "magic," closed, 5-shell polyhedron (561 atoms). Powder diffraction measurements of the molecules were performed as a function of temperature, T, between 25 and 850 K. Figure 1 shows the diffraction pattern obtained from the sample at T = 25 K. Open circles are the measured points. The data have been corrected for background scattering from the sample holder, absorption in the sample and its holder, the Lorentz factor, and the decreasing arc of the Debye-Scherrer rings intercepted at successively larger scattering angles. Immediately evident in Fig. 1 is the large number of diffraction peaks. From these we immediately conclude that the Pd core of the molecules is crystalline. Also shown in Fig. 1 are vertical dashed lines and labels indicating the positions of bulk face-centered-cubic (fcc) Bragg reflections. Remarkably, a solid containing only ~ 8 atomic layers already reveals a diffraction pattern reminiscent of the bulk. Ongoing analysis has, however, demonstrated that the Pd core has neither the structure of a perfect fcc crystal nor a simple Mackay icosahedron.

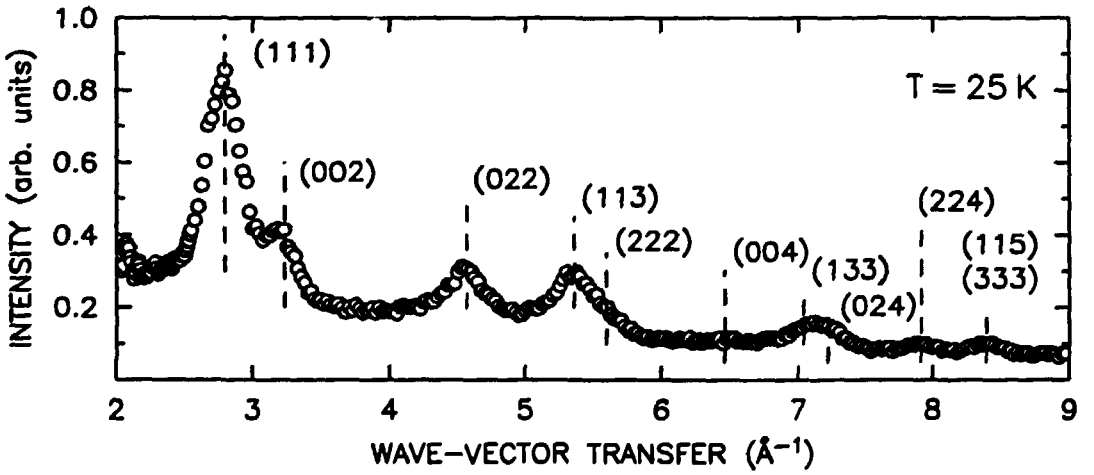

Fig. 1. Powder diffraction pattern of the Pd cluster molecule obtained at T = 25 K.

[1] R.W. Siegel, (1993). Physics Today **46**, No. 10, 64.

[2] M.N. Vargaftik, V.P. Zagorodnikov, I.P. Stolyarov, I.I. Moiseev, V.A. Likholobov, D.I. Kochubey, A.L. Chuvilin, V.I. Zaikovsky, K.I. Zamaraev, and G.I. Timofeeva, (1985). J. Chem. Soc. Chem. Comm., 937.

1.41 Small-angle Neutron Scattering on Ni-11 at.% Ti

P. Vyskocil, B. Schönfeld, G. Kostorz, *Institute of Applied Physics, ETH Zürich, Switzerland*, and J. Skov Pedersen, *Department of Solid State Physics, Risø National Laboratory, Denmark*

The phase separation at 580°C in single and polycrystalline Ni-Ti alloys with Ti concentrations between 10.5 and 12.0 at.% was followed by SANS measurements after various aging treatments. The integrated intensities of two polycrystalline alloys exhibit an early and a late plateau (see Fig. 1). The particle and the matrix compositions were calculated, and they indicate that before the formation of the stable precipitates (η-phase, Ni_3Ti, $D0_{24}$ structure) two consecutive metastable phases appear with Ti concentrations of 18.4 and 22 at.%, respectively. The Ti concentration of the matrix is near 8.5 at.% for both plateaus.

A scaling analysis performed for polycrystals as well as for different crystallographic directions of single crystals suggests that the first metastable phase is formed by spinodal decomposition and that the amplitude of concentration modulations grows linearly with aging time.

Special effort was made to model precipitate arrangements which give scattering cross-sections compatible with the anisotropic scattering of single crystals (see Fig. 2). A cluster model was introduced which may be applied for distinct quasi-periodic particle arrangements. It provides a discrete particle size distribution, the scattering contrast between particles and matrix, and a measure for the degree of order within each cluster. The linear increase of the scattering contrast during the first two hours of aging as suggested by the scaling analysis was confirmed. It was also shown that the particle arrangement becomes more and more regular with increasing aging time.

Deviations from the Porod law served to calculate the width of the particle-matrix interface. It is rather broad in the early stages of decomposition (20 Å, about half the diameter of the Ti-enriched zones) while for later stages the precipitates are larger and the interface width is only about 10 Å.

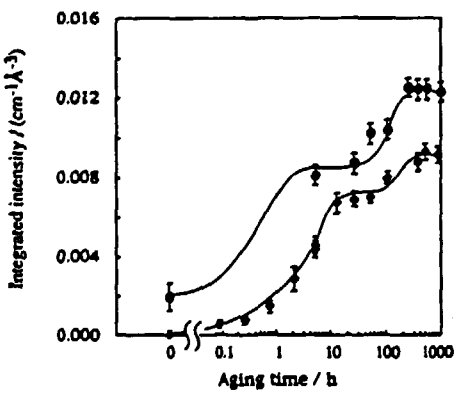

Fig. 1. Integrated SANS intensities of Ni-11.8 at% Ti (•) and Ni-10.8 at.% Ti (o).

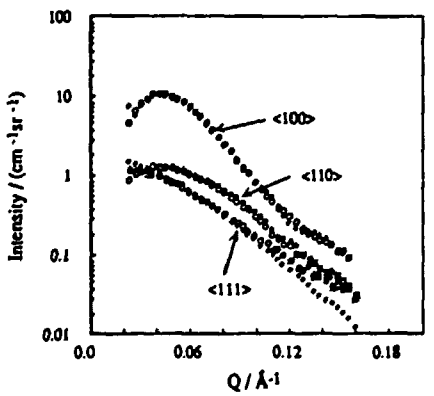

Fig. 2. SANS intensities for three crystallographic directions after annealing for 25 h at 580°: (o) data and (•) fit.

1.42 Study of Bimodal Size Distributions of γ' Precipitates in Ni-Al-Mo

A.D. Sequeira, H.A. Calderon, G. Kostorz, *Institute of Applied Physics, ETH Zürich, Switzerland*, and J. Skov Pedersen, *Solid State Physics Department, Riso National Laboratory, Denmark*

The presence of an ordered phase of hard, coherent γ' (Ni_3Al) precipitates embedded in a disordered Ni-rich matrix (γ) gives rise to outstanding mechanical properties at high temperatures. The typical microstructure of a practical alloy may consist of a class of aged, coarse precipitates and a second class of finely dispersed ones. Small-angle neutron scattering (SANS) is particularly suitable to study inhomogeneities. However, data analysis becomes difficult for non-dilute systems. Furthermore the most common shapes for the precipitates in the alloys of interest are usually non-spherical (cuboidal) and the size distributions are generally polydisperse and multimodal. Therefore the use of a complementary technique is mandatory. Transmission electron microscopy (TEM) is an excellent complement to SANS. In the present study two Ni-Al-Mo alloys were prepared and heat treated to contain a bimodal size distribution of precipitates. The determination of particle size distributions (PSDs), the evolution of the morphology, and the spatial arrangement of both classes of precipitates were studied using TEM and SANS. The particle size distribution of the small precipitates was determined from the SANS data by the method described in contribution 1.10 employing the local monodisperse approximation.

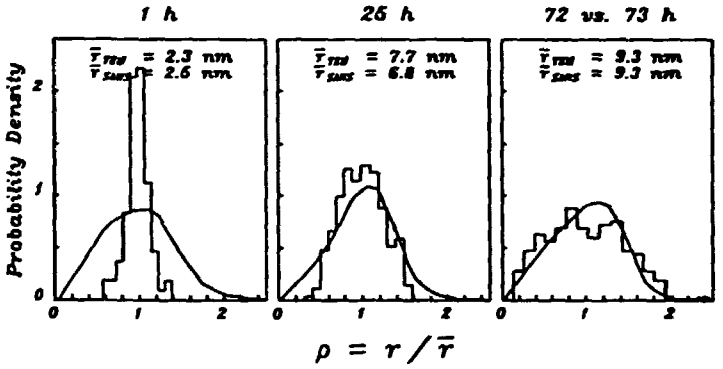

Fig. 1. Particle size distributions determined by TEM (histograms) and by SANS (solid line) for the Ni-9.5Al-5.4Mo alloy for the aging states which were measured by both techniques.

Some PSDs for one of the alloys obtained from both techniques are displayed in Fig. 1. The average size of the precipitates determined by both techniques are indicated in the figure and agree within 15%. The SANS size distributions are systematically wider than those determined by TEM but, apart from the state corresponding to 1 h where the shapes are completely different, the overall agreement is very good. The differences in shape observed can be understood if one considers the different size sensitivities of the two techniques. The size distributions determined by SANS for the whole range of aging times (1 to 1000 h) prove that the present SANS analysis is insensitive to changes in the polydispersity observed during the decomposition of this alloy. This is probably related to the fact that in this treatment the high anisotropy of the system was ignored by radially averaging the two-dimensional scattering patterns. Considering the different "nature" of the two techniques and their different size sensitivities, the overall agreement of the size distributions is excellent.

1.43 A SANS Investigation of the Influence of Hydrogen on the Age-hardening of Commercial Aluminimum-Lithium Alloys

D.M. Henry, D.E.J. Talbot, *Department of Material Scince and Technology, Brunel University, Uxbridge, Middlesex, UK*, and J. Skov Pedersen, *Department of Solid State Physics, Risø National Laboratory, Denmark*

Dissolved hydrogen has previously been found to delay the development of precipitate precursors during the early stages of ageing in a single phase Al-2wt%Li at 95°C [1]. The effect was ascribed to an association of the hydrogen solute with lithium-rich zones within the α-matrix. Since ageing of commercial aluminium-lithium alloys show erratic behaviour and hydrogen is a normal impurity present to a variable degree it is probable that the erratic respeonse could, in part, be due to the presence of hydrogen.

Small-angle neutron scattering has been imployed to assess the influence on the early stages of the ageing of three commercial Al-Li alloys: AA2090 (Al-2.2wt%Li-2.6wt%Cu), AA8090 (Al-2.33wt%Li-1.06wt%Cu-0.64wt%Mg), Weldalite 049^{TM} (Al-4.75wt%Cu-1.25-wt%Li-0.40wt%Mg-0.40wt%Ag-0.12wt%Zr), and a laboratory ternary alloy (Al-2.38wt%-Li-0.66wt%Mg-0.11wt%Zr-0.4wt%Fe). The samples were solution heat treated and loaded with varying amounts of hydrogen, aged for various times between 0 and 62 h at 423 K.

The complex nature of the alloys has made the understanding of their ageing behaviour difficult. Analysis of the results is on-going. In this report we give some results for the AA8090 system. Despite the apparent complexity of AA8090 only δ' (Al_3Li) and possibly α' ($Al_3(Li,Zr)$) are expected to influence the SANS results. Predominance of spherical δ' particles makes analysis in terms of a monodisperse hard-sphere model possible. From the results of cluster growth (Fig. 1) we can confirm that hydrogen inhibits cluster growth, the greater the hydrogen content the slower the growth. The cluster radius depends linearly on the cube-root of time, suggesting diffusion controlled growth or Ostwald ripening.

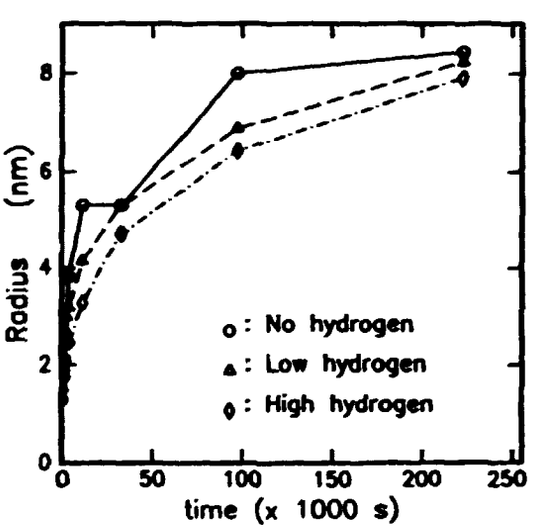

Fig. 1. Time evolution of cluster radius in AA8090 during ageing at 423 K.

[1] C. McCracken, D.E.J. Talbot, and J. Skov Pedersen, (1991). Contribution 1.70 in Risø-R-610(EN).

1.44 Sputtering of Solid Deuterium by keV Electrons

B. Thestrup, W. Svendsen, J. Schou, *Department of Solid State Physics, Risø National Laboratory, Denmark*, O. Ellegaard, *University of Odense, Denmark*, and R. Pedrys, *Jagellonian University, Krakow, Poland*

Solid deuterium is one of the most volatile elements that can exist in equilibrium with laboratory vacuum. Electron irradiation without significant evaporation from a deuterium film is only possible at temperatures below 3 K and with currents below 200 nA. Sputtering yield measurements were carried out for 1.5 and 2.0 keV electrons at an existing setup.

The yield increased drastically for deuterium films that exceeded the range of the electrons. For 1.5 keV electrons the yield increased from a few molecules per electron up to the saturation value of about 400 D_2/electron around 30000 Å (see Fig. 1).

This strange yield behaviour which has not been seen for other condensed gases, is correlated with the formation of a space charge in solid deuterium. This space charge of trapped electrons is likely to drive slow internal electrons to the surface. How these electrons contribute to sputtering is not yet known.

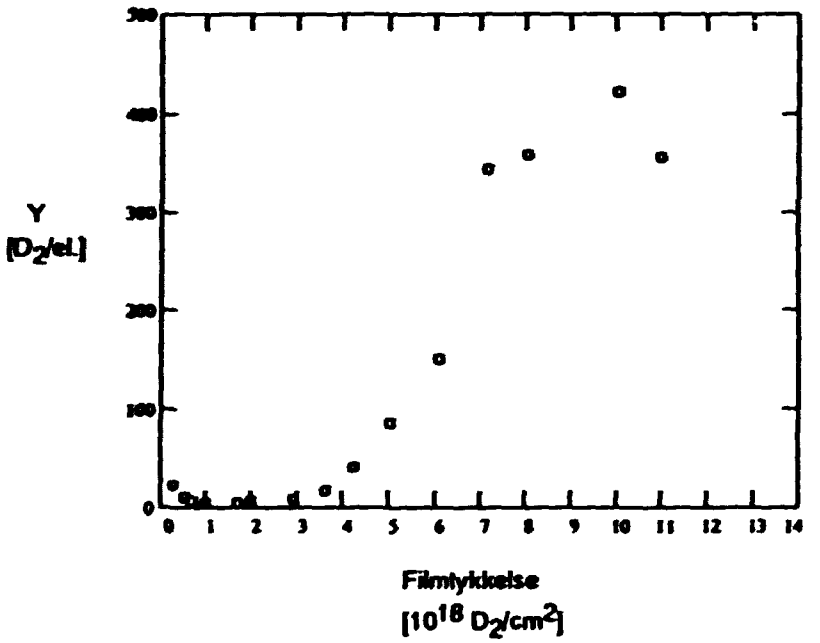

Fig. 1. Sputtering yield of 1.5 keV electrons on D_2/Ag versus film thickness.

1.45 Fundamental Laser Ablation of Simple Materials

J. Schou, W. Svendsen, A. Nordskov, *Department of Solid State Physics, Risø National Laboratory, Denmark,* and O. Ellegaard, *University of Odense, Denmark*

Laser ablation of solids, *i.e.* erosion by an intense laser beam, becomes gradually one of the most important methods to deposit thin films and to investigate the mass composition of complicated organic mixtures. In particular, epitaxial films of high T_c-superconductors have been produced by UV-laser ablation deposition at many laboratories. Mass spectrometry of organic matrices doped with small amounts of bioorganic materials can be carried out in a fast and convenient manner by UV-laser irradiation as well.

However, the success of these methods does not mean that the basic processes are known. In most of the cases, the studies have been performed in an empirical manner. In contrast to the main areas in physics, most of the materials investigated so far are fairly complex, whereas the simple ones have been studied relatively little.

These partly unexplored phenomena have stimulated a program in which the basic processes of laser ablation from simple materials will be studied. The setup is shown in Fig. 1. The laser beam from a pulsed Nd:YAG laser strikes the target and produces a plume of material that leaves the target within a few nanoseconds. The ablated material will be collected on microbalances so that the erosion and deposition yield can be determined as a function of intensity and wavelength. Simultaneously with these measurements, the plume will be studied optically with a VUV-monochromator, and the emission of positive ions from the biased target will be estimated from the current collected.

Silver will be studied, since there exist a few measurements of ablation from thin silver films and massive targets. Furthermore, silver surfaces develop comparatively little contaminants in vacuum. Water ice will be studied as well, since this is one of the simplest oxides. Relatively many of the electronic transitions are known for the water molecule. Water ice has been utilized recently as a matrix for sequences of DNA-dopants. With respect to the vacuum conditions, films of water ice are relatively easy to produce *in-situ* and can, therefore, be kept relatively clean.

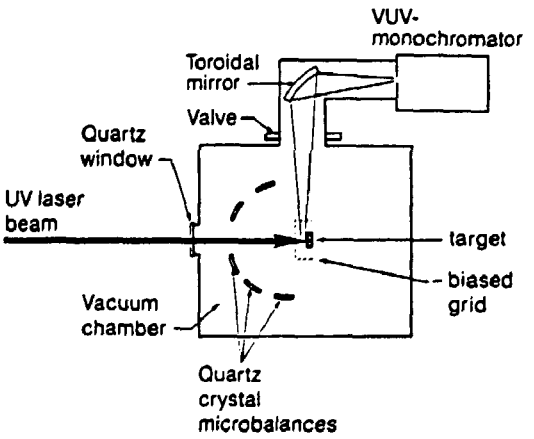

Fig. 1. Schematic drawing of the setup for fundamental laser ablation.

1.46 X-ray Scattering from Free-standing Amorphous Diamond-like Carbon Films

E. Findeisen, R. Feidenhans'l, M. Nielsen, *Department of Solid State Physics, Risø National Laboratory, Denmark*, G. Grübel, J. Als-Nielsen, *ESRF, Grenoble, France*, and M. Foss, *Institute for Physics and Astronomy, Aarhus University, Denmark.*

X-ray scattering from free-standing amorphous diamond-like carbon (DLC) films [1] has been carried out at the Troika beamline ID10 at the ESRF. For large momentum transfer most of the photons are scattered inelastically (Compton scattering). However, only the elastic signal of 23.89 keV contains structural information about the average distance between carbon atoms and their hybridization states. The shift in energy due to the Compton scattering is $\Delta E = E - E' \approx \hbar^2 q^2 / (2m_e)$. In order to get direct access to the structural information both scattering contributions were separated by using a Ge-detector with high energy resolution.

Figure 1 shows the energy dependence of the scattered intensity at $q = 14$ Å^{-1} for a free-standing DLC-film. The elastic peak is fitted with a gaussian distribution and the peak corresponding to the Compton scattering with a Voigt function. The calculated energy of the Compton scattering, $E' = 23.15$ keV, shown by the line is, within errorbars, in agreement with the experimental data. The experimentally determined energy shift is $\Delta E = 747$ eV.

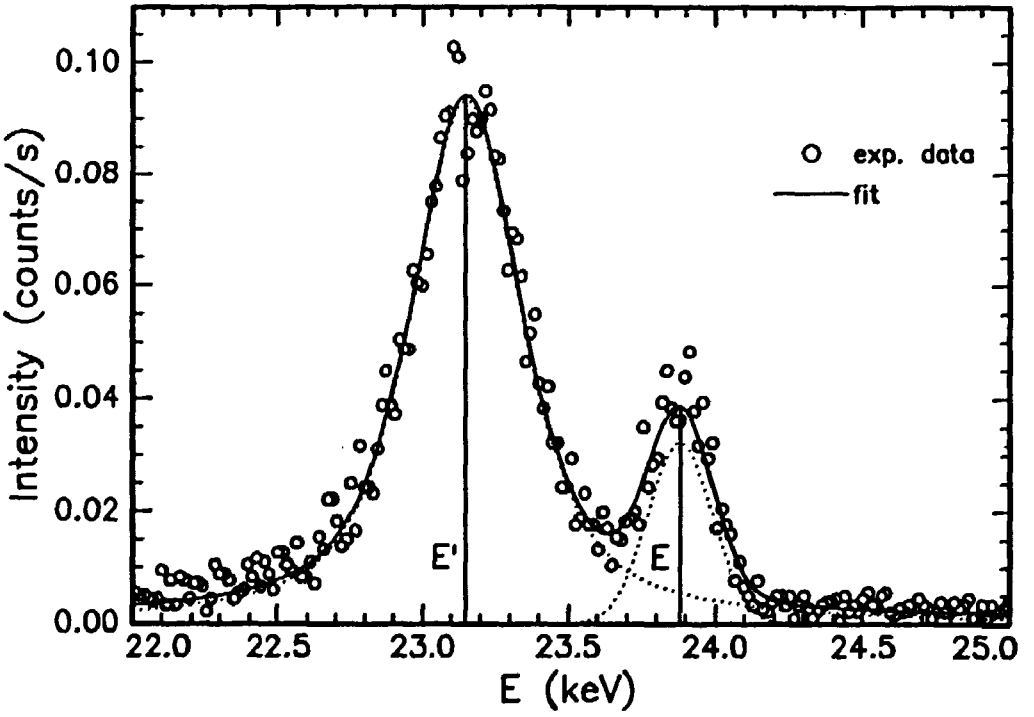

Fig. 1. Energy dependence of the scattered intensity at $q = 14$ Å^{-1}. The lines indicate the calculated values for the elastic E and Compton peak E'.

[1] E. Findeisen, R. Feidenhans'l, M. Nielsen, J.B. Hansen, and M. Benzon, (1992). Contribution 1.48 in Risø-R-660(EN).

1.47 Material Properties and Production Parameters of Diamond-like Carbon Thin Films

M.E. Vigild, E. Findeisen, R.Feidenhans'l, *Department of Solid State Physics, Risø National Laboratory, Denmark*, C. Barholm-Hansen, M.D. Bentzon, and J.B. Hansen *NKT Research Center, Denmark*

Diamond-like carbon (DLC) is an amorphous material and can be produced by low pressure deposition techniques. Diamond-like carbon exhibits material properties close to those of crystalline diamond. It is a very hard material with a high thermal conductivity. It is resistant to corrosion, transparent to ultra violet light, electrically insulating, and has a low coefficient of friction. Diamond-like carbon is a very interesting material in view of its applications as a coating material.

We have studied thin films of DLC on silicon substrates made by plasma enhanced radio frequency vapour deposition (PE-RFCVD). With this method of preperation the carbon feedstock - methane CH_4 - flows steadily through the growth chamber. The substrates sit on an electrode around which a plasma is excited by the radio frequency electrical field. The aim of the experimental effort was to map out the dependance on the methane flow of the mass density ρ and the hydrogen content γ of the DLC film. This was possible by combining X-ray and neutron reflectivity measurements.

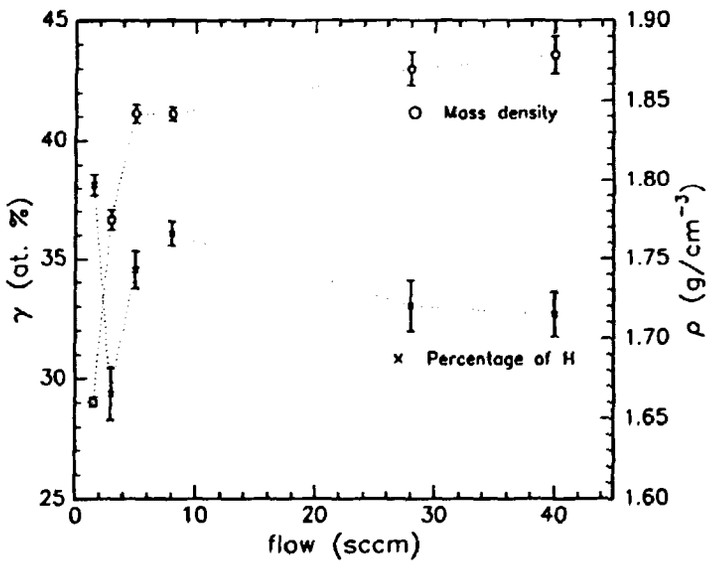

Fig. 1. Mass density ρ and hydrogen atomic percentage γ as a function of the methane flow.

The flow parameter was found to be important to both mass densities and atomic hydrogen contents. Mass densities were found in the interval from 1.66 g/cm^3 to 1.88 g/cm^3. Atomic hydrogen contents were found in the interval from 29 % to 38 %. The mass density shows a fast growing dependance on the flow at low values and a tendency to stabilize at higher flow values. The atomic content of hydrogen does not show any such simple relationship with the flow parameter. Above a critical flow of approximately 10 sccm the film parameters stabilise at mass densities of 1.87 g/cm^3 and hydrogen content of approximately 33 %. Further experiments are planned to explore the low flow interval of 1 - 10 sccm.

1.48 Order-disorder Transition in Sandwiched Cu_3Au Films

C.P. Jensen and R. Feidenhans'l, *Department of Solid State Physics, Risø National Laboratory, Denmark*

Cu_3Au is a classical system for studying an order-disorder phase transition. The bulk phase transition is first order, but at the (100) surface it is second order. The critical temperature for both bulk and surfaces is 663 K.

We have looked on a 400 Å thick Cu_3Au film in a Ag sandwich. It has been grown in the Molecular Beam Epitaxy (MBE) chamber. The substrate is the (001)-surface of a perfect MgO crystal. As a buffer layer to ensure good crystallinity we have grown a layer of 300 Å Ag. On top of the buffer layer was grown 400 Å Cu_3Au. This was done with two Knudsen cells, one with Cu and one with Au. The two cells were evaporating at the same time and the temperature of the two cells was set such that the stoichiometry of Cu and Au was three to one. As a cap we grew 300 Å Ag. The substrate has all the time been at room temperature. The stoichiometry of the Cu_3Au layer was checked with Rutherford backscattering spectrometry and it gave 74.8% Cu and 25.2% Au.

With X-ray diffraction we measured the Cu_3Au (001)-superstructure peak at different temperatures. The measurements were performed at a rotating Cu anode using a graphite monochromator. The figure shows the (001) peaks as a function of time and there is indicated where the temperature has been changed. At 629 K there was no peak at the (001) position. That means that there was no long range ordering and T was above the critical temperature. At $t = 0$ the temperature was changed from 629 K to 625 K and the (001) peak begins to grow up. After about 40 hours the temperature was raised 1 K, even though equilibrium was not reached. The lines are exponetial fits to the points. It can been seen that the time constants are about 9.5 and 21 hours which is much larger equlibrium times than for the bulk. Notice that the critical temperature for the thin film is 34 K below the critical temperature for the bulk. One reason for the slow kinetics might be interdiffusion between the layers.

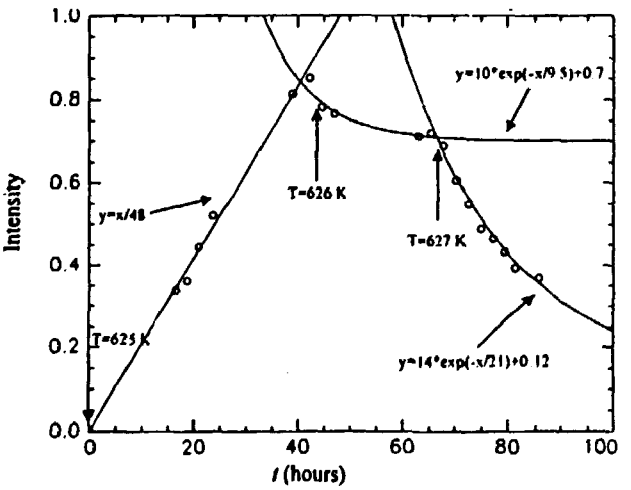

Fig. 1. The intensity of the Cu_3Au (001) peak as a function of time. At $t = 0$ the temperature is 629 K.

1.49 Investigation of the (1×2)-phases of Bi/GaSb(110)

T. van Gemmeren, L. Lottermoser, R.L. Johnson, *II. Institut für Experimentalphysik, Universität Hamburg, Germany,* R. Feidenhans'l, and M. Nielsen, *Department of Solid State Physics, Risø National Laboratory, Denmark*

Ordered nonreactive systems provide the best starting point for studying the structural and electronic properties of metal-semiconductor interfaces. Both bismuth and antimony adsorbed on (110) surfaces of many III-V compound semiconductors form well-ordered interfaces. Skeath *et al.*[1] observed that a monolayer (ML) of Sb deposited on GaAs(110) at room temperature forms zigzag chains of Sb atoms bonded alternately to Ga and As atoms. In contrast to Sb the system Bi/GaAs(110) exhibits regular dislocations with missing adatoms every sixth unit cell[2], which are attributed to strain induced in the Bi chains resulting from the poor lattice match between the Bi chains and the substrate. GaSb has a larger lattice constant than GaAs and thus should be able to accommodate Bi better. Although Bi deposited on GaSb(110) at room temperature shows an ordered (1×1) reconstruction also consisting of Bi zigzag chains[3], the thermally stable phase is the (1×2) reconstruction.

In different runs we annealed Bi films with coverages between 1 and 8.9 ML in the temperature range between 200 and 410°C. Up to a temperature of approximately 350°C we observe half-order peaks along the [001] direction. Beyond this temperature a (1×1) LEED reconstruction of the clean surface is formed, which coincides with the disappearance of the Bi photoemission signal. In the temperature range, where we observe the (1×2) pattern, the Bi intensity decreases and the substrate intensity increases slightly. The Bi signal corresponded to a coverage of 0.6 ± 0.1 ML. The Bi($5d$) core-level spectra could be fitted with two components and the substrate lines were fitted with two peaks corresponding to the surface and bulk components from the clean surface. The surface contribution from the substrate core levels was strongly attenuated indicating that the Bi adsorbate reduces the strain in the near-surface region.

In addition to the photoemission studies the atomic structure of the (1×2) reconstruction has been studied by surface diffraction at the Wiggler beamline BW2 at HASYLAB in Hamburg. For the structure analysis 61 fractional-order and 17 integer-order in-plane reflections were measured, out of which 25 and 13 were non-equivalent. The data set included six fractional-order rod-scans and three integer-order rod scans. All of the fractional-order reflections can be indexed in terms of a (1×2) unit cell. A Fourier transformation of the data gives directly the electron-density auto-correlation function (Patterson function). A detailed analysis of the data and a refinement of the structural model for the GaSb(110) (1×2) - Bi reconstruction is currently in progress.

[1] P. Skeath, I. Lindau, C. Y. Su, and W. E. Spicer, (1989). J. Vac. Sci. Technol. **19**, 556.
[2] R. Ludeke, A. Taleb-Ibrahimi, R. M. Feenstra, and A. B. McLean, (1989). J. Vac. Sci. Technol. **B7**, 936.
[3] D.N. McIlroy, D. Hesket, A.B. McLean, R. Ludeke, H. Munekata, and N. J. DiNardo, (1993). Phys. Rev. **B48**, 11897.

1.50 Investigations of Surface Structures at Beamline BW2

R. Feidenhans'l, E. Findeisen, M. Nielsen, *Department of Solid State Physics, Risø National Laboratory, Denmark*, M. Foss, *Institute for Physics and Astronomy, Aarhus University, Denmark*, L. Seehofer, G. Falkenberg, L. Lotteimoser, T. Buslaps, and R. L. Johnson, *II. Institut für Experimentalphysik, Universität Hamburg, Germany*

For a number of surface structures it is necessary to obtain not only information about the in-plane atomic geometry but also about the geometry in the direction normal to the surface. Hence, it is neccassary to be able to measure the intensity along the Bragg rods normal to the surface. At the surface X-ray diffractometer we have set up a new procedure to perform rod scans. We have possibilities to vary both the angle of incidence α_i to the surface as well as the angle of exit α_f up the 20°. The momentum transfer in the direction normal to the surface is $q = k(\sin\alpha_i + \sin\alpha_f)$. For an X-ray wavelength of 1.2 Å the accessible momentum transfer range is 3.5 $Å^{-1}$. We have investigated a number of different surface structures.

The structure of Ge(111)$\sqrt{3} \times \sqrt{3}$-Ag is controversial. We have previously on basis of in-plane X-ray diffraction derived a Ag trimer structure with Ag-Ag bonds, a structure similar to Au/Ge(111). Recently, however, a Low-Energy-Electron-Diffraction (LEED) study have found a structure similar to the Ag/Si(111) structure which does not have the Ag trimer. In order to resolve this controversy we have performed extended rod scans on several fractionel and integer-order reflections.

We have investigated the β-Ge(111)$\sqrt{3} \times \sqrt{3}$-Pb surface. We have previously determined the in-plane structure to be a distorted (111) Pb overlayer. New rod scans have been performed to cast light on the registry of the Pb-layer with respect to the Ge(111) substrate.

The Cu(110)2×1-O structure is a missing-row structure with rows along (001) direction of almost co-planer Cu-O-Cu atoms. We have performed new fractional and integer-order rod scans on this structure in order to determine whether the oxygen sits above or below the Cu atoms.

Finally we have collected an in-plane and out-of-plane data sets of the Cu(110)4×1-Bi structure. This is a first step to determine the Bi phase diagram as a function of temperature and coverage on the Cu(110) surface.

Structural models for all these structures are in progress.

1.51 The Specular Reflectivity as a Structural Probe

R. Feidenhans'l, M. Nielsen, *Department of Solid State Physics, Risø National Laboratory, Denmark*, M. Böhringer, P. Molinas-Mata, J. Zegenhagen, *Max-Planck-Institute für Festkörperforschung, Stuttgart, Germany*, G. Falkenberg, L. Seehofer, L. Lotteimoser, T. Buslaps, and R. L. Johnson, *II. Institut für Experimentalphysik, Universität Hamburg, Germany*

Ga on Ge(111) shows a rather complicated phase diagram with several discommensurate structures as a function of Ga coverage. In order to obtain structural information without necessarily knowing the in-plane coordinates of all the atoms involved in the reconstructions we have performed specular reflectivity scans along the (00) crystal truncation rod. Along this rod the momentum transfer is only in the direction normal to surface and hence independent of the in-plane atomic arrangements. We have measured the the (00) rod for the γ and the β-H_3 phase for Ga/Ge(111). Furthermore, we have also measured the (00) rods for Pb/Ge(111) β-phase and for the Ag/Ge(111)$\sqrt{3} \times \sqrt{3}$ structure. The data are shown in Fig. 1. At every datapoint along the rod we have performed an ω(rocking)-scan to obtain the integrated intensity. The integrated intensities were corrected for effective area and Lorentz factors.

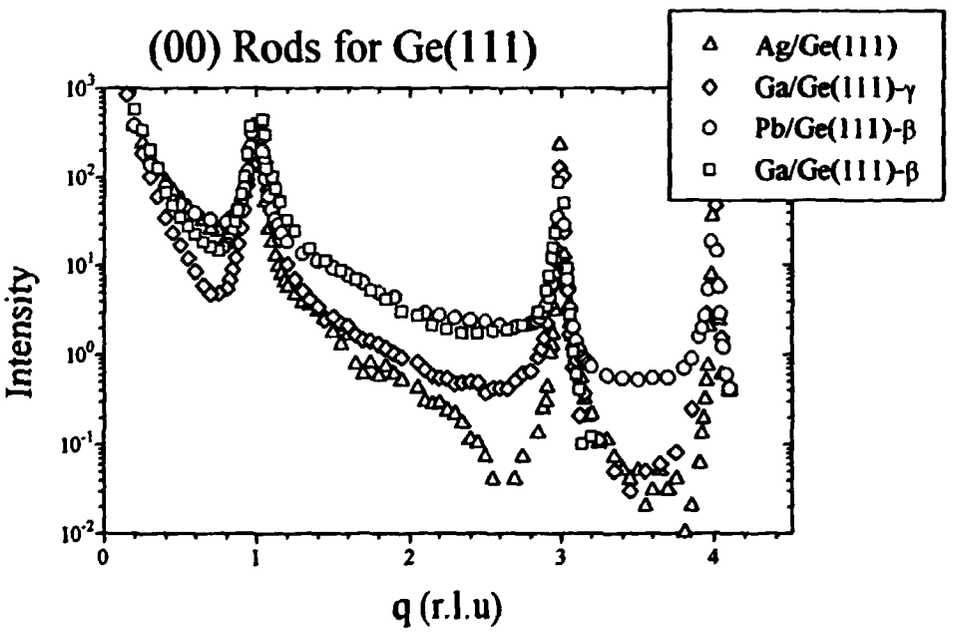

Fig. 1. The specular reflectivity scans for four different structures on the Ge(111) surface.

Clearly, there is a huge difference in intensity for the four different structures. A crude analysis shows that the rod for the Ga/Ge(111) γ-phase surface can be explained by a structure with 0.7 ML Ga substituting for the upper half bilayer of Ge with an inward contraction of about 0.5 Å. The rod for Ag/Ge(111) can roughly be explained by 1 ML of Ag substituting for half a bilayer of Ge(111) and the Pb/Ge(111) rod can be explained by 1.3 ML Pb sitting about 2.7 Å above an undisturbed Ge(111) latttice. More accurate modeling are in progress.

1.52 X-ray Scattering Investigations of the Discommensurate Structures of Ga on Ge(111)

R. Feidenhans'l, M. Nielsen, *Department of Solid State Physics, Risø National Laboratory, Denmark*, M. Böhringer, P. Molinas-Mata, J. Zegenhagen, *Max-Planck-Institute für Festkörperforschung, Stuttgart, Germany*, G. Falkenberg, L. Seehofer, L. Lottermoser, T. Buslaps, and R. L. Johnson, *II. Institut für Experimentalphysik, Universität Hamburg, Germany*

A few metals like Cu and Ga make discommensurate structures when deposited on Si(111) and Ge(111) surfaces. We have continued our X-ray scattering studies of the Ga/Ge(111) system at the beamline BW2 in HASYLAB. Several phases - labelled γ, β and β-H_3 exist as a function of coverage of Ga. We are now able to produce single phases of each of these structures, which simplifies the data analysis. The surfaces were prepared and characterized in the STM/MBE chamber at the II. Institute für Experimentalphysik. Prior to the X-ray scattering investigations the surfaces were studied by Scanning Tunneling Microscopy (STM).

For the γ and the β phases we have performed in-plane scans around the integer-order reflections to identify the discommensurability. The main satellite reflection is at (0.867,0) for the γ-phase and (0.9325,0) for the β phase. We have also performed scans along the (10) and (01) Crystal Truncation Rods (CTR) and along the rods of the main satellite reflections. In the figure the rods are shown for the β-phase. The right side shows the (10) CTR (note the logarithmic scale). The peak at l=0.333 is the (11$\bar{1}$) bulk Bragg reflection. The left side shows the (0.9325,0) rod. Very surprisingly, the (0.9325,0) rod shows a sharp feature at l=0.36. This means that the discommensurations penetrate several layers down and that the outmost layer spacings are slightly contracted. Similar features are observed for the rods of the γ phase.

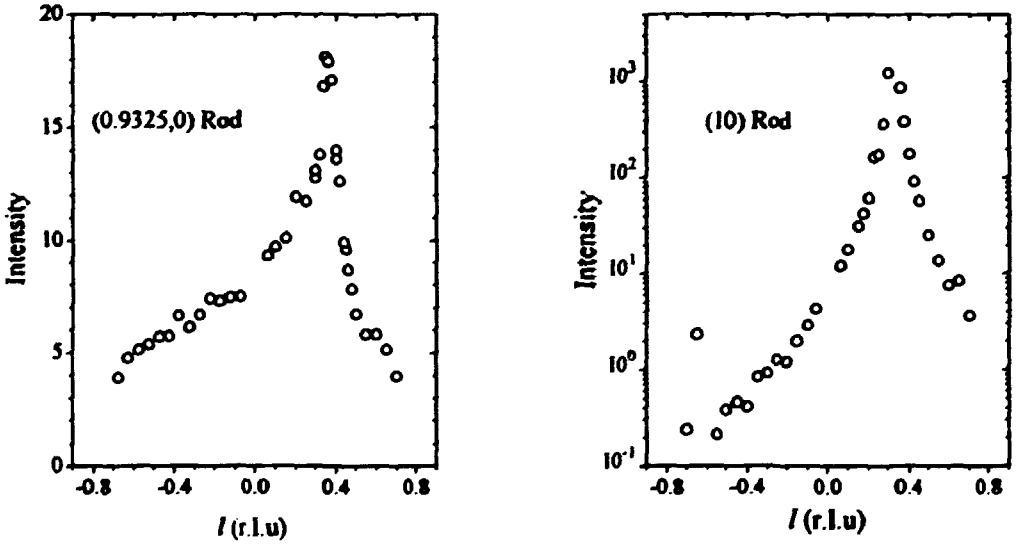

Fig. 1. Rodscans of the (10) CTR and the main satellite at (0.9325,0) for the Ga/Ge(111) β-phase structure.

1.53 Metal on Metal Growth: Au on Ni(110)

M. Foss, L. P. Nielsen, F. Besenbacher, *Institute for Physics and Astronomy, Aarhus University, Denmark*, R. Feidenhans'l, M. Nielsen, *Department of Solid State Physics, Risø National Laboratory, Denmark*, L. Seehofer, G. Falkenberg, L. Lotteimoser, T. Buslaps, and R. L. Johnson, *II. Institut für Experimentalphysik, Universität Hamburg, Germany*

Understanding epitaxial growth is a key to control structures on an atomic level. Heterogeneous growth of metals on metals surfaces have recently shown unexpected behavior. Intermixing of two metals, which are immicible in bulk crystals, has been identified by Scanning Tunneling Microscopy (STM) in the monolayer regime[1]. For small coverages (less than 0.5 monolayers (ML)) Au substitutes for Ni in the first layer of the Ni(110) surface. At higher coverages the surface alloy becomes unstable and it is believed that the Au atoms 'pop' out again.

At beamline BW2 in HASYLAB we have studied the Ni(110)5×1-Au at about 0.7 ML and also the structure at about 1 ML Au. At 0.7 ML a "worm-like" structure is observed by STM as shown in Fig. 1. The white chains probably consist of Au atoms with a coverage of 0.2 ML. The remaining 0.5 ML must still be embedded in the Ni(110) top layer, but ordered in between the upper Au chains. In order to clarify this we have collected an in-plane crystallographic data set of the 5×1 structure. A contour plot of the Patterson function is shown in Fig. 1. At higher Au coverage an c(2×4) structure appears. The X-ray scattering measurements shows that this phase is not commensurate and that it consists of a distorted (111) Au overlayer.

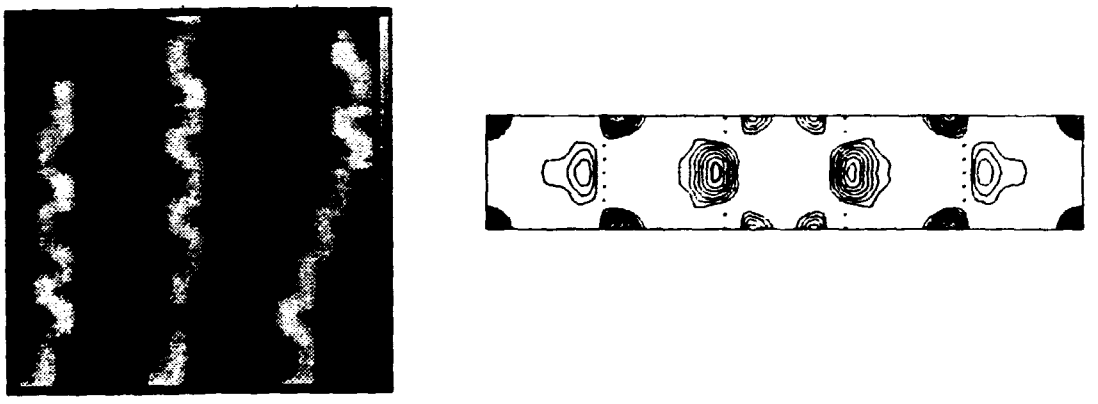

Fig. 1. On the left is shown an STM image of the "worm-like" 5×1 Au/Ni(110) structure. On the right a contour map of the Patterson function is shown.

[1] L.P. Nielsen, F. Besenbacher, I. Stensgaard, E. Lægsgaard C. Engdahl, P. Stoltze, K.W. Jacobsen, and J.K. Nørskov, (1993). Phys. Rev. Lett. 71, 754.

1.54 Metal on Metal Growth: Au on Ni(111)

M. Foss, L.P. Nielsen, F. Besenbacher, *Institute for Physics and Astronomy, Aarhus University, Denmark*, R. Feidenhans'l, M. Nielsen, *Department of Solid State Physics, Risø National Laboratory, Denmark*, L. Seehofer, G. Falkenberg, L. Lotteimoser, T. Buslaps, and R.L. Johnson, *II. Institut für Experimentalphysik, Universität Hamburg, Germany*

Although Au substitutes for Ni atoms in the outermost layer for the Ni(110) surface, this is not expected to happen for the close packed (111) surfaces, where it is too costly in energy to remove a Ni atom. At beamline BW2, HASYLAB, we have studied the growth of Au on Ni(111) at two different preparation procedures with X-ray scattering. After a standard ion-sputter cleaning and annealing of the Ni(111) surface, about 0.7 monolayers (ML) of Au was deposited onto the surface at room temperature. Extra satellites reflections were only observed at multiples of (0.896,0) (and symmetry equivalents) where (1,0) is the shortest in-plane reflection for the Ni(111) substrate. This corresponds to a "9.6×9.6" structure. Apart from Debye-Waller and form factors there is little intensity variation between the satellite reflections. Also, scans along the satellite rods show little intensity variation. This indicates that the structure is mainly a (111) Au overlayer on a undisturbed Ni(111) substrate. In order to determine the structure of the underlying Ni(111) crystal, we have measured the (10) Crystal Truncation Rod (CTR) as shown in Fig. 1.

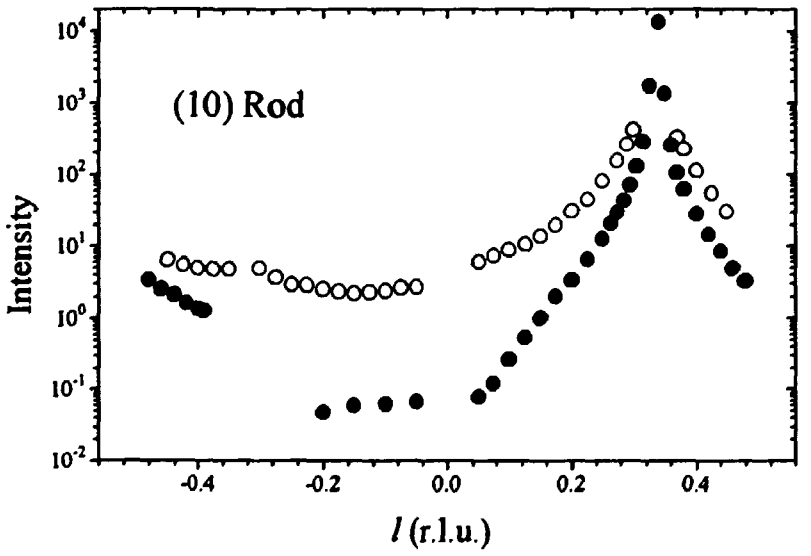

Fig. 1. The (10) CRT of the Ni(111) substrate with 0.7 ML Au deposited. The open circles represents the unannealed surface. The filled circles represents the surface which has been annealed to 600°C. The sharper intensity decay away from the bulk Bragg point (l=0.33) indicate a rougher surface. A peak at l=-0.33 coming from stacking faults in the bulk crystal has been omitted.

After annealing to 600°C, the picture changes dramatically. Several rather broad in-plane satellite reflections appear. The strongest is the (0.95,0) reflections indicating a "20×20" structure. The (10) CTR rod has also changed. The intensity decays much faster away from the bulk Bragg points. This indicates that the Ni(111) interface has become rougher, eventually due to intermixing between Au and Ni. Further analysis is in progress.

1.55 The Ni(111)(5$\sqrt{3}$×2)-S Reconstruction Examined by Surface X-ray Diffraction

M. Foss, *Institute for Physics and Astronomy, Aarhus University, Denmark*, R. Feidenhans'l, E. Findeisen, M. Nielsen, *Department of Solid State Physics, Risø National Laboratory, Denmark*, R. Johnson, and T. Buslaps, *II. Institut für Experimentalphysik, Universität Hamburg, Germany*

Chemisorption of sulphur on metal surfaces has received considerable attention because of the technological importance in catalytic reactions. In some catalytic processes, for example in steam-reforming of hydrocarbons, sulphur acts as a poison on a Ni catalyst, whereas in other reactions like hydrodesulfurization it is a promotor.

The examination of this system was initiated because of an investigation by L. Ruan *et al.*[1], where a missing row model is proposed to account for STM data. Such a reconstruction has never been observed on a close packed metal surface before.

The X-ray diffraction measurements were performed at BW2, HASYLAB. Two series of measurements on this reconstruction gave very similar results. The Patterson function is shown in the figure.

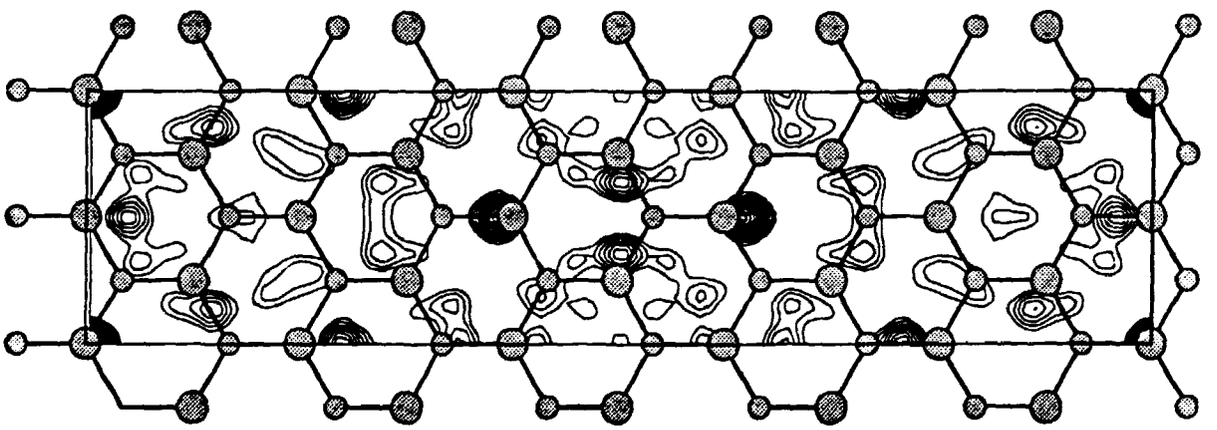

Fig. 1. Contour plot of the experimental Patterson function of Ni(111)(5$\sqrt{3}$×2)-S. The two solid lines are mirror lines.

The experimental results do not seem to confirm the missing row model even though there is some indication of a distorted (111) layer. It also does not support the other proposed model for this system - a pseudo Ni(100)c(2×2)-S overlayer[2]. No detailed model has been found yet - but STM shows that a large amount of Ni (about 80% of a monolayer) is involved in the reconstruction, making the data analysis difficult.

[1] L. Ruan, I. Stensgaard, F. Besenbacher, and E. Lægsgaard, (1993). Phys. Rev. Lett. **71**, 2962.
[2] D.R. Warburton, P.L. Wincott, G. Thornton, F.M. Quinn, and D. Norman, (1989). Surf. Science **211/212**, 71.

1.56 The Cu(111)-S "Zig-zag" Structure Examined by Surface X-ray Diffraction

M. Foss, *Institute for Physics and Astronomy, Aarhus University, Denmark*, R. Feidenhans'l, E. Findeisen, M. Nielsen, *Department of Solid State Physics, Risø National Laboratory, Denmark*, R. Johnson, and T. Buslaps, *II. Institut für Experimentalphysik, Universität Hamburg, Germany*

Two sulphur induced reconstructions exist on Cu(111) - a high ($\sqrt{7} \times \sqrt{7}$R19°) and a low coverage phase (zig-zag)[1]. The high coverage phase was measured by surface X-ray diffraction and a structural model proposed[2] and since the two phases seem to have a very similar structural unit, also the zig-zag structure attracted attention. The low coverage phase is a complicated structure with six domains, which are not describable in Wood's notation but only in matrix notation[1]. The SXRD measurements were performed at BW2, HASYLAB. The Patterson function is shown in the figure.

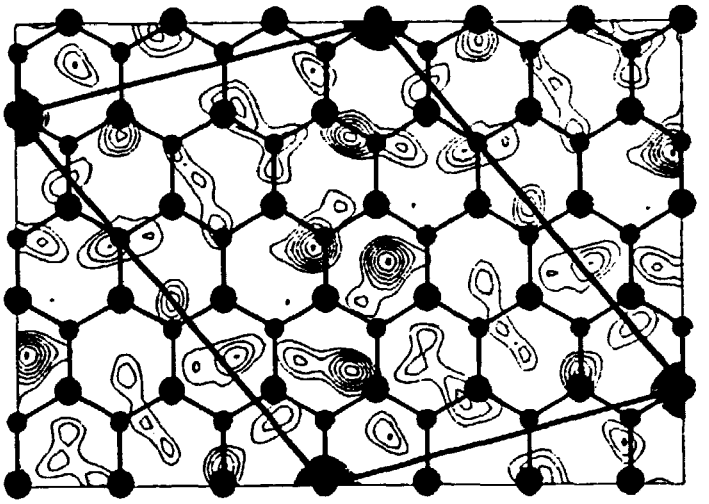

Fig. 1. The contour map of the experimental Patterson function of the Cu(111)-S "zig- zag" structure. The unit cell is indicated by solid lines and the two top layers of Cu has been included.

The structure has not yet been solved. Rod scans show, however, that it is a single layer reconstruction, meaning that sub-surface relaxations probably are small. Also an approximate Cu coverage is known from dynamic visualization scanning tunneling microscopy[1]. The reconstruction has a large unit cell of 17 times the (1×1) unit cell, so more than 100 in-plane integrated intensities were measured. Because of the size of the unit cell and the small number of atoms contributing to the scattering, the intensities were small making the uncertainties large.

[1] L. Ruan, I. Stensgaard, F. Besenbacher, and E. Lægsgaard, (1992). Ultramicroscopy **42-44**, 498.
[2] M. Foss, F. Besenbacher, L. Ruan, I. Stensgaard, E. Findeisen, R. Feidenhans'l, M. Nielsen, T. Buslaps, and R.L. Johnson, (1992). Contribution 1.41 in Risø-R-660(EN).

1.57 Phase Transitions in Di-glyceride Monolayers Studied by Molecular Dynamics Simulation and Synchrotron X-ray Diffraction

G.H. Peters, S. Toxværd, *Department of Chemistry, University of Copenhagen, Denmark*, N.B. Larsen, T. Bjørnholm, K. Schaumburg, *Centre for Interdisciplinary Studies of Molecular Interactions, Department of Chemistry, University of Copenhagen, Denmark*, and K. Kjær, *Department of Solid State Physics, Risø National Laboratory, Denmark*

Lipids are widespread in biological systems forming monolayers, micelles or bilayers in aqueous solution. Recently it has been suggested[1] that phase transitions in lipids may have important regulatory functions in biological systems, leading to enhanced interest in the phase behavior of lipid systems. For the present study we have chosen monolayers of the di-glyceride 1,2-sn-dipalmitoyl-glycerol, $(CH_3(CH_2)_{14}(CO)O\text{-})_2(\text{-}CH_2)(\text{-}CH)CH_2OH$. A layer of 48 molecules (periodic boundary conditions) was simulated for different areas per molecule. The isotherm showed two discontinuities in slope in accordance with experiment. Within the high and medium surface pressure region the lateral ordering of the chains was found to be essentially untilted hexagonal, while the structure of the low surface pressure region was distorted hexagonal, the chains tilting by 13±3°, roughly towards nearest neighbour. A synchrotron X-ray diffraction study of the structure within each region of the isotherm was performed, *cf.* Fig. 1. Analysis of the X-ray diffraction data indicates a chain tilt of 13.5±3° towards nearest neighbours. The good agreement of the simulation results with experiments indicates that the description of interactions used in the computer simulation is adequate for modeling such lipid systems.

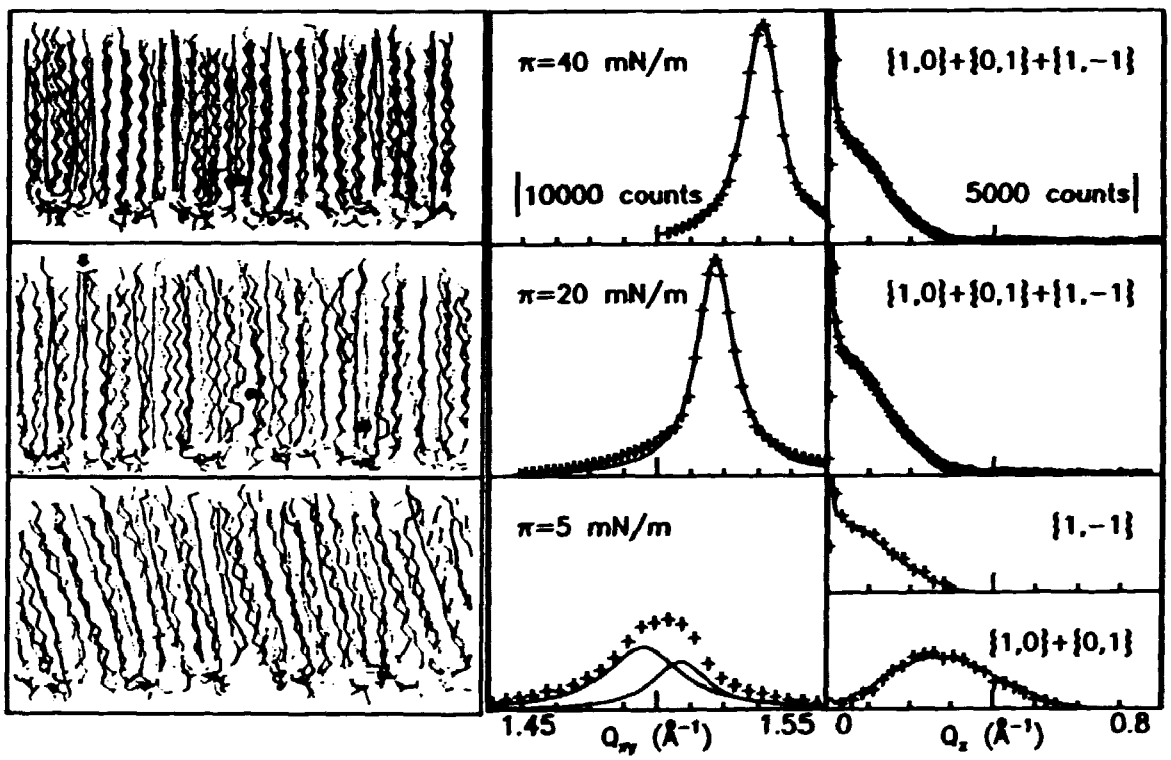

Fig. 1. Left: Side view of simulations. Centre: Diffraction peaks. Right: Bragg rods.

[1] P.K.J. Kinnunen, (1991). Chem. Phys. Lipids 57, 375.

1.58 Langmuir and Langmuir-Blodgett Films of Functionalized Molecules with Cross-sectional Mismatch between Head and Tail

N.B. Larsen, T. Bjørnholm, M. Jørgensen, K. Schaumburg, *Centre for Interdisciplinary Studies of Molecular Interactions, Department of Chemistry, University of Copenhagen, Denmark*, J. Garnæs, *Danish Institute of Fundamental Metrology, Denmark*, J.A.N. Zasadzinski, *Department of Chemical and Nuclear Engineering, University of California, Santa Barbara, USA*, and K. Kjær, *Department of Solid State Physics, Risø National Laboratory, Denmark*

Functionalized surfactant molecules for molecular electronics often have a mismatch between the cross-sectional areas of the head and tail groups. The way these molecules organize in Langmuir-Blodgett films is of vital importance for the possible use of such films in devices. An important parameter in the optimization of the film structure is the degree of molecular reorganization which occurs when the floating monolayers are transferred to solid supports. To gain knowledge about the extent of reorganization to be expected we have investigated the molecular structure of layers of a typical functionalized surfactant (an electron acceptor, see inset of Fig. 1) by synchrotron X-ray diffraction at the water surface and by atomic force microscopy (AFM) of transferred layers. The diffraction peaks, Bragg rods, and a representative AFM image are shown in Fig. 1 with results of the analysis given in the table. Comparison shows that the unit cell expands slightly along both axes at transfer but the shape of the oblique unit cell is retained. The size of the (apparently quite perfect) domains in the transferred film is comparable to the (rather short) coherence length deduced from the widths of the diffraction peaks. In conclusion no major molecular reorganization appears to happen.

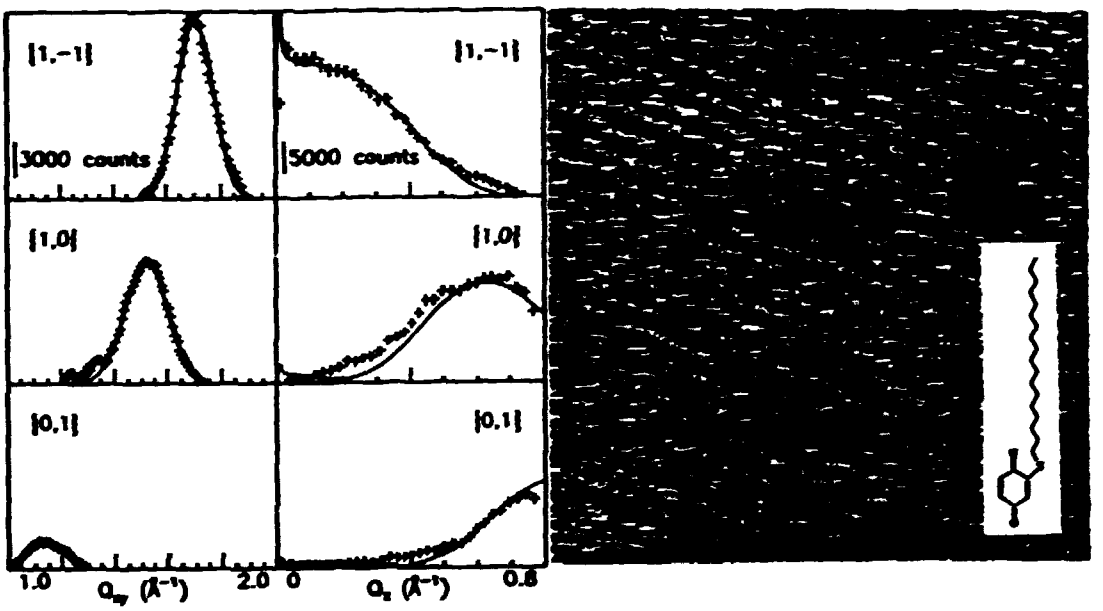

Fig. 1. Left: Diffraction peaks. Centre: Bragg rods. Right: AFM image. Inset: The investigated molecule, with head group about 50 % larger than tail group.

	Unit cell parameters	Tilt angle	Coherence length
Floating monolayer	$a = 0.560$, $b = 0.419$ nm, $\gamma = 80°$	$39 \pm 2°$	$3 - 9$ nm
Transferred film	$a = 0.59$, $b = 0.46$ nm, $\gamma = 82°$	$40 \pm 5°$	$\leq 7 - 20$ nm

1.59 Structure of Relaxed Monolayers of Shorter-chain Alcohols on Water

J. Majewski, M. Lahav, L. Leiserowitz, *Department of Materials and Interfaces, Weizmann Institute of Science, Rehovot, Israel*, J. Als-Nielsen, W. G. Bouwman, and K. Kjær, *Department of Solid State Physics, Risø National Laboratory, Denmark*

Monolayers of alcohols $C_nH_{2n+1}OH$ ($n \geq 16$) nucleate ice in super-cooled water, the efficiency being dependent on the (odd/even) number n of CH_2 groups in the chain and decreasing with shorter chain length[1,2]. Grazing Incidence X-Ray Diffraction (GID) data from monolayers of $C_nH_{2n+1}OH$ ($n = 20, 23, 30, 31$) showed that, in the relaxed state, at temperatures below ~20°C these monolayers spontaneously crystallize and yielded information on their 2D-crystalline properties and packing modes[3]. This was correlated with ice nucleation properties in terms of epitaxial match[2,3] In order to understand the poorer ice nucleating properties of alcohol monolayers on reducing n, and to establish how short a chain would still form a 2D crystal at zero pressure we have examined, by GID, monolayers of $C_nH_{2n+1}OH$ ($n = 18, 16, 14$). The GID patterns for $n = 18, 16, 14$ on water at 5°C (*cf.* Fig. 1) were indexed as the {1,±1} and {0,2} reflections, yielding a rectangular a,b unit cell. The spacing $d_{\{0,2\}}$ increases with decreasing n, in keeping with the results for $n = 20$ to 31[2,3]. Interestingly, for $n = 16$ the {1,±1} and the {0,2} reflections coincide yielding what, without Q_z resolved, might have been interpreted as a hexagonal structure. However, the molecules are tilted along the b axis by an angle of ~16° from the surface normal, breaking the symmetry. We note that for $n = 14$ the $d_{\{0,2\}}$ spacing is longer than $d_{\{1,\pm1\}}$. Thus, there is an increased lattice mismatch to ice with decreasing n, in keeping with the ice nucleation experiments.

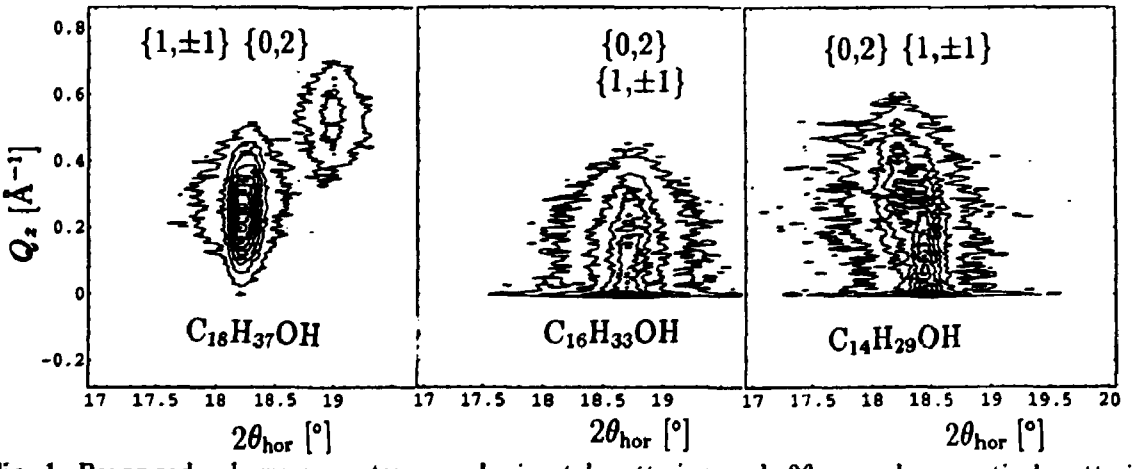

Fig. 1. Bragg rods, shown as contours *vs.* horizontal scattering angle $2\theta_{hor}$ and *vs.* vertical scattering vector Q_z for monolayers of $C_nH_{2n+1}OH$ (n = 18, 16 and 14) at zero pressure on water at 5°C. Note that for $n = 18$ the {1,±1} and {0,2} reflections are resolved, for $n = 16$ they coincide in $2\theta_{hor}$, and for $n = 14$ the {0,2} reflection appears on the lower $2\theta_{hor}$ side of the {1,±1}. Data from beamline BW1, HASYLAB, Hamburg.

[1] M. Gavish, R. Popovitz-Biro, M. Lahav, and L. Leiserowitz, (1990). Science **250**, 973.
[2] R. Popovitz-Biro, J.L. Wang, J. Majewski, E. Shavit, L. Leiserowitz, and M. Lahav, (1993). J. Am. Chem. Soc., *in press.*
[3] J.L. Wang, F. Leveiller, D. Jacquemain, K. Kjaer, J. Als-Nielsen, M. Lahav, and L. Leiserowitz, (1993). J. Am. Chem. Soc., *in press.*

1.60 Grazing Incidence X-Ray Diffraction (GID) Studies of Monolayers of Mixed Amphiphilic Alcohols

J. Majewski, M. Lahav, L. Leiserowitz, *Department of Materials and Interfaces, Weizmann Institute of Science, Rehovot, Israel*, J. Als-Nielsen, W.G. Bouwman, and K. Kjær, *Department of Solid State Physics, Risø National Laboratory, Denmark*

Monolayers of $C_{31}H_{63}OH$ alcohol efficiently nucleate ice in supercooled water, in contrast to monolayers of $C_{20}H_{41}OH$[1]. The structures of these two monolayers in the relaxed state (*e.g.*, 70% coverage of the available surface) at 5°C were determined by Grazing-Incidence X-ray Diffraction (GID)[1], showing that the long chain $C_{31}H_{63}OH$ molecules are aligned almost vertical on the water surface, whereas the $C_{20}H_{41}OH$ are tilted by ~19°. This difference in molecular tilt manifests itself in significantly different dimensions of their rectangular unit cells (a = 5.0 Å, b = 7.45 Å, resp. a = 5.05 Å, b = 8.0 Å). For mixed monolayers of these two compounds we expect a tendency for phase separation because of the loss of intermolecular energy in case of a mixed single phase. Separated phases should be recognizable by their different structures. We have attempted to engineer islands of $C_{31}H_{63}OH$ monolayers of variable size embedded in a sea of $C_{20}H_{41}OH$, to study these systems by GID and to correlate such data with the ice nucleation temperatures induced by the mixed monolayers. The GID patterns for three $C_{20}H_{41}OH$:$C_{31}H_{63}OH$ mixtures are shown in Fig. 1. The GID patterns are presently being analyzed. We observe that, in-between the scattering signatures of pure $C_{31}H_{63}OH$ and pure $C_{20}H_{41}OH$, there is also some high intensity. This intensity is *not* on the locus of a Scherrer ring, and thus cannot be due to a powder of 3D-crystallites of the monolayer material. We have to consider whether it could be caused by (several?) mixed phases showing intermediate 2D-crystal structures.

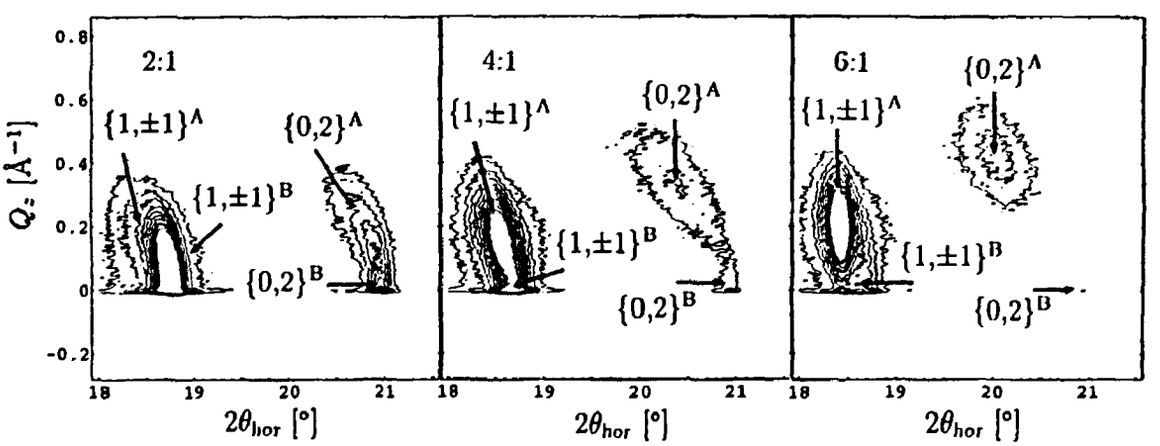

Fig. 1. {1,1} and {0,2} Bragg rods, shown as iso-intensity contours *vs.* horizontal scattering angle $2\theta_{hor}$ and *vs.* vertical scattering vector Q_z for mixed monolayers (in the relaxed state at 5°C) of $C_{20}H_{41}OH$ (A) and $C_{31}H_{63}OH$ (B) amphiphilic alcohols for molar ratios A:B = 2:1, 4:1 and 6:1. The positions of Bragg rods of A and B are indicated by arrows. The $2\theta_{hor}$-resolution was ca. 0.1°.

[1] (a) R. Popovitz-Biro, J. L. Wang, J. Majewski, E. Shavit, L. Leiserowitz, M. Lahav, (1993). J. Am. Chem. Soc., *to appear.* (b) J. L. Wang, F. Leveiller, D. Jacquemain, K. Kjaer, J. Als-Nielsen, M. Lahav, and L. Leiserowitz, (1993). J. Am. Chem. Soc., *in press.*

1.61 Two-dimensional Crystal Structure of a Long-chain Amino Acid

I. Weissbuch, J. Majewski, M. Berfeld, M. Lahav, L. Leiserowitz, *Department of Materials and Interfaces, Weizmann Institute of Science, Rehovot, Israel*, and J. Als-Nielsen, W.G. Bouwman and K. Kjær, *Department of Solid State Physics, Risø National Laboratory, Denmark*

It is known that the packing of water soluble hydrophobic α-amino acids in 3D crystal structures is dominated by a 2D network of hydrogen bonds which link the carboxylate and the amino groups of the zwitterionic molecules. This H-bonding requires a 5.1 × 5.4 Å cell ($\gamma = 113°$) within the molecular layer. For insoluble long chain α-amino acids spread on water, there is an apparent discrepancy between the packing of the chains that require a cross-sectional area of ~18.5 Å^2 and that of the α-amino acid head groups that require ~25 Å^2. We have previously reported[1] the 2D structure of compressed monolayers of N$^\epsilon$-(palmitoyl)-(R) lysine ($CH_3(CH_2)_nCO$-NH-$(CH_2)_4$-$CH(NH3)^+CO_2^-$, n=14). This compound packs in a cell ($a = 5.03$, $b = 5.46$ Å, $\gamma = 117.8°$) of 24.3 Å^2 molecular area, with relatively long N-H···O(amide) bonds along the $a+b$ diagonal and a net of H-bonds between the O(carboxylate)···H-N(amino) groups. To adress the question, whether a longer alkyl chain, with more van der Waals contacts between the CH_2 groups, modifies the packing of the α-amino acid moieties, we have studied monolayers of N$^\epsilon$-(docosanoyl)-(S) lysine, ($n = 20$). Figure 1 shows Grazing-Incidence Diffraction (GID) data for a self-assembled monolayer at 70% coverage, zero surface pressure and 5°C. We assigned the GID peaks as arising from two 2D-crystalline phases of very similar cell dimensions. The diffraction peaks arising from the major phase were assigned as {1,±1} at $q_{xy} = 1.367$ Å^{-1} and {0,2} at q_{xy} =1.583 Å^{-1}, resulting in a rectangular cell of dimensions $a = 5.64$ Å, $b = 7.94$ Å and molecular area 22.4 Å^2. This area is smaller than that observed in the structure of the $n = 14$ compound[1], but still allows a good hydrogen bonding along the 4.87 Å $\frac{1}{2}(a+b)$ cell diagonal. From the Bragg rod data a molecular tilt of 22° along the b axis was deduced. A detailed molecular model was constructed by comparison to 3D crystal structures.

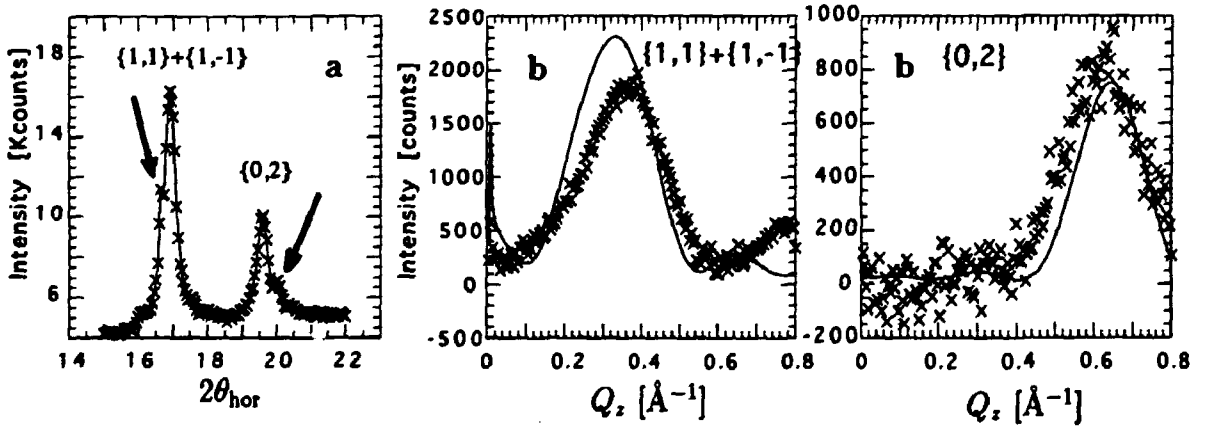

Fig. 1. a) Q_z-integrated intensity *vs.* horizontal $2\theta_{hor}$. The arrows mark the peaks from the minor phase. b) 2θ-integrated intensity *vs.* Q_z.

[1] S. Grayer Wolf, L. Leiserowitz, M. Lahav, M. Deutsch, K. Kjaer, and J. Als-Nielsen, (1987). Nature **328**, 63.

1.62 Controlled Formation of Amphiphilic Amide Multilayers and Monolayers at the Air-liquid Interface

S.P. Weinbach, M. Lahav, L. Leiserowitz, *Department of Materials and Interfaces, Weizmann Institute of Science, Rehovot, Israel*, W.G. Bouwman, J. Als-Nielsen, and K. Kjær, *Department of Solid State Physics, Risø National Laboratory, Denmark*

As part of an ongoing investigation of thin films at the air-liquid interface as models for three-dimensional crystal nucleation and growth we last year reported the spontaneous formation of molecular monolayers and trilayers at air-water and air-formamide interfaces[1,2]. The current work demonstrates the use of "tailor made" additive molecules, which are slightly modified from the bulk material, to control multilayer formation. Uncompressed films of the amphiphile arachidamide ($C_{19}H_{39}CONH_2$) spontaneously form monolayers ($m_{||}$) on water with the hydrocarbon chains parallel to one another and inclined from the vertical. Over formamide subphases, however, two coexisting trilayer phases spontaneously form: $t_\perp$ with the molecules packed in a herringbone pattern in which the planes of the hydrocarbon chains are approximately orthogonal to one another and with the axes vertical, and $t_{||}$ with the chains parallel and tilted relative to the surface normal. The presence of small quantities of modified additive[3] inhibits the formation of trilayers over formamide, resulting in formation primarily of a monolayer ($m_\perp$) with the same packing arrangement as found for the vertically oriented trilayer $t_\perp$.

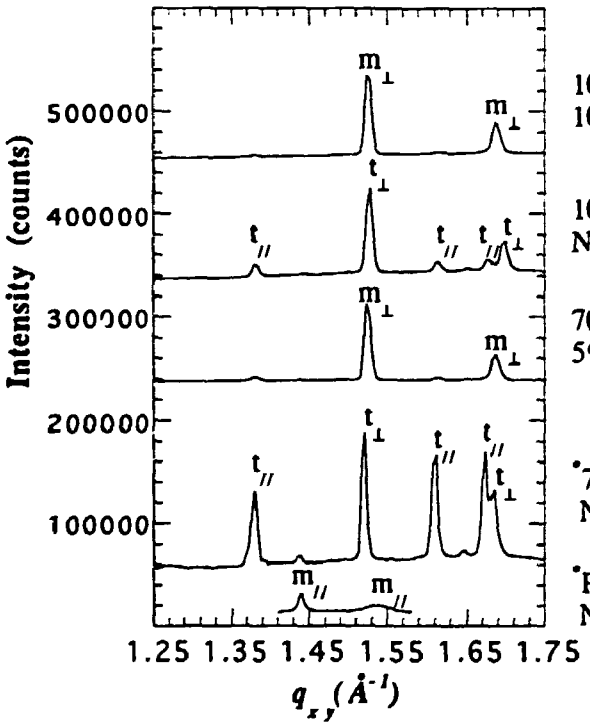

Fig. 1. Grazing incidence X-ray diffraction (GID) patterns for uncompressed arachidamide on water, formamide, and 70 mole% formamide subphases at 5 ± 1°C. The GID patterns are shown for both arachidamide alone and with "tailor-made" additives[3]. The marked (*) data sets were obtained at the undulator beamline Troika, ESRF, Grenoble. All other data were obtained at the undulator beamline BW1, HASYLAB, DESY.

[1] S.P. Weinbach, K. Kjaer, J. Als-Nielsen, M. Lahav, and L. Leiserowitz, (1993). J. Phys. Chem. **97**, 5200.

[2] S.P. Weinbach, D. Jacquemain, F. Leveiller, K. Kjaer, J. Als-Nielsen, and L. Leiserowitz, (1993). J. Am. Chem. Soc. **115**, 11110.

[3] "APA" is the diamide $C_{19}H_{39}CONHC_2H_4CONH_2$; "N-methylamide" is $C_{19}H_{39}CONHCH_3$.

1.63 Spontaneous Formation of Crystalline Multilayers of HO-$C_{22}H_{44}$-OH at the Air/Water Interface Studied by Grazing Incidence X-ray Diffraction

J. Majewski, R. Popovitz-Biro, M. Lahav, L. Leiserowitz, *Department of Materials and Interfaces, Weizmann Institute of Science, Rehovot, Israel*, J. Als-Nielsen, W.G. Bouwman, and K. Kjær, *Department of Solid State Physics, Risø National Laboratory, Denmark*

Induced nucleation of ice by α-ω diols (HO-C_nH_{2n}-OH, $n > 20$) has suggested, in contrast to previous reports[1], that such molecules do not reside bent on the water surface with the two OH groups in the water, but rather form crystalline multilayers on the water surface. This hypothesis was substantiated by various methods including surface pressure-area isotherms, infra red spectroscopy, cryo-electron microscopy, atomic force microscopy and X-ray specular reflectivity. Spontaneous formation of crystalline multilayers was previously observed with other surfactant systems[2] of the type $C_nH_{2n+1}X$ (X = $CONH_2$ or $CONHC_2H_4CONH_2$). Thus we undertook a GID study of the structure of HO-$C_{22}H_{44}$-OH deposited on the water surface for a coverage of 70% of that required to complete a monolayer. The GID measurements were conducted on the liquid surface diffractometer at beamline BW1 at HASYLAB. The GID yielded two Bragg peaks (Fig. 1a). Their Bragg rods (Fig. 1b,c) are so narrow in Q_z that they could be modeled by structure factor calculations only if a partial bilayer is assumed. This is the first example demonstrating crystallinity of a thin film of bifunctional molecules of the type X-C_nH_{2n+1}-X (X is hydrophilic) on the water surface. We note that previous GID studies of mono-alcohols $C_nH_{2n+1}OH$ over water had demonstrated the presence of highly crystalline *monolayers*[3].

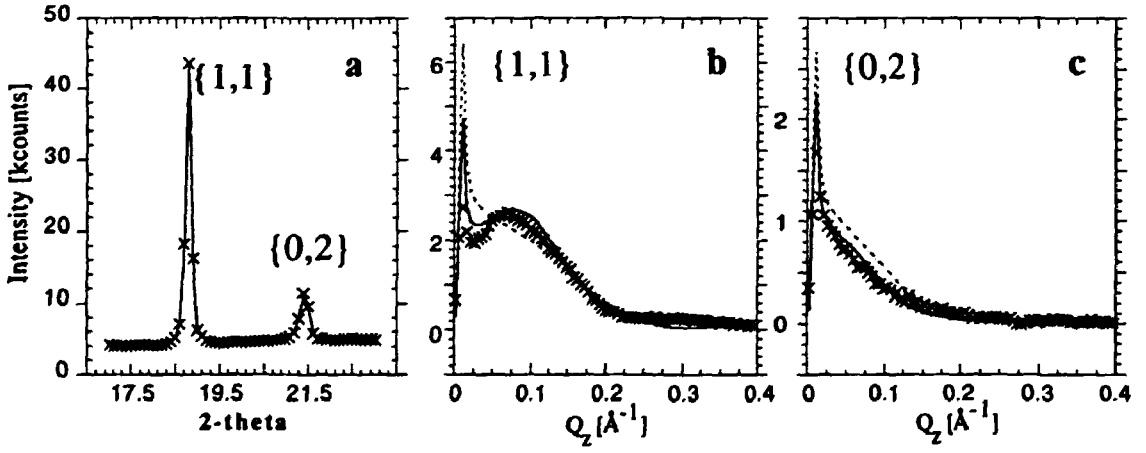

Fig. 1. a) Intensity *vs.* horizontal 2θ at 5°C. The two observed reflections indicate a rectangular unit cell a = 5.0 Å, b = 7.27 Å and area per molecule 18.2 Å^2. b, c) Bragg rod profiles. The full lines were calculated taking into account the presence of bilayer with the molecular occupancy of the top layer ~15%. Molecules were tilted in the direction of the a axis by an angle of 4° and in the direction of the b axis by 1.3°. The dashed lines show the poorer fit when assuming the presence of monolayer only.

[1] M. Ueno, M. Kawanabe, and K. Meguro, (1975). J. Colloid Interface Sci. **51**, 32.
[2] S.P. Weinbach, K. Kjaer, J. Als-Nielsen, M. Lahav, and L. Leiserowitz, (1993). J. Phys. Chem. **97** , 5200.
[3] R. Popovitz-Biro, J.L. Wang, J. Majewski, E. Shavit, L. Leiserowitz, and M. Lahav, (1993). J. Am. Chem. Soc., *in press.*

1.64 Phase-separated Two-component Monolayer Systems

I. Weissbuch, J. Majewski, M. Lahav, L. Leiserowitz, *Department of Materials and Interfaces, Weizmann Institute of Science, Rehovot, Israel*, J. Als-Nielsen, W.G. Bouwman, and K. Kjær, *Department of Solid State Physics, Risø National Laboratory, Denmark*

The 2D structure of mixed Langmuir monolayers designed to undergo spontaneous phase separation was studied, *in situ*, as a function of their composition. Such mixtures are used as models simulating structured "nuclei" to induce oriented 3-D crystallization and are part of a long-range study directed towards a determination of the structural and size requirements for nucleation of 3D crystals. The two components were Eicosanoamide, $CH_3(CH_2)_{18}CONH_2$ (1), forming the matrix to which N-(triacontanoyl)-aminopropionic acid, $CH_3(CH_2)_{28}CONH(CH_2)_2COOH$ (2), was added in various proportions. This monolayer mixture was expected to form separated crystalline domains due to the large difference in length of the aliphatic chains above the amide (CONH) group and due to favourable interactions between the $(CH_2)_2$ spacers below the amide group and either hydrogen-bonding or metal ions binding to the carboxylate groups of the component 2 as already reported for another system[1]. However, the common feature of the two molecules is their amide group which is believed to ensure phase continuity between the separated domains by hydrogen bonding. Grazing-Incidence Diffraction (GID) patterns of monolayer mixtures are shown in Fig. 1. The GID patterns (a) and (d) are similar: The minor component, 2, forms domains still visible at 10% concentration and of coherence length as low as ~50 Å (peak at $2\theta_{hor} = 20.43$). However, for (b) and (c) the influence of the Cd^{2+} ions bound to component 2 is remarkable. The banana-shaped feature could be interpreted in terms of a gradual change of tilt and spacing of type-1 domains that must adjust in order to ensure structural continuity. However, it must be noted that the "banana" is on the locus expected for a Scherrer ring from a powder of 3D crystallites. Also X-ray reflectivity showed evidence of partial multilayer formation. The data require further analysis.

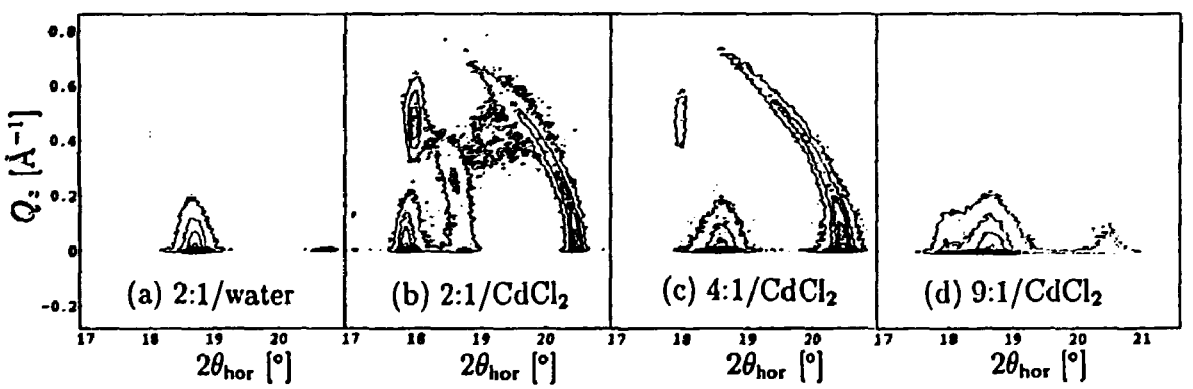

Fig. 1. GID intensity *vs.* (horizontal) $2\theta_{hor}$ and *vs.* (vertical) Q_z for mixed monolayers of molar ratios: (a) 2:1 on water; (b) 2:1 on 1mM $CdCl_2$; (c) 4:1 on 1mM $CdCl_2$; (d) 9:1 on 1mM $CdCl_2$, at 5°C.

[1] I. Weissbuch, J. Majewski, K. Kjaer, J. Als-Nielsen, M. Lahav, and L. Leiserowitz, (1993). J. Phys. Chem. **97**, 12848.

1.65 The Adsorption of Molecular Polymer Layers to Lipid Monolayers

M. Lösche, G. Brezesinsky, *Institut für Physikalische Chemie*, and T. Bohanon, *Institut für Organische Chemie, Johannes-Gutenberg-Universität, Mainz, Germany*, W.G. Bouwman, and K. Kjær, *Department of Solid State Physics, Risø National Laboratory, Denmark*

The adsorption of polymers to monolayers of fatty acids on aqueous polymer solutions has been studied by X-ray reflectivity and grazing incidence diffraction measurements. Preliminary evaluation of the reflectivity measurements hints that the polymer, poly(ethylene imine) (PEI, ~40 monomers), does adsorb to a floating surface monolayer of stearic acid in a molecular thin film. Since the electron density of PEI differs only slightly from that of water, the effect of the polymer on the reflectivity is however marginal. Nonetheless surface isotherms suggest that the phase diagram of fatty acid monolayers is drastically different on water subphases and on polyelectrolytic solutions[1]. A much clearer indication of the presence of a polymer layer at the interface comes from diffraction data obtained from such systems *in situ* (see Fig. 1), which indicate that the microscopic monolayer structure on polymeric counterion solutions is quite different from that observed on pure water[2,3]. In particular, the data seem to suggest the formation of a triclinic lattice of the fatty acid's hydrophobic tails. A more elaborate evaluation is pending.

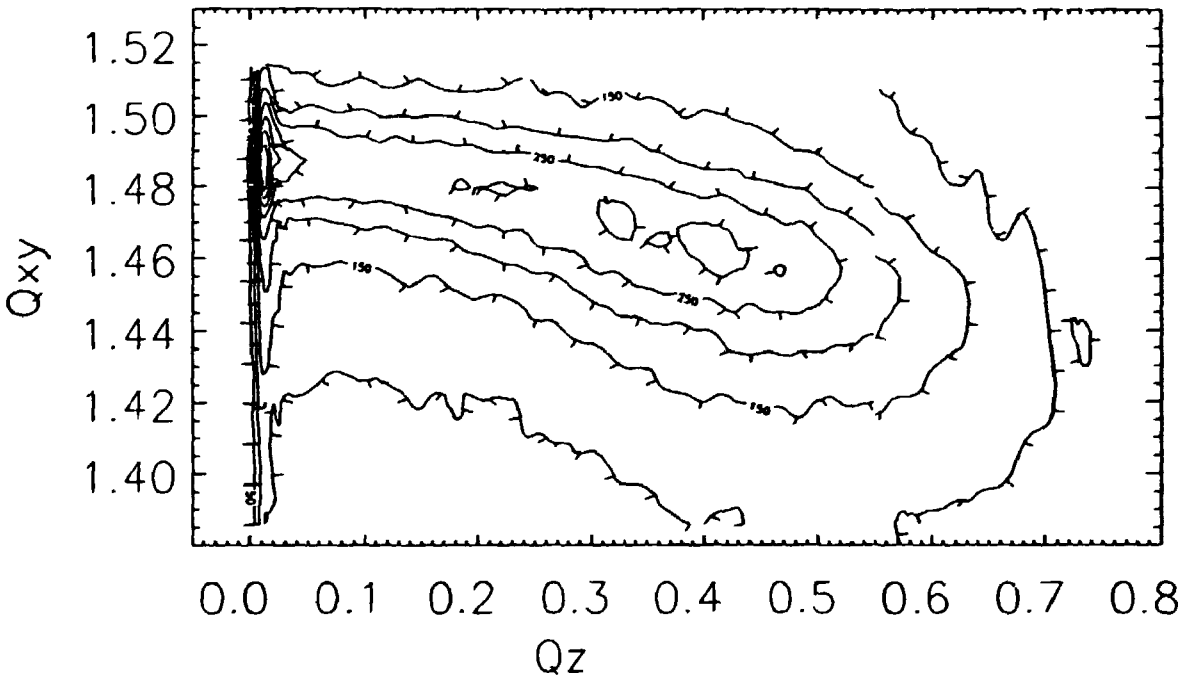

Fig. 1. Contour plot of the diffracted x-ray intensity from the system investigated. Q_z and Q_{xy} are the vertical and horizontal components of the scattering vector, respectively.

[1] L.F. Chi, R.R. Johnston, and H. Ringsdorf, (1991). Langmuir **7**, 2323.
[2] R.M. Kenn, C.Böhm, A.M. Bibo, I.R. Peterson, H. Möhwald, J. Als-Nielsen, and K. Kjær, (1991). J. Phys. Chem. **95**, 2092.
[3] D. Jacquemain, S. Grayer Wolf, F. Leveiller, M. Deutsch, K. Kjær, J. Als-Nielsen, M. Lahav, and L. Leiserowitz, (1992). Angew. Chemie. Int. Ed. Engl. **31**, 130.

1.66 Influence of Chirality on the Structure of a Diol Monolayer

G. Brezesinski, H. Möhwald, *Institut für Physikalische Chemie, Johannes-Gutenberg-Universität, Mainz, Germany*, R. Rietz, *Physical Chemistry Department, Halle University, Germany*, W.G. Bouwman, and K. Kjær, *Department of Solid State Physics, Risø National Laboratory, Denmark*

3-Alkoxy-propane-1,2-diols (*e.g.*, $C_{16}H_{33}O\text{-}CH_2\text{-}CHOH\text{-}CH_2OH$) may be looked upon as the parent compounds of the large family of phosphatidylcholines. One of the influences on the packing of the monolayer is certainly the head group, as a result both of steric hindrance and of its specific interactions with the monolayer environment. In the present study we have reduced the lipid head group to the glycerol backbone with a chiral center at the C-2 carbon atom. Fluorescence measurements have shown that above the main transition from a liquid-expanded to a condensed phase domains with a polygonal shape appear. On further compression shape instabilities occur. While the spirals of the enantiomer turn only in one direction, the spirals arising from one domain of the racemate exhibit opposite handedness. This behavior is explained by a separation of enantiomers on the molecular level[1]. In order to further understand the influence of chirality on the monolayer structure the condensed monolayer phases have been investigated by means of Grazing Incidence X-ray Diffraction (GID) measurements using the liquid-surface diffractometer at beamline BW1 in HASYLAB, Hamburg. Figure 1a shows the results for the chiral resolved (R) compound at 20°C and a lateral pressure well above the main transition. Three diffraction peaks at Q_{xy}=1.43 Å^{-1}, Q_{xy}=1.39 Å^{-1} and Q_{xy}=1.31 Å^{-1} could be observed. All three peaks have their maximum at non-zero Q_z. For the racemic compound only two peaks at Q_{xy}=1.42 Å^{-1} and Q_{xy}=1.32 Å^{-1} could be resolved under the same conditions (Fig. 1b). This behavior is similar to that observed for DPPE monolayers[2] where a rectangular cell was found in the case of the racemate and a symmetry reduction to an oblique cell for the enantiomer. The data are currently being evaluated.

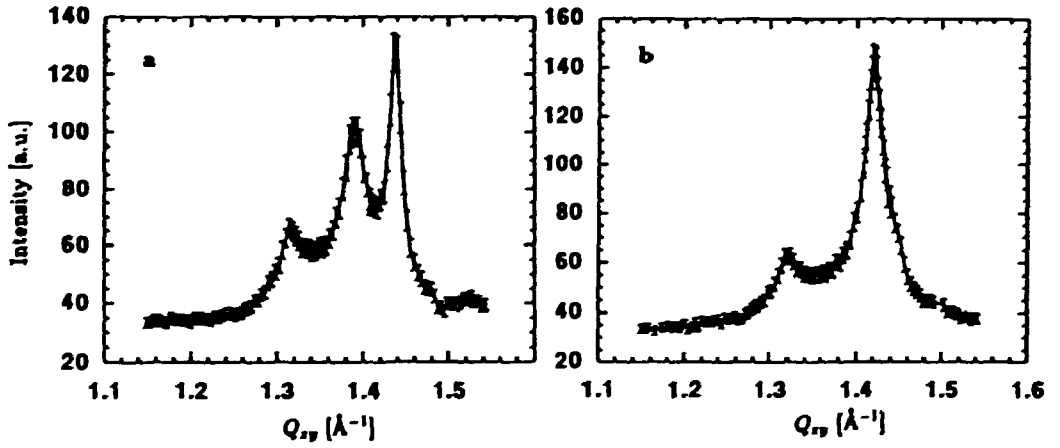

Fig. 1. GID data for monolayers of (a) chiral resolved and (b) racemic $C_{16}H_{33}O\text{-}CH_2\text{-}CHOH\text{-}CH_2OH$ on water.

[1] R. Rietz, G. Brezesinski, and H. Möhwald, (1993). Ber. Bunsenges. Phys. Chem. **97**, 1394.

[2] C. Böhm, H. Möhwald, L. Leiserowitz, J. Als-Nielsen, and K. Kjaer, (1993). Biophys. J. **64**, 553.

1.67 Condensed Phases in Monolayers of Double-chain Lecithins on Water

A. Dietrich, G. Brezesinski, B. Struth, H. Möhwald, *Institut für Physikalische Chemie, Johannes-Gutenberg-Universität, Mainz, Germany*, F. Bringezu, *Department of Pharmacy, Halle University, Germany*, W.G. Bouwman, and K. Kjær, *Department of Solid State Physics, Risø National Laboratory, Denmark*

Phospholipids consist of two hydrophobic chains which are linked via an ether- or an ester-bond to a hydrophilic head group. The mixed ester- and ether-linked lecithins (PCs) are the first members in the homologous series of monobranched PCs[1]. Investigation of the bulk phases of aqueous lipid dispersions shows that the chain linkage has a strong influence on the structure of gel phases. Therefore we have investigated monolayers of two mixed-linked PCs 1P-2H-PC (1-palmitoyl-2-hexadecyl-phosphatidylcholine) and 1H-2P-PC (1-hexadecyl-2-palmitoyl-phosphatidylcholine). Figure 1 shows the Grazing-Incidence X-ray Diffraction (GID) results, obtained with the liquid-surface diffractometer at beamline BW1 in HASYLAB, for monolayers of 1H-2P-PC on water at 15°C and surface pressures of 27 mN/m and 41 mN/m. The GID results for 1P-2H-PC are qualitatively similar. One Bragg peak has its maximum at $Q_z = 0$ Å^{-1} whereas the intensity of the second peak extends in the region $0.5 < Q_z < 0.9$ Å^{-1}. By indexing the peak at high Q_z as the $\{1,\pm1\}$ reflections and the peak at $Q_z = 0$ Å^{-1} as the (0,2) reflection of a rectangular unit cell with the chains tilted towards their nearest neighbours, a molecular tilt of the hydrocarbon chains can be calculated from the maximum position in Q_z for the $\{1,\pm1\}$ peak of 29° (1P-2H-PC) and of 31° (1H-2P-PC) at a lateral pressure of 27 mN/m and of 25° and 26°, respectively, at 41 mN/m. The cross-sectional area normal to the molecular axis amounts to 0.206 nm^2 and 0.203 nm^2, respectively, which indicates that molecular rotation of the chains about their long axes is possible. A more detailed structure analysis is under way.

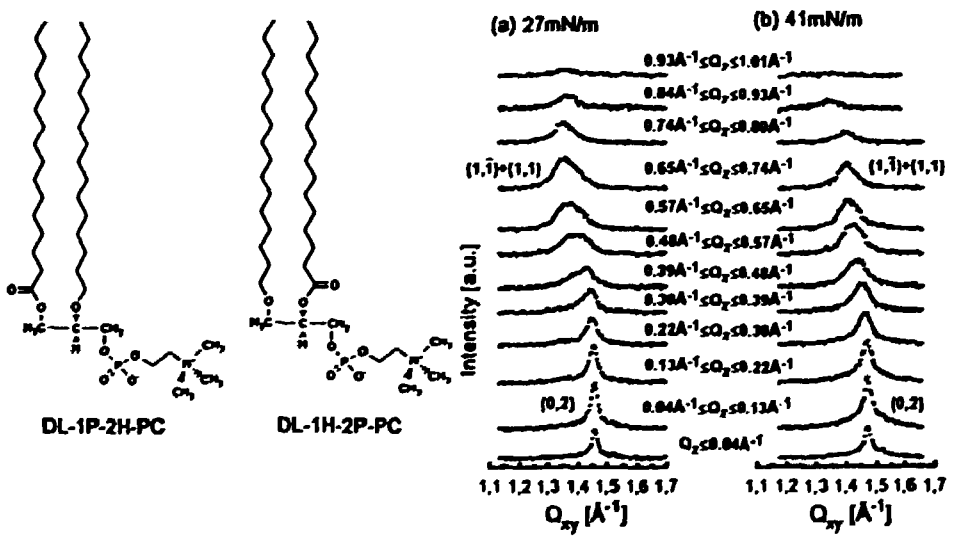

Fig. 1. Structural formulas of both lecithins (left) and GID data (intensity versus horizontal momentum transfer Q_{xy}), partially resolved in the vertical momentum transfer Q_z, of 1H-2P-PC at 15°C.

[1] A. Dietrich, H. Möhwald, W. Rettig, and G. Brezesinski, (1991). Langmuir 7, 539.

1.68 Influence of Changes in the Hydrophobic Region on the Monolayer Structure of Lecithins

G. Brezesinski, A. Dietrich, B. Struth, H. Möhwald, *Institut für Physikalische Chemie, Johannes-Gutenberg-Universität, Mainz, Germany*, F. Bringezu, *Department of Pharmacy*, and R. Rietz, *Physical Chemistry Department, Halle University, Germany*, W.G. Bouwman, and K. Kjær, *Department of Solid State Physics, Risø National Laboratory, Denmark*

Branched-chain phospholipid monolayers are model systems for the study of biological membranes. Variation of the positions and lengths of the hydrophobic side branches can change intermolecular interactions as well as the relative sizes of the hydrophobic and the hydrophilic moieties. Due to the side chains the area per molecule is larger than that required by the head group, in contrast to the situation for nonbranched lecithins. Introduction of long chain branches in the 2-position of one or both main chains leads to a triple- or quadruple-chain lipid. Branched-chain lipid monolayers at the air-water interface have been investigated by means of Grazing-Incidence X-ray Diffraction (GID) at beam-line BW1 in HASYLAB. For the triple-chain lecithin the analysis of the Bragg rod profiles parallel and perpendicular to the surface indicates three different ordered phases. On increasing the lateral pressure at different temperatures the hydrocarbon chains form tilted phases with a tilt toward the nearest neighbours and eventually a hexagonal lattice with vertical chain orientation[1]. Figure 1 shows GID results for a quadruple-chain phosphatidylcholine at 15°C and lateral pressures of 21 mN/m and 33.7 mN/m. In both cases one sharp diffraction peak with a d spacing of 4.25 Å is apparent, indicating a hexagonal packing. The maximum intensity in the Q_z-resolved scan occurs in the plane of the water surface ($Q_z = 0$ Å^{-1}) extending to $Q_z = 0.3$ Å^{-1}, indicating a nearly vertical chain orientation. The cross section per chain amounts to 0.208 nm^2 characteristic for a rotator phase.

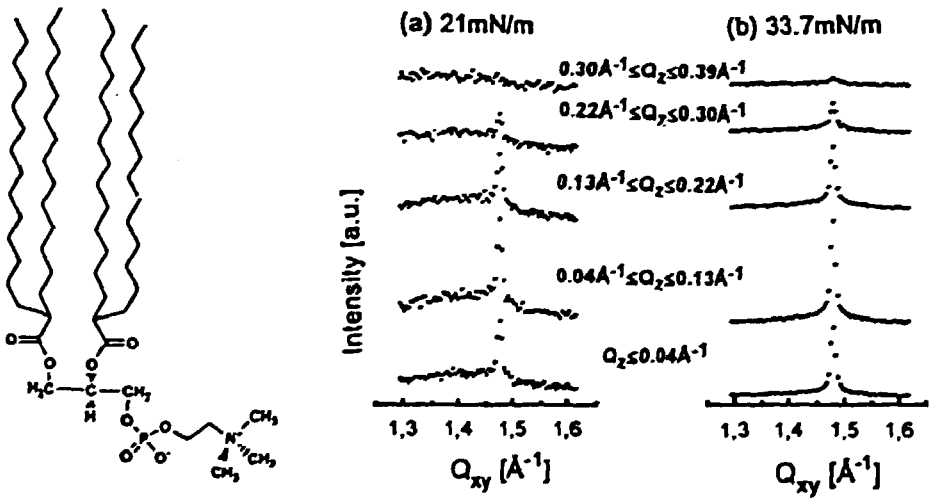

Fig. 1. Structural formula (left) and GID data (intensity versus horizontal momentum transfer Q_{xy}) of the monolayers of the quadruple-chain lipid 1,2-di(2-tetradecyl-palmitoyl)-phosphatidylcholine at 15°C. Data are shown partially resolved in the vertical momentum transfer Q_z.

[1] G. Brezesinski, C. Böhm, A. Dietrich, and H. Möhwald, (1994). Physica B, *in press.*

1.69 A New Phase Transition in a Fatty Acid Monolayer on Water

I.R. Peterson, R.M. Kenn, A. Goudot, P. Fontaine, F. Rondelez, *Institut Curie, Paris, France*, W.G. Bouwman, and K. Kjær, *Department of Solid State Physics, Risø National Laboratory, Denmark*

Although monolayers of fatty acids on the surface of water have been investigated since the beginning of the century, Grazing-Incidence X-ray Diffraction (GID) measurements[1] have proved that their phase behaviour is much richer than previously thought: up to now, seven distinct phases could be identified. For monolayers of Eicosanoic Acid ($CH_3(CH_2)_{18}COOH$), in what was first thought to be *one* nearest-neighbour(NN)-tilted phase an axial order–disorder transition was indicated by comparison of two such studies[1,2] and is predicted by a recent theory[3]. The present measurements had two aims: (1) to complete previous data, characterizing the separate thermodynamic contributions from the headgroup and chain[4] and (2) to determine the temperature variation of the molecular packing across the axial order–disorder transition. Figure 1 shows GID data from a typical run. The pattern of two broad reflections, one in the plane and one above of it, is characteristic for NN–tilted hexatic phases. Initial evaluation of the data shows that the details of the order–disorder transition are not as expected. At low pressures, the transition temperature is considerably higher than previously found[2]. Although the transition was thought to be first order, the variation of the out–of–plane reflection with surface pressure appears to be continuous.

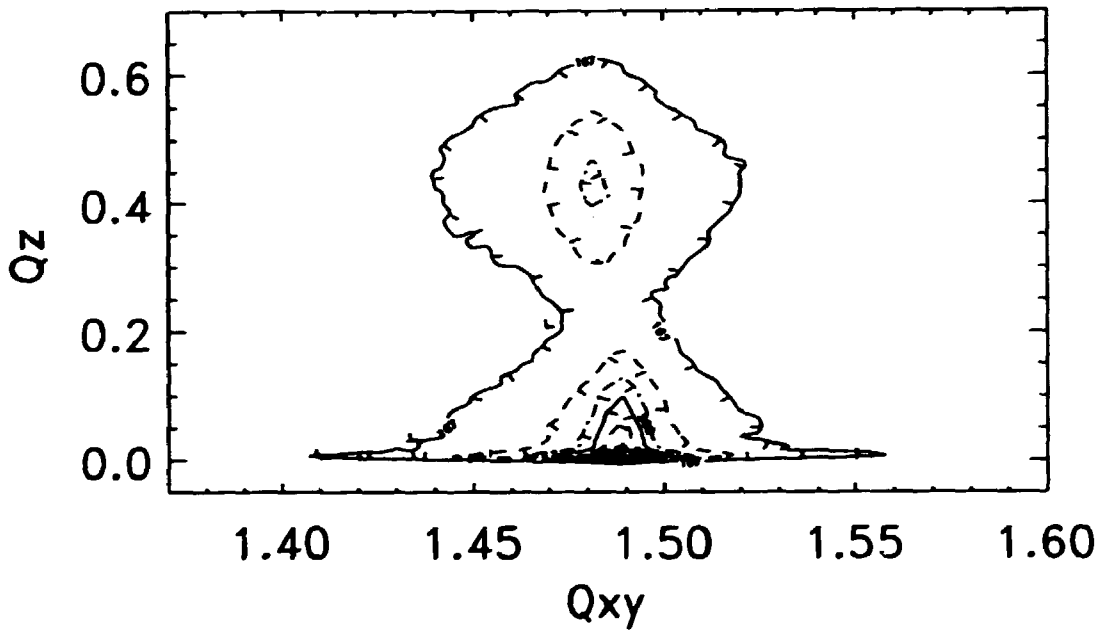

Fig. 1. GID intensity-contours in reciprocal space at 23°C and surface pressure Π=15mN/m. (Q_{xy},Q_z) are the (horizontal,vertical) components of the scattering vector.

[1] R. M. Kenn, C. Böhm, A. M. Bibo, I. R. Peterson, H. Möhwald, J. Als-Nielsen, and K. Kjær, (1991). J. Phys. Chem. **95**, 2092.
[2] P. Tippmann-Krayer and H. Möhwald, (1991). Langmuir **7**, 2303.
[3] V. M. Kaganer and E. B. Loginov, (1993). Phys. Rev. Lett. **71**, 2599.
[4] I. R. Peterson, V. Brezezinski, R. M. Kenn, and R. Steitz, (1992). Langmuir **8**, 2995.

1.70 Tilted Structures in Monolayers of Fluorinated Molecules

A. Goudot, I.R. Peterson, P. Fontaine, R.M. Kenn and F. Rondelez, *Institut Curie, Paris, France*, W.G. Bouwman, and K. Kjær, *Department of Solid State Physics, Risø National Laboratory, Denmark*

Perfluorinated carbon chains, in contrast to hydrogenated chains, are almost free of gauche defects. In monolayers of hydrogenated amphiphiles (carboxylic acids, alcohols or phospholipids) at the air-water interface these gauche defects have often been believed to be important for the structural behaviour of monolayers[1], but this has never been clearly evidenced. Investigation of the structures exhibited by monolayers of fluorinated linear molecules and comparison to those of hydrogenated molecules can therefore bring interesting insight into the physics of these quasi-2D systems. The structures and molecular orientations in the "liquid condensed" part of the phase diagram of the perfluorinated acid $C_{11}F_{23}COOH$ have recently been studied by both molecular dynamics simulations[2] and X-ray scattering experiments (grazing incidence diffraction (GID)[3] and reflectivity[4]. The results obtained were quite contradictory: Whereas the X-ray diffraction and some simulations indicated that the molecules were normal to the water surface, other simulations and the X-ray reflectivity lead to the conclusion that this system does exhibit a tilted phase. The aim of this study was to clarify the situation on this compound by use of the high-brilliance X-ray source BW1 in HASYLAB at DESY, Hamburg. In Fig. 1 a splitting of the peak can be observed, indicating a break of the hexagonal symmetry by a uniform molecular tilt by *ca.* 10° towards nearest neighbours. By contrast, in monolayers of the related molecule $C_{10}F_{21}CH_2COOH$, no tilted phase was found.

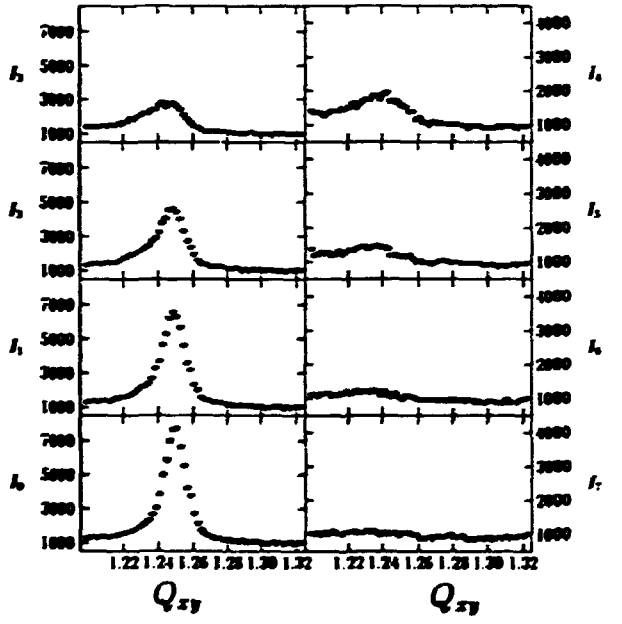

Fig. 1. GID intensity *vs.* horizontal scattering vector Q_{xy} for a monolayer of $C_{11}F_{23}COOH$ at a molecular area of 44 Å^2 and a lateral pressure of 6 mN/m. The data are shown partially resolved in vertical scattering vector Q_z: I_0 to I_7 are the intensities for consecutive Q_z-intervals of $\simeq 0.08$Å^{-1}.

[1] D. Andelman, F. Brochard, C. Knobler, and F. Rondelez, (1993). In: Modern Ideas and Problems in Amphiphilic Science, M. Gelbert, D. Roux and A. B. Shoul, eds., *in press.*

[2] S. Shin, N. Collazo, and S. A. Rice, (1993). J. Chem. Phys. **98**, 3469, and **96**, 4735.

[3] A. A. Acero *et al.*, (1993). J. Chem. Phys. **99**, 7214.

[4] A. Goudot, (1993). These de doctorat, Universite Paris VI.

1.71 Microscopic Structure of a Polymerizable Langmuir Monolayer

P. Fontaine, A. Goudot, I.R. Peterson, R.M. Kenn, F. Rondelez, *Institut Curie, Paris, France*, W.G. Bouwman, and K. Kjær, *Department of Solid State Physics, Risø National Laboratory, Denmark*

Polymerizable Langmuir monolayers of Octadecyltrimethoxysilane ($CH_3(CH_2)_{17}Si(OCH_3)_3$) have been studied by means of Grazing-Incidence X-ray Diffraction (GID). These molecules undergo chemical reactions on contact with water: First, hydrolysis according to

$$CH_3(CH_2)_{17}Si(OCH_3)_3 + 3H_2O \rightarrow CH_3(CH_2)_{17}Si(OH)_3 + 3CH_3OH$$

Second, cross-linkage according to

$$nCH_3(CH_2)_{17}Si(OH)_3 \rightarrow CH_3(CH_2)_{17}Si(OH)_2\text{-}O\text{-}CH_3(CH_2)_{17}Si(OH)_2\text{-}O\text{-}\ldots$$

The second step is *pH*-dependent. The final result is a 2D-polymer network adsorbed at the air-water interface.

A GID experiment was performed at beam-line BW1 in HASYLAT at DESY, Hamburg with the aim of characterizing the microscopic structure of the polymerized state, and to study the structural changes induced by surface pressure and temperature. The data obtained at $pH=2$ are consistent with a hexagonal structure in the final state of the monolayer. The molecules are vertical at all temperatures (20-30°C) and surface pressures (0.5, 5, 10, 15, 20 mN/m). Thus the results seem to indicate that these monolayers are close-packed. Further, this structure is preserved on variation of temperature and surface pressure, indicating that a kind of "gelation" has occurred in the system, as expected in case of formation of a polymerized network.

1.72 Internal Structure of Electrostatically Adsorbed Polyelectrolyte Films

M. Lösche, J. Schmitt, T. Grünewald, G. Decher, *Institut für Physikalische Chemie, Johannes-Gutenberg-Universität, Mainz, Germany*, P.S. Pershan, W.G. Bouwman, and K. Kjær, *Department of Solid State Physics, Risø National Laboratory, Denmark*

The internal structure of ultrathin polymer films deposited by sequential adsorption of alternately charged polyelectrolyte layers to Silicon wafers has been characterized by neutron and X-ray reflection. These polymer films are novel materials for which macroscopic properties may be custom tailored via the control of their structure on the molecular length scale. Such a sample is prepared by dipping a Si wafer, which is surface charged by coating with a molecular layer of butyl-aminosilane, into an aqueous solution of a polyanion, polystyrene sulfonate (PSS). This results in the deposition of an ultrathin layer of the polyelectrolyte, accompanied by charge reversal of the functionalized surface. Upon immersion into a polycationic solution (polyallylamine hydrochloride, PAH), a second polyelectrolyte layer is deposited and the surface charge is again reversed. Cycling between the two solutions leads to the growth of a polymer multilayer film. X-ray and neutron reflectivity investigations of such samples, into which perdeuterated polyelectrolyte components were incorporated, showed that the process leads to materials that are well organized on the molecular length scale, as they retain their stratified structure[1]. The molecular composition of the films could be assessed in terms of polymer concentration at the interface and content of water and inorganic counter-ions. The roughnesses of external and internal interfaces have been determined; the internal roughness is significantly larger than that of the external interface leading to a quantitative estimate of the interdigitation of polymer segments between neighbouring layers. The interaction of the polymer with the substrate is different from the interaction between adjacent polymer layers, leading to a smaller layer thickness close to the Si wafer than far from it, where the thickness attains an equilibrium value.

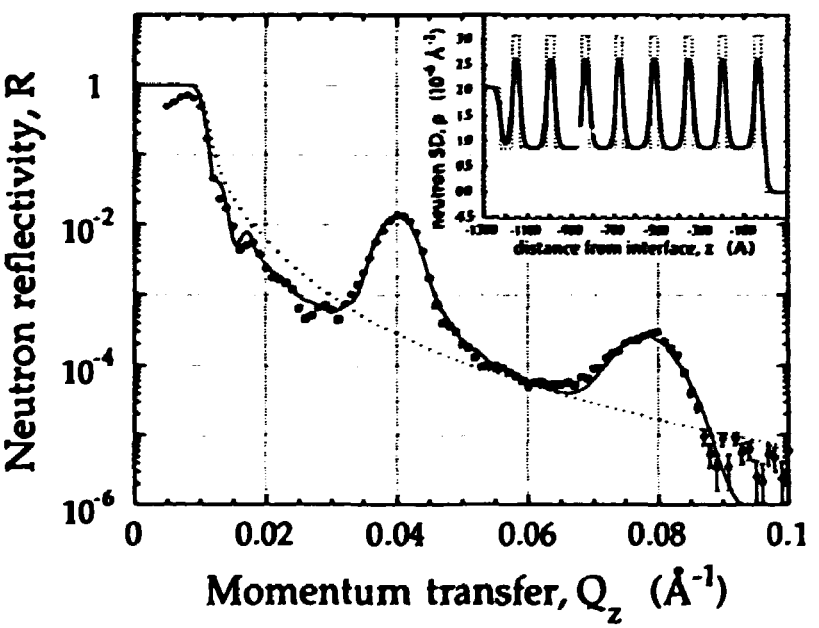

Fig. 1. Neutron reflectivity of a 48-layer polymer film on a Silicon wafer. The sample consisted of a 6-layer superlattice of deuterated and protonated polymer films (8 repeat units).

[1] J. Schmitt, T. Grünewald, G. Decher, P.S. Pershan, K. Kjaer, and M. Lösche, (1993). Macromolecules **26**, 7058.

1.73 Interfacial Melting (?) at an Ice/Silicon Interface

A. Lied, H. Dosch, *Sektion Physik der Universität München, München, Germany*, J. H. Bilgram, ETH Zürich, Switzerland, and K. Kjær, *Department of Solid State Physics, Risø National Laboratory, Denmark*

Interfacial melting of ice on different substrates plays an important role in our everyday lives, *e.g.*, frost heave or skiing and skating. The neutron is an ideal probe for studying buried interfaces because it is absorbed only weakly by many materials. Silicon is a favourable material to start with because it is wetted by water or ice. By neutron reflectivity we have investigated the interface of a (100) D_2O single crystal frozen onto a Si (111) wafer. The experiment was performed in the following way: A cold neutron beam passes through the edges of the Silicon substrate and hits the interface under a glancing angle α_i (*cf.* Fig. 1, insert). The transmission of the 10 cm diameter Silicon wafer is *ca.* 80% at a wavelength of 4.3 Å. Due to the rather large scattering length density of D_2O, total reflection occurs at the Si-ice interface ($n_{D_2O} < n_{Si}$) for neutron incidence angles α_i less than the critical angle α_c which is given in this geometry by

$$\alpha_c = \cos^{-1}\left(\frac{n_{D_2O}}{n_{Si}}\right) \simeq \sqrt{2(n_{D_2O} - n_{Si})}\,.$$

In principle, reflectivity data allow to determine the scattering length density profile perpendicular to the interface. Figure 1 shows reflectivity data for two different temperatures. The low temperature curve can be theoretically reproduced by the (independently determined) roughness and wavyness parameters of the silicon surface. This indicates that the interface is rather perfect. Closer to the bulk melting point T_m the higher reflectivity observed at large α_i speaks in favour of a denser interfacial layer between the ice and the Si. With a detailed analysis of the data it should be possible to calculate the density of the interfacial region. This is currently under way.

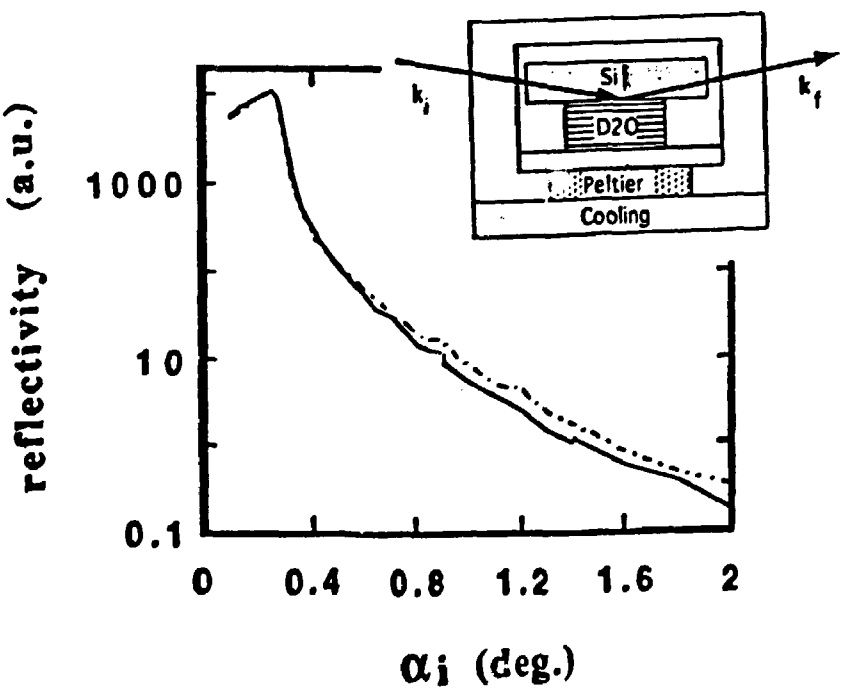

Fig. 1. Neutron reflectivity data from a D_2O-silicon interface at (full line) $T_m - T = 26$ K and (dashed line) $T_m - T = 0.31$ K. The insert shows the scattering geometry.

1.74 Confined Motion in the Amorphous Regions of Partially Crystalline Polyethylene

B. Holzer, G. Strobl, and B. Stühn, *Department of Physics, University of Freiburg, Germany*, and N.H. Andersen, *Department of Solid State Physics, Risø National Laboratory, Denmark*

The glass transition in amorphous polymers as well as in low molecular weight glass forming liquids is known to be accompanied by a fast relaxation process besides the α-relaxation, which is the relaxation that actually becomes infinitely slow below the glass transition temperature, T_G. The detailed molecular mechanism underlying the fast process is still unknown[1]. It is believed to be a localized diffusion in a cage ('cage process').

We investigated the cage process in partially crystalline polyethylene (PE) with incoherent and coherent quasielastic neutron scattering. Thus we are able to determine the relaxation times and the spatial extension of motion. In the incoherent experiment the process showed up as a quasielastic contribution to the elastic part in the range of energy transfer 0.2-0.3 meV (FWHM), and is activated around the glass transition temperature T_G. The linewidth turns out to be independent of q (0.5 Å^{-1} $\leq q \leq$ 2 Å^{-1}) and is nearly independent of the temperature (see Fig. 1). Only the intensity increase with the temperature. The spatial extension can be determined by analysing the q-dependence of the elastic line (Debye-Waller Factor) and the mean squared displacements $\langle u^2 \rangle$ turns out to be in the range of 1-4 Å (see Fig. 2). The coherent dynamic structure factor of deuterated PE (d-PE) was measured in the regime of the halo caused by interchain interference (1.1 Å^{-1} $\leq q \leq$ 2 Å^{-1}). In addition to the unresolved elastic line, there exists a quasielastic contribution of 0.2 meV (FWHM). The width is independent of q and nearly identical to the value obtained in the incoherent experiment.

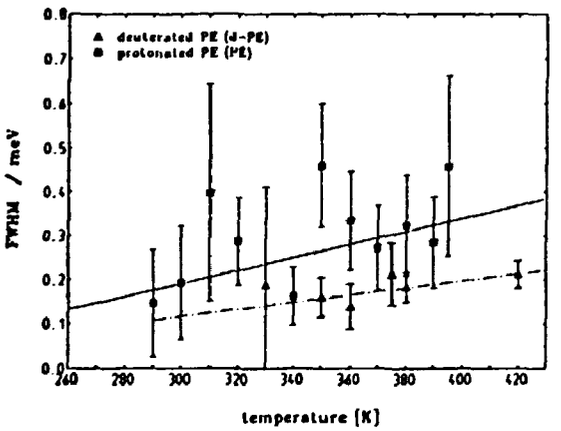

Fig. 1. Temperature dependence of relaxation rate for PE and d-PE cage mode: q = 2 Å^{-1} for PE and q = 1.3 Å^{-1} for d-PE.

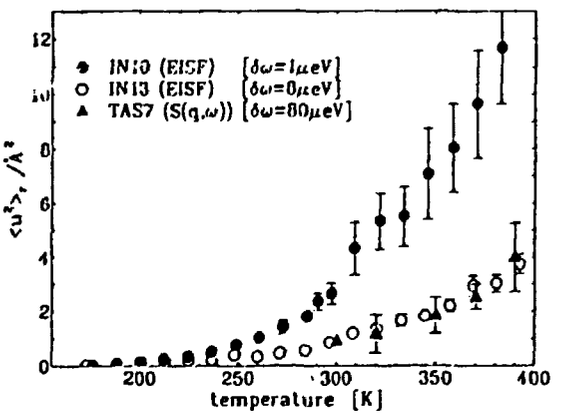

Fig. 2. Temperature dependence of $\langle u^2 \rangle$ of PE obtained by analysis of the elastic line and the quasielastic decomposition.

[1] Polymer Motion in Dense Systems, Ed. D. Richter & T. Springer, Springer Verlag (1988), 138.

1.75 Towards a Phenomenological Definition of the Term 'Gel'

K. Almdal, *Department of Solids State Physics, Risø National Laboratory, Denmark*, J. Dyre, S. Hvidt, *Roskilde University Center, Denmark*, and O. Kramer, *Department of Chemistry, University of Copenhagen, Denmark*

The term 'gel' has been associated with widely different materials studied by scientists with different backgrounds, *e.g.* physicists and food scientists. In fact, the concept 'gel' has become unclear to such an extent that it often creates more confusion than enlightening. Therefore, we propose a definition which has a purely phenomenological basis[1]. Typical gels include biological systems such as gelatin, carrageenan and agar gels. Covalently cross-linked styrene-divinylbenzene copolymer swollen in an organic solvent is also a typical gel. Characteristics of these systems are that they contain two or more components, one of which is a liquid present in substantial amounts and that they are soft solid or solid-like materials. We adopt these characteristics as generic phenomenological characteristics of gels. However, a number of 'dry' systems such as dried silica gel, unswollen cross-linked rubber, and aerogels have also been termed 'gels' in the literature and they are as such in our opinion examples of an indiscriminate use of the concept. We propose the following phenomenological definition of a gel:

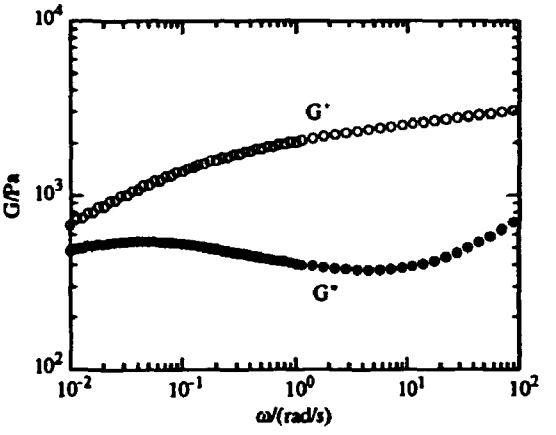

Fig. 1. Log-log plot of storage modulus $G'(\omega)$, and loss modulus, $G''(\omega)$, versus angular frequency for a 13.9 % (w/w) solution of polystyrene in di(2-ethylhexyl)phthalate. The molar mass of polystyrene is 4.7×10^6 g/mol. Measurements were made at 25°C on a Rheometrics RMS 800 instrument, using parallel plates.

A gel is a soft, solid-like material containing two or more components one of which is a liquid, present in substantial quantity. Solid-like gels are characterized by the absence of an equilibrium modulus, by a storage modulus, $G'(\omega)$, which exhibits a pronounced plateau extending to times at least of the order of seconds, and by a loss modulus, $G''(\omega)$, which is considerably smaller than the storage modulus in the plateau region.

It should be noted that this definition includes certain viscoelastic liquids. The mechanical properties of such a liquid is illustrated in Fig. 1. In consideration of the limitation of human perception, we have specified that the plateau in the storage modulus must include times 'at least of the order of seconds'. We have not been able to specify a natural upper limit to define the term 'soft' due the different meaning of the word in different areas of science. However materials with storage modulus in the plateau region of the order of 10^8 Pa are in our opinion much to rigid to be included in the family of gels.

[1] K. Almdal, J. Dyre, S. Hvidt, and O. Kramer, (1993). Polymer Gels and Networks **1**, 5. 5.

1.76 Structural Characterization of a Bis-arborol-tetrathiafulvalene Gel

K. Mortensen, K. Bechgaard, *Department of Solid State Physics, Risø National Laboratory, Roskilde, Denmark.* and M. Jørgensen, *CISMI, Chemistry Department, University of Copenhagen, Denmark*

One of the interesting fields of organic chemistry is the potential of manufacturing molecular scale electronic and optical components, such as rectifiers, switches, and wires. The aim of the present study is to combine the knowledge on electronic character as experienced from studies on organic conduction salts of the TTF type, with new insight into the molecular requirements of self-assembling structures. In the combination, it might be possibly to make self-assembling "molecular wires".

With this goal, a bis-arborol-TTF molecule has been synthesized[1]. Bis-arborols are bi-directional molecules with a lipophilic central unit substituted on the ends with hydrophilic polyalcohol groups. In water, the bis-arborol-TTF molecules self-assemblies into string-like aggregates, forming a viscous gel, when the concentration exceeds approximately 1%. The scattering function gives pronounced side maxima revealing relative well characterized cross-sectional characteristics. When exposed to shear, the strings easily align, as demonstrated by the scattering spectrum shown in Fig. 1.

It is likely, that the hydrophilic polyalcohols in the aggregates form an electrically insulating layer around an internal core of conducting TTF stack, thereby selfassembling a prototype molecular wire. Since the TTF moities are easily oxidized to the cation radical stage, a small amount aliquots of iodine added to the gel might create the necessary unfilled states required for electrical conduction.

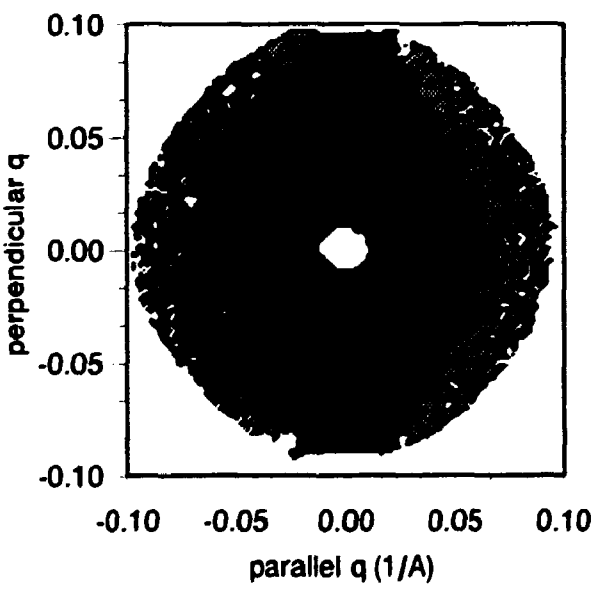

Fig. 1. Two dimensional contour plot of the scattering pattern of bis-arborol TTF dissolved in D_2O when aligned by shear in a couette cell.

[1] M. Jørgensen, T. Bjørnholm, P. Sommer-Larsen, L. Lithen-Madsen, L.G. Hansen, K. Schaumburg, K. Bechgaard, M.N. Nielsen, A. Henschel, and A. Thölen, (1993). J. Org. Chem., *submitted.*

1.77 SANS Investigation of Tube Constraints in Polymer Networks

V. Urban, W. Pyckhout-Hintzen, D. Richter, *Forschungszentrum Jülich, Germany* E. Straube, *Martin-Luther University, Halle-Wittenberg, Germany*, and K. Mortensen, *Department of Solid State Physics, Risø National Laboratory, Denmark*

The tube model[1)] has been quite successful in accounting for the effect of topological constraints in polymer melts and recently also in networks. We have tested the assumptions of a newly extended theory based on the tube concept with the deformation dependent tube diameter measured by SANS. The model, which has been used to calculate stress-strain properties, include a possible strain dependent deformation of the tube diameter, d_o. This microscopic constraint-release modifies the macroscopic strain L to a reduced strain, defined as L^b with $0 \leq b \leq 1$. The anisotropic form factor calculated from the model follows a powerlaw in d_o with the exponent given by the constraint-release parameter b.

The experiments on randomly cross-linked poly(isoprene) networks for which the melt topology was conserved upon cross-linking proved to be very sensitive to b whereas the tube had not changed its size from that of the uncross-linked melt. The constraint-release parameter is seen to approach unity for higher cross-linking densities and longer primary chains. The model is able - as a unique result - to describe the scattering for different strains and directions parallel and perpendicular to the strain simultaneously. Additional experiments involving defect density as well as deformation dependence of the tube are under way.

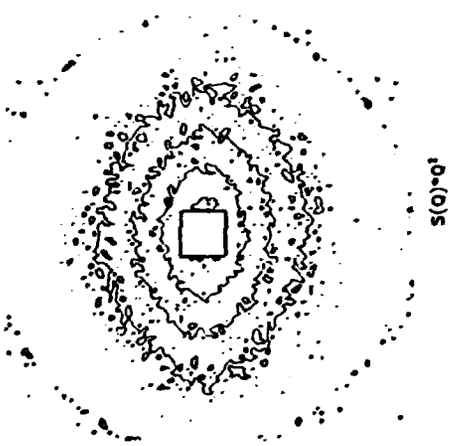

Fig. 1. Two-dimensional scattering intensities showing typical ellipsoidal shape.

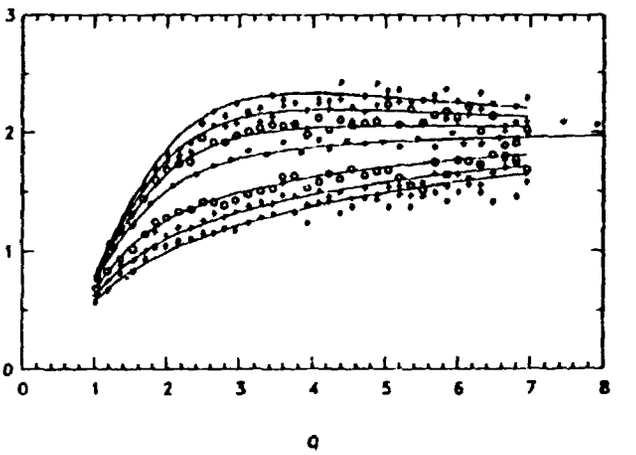

Fig. 2. Kratky representation of scattering intensities of a strained network at different strains for parallel and perpendicular direction of the strain.

1) P.G. de Gennes, (1971) J. Chem. Phys. **55**, 572.

1.78 On the Cross-over from Ising to Mean-field Behaviour in Binary Polymer Blends

G. Meier, *Max Planck Institut for Polymer Research, Mainz, Germany,* D. Schwahn, S. Janssen, *Forschungzentrum Jülich, Germany,* and K. Mortensen, *Department of Solid State Physics, Risø National Laboratory, Denmark*

In contrast to simple binary fluids which show $3d$–Ising critical behavior, polymer mixtures are usually described by mean-field type of theory. In the vicinity of the critical temperature T_c deviations are present because fluctuations become dominant. This results in a temperature width for the Ising regime around T_c, as manifested by the Ginzburg criterion[1,2]. Experimental scattering data, probing the critical fluctuations, for various binary polymer blends at critical composition far from and near the critical point of phase separation confirm the crossover character[2,3,4]. We have compared these susceptibility data with a theoretical expression[5] describing the crossover from critical mean-field to a $3d$-Ising behaviour close to the critical point. The crossover function used is an explicit solution to first order in the perturbation parameter ϵ=4-d based upon a renormalization group analysis[1]. The results obtained using the crossover function are compared with those obtained using the Flory-Huggins form of the bare free-energy density. The observed differences can be interpreted as being due to an underestimate of the perturbation caused by fluctuations in the Flory-Huggins model. In Fig. 1 is shown experimental reduced susceptibility, $\hat{S}(0)=S(0)a_0G_i$ versus reduced temperature $\hat{\tau}/G_i$, where $\tau=(T-T_c)/T_c$ and $S(0)$ is the scattering function at zero angle, a_0 a mass term, and G_i the Ginzburg number. The Ginzburg number G_i, calculated from the crossover function, can be related to the proposed universal constant c of the Ginzburg criterium[2] which is a measure for the width of the Ising regime.

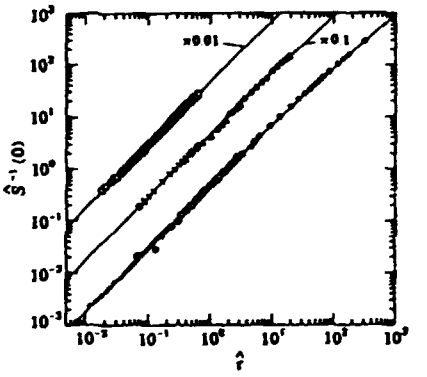

Fig. 1. $\hat{S}(0)$ *vs.* $\hat{\tau}$ for six polymer blends: dPB/PS o, PVME/dPS ⋆, PDMS/PEMS Δ, PPMS/dPS(1) ×, PPMS/dPS(2) □, PPMS/dPS(3) +. Data for PDMS/PEMS and PPMS/dPS are multiplied by 10, and data for PPMS/dPS by *100* for visibility. Full lines are plots of the the theoretical expression.

[1] P.G. de Gennes, (1977). J. Phys. Lett. **38**, 441.
[2] F.S. Bates, J.H. Rosedale, P. Stepanek. T.P. Lodge, P. Wiltzius, G.H. Fredrickson, and R.P. Helm, (1990). Phys. Rev. Lett. **65**, 1893.
[3] D. Schwahn, K. Mortensen, and H. Yee-Madeira, (1987). Phys. Rev. Lett. **58**, 1544.
[4] G. Meier, D. Schwahn, K. Mortensen, and S. Janssen, (1993). Europhys. Lett. **22**, 577.
[5] D. Schwahn, G. Meier, K. Mortensen, and S. Janssen, (1993), *submitted.*

1.79 Pressure Dependent SANS on Polymer Blends and a Comparison to the Lattice Cluster Theory

S. Janssen, D. Schwahn, J. Dudowicz, K.F. Freed, T. Springer, *Forschungzentrum Jülich, Germany*, K. Mortensen, *Department of Solid State Physics, Risø Natinal Laboratory, Denmark*, and H. Hasegawa, *Department of Polymer Chemistry, Kyoto University, Japan*

Compatible polymer blends either show decomposition by lowering (UCST behaviour) or by increasing temperatures (LCST behaviour). In LCST systems the decomposition process is entropy driven, because here free volume is gained during the decomposition. The interaction of the single chain segments is described phenomenologically by the Flory-Huggins interaction parameter Γ. It consists of an enthalpic and an entropic contribution Γ_h and Γ_s, respectively, and depends on temperature, composition, and pressure.

By means of SANS the pressure dependence of Γ was investigated for three different polymer blends, namely *d*-PS/PVME, *d*-PB/PI (LCST), and *d*-PS/PPMS (UCST). It is one aim of the study to examine the free volume concept, which states that Γ_s is an additional segmental entropy that is correlated to the free volume of the blend.

The experiments show that for all the three blends the enthalpic contribution Γ_h is almost pressure independent in the investigated range $1 \leq p \leq 1200$ bar (Fig. 1), whereas the absolute value of Γ_s is a decreasing function of pressure due to the fact of a decreasing amount of free volume (Fig. 2).

Recently, the Lattice Cluster Theory (LCT) for polymer blends has been formulated by Dudowicz and Freed. In addition to the original Flory-Huggins theory it implies free volume correlations between the single monomer bonds and it takes care of the monomer structures of the two species. The experimentally observed pressure dependence is fairly well represented by this theory. An additional improvement might be obtained by the introduction of a pressure dependent lattice constant into the theory.

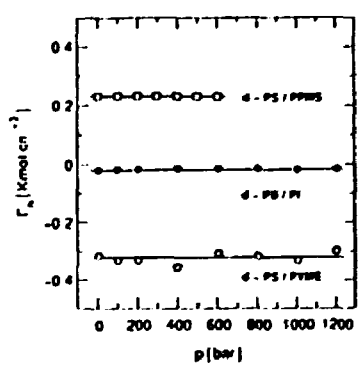

Fig. 1. The enthalpic contribution Γ_h of the Flory-Huggins parameter for the three investigated blends. Γ_h is almost pressure independent in the range ($1 \leq P \leq 1200$) bar.

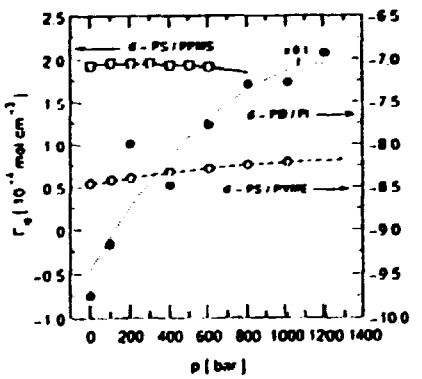

Fig. 2. The entropic contribution Γ_s of the Flory-Huggins parameter for the three investigated blends.

1.80 Pressure Dependence of Spinodal Temperature in DPB-HPI Block Copolymer with LCST-type Phase Behavior

H. Hasegawa, T. Hashimoto, *Department of Polymer Chemistry, Kyoto University, Japan*
S. Janssen, D. Schwahn, *Forschungzentrum Jülich, Germany*, and K. Mortensen, *Department of Solid State Physics, Risø National Laboratory, Denmark*

Mixtures of perdeuterated polybutadiene (DPB) and protonated polyisoprene (HPI) exhibit a lower critical solution temperature (LCST)-type phase behaviour[1]. Therefore, it is expected that block copolymers of DPB and HPI show a LCST-type behavior, *i.e.* ordered state at high temperatures and disordered structure at low temperatures. This system might be a representative of a very interesting class of systems because most block copolymers studied so far show ordering at low temperatures, and because the ordering process in this system is driven by the entropic term of the Flory-Huggins parameter. The DPB-HPI diblock copolymer used was synthesized by sequential living anionic polymerization and has a molecular weight of 3.3×10^5 and 31 mol% of DPB. We measured the scattering profile at 55, 73, and 88°C with varying pressure from 1 to 600 bar. All scattering profiles show a single peak typical for the disordered state. Figure 1 shows the pressure dependence of the scattering profiles at 88°C. The intensity decreases with increasing pressure indicating a shift of the phase diagram toward higher temperature as found for the DBP/HPI homopolymer blend[2]. The spinodal temperature, T_s, was obtained from the linear $1/I_{max}$ versus $1/T$ dependence. It is shown in Fig. 2 as a function of pressure together with the results for the DPB/HPI blend. Surprisingly, the pressure effect on the spinodal temperature for DPB-HPI block copolymer is almost four times larger than that for the homopolymer blend. The extrapolation to $1/I_{max}=0$ introduces some ambiguity to T_s values. The estimated T_s at 1 bar is 164°C but the order-disorder transition could not be reached due to cross linking of the polymer at temperatures higher than 130°C.

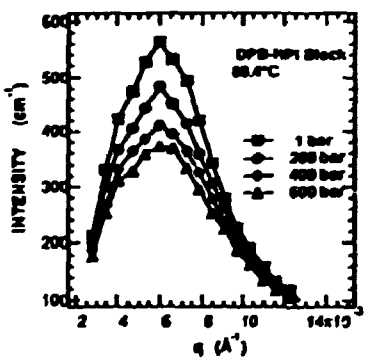

Fig. 1. SANS profiles of DPB-HPI diblock copolymer at 88°C for pressures between 1 and 600 bar.

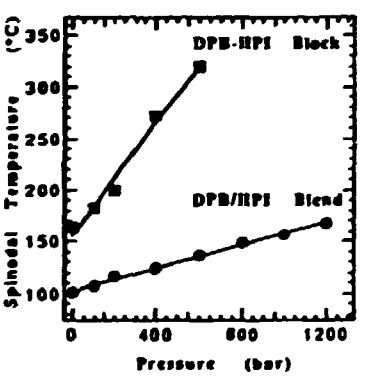

Fig. 2. Pressure dependence of spinodal temperature for DPB-HPI block copolymer and DPB/HPI homopolymer blend

[1] H. Takahashi, S. Sakurai, M. Takenaka, T. Hashimoto, and C.C. Han, (1991). Macromol. **24**, 1813.
[2] *Contribution 1.79 in this report.*

1.81 Mesophase Formation in a Symmetric Poly(styrene-b-paramethylstyrene) Diblock Copolymer

M. Stamm, V.T. Bartels, V. Abetz, *Max Planck Institut für Polymerforschung, Mainz, Germany*, and K. Mortensen, *Department of Solid State Physics, Risø National Laboratory, Denmark*

The microphase separation transition and formation of crystalline mesophases in diblock copolymers has attracted great interests in recent years. A fundamental question raised has been the temperature (T) dependence of the characteristic length scale, as determined by the value, q^*, of the first order correlation peak of the scattering function. According to mean-field theory[1], there should be no T-dependence of q^*. Experimentally, however, a significant change in q^* is observed, not only at the mesophase transition temperature, but far into the disordered regime, suggesting that the chain is stretch as the concentration fluctuations increases[2]. In the attempt to learn the detailed fu ctionality of $q^*(T)$ for not only the PEP-PEE-block copolymers[2], but also for significantly different systems, we have studied the symmetric diblock copolymer of deuterated poly(styrene) (PS) and poly(paramethylstyrene), P(S-b-pMS) by small-angle neutron scattering. The most important sample characteristic for the present study, is the similar glass transition for both blocks (T_g=100°C) and a microphase separation temperature with upper critical solution temperature (UCST) at 180°C. The scattering pattern is within the whole temperature range characterized by a pronounced correlation peak, which within the whole temperature range shows Lorentzial character. In Fig. 1 is shown the peak characteristics versus reciprocal temperature, as obtained by least-square fits to the Lorentz function, including instrumental smearing. The peak width decreases as the MST is approached. But even in the ordered lamellae mesophase, the peak is not resolution limited. The peak position q^* changes like a *tanh*-function (full line in Fig. 1a).

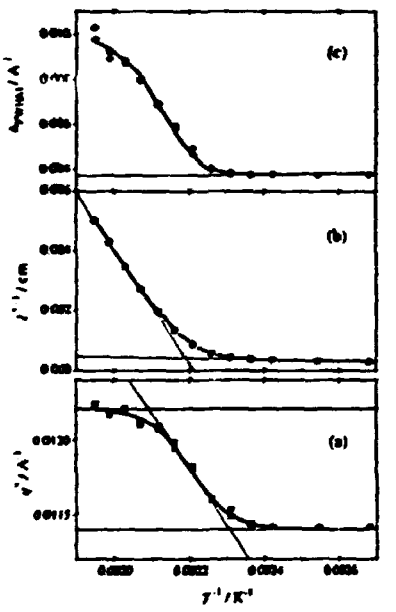

Fig. 1. Characteristics of the first order correlation peak near the microphase separation temperature of PS-P(S-b-pMS), vs $1/T$. The solid line in a) corresponds to a tanh fit, whereas the solid lines in b) and c) are guides to the eye.

[1] L. Leibler, (1980). Macromolecules **13**, 1602.
[2] K. Almdal, J. Rosedale, F.S. Bates, G. Wignall, and G. Fredrickson, (1990). Phys. Rev. Lett. **65**, 1112.
[3] V.T. Bartels, V. Abetz, M. Stamm, and K. Mortensen, (1994). Polymer Preprint, *submitted*

1.82 Diblock Copolymers as Compatibilisers for Rubber Toughened Blends

H.E. James, J.S. Higgins, *Imperial College, London, UK*, R.L. Scherrenberg, *DSM Research, The Netherlands*, and K. Mortensen, *Department of Solid State Physics, Risø National Laboratory, Denmark*

Polymers such as polystyrene (PS) have desirable properties such as high tensile strength but are brittle under normal use conditions. Rubber can be incorporated into a matrix of such a polymer to toughen it. To be effective the rubbery particles must be dispersed randomly, have an average particle diameter near the optimum for that material and there must be good adhesion between the matrix and the rubbery material. Diblock copolymers of suitable molecular weight and composition can be used to compatibilise polymer blends. The diblock copolymers segregate to the interface between the homopolymers where they lower the interfacial tension and, hence, make the dispersion of the blend finer[1]. If the blocks of the copolymer are of sufficient length they can also improve the mechanical properties of the blends by penetrating into the respective homopolymer phases and hence increasing the adhesion between the phases[2]. The aim of this project is to find a relationship between the morphology and mechanical properties of homopolymer/diblock copolymer blends in particular the relationship between impact properties and adhesion. The impetus for this project is the desire to produce rubber-toughened plastics by simple blending. This is desirable as blending requires less complicated equipment and is more flexible than traditional methods such as *in-situ* polymerization and reactive blending. We have used SANS and TEM to investigate the morphology of polystyrene (PS)/rubber/diblock copolymer ternary blends. Two systems, with respectively polyisoprene (PI) and low density polyethylene (VLDPE) as the rubber, and *d*-PS-PI as copolymer, where *d*-PS is deuterated PS. For each system the effect of two diblock copolymers of differing molecular weight were studied. Examples of scattering data are shown in Fig. 1. The peaks visible in the data indicate segregation and ordering of the diblock copolymer. Detailed analysis, which will give details on the rubber domains as well as the copolymer interfacial structure, have still to be done.

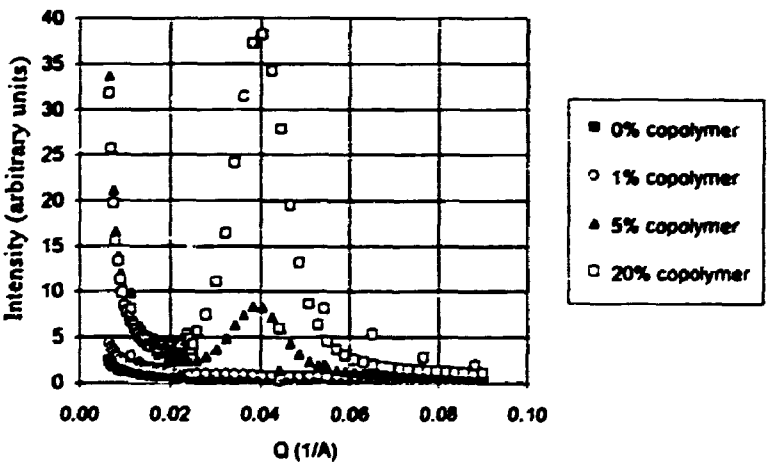

Fig. 1. Scattering data of polystyrene/polyisoprene blend in the ratio 65:35 incorporated with PSd-PI block copolymers in various amounts ranging from 0 to 20%.

[1] D.G. Bucknall, (1991). PhD thesis, Imperial College, London, UK.
[2] H.R. Brown, (1989). Macromolecules **22**, 2859.

1.83 Microstructural Characteristics of Microhpase-separated Tapered Block Copolymers

R.J. Spontak, *North Caroline State University, USA*, S.D. Smith, *The Procter & Gamble Co., USA*, J. Samseth, *Institutt for Energiteknikk, Kjeller, Norway*, and K. Mortensen, Department of Solid State Physics, Risø National Laboratory, Denmark

Ideal AB block copolymers self organize above the order-disorder transition (ODT) into periodic morphologies when the constituent blocks are sufficiently long and incompatible. To facilitate processing (in the disordered state), the ODT of a symmetric copolymer can be lowered, and the extend of mixing increased, by modifying the junction between the A and the B blocks. In this case, the contiguous A and B blocks are not covalently bonded together, as they are in an ideal copolymer, but are instead separated by a sequence of A/B monomers. Four symmetric styrene-isoprene block copolymers possessing comparable molecular weights but different fractions of the middle A/B sequence (from 10-40 wt%) have been synthesized via living anionic polymerization in this work. The A monomer in the A/B sequence is perdeuterated to enhance contrast in small-angle neutron scattering (SANS). Anisotropic two-dimensional SANS patterns indicate that all four materials are microphase separated and exhibit lamellae morphologies. Micrographs collected with transmission electron microscopy (TEM) also reveal that lamellae form in each of these copolymers. Microdomain periodicities, measured from integrated SANS profiles, and TEM micrographs, are obtained and correlated with molecular characteristics. Interphase thicknesses have also been discerned from SANS for each mterial. The microstructural dimensions presented here are compared quantitatively with theoretical predictions and data from related systems.

1.84 Structural Studies of ABA-triblock Copolymer Gels

K. Reynaers, N. Mischenko, H. Reynaers, *Macromoleculaire Structuurchemie, Katholieke Universiteit Leuven, Belgium*, K. Mortensen, *Department of Solid State Physics, Risø National Laboratory, Roskilde, Denmark*, and R. Graulus, *Raychem, Kessel-Lo, Belgium*.

Triblock copolymer gels possess unique properties and are finding many practical applications. The properties and specific morphology depend strongly on the condition of preparation. Using small-angle X-ray and neutron scattering, we have investigated commercial gels of the Kraton type: poly(styrene)-poly(ethylene/butylene)-poly(styrene) triblock copolymers, prepared with an extender oil of aliphatic and alicyclic hydrocarbons. The oil acts as a good solvent for the ethyle/butylene block, whereas poly(styrene) does not dissolve. The poly(styrene) end blocks therefore tend to aggregate into poly(styrene) rich domains. Structural data, as the example shown in Fig. 1, is in agreement with the formation of an interconnected three-dimensional network of poly(styrene) micelles[1]. The soluble poly(ethylene/butylene) middle block connects neighbouring micellar cores, as schematically drawn in Fig. 2. The poly(styrene) core size is, relatively independent of the polymer concentration, c, whereas a systematic change in the intermicellar distance is observed as a function of c. The effective micellar volumen fraction, as determined assuming that the micelles are interacting through a *hard-sphere* interaction potential, goes through a weak maximum close to 12 vol.% polymer. The Kraton gel is rubber-like. When macroscopically deformed, the internal network deforms affinely for elongation up to roughly two times, as seen experimentally from the ellipsoidal correlation ring.

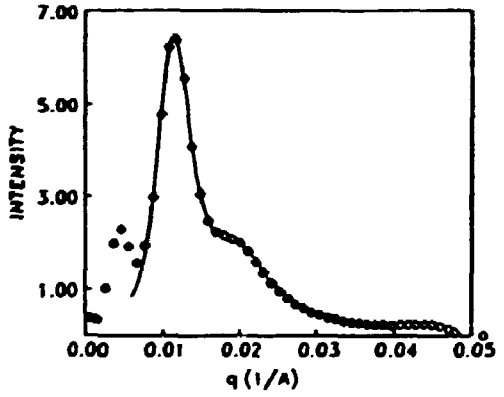

Fig. 1. Scattering function of Kraton gel (12% G1651). The solid line is a fit using a hard-sphere model

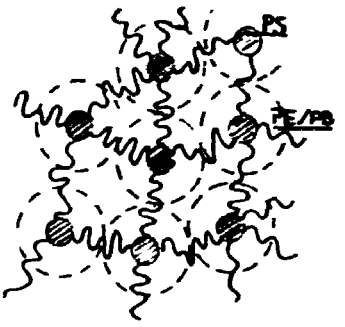

Fig. 2. Schematic model for the interconnected micellar Kraton network.

[1] N. Mischenko, K. Reynaers, K. Mortensen, R. Scherrenberg, F. Fontaine, R. Graulus, and H. Reynaers, (1993), Macromolecules, *submitted*.

1.85 Pressure Induced Melting of Poly(ethylene Oxide)-poly(propylene oxide)-poly(ethylene oxide) Triblock Copolymer Micellar Crystal

K. Mortensen, *Department of Solid State Physics, Risø National Laboratory, Denmark*,
D. Schwahn, and S. Janssen, *Forschungszentrum Jülich, Germany*

Poly(ethylene oxide), PEO, and poly(propylene oxide), PPO, are water soluble polymers due to hydrogen bonding through structured water near the polymer backbone. While PEO remains water soluble up to typically 100°C (depending on molecular weight), PPO becomes insoluble already below ambient temperature. Upon application of hydrostatic pressure, the phase-separation temperature increases on the order of 2°C/kbar and 20°C/kbar for PEO[1] and PPO[2] respectively. Aqueous solutions of the combined triblock-copolymer PEO-PPO-PEO self assemble into micelles in the temperature regime where water is a good solvent for PEO, only. Micelles and dissolved copolymers are in thermodynamic equilibrium, with a temperature dependence which leads to a roughly linear increase in micellar volume fraction. At a critical temperature, the micellar volume fraction approach the critical value for hard-sphere crystallization, resulting in an apparent inverted crystallization transition into a cubatic phase[3]. Since hydrostatic pressure increases the solvent quality, micelles dissolves into unimers, resulting in pressure induced melting[2], as shown in the resulting T-P phase diagram of 28% EPE-copolymer (F88) in D_2O.

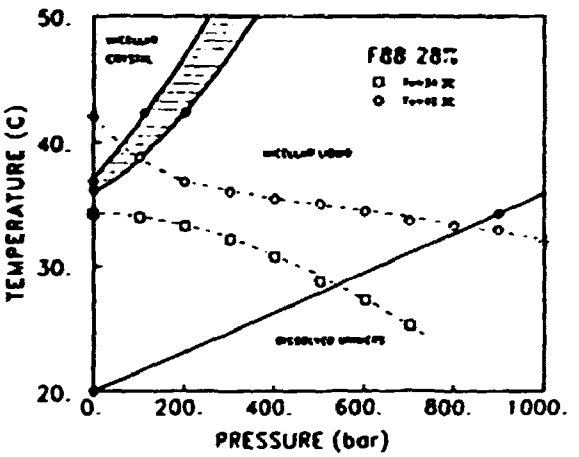

Fig. 1. Temperature-pressure phase diagram of 28% aqueous F88 solution.

[1] R.L. Cook, H.E. King, and D.G. Pfeiffer, (1992). Phys. Rev. Lett. 69, 3072.
[2] K. Mortensen, D. Schwahn, and S. Janssen, (1993). Phys. Rev. Lett. 71, 1728.
[3] K. Mortensen, W. Brown, and B. Nordén, (1992). Phys. Rev. Lett. 68, 2340.

1.86 Structural Investigations of PEP, Poly(propylene oxide)-poly(ethylene oxide)-poly(propylene oxide), Triblock Copolymers in Aqueous Solution

K. Mortensen, *Department of Solid State Physics, Risø National Laboratory, Denmark*, and W. Brown, *Department of Physical Chemistry, University of Uppsala, Sweden*

Recently the Pluronic surfactants based on the triblock copolymer EPE, where E is poly(ethylene oxide) and P is poly(propylene oxide), have attracted great interests within applications as well as within basic research on micelle formation, micellar form transformation and micellar crystallization[1,2]. The proven commercial utility of the EPE surfactant macromolecules has led to further research to find structural modifications that would offer even broader selections of surfactant properties and characteristics. Reversing the hydrophobic and hydrophilic blocks into the PEP triblock copolymer (Pluronic-R) is among such new candidates. In acqueous solutions, these PEP copolymers show distinct differencies from the related EPE copolymers. Of particular interests is the low foaming and good wetting properties. Among the utilities is cleansing agents, in such products as cosmetic face creams, shampoos, and lotions, and in cleaning applications. We have made structural studies on the 25R8 copolymer, which have 80% poly(ethylene oxide), using small-angle neutron scattering and dynamic light scattering. In Fig. 1 is shown the SANS data of 2% copolymers in D_2O. At low temperatures (and low copolymer concentrations) the PEP copolymers are dissolved as independent macromolecules. In a specific temperature range, the scattering pattern indicates formation of an interconnected network of micelles, where the micellar cores of hydrophobic poly(propylene oxide) are interconnected by poly(ethylene oxide) strands. In contrast to the Kraton micellar networks of similar structure[3], which forms a rubber-like material, the PEP-structure is so dynamic that it is still a true liquid.

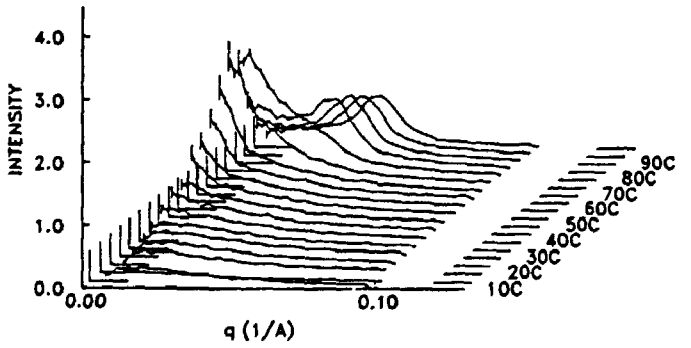

Fig. 1. Scattering function of 2% PEP triblock copolymer (25R8) in D_2O, as obtained in the temperature range 5-95°C.

[1] K. Mortensen, W. Brown, and B. Nordén, (1992). Phys. Rev. Lett. **68**, 2340.
[2] K. Mortensen and J.S. Pedersen, (1993). Macromolecules **26**, 805.
[3] N. Mischenko, K. Reynaers, K. Mortensen, R. Scherrenberg, F. Fontaine, R. Graulus, and H. Reynaers, (1993). Macromolecules, *submitted.*

1.87 Shear-induced Order in a Diblock Copolymer Solution

D. Schneiders, W. Pyckhout-Hintzen, D. Richter, *Forschungszentrum Jülich, Germany*, K. Mortensen, *Department of Solid State Physics, Risø National Laboratory, Denmark*, J. Huang, and L.J. Fetters, *Exxon Research and Engineering Co., Annandale, New Jersey, USA*

In the selective solvent decane, linear poly(ethylene)-poly(ethylene propylene) (PE-PEP) diblock chains (M_w=5000-8000) aggregate into flat, pancake-like, micelles with a PE core and a PEP brush, on both sides of the core. Light and X-ray scattering indicate a PE core thickness of 90 Å and a typical lateral dimension of 3000 Å. Neutron scattering on micelles with deuterated PE and protonated PEP in decane yields a core thickness of 45 Å and a lateral dimension of several 1000 Å. The PEP brush density profile seems to be parabolic, extending over a length of 180 Å, as theoretically expected [1].

In addition to the form factor of the micelles, the SANS data indicate a structure factor, which arises from an aggregation of several micelles, presumably with nearest neighbor lamellae type of ordering. Figure 1 shows the scattering pattern of a jelly 10% solution sheared in a couette type of shear cell at T = 20°C. The scattering pattern shows that the micellar gel responds to shear quite similar to lamellae systems making 'perpendicular'[2] orientation.

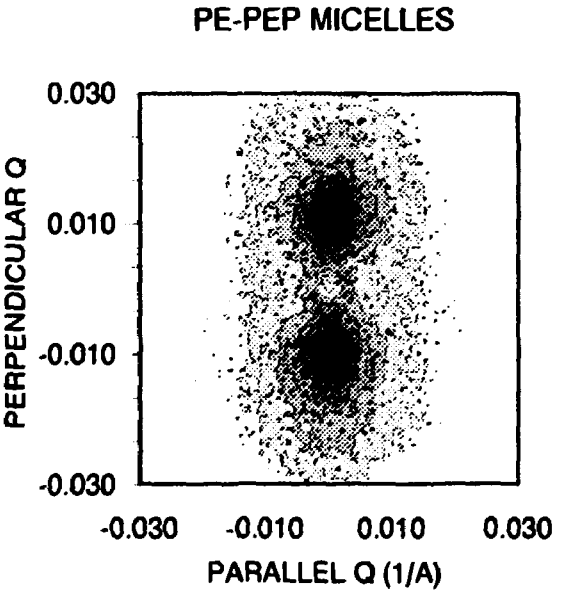

Fig. 1. Scattering pattern of 10% PE-PEP micellar gel oriented by shear. Parallel Q is the scattering vector parallel to the flow. Perpendicular Q is the scattering vector perpendicular to both flow and shear gradient.

[1] S.T. Milner, T.A. Witten, and M.E. Cates, (1988). Macromolecules **21**, 2610.
[2] K. Koppi, M. Tirell, F.S. Bates, K. Almdal, and R.H. Colby, (1992). J. Phys. II **2**, 1941.

1.88 Lamellae Orientation in Dynamically Sheared Diblock Copolymer Melts

K. Almdal, *Department of Solids State Physics, Risø National Laboratory, Denmark,* K.A. Koppi, M. Tirrell, F.S. Bates, *Department of Chemical Engineering and Materials Science, University of Minnesota, USA,* and R.H. Colby, *Corporate Research Laboratories, Eastman Kodak Company, Rochester, New York, USA*

In this study[1] we have used two poly(ethylene-propylene)-poly(ethylethylene) (PEP-PEE) diblock copolymer melts containing 55% by volume PEP to probe the response of ordered microstructures in 'soft' materials to deformation. (Sample PEP-PEE-2D: $M_n = 5.01 \times 10^4$ g/mol, $M_w/M_n = 1.07$, $T_{ODT} = 93°C$; here ODT denotes the order to disorder transition). We have subjected these materials to reciprocating shear at various angular frequencies, ω, in all cases with strain amplitudes of 100%.

The structure of PEP-PEE-2D specimens sheared at low frequency ($\omega = 0.02$ rad/s) or high frequency ($\omega = 1$ rad/s) in both cases for 15 hours at a temperature close to the ODT (83°C) were characterized by small-angle neutron scattering (SANS). High frequency shearing leads to a certain lamellar microstructure which we denote 'perpendicular lamellae'. The unit normal to the lamellae is perpendicular to both the shear and shear gradient directions - *i.e.* parallel to the z-direction in Fig. 1. Low frequency shearing leads to a different lamellar microstructure - 'parallel lamellae'. Here the unit normal is parallel to the shear gradient direction - *i.e.* the y-direction in Fig. 1. This orientation is also obtained when shearing at temperatures far from the ODT irrespective of the frequency.

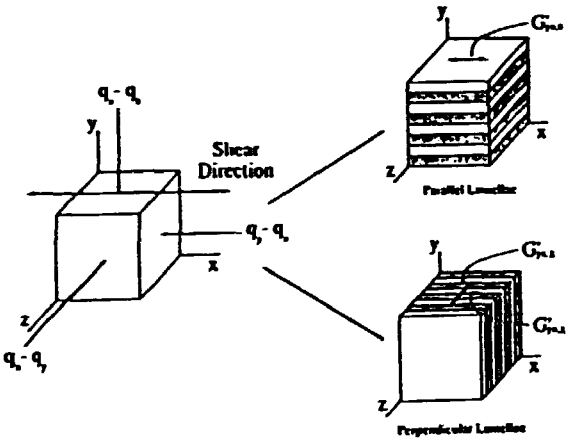

Fig. 1. Coordinate system used for the description of the experiments. Shearing directions are indicated with double ended arrows for both large and small amplitude shearing (processing and dynamical testing, respectively).

Based on rheological measurements we propose two different mechanisms to account for these results. At high frequencies and temperatures close to the ODT the perpendicular orientation arises from a process involving the shear-induced melting of the microstructure due to the effect of vorticity followed by the suppression of composition fluctuations in the disordered state by the shear field in all directions but the one that gives rise to the reordering of the lamellae into the perpendicular orientation. At temperatures far from the ODT or at low frequency the shear-induced melting is not possible. Instead we propose a different mechanism that involves the movement of defects in the structure and results in the formation of microstructures with the parallel orientation.

[1]K.A. Koppi, M. Tirrell, F.S. Bates, K. Almdal, and R.H. Colby, (1993). J. Phys. France II, **2**, 1941.

1.89 Dynamically Sheared bcc Ordered Diblock Copolymer Melts

K. Almdal, *Department of Solids State Physics, Risø National Laboratory, Denmark*, K.A. Koppi, and F.S. Bates, *Department of Chemical Engineering and Materials Science, University of Minnesota, USA*

We have studied the susceptibility of ordered block copolymer melts to symmetry breaking fields, *e.g.* a shear field. Considering the symmetry of a lamellar or a cylindrical domain it is not surprising that such domains respond to the influence of a symmetry breaking field. It is less obvious what happens with a structure consisting of spherical domains under symmetry breaking conditions. In this study we have used a poly(ethylene-propylene)-poly(ethylethylene) (PEP-PEE) diblock copolymer melt, containing 83% by volume PEP; $M_n = 1.7 \times 10^5$ g/mol, $M_w/M_n = 1.05$ $T_{ODT} = 104$°C; where ODT denotes the order to disorder transition. The sample was subjected to a reciprocating shear deformation using a frequency of $\omega = 0.02$ rad/s and strain amplitude of $\gamma_0 = 100\%$ for 12 hours at 90°C followed by 1 hour at 80°C and 4 hours at 70°C. The constant shear rate was $|\dot{\gamma}| = 0.01 s^{-1}$.

The resulting sample was investigated using small-angle neutron scattering (SANS). The neutron beam was passed through the sample in three orthogonal direction simply by cutting the sheared specimen and mounting pieces with different orientations in the sample position on the neutron instrument to obtain the SANS patterns given in Fig. 1. The patterns are characterized by resolution limited diffraction spots at $|\mathbf{q}| = q^* = 0.012$ Å^{-1}. The patterns correspond to a perfectly twinned body centred cubic crystal structure. Using the same coordinate system as given in Fig. 1 of Ref. 1, the x-axis (shear direction) is a $\langle 111 \rangle$-axis in the bcc unit cell, the y-axis (shear gradient) is a $\langle 1\bar{1}0 \rangle$-axis, and the z-axis (orthogonal to x and y) is a $\langle 11\bar{2} \rangle$-axis. The weak reflections seen in the q_x-q_z scattering plane at $\sqrt{2}q^*$ are (200) reflection. Thus the ordered collection of spheres in the bcc structure responds anisotropically to an applied force.

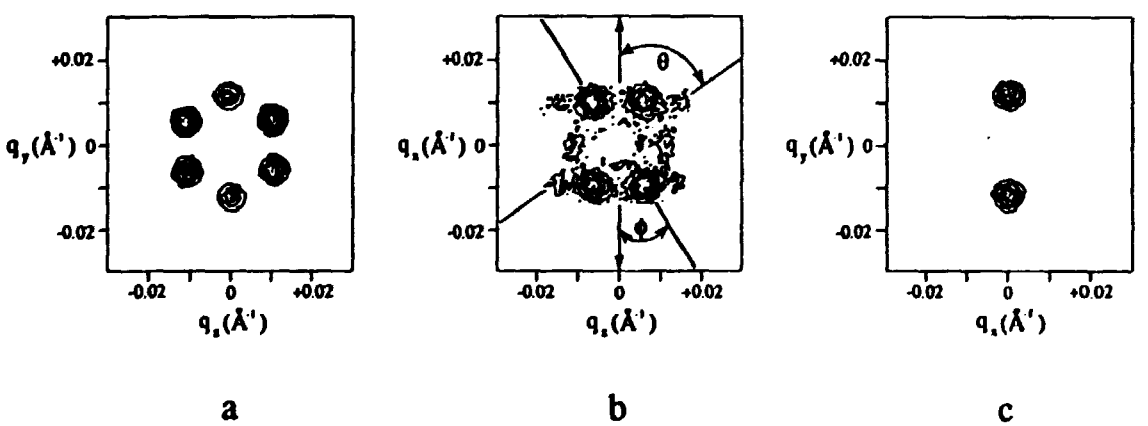

Fig. 1. SANS patterns obtained with the neutron beam directed along three orthogonal directions; (a) the x (shear) direction, (b) the y (shear gradient) direction, and (c) the z (orthogonal to x and y) direction.

[1] Contribution 1.88 in this report.

[2] K. Almdal, K.A. Koppi, and F.S. Bates, (1993). Macromol. **26**, 4058.

1.90 Orientational Ordering in Nematic Liquid Crystals: Isotope Labelling Neutron Diffraction Experiments

I.W. Hamley, *Department of Physics, University of Durham, UK,* R.M. Richardson, *Department of Chemistry, University of Bristol, UK,* J.M. Seddon, *Department of Chemistry, Imperial College, London, UK,* G.R. Luckhurst, *Department of Chemistry, University of Southampton, UK,* and J. Skov Pedersen, *Department of Solid State Physics, Risø National Laboratory, Denmark*

Liquid crystals are characterised by long-range molecular orientational order - in the nematic phase there is no additional translational order. A complete description of orientational order has not yet been obtained. Spectroscopic techniques such as NMR or depolarized Raman scattering have been employed, but they only provide orientational order parameters of a certain rank, which are not sufficient to characterise the complete orientation distribution function. In contrast, diffraction can be used to obtain the complete molecular orientational distribution function [1]. It is important, however, to obtain largely intramolecular diffraction. We have recently shown[2,3] how such scattering can be obtained using the isotope labelling technique in neutron diffraction. When mixtures of deuterated and protonated molecules are used, scattering depending on molecular contrast is obtained for $Q < 0.8$ Å^{-1}. For an aligned liquid crystal phase, the anisotropy of this scattering is related to the molecular orientational order. A series expansion approach [3] has been used to obtain a set of order parameters directly from this scattering. The number of the order parameters which can be obtained is not *a priori* limited but in practice depends on molecular anisotropy[4].

We obtained anisotropic intramolecular scattering patterns for the nematogens 4,4′-dimethoxyazoxybenzene (PAA) and 4-pentyl-4′-cyanobiphenyl (5CB). Mixtures of about 80% perdeuterated molecules were used which ensures maximal intramolecular scattering compared to the incoherent background. Samples were aligned between rare earth magnets within an electrically-heated oven. The orientational order parameters obtained for 5CB are not in accord with the predictions of the Maier-Saupe theory for nematogens[3] (the ratio $\overline{P}_4/\overline{P}_2$ is much greater than predicted, where $\overline{P}_L$ denotes an Lth rank Legendre polynomial order parameter). Values of $\overline{P}_2$ are slightly lower than those obtained from NMR. For PAA, the order parameters extracted do not agree with those obtained by us previously at the ILL, Grenoble[3] - in particular the ratio $\overline{P}_4/\overline{P}_2$ is much larger. We are currently attempting to resolve the source of this discrepancy.

[1] P.G. de Gennes, (1972). C.R. Acad. Sci. (Paris) **274B**, 142.
[2] R.M. Richardson, J.M. Allman, and G. McIntyre, (1990). Liq. Crystals **7**, 701.
[3] R.W. Date, I.W. Hamley, G.R. Luckhurst, J.M. Seddon, and R.M. Richardson, (1992). Molec. Phys. **76**, 951.
[4] I.W. Hamley, (1991). J. Chem. Phys. **95**, 9376.

1.91 Side-chain Liquid Crystalline Polyesters for Optical Information Processing

S. Hvilsted, *Department of Solid State Physics, Risø National Laboratory, Denmark*, P. S. Ramanujam, *Optics and Fluid Dynamics Department, Risø National Laboratory, Denmark*, H. W. Siesler, *Department of Physical Chemistry, University of Essen, Germany*, P. Magagnini, *Chemical Engineering Department, University of Pisa, Italy*, and F. Andruzzi, *CNR, Chemical Engineering Department, University of Pisa, Italy*

This project is a collaborative focussed fundamental research planned by the listed international consortium and supported financially in part by the European Economic Community under the Brite/EuRam programme. The work programme just launched is set up for three years with the management of the project in the Department of Solid State Physics, Risø.

The objectives of the project are to develop, fabricate and test side-chain liquid crystalline (SCLC) polyester materials and devices for optical storage and processing. Specifically, the planned research is directed towards the development of an erasable and rewritable optical memory providing a high storage capacity of about 1 Gbits/cm^2. The major research tasks are:

i) initial synthesis and subsequent characterization by thermal, optical microscopic, molecular spectroscopic, mechanical, and electrical measurements of a variety of SCLC polyesters for screening of useful opto-electrical properties.

ii) optical information storage applications of SCLC polyester films, such as computer generated holograms for filtering and mapping applications.

iii) design, synthesis and characterization of new functional SCLC polyesters with the aim of achieving a recording energy of 10 to 100 mJ/cm^2.

iv) investigation of novel biphotonic processes and their use in joint transform correlators, spatial light modulators, and thick holograms for optical interconnects.

The materials and components developed under this project could be used in state-of-the-art apparatus performing analog optical processing such as vision systems and optical neural networks and in digital devices, like optical computer memories and audiovisual entertainment systems.

In the initial phase the efforts have been concentrating on the preparation of the necessary building blocks and preparation and characterization of the first selected side-chain liquid crystalline polyesters. Initial optical investigations have also been performed.

1.92 Characterization of the Segmental Mobility of Side-chain Liquid Crystalline Polyesters by FTIR Spectroscopy and Optical Anisotropy

C. Kulinna, I. Zebger, H.W. Siesler, *Department of Physical Chemistry, University of Essen, Germany*, F. Andruzzi, *CNR, Chemical Engineering Department, University of Pisa, Italy*, P. S. Ramanujam, *Optics and Fluid Dynamics Department, Risø National Laboratory, Denmark*, and S. Hvilsted, *Department of Solid State Physics, Risø National Laboratory, Denmark*

Side-chain liquid crystalline (SCLC) polyesters containing pendant azo dyes exhibit permanent local polymer main-chain conformational reorganization in response to light, due to trans-cis isomerization resulting in local changes in refractive index. The light induced orientational behaviour of the SCLC polyesters under investigation shows that the materials comply with the requirements for reversible optical data storage. The implications of changing the number of main-chain methylene spacers from 3 to 12 in polyesters with 6 methylene spacers in the side-chains linking the cyanobenzene to 1,3-propanediol in the main-chain have been studied by analyzing laser irradiated polyester films with polarized infrared light.

No prealignment of the samples is necessary to achieve orientation of the liquid crystalline side-chains relative to the polarization of the writing beam. Furthermore, small changes in the number of methylene units in the main-chain result in changes in the light induced behaviour, depending on the response of the polymers to the applied argon ion laser beam.

In addition, it has been demonstrated[1,2] that FTIR spectroscopy employing polarized radiation is a useful tool for the quantitative determination of the order parameter. This can be used for the derivation of a model for light induced alignment of the molecules by focusing on specific absorption bands. Moreover, FTIR spectroscopy can be used to follow the time dependent development of alignment and the temperature dependent erasure of the laser induced orientation.

The influence of varying the flexible spacer length in the side chains from 6 over 8 to 10 methylenes of polyesters with a dodecamethylene (12) spacing of the ester groups was also studied by time dependent measurement of the optically induced anisotropy with the polyester films between crossed linear polarizers. A He-Ne laser was used to measure the transmission through films. A polarized argon ion laser beam at 488 nm with its polarization at 45° to the linear polarizer orientation was used to induce the optical anisotropy in the film. It is shown that the transmission through the films depends on the laser intensity, and that the polyesters with shorter flexible spacers respond more readily to low irradiation intensities albeit with longer time constants.

[1] P.S. Ramanujam, S. Hvilsted, F. Andruzzi, C. Kulinna, and H.W. Siesler, (1993). Organic Thin Films for Photonic Applications, 1993 Technical Digest Series Vol. 17 (Optical Society of America, Washington D.C.), 244.
[2] C. Kulinna, I. Zebger, S. Hvilsted, P.S. Ramanujam, and H.W. Siesler, (1994). Makromol. Chem., Makromol. Symp., *in press.*

1.93 New Polymer Materials for Optical Storage

M. Pedersen, S. Hvilsted, *Department of Solid State Physics, Risø National Laboratory, Denmark*, P.S. Ramanujam, *Optics and Fluid Dynamics Department, Risø National Laboratory, Denmark*, and J. Kops, *Department of Chemical Engineering, The Technical University of Denmark, Denmark*

Several different polymer systems have a potential for optical storage applications, however, all systems seem to be centered around pendant cyanoazobenzene. Our flexible aliphatic side-chain liquid crystalline (SCLC) polyester architecture has four adjustable molecular design parameters. Two of these, length of methylene sequence in polyester main-chain and length of flexible methylene spacer linking cyanoazobenzene to 1,3-propanediol in main-chain, have been demonstrated[1,2,3] to dramatically influence the optical storage possibilities. The third parameter, the polyester molar mass, is also of importance although the influence on optical behaviour is not yet fully investigated.

The fourth parameter, substituents different from cyano on azobenzene, will affect the light absorption behaviour and the dipole character of the azo dyes. Both inherently physical properties are expected to significantly influence the azobenzene response to laser irradiation and consequently the optical properties of SCLC polyesters with these new dyes incorporated.

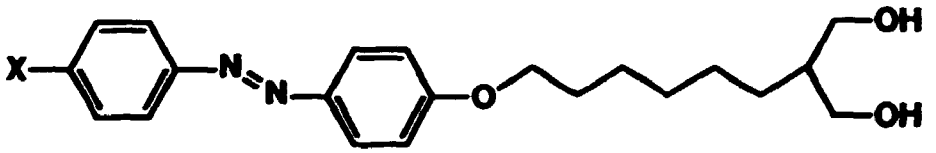

X = CN, H, NO_2, OCH_3

Fig. 1. Basic structure of the photosensitive azobenzene diols with six methylene groups in the flexible spacer. The different substituents are shown.

The indispensable precursers for the diols illustrated in Fig. 1, the corresponding azophenols are prepared and the absorption characteristics (λ_{max}(nm), ϵ_{max}(1/cm·mol))in tetrahydrofuran are determined: CN: 367, 26000, H: 350, 20000, NO_2: 379, 24000, OCH_3: 358, 27000. In addition, improvements in the necessary purification procedure of the aliphatic linking part of the diols are worked out.

[1] S. Hvilsted, F Andruzzi, and P. S. Ramanujam, (1992). Opt. Lett. **17**, 1234.
[2] P. S. Ramanujam, S. Hvilsted, and F. Andruzzi, (1993). Appl. Phys. Lett. **62**, 1041.
[3] Contribution 1.92 in this report.

1.94 Layered Materials Derived from Calixarenes

H. Nishikawa and K. Bechgaard, *Department of Solid State Physics, Risø National Laboratory, Denmark*

The calixarenes are a class of cyclic oligomers of 2-methyl-phenol and models for bakelite, the condensation product of formaldehyde and phenol. The structural characteristic shape of calix (4) arene is in selected cases that of a "cone" presenting a upper and a lower rim. Inside the cone small molecules can be trapped. The circular structure of the molecule makes it an ideal structure for building layered structures with isotropic interactions in the plane.

In the project we have functionalised the calixarenes on both the upper and lower rim in order to build weakly interacting high-spin systems, where the main intermolecular interactions are expected in planes seperated by about 20 Å. Severeal model molecules are under investigation, both theoretically and experimentally. So far a holmium complex has been prepared in amorphous form and further functionalisation of the calixarene is underway in order to improve the quality of the material.

In another part of the project, we attempt to couple the calixarenes in order to generate cylindrical macromolecules.

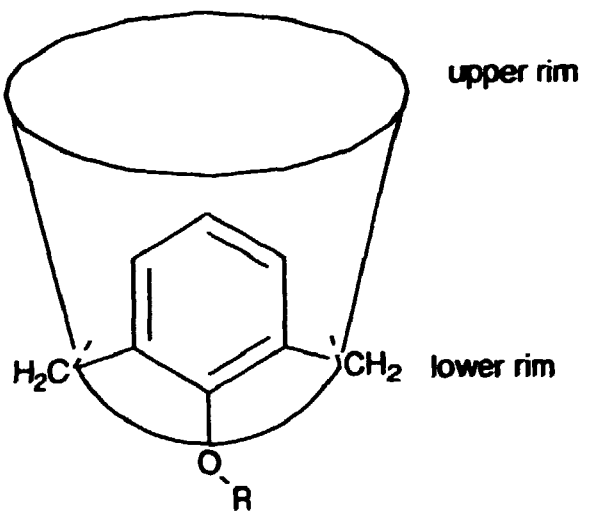

1.95 Peptide Nucleic Acids (PNA)

M. Egholm, O. Buchardt, *Research Center for Medical Biotechnology, The H.C. Ørsted Institute, University of Copenhagen, Denmark*, P.E. Nielsen, *Department of Biochemistry B, The Panum Institute, University of Copenhagen, Denmark*, and R.H. Berg, *Department of Solid State Physics, Risø National Laboratory, Denmark*

We recently designed a DNA analog, PNA (see Fig. 1), in which the entire sugar-phosphate backbone has been replaced with a backbone based on amino acids[1–5]. It was shown that PNAs containing solely T and C nucleobases can bind to complementary nucleic acids through $(PNA)_2$-DNA triplex formation and to double-stranded DNA by strand displacement. PNA containing all four natural nucleobases (T, C, A, G) has now been synthesized and found to exhibit sequence-specific binding to complementary nucleic acids obeying the Watson-Crick hydrogen bonding rules[4]. Thus, PNA is a true DNA mimic in terms of base-pair recognition. Furthermore, PNAs bind with higher affinities and specificities than unmodified DNA and they are stable against nuclease and protease cleavage. Thus, PNA has potential for applications in diagnostics and as biomolecular tools and, possibly, in drug therapies.

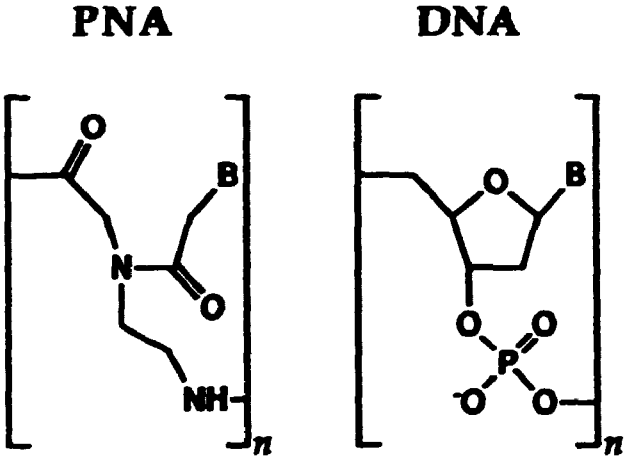

Fig. 1. Chemical structure of peptide nucleic acid(PNA) versus that of deoxyribonucleic acid(DNA). B = nucleobase.

[1] P.E. Nielsen, M. Egholm, R.H. Berg, and O. Buchardt, (1991). Science **254**, 1497.
[2] M. Egholm, O. Buchardt, P.E. Nielsen, and R.H. Berg, (1992). J. Am. Chem. Soc. **114**, 1895.
[3] M. Egholm, P.E. Nielsen, O. Buchardt, and R.H. Berg, (1992). J. Am. Chem. Soc. **114**, 9677.
[4] M. Egholm, O. Buchardt, L. Christensen, C. Behrens, S.M. Freier, D.A. Driver, R.H. Berg, S.K. Kim, B. Nordén, and P.E. Nielsen, (1993). Nature **365**, 566.
[5] For an introduction to our work, see: M. Frank-Kamenetskii, (1991). Nature **354**, 505 (News and Views); D.J. Patel, (1993). Nature **365**, 490 (News and Views); F. Flam, (1993). Science **262**, 1647 (Research News).

1.96 Film-based Solid-phase Synthesis

W. Batsberg Pedersen, L. Winther, K. Almdal, and R.H. Berg, *Department of Solid State Physics, Risø National Laboratory, Denmark*

Solid-phase synthesis employs an insoluble matrix on which to build up macromolecules such as peptides and nucleic acids in a stepwise manner[1,2]. Established methods for the solid-phase assembly of peptides normally employ a beaded matrix of cross-linked polystyrene. A few years ago, we developed a film-based matrix, which we refer to as a "long-chain polystyrene-grafted polyethylene film", abbreviated to PEPS[3]. The development of PEPS is based on the invention of a γ-radiation-induced grafting procedure which is performed in a mixture of a solvent and a non-solvent for polystyrene. PEPS provides state-of-the-art peptide synthesis and, in addition, it offers exceptional ease of handling, permitting the simultaneous production of multiple peptides in a parallel fashion: Each peptide is synthesized on a labeled sheet of PEPS and the common steps of deprotection, neutralization, washings, and coupling of identical amino acids are carried out simultaneously in a *single* reaction vessel. It is believed that the PEPS invention offers new possibilities in areas such as stucture-activity studies or screening of bioactive peptides. A patent for the whole concept was issued in 1993[4]. More recently, we have shown that cross-linking of the polyethylene film (with high energy electrons) prior to the grafting of polystyrene leads to very significant improvements in the properties and the quality of the PEPS film[5]. Thus, the cross-linked PEPS film possesses excellent mechanical and thermal properties and, most surprisingly, and in contrast with noncross-linked PEPS films, no inhomogeneities due to bubbles containing occluded homopolymer are visible in the grafted polymer. Another feature of the new technology is that peptides may be built up stepwise and then remain attached to the PEPS support via a permanent covalent bond. By nature the PEPS film is hydrophobic, but the cross-linked film can be modified to a version which is both hydrophilic and hydrophobic. This modified film is still well-suited for peptide synthesis in organic solvents and, in addition, it exhibits a high level of solvation in aqueous solution. Based on these findings we predict that it should be possible to construct versatile systems for certain biotechnological applications such as diagnostic testing and affinity purification by using hydrophilic versions of the PEPS material.

1) R.B. Merrifield, (1963). J. Am. Chem. Soc. **85**, 2149.
2) R.B. Merrifield, (1986). Science **232**, 341. (Nobel Lecture)
3) R.H. Berg, K. Almdal, W. Batsberg Pedersen, A. Holm, J.P. Tam, and R.B. Merrifield, (1989). J. Am. Chem. Soc. **111**, 8024.
4) R.H. Berg, K. Almdal, W. Batsberg Pedersen, A. Holm, J.P. Tam, and R.B. Merrifield, (1993). US Patent 5,258,454.
5) R.H. Berg, K. Almdal, W. Batsberg Pedersen, and L. Winther, (1993). DK Patent Appl. 930724 (filed 18 Jun 1993).

1.97 Flexibility and Local Structure of Polymer-like Reverse Micelles

P. Schurtenberger, C. Cavaco, *Institut für Polymere, ETH Zürich, Switzerland*, P. Lindner *Institute Laue-Langevin, Grenoble, France*, and J. Skov Pedersen, *Department of Solid State Physics, Risø National Laboratory, Denmark*

We have studied the structural properties of polymer-like lecithin reverse micelles in deuterated cyclohexane as a function of the water to lecithin molar ratio, w_o, and the volume fraction, Φ. At very low values of w_o, the micelles are small and the solutions have static and dynamic properties which are typical for classical micellar or colloidal solutions. At high values of w_o, the micellar size can be extremely large, and the micelles have polymer-like properties. Experiments were performed using an extended Q-range of 2.8×10^{-3} Å$^{-1} \leq Q \leq 0.45$ Å^{-1}, which permits us to study overall dimensions, flexibility, and local structure. For very low values of Q ($1/Q < R_g$), the scattered intensity $I(Q)$ becomes insensitive to structural details. $I(Q)$ reduces to Guinier's law, and we can determine the radius of gyration R_g of the particles. The low-Q regime thus reflects the water-induced aggregate growth postulated in our model. At intermediate Q ($R \ll 1/Q \ll R_g$), $I(Q)$ becomes much more sensitive to the local aggregate structure. Polymer theory predicts for flexible polymer coils that $I(Q)$ should decay with a power law of the form $I(Q) \sim Q^{-x}$, where $1.7 \leq x \leq 2.0$. At large values of Q, $I(Q)$ is controlled by distances over which polymers are rod-like rather than flexible, and a crossover to an asymptotic Q^{-1}-dependence for $I(Q)$ can be expected, which is typical for locally cylindrical structures. At still larger Q-values, the finite cross-sectional radius of the polymer can be studied, which results first in $I(Q) \sim (1/Q)\exp(-R_c^2Q^2/2)$, where R_c is the cross-sectional radius of gyration, before $I(Q)$ finally crosses over to a classical Porod law. Figure 1 shows that these different regimes can indeed be observed for lecithin reverse micelles. We also see for example clearly the dramatic micellar growth induced by the addition of only 4 molecules of water per lecithin molecule at low Q, whereas the flexibility and local packing remains unchanged. However, a major obstacle in a quantitative analysis of the full scattering curve still remains in a consistent incorporation of excluded volume effects. While our (preliminary) data shows that we can obtain most of the required structural information from the low (R_g), intermediate (persistence length l_p) and high (cross-sectional radius R) Q part of the data, the micelles are so giant that excluded volume effects become important in the low and intermediate Q-range. We are therefore currently investigating different forms for the segment distribution function known from polymer physics which we could use in order to model the scattering curve obtained with our solutions.

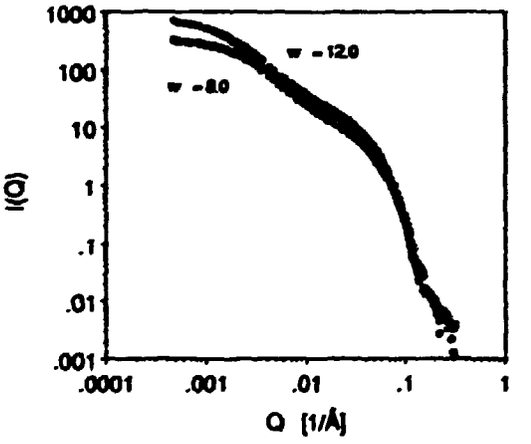

Fig. 1. Plot of $I(Q)$ versus Q for solutions of lecithin in deuterated cyclohexane (molar ratio water to lecithin $w_o = 8.0$ and $w_o = 12.0$) at a volume fraction $\Phi = 0.0036$. Data shown is obtained from a combination of light and neutron scattering experiments.

1.98 Shear Melting and Orientation of a Lyotropic Cubic Phase

U. Olsson, *Physical Chemistry 1, Chemical Center, Lund University, Sweden*, and K. Mortensen, *Department of Solid State Physics, Risø National Laboratory, Denmark*

Bicontinuous lyotropic cubic phases, made up of infinite multiply connected bilayer membranes, are found in a number of surfactant-water-oil systems. Here we report on a study of a bicontinuous cubic phase in the system pentaethyleneglycol dodecyl ether (C12E5)/heavy water (D_2O)/tetradecane with the composition 0.341/0.220/0.439, in volume fractions. Since the area per C12E5 molecule at the polar/apolar interface is well known, it is possible to calculate the lattice parameter from the composition for different minimal surface structures. Using the parallel surface model, a good agreement between area and q-value of the first order correlation peak is found for the Gyroid minimal surface structure of space group Ia3d, assuming the peak corresponds to the lowest order reflection allowed for this structure which is [hkl]=[211]. Further support for this assignment is given by the shear cell experiments, as illustrated in Fig. 1. Upon shear an essentially circular symmetric scattering pattern was observed on the two dimensional detector (Fig. 1a). However, after turning off the shear, a preferred orientation of the cubic phase sample is obtained (Fig. 1b). The scattering pattern of Fig. 1b contains 6 stronger reflections at the polar angles: 20°, 90° and 160°. In addition, one can also observe 4 weaker reflections, one on either side of the 90° reflections. The stronger reflections can be assigned to the [211] planes, with an orientation of the ⟨111⟩ axis parallel with the shear field (horizontal). The four weaker reflections can be ascribed to a smaller population of an orientation of the ⟨111⟩ axis parallel to the symmetry axis of the Couette cell. Here, the reflections at 0° and 180° are not resolved between the stronger reflections at 20° and 160°, respectively. Bicontinuous cubic phases cannot swell continuously with solvent[1], since the shear moduli decreases upon swelling. This can result in a first order 'melting' phase transition to a fluid L3 phase where the bilayer topology is retained[2,3]. The present sample is very close in composition to such a transition[3]. This suggests the possibility of melting the cubic crystalline order under shear.

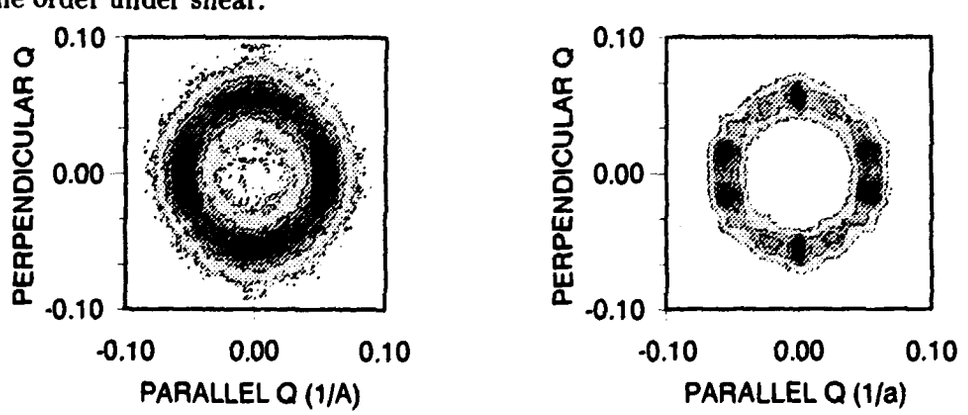

Fig. 1. Contour plots of scattering pattern of C12E5 with shear 300/s and relaxed from shear.

[1] R. Bruinsma, (1992). J. Phys. II **2**, 425.
[2] U. Olsson, B. Balinov, and O. Soderman, (1992) in 'The Structure and Conformation of Amphiphilic Membranes', (Springer-Verlag) p. 287.
[3] U. Olsson, U. Wurz, and R. Strey, (1993). J. Phys. Chem. **97**, 4535.

1.99 Structural Studies of the Sodium Deoxycholate Surfactant System both with and without Lipopolysaccharide

F. Lopez, J. Rouch, *CPMOH, Un.versity of Bordeaux I, France*, J. Samseth, *Institutt for Energiteknikk, Kjeller, Norway*, E. Rosenquist, *National Institute of Public Health of Norway*, K. Mortensen, *Department of Solid State Physics, Risø National Laboratory, Denmark.*

Meningitis is a very serious disease among young people. The National Institute of Health of Norway has developed a vaccine in order to fight the disease. In the production of this vaccine it is neccessary to remove a lipopolysaccharide (LPS). LPS is found in the cell membranes of the cells that produce the vaccine. In the human body LPS will cause a high fever if it is not removed. When sodium deoxycholate (DOC) is added, the DOC and LPS will form a complex depending on the the pH. DOC is a bile salt and thus has no harmful effects on the body. DOC can also be synthesized and is available in large quantities.

In this work we have investigated structural properties of the pure DOC as well as the pure LPS system. Further we have studied the DOC and LPS complex. DOC is a surfactant and will form micelles. These micelles has been found to be rodshaped. Both the radius and the aspect ratio of the rod decreases with increasing pH from 7.5 to 10. The LPS macromolecule has been found to be of approximately the same size as the DOC micelle at high pH. Together with DOC it forms micellar complexes. The nature of these complexes can be modified by adding magnesium chloride. More investigations need to be done on the DOC-LPS complex.

1.100 Bending Rigidity of Sodium Octyl Sulfate/Water/Decanol Lamellae

E.Y. Sheu, *Texaco R&D, Beacon, New York, USA*, J. Samseth, *Institut for Energiteknikk, Kjeller, Norway*, S.-H. Chen, *Massachusetts Institute of Technology, USA*, and K. Mortensen, *Department of Solid State Physics, Risø National Laboratory, Denmark*

The bending rigidity of microemulsion lamellae is an important characterization parameter. Experimentally, it can be determined by the structure factor from a scattering measurement. The conventional data analysis involves the analysis of the peak shape, particularly, its dependence upon the scattering vector q near the peak. The other alternative to obtain the bending rigidity is to analyze the small-angle regime where the scattering contribution is mainly from the fluctuation of the lamellar layers, thereby providing the information about the bending rigidity. In this SANS experiment, we measured the sodium octyl sulfate (SOS)/water/decanol system in the lamellar neat phase, along the water dilution line with SOS/decanol weight ratio, W, kept at 45:55. The scattering pattern shows a pronounced correlation peak. The peak evolves toward higher scattering vectors q with decreasing water content, indicating a decreasing inter-layer spacing. The small-angle scattering is substantial for all samples, signifying the high fluctuations of the lamellae. If the small-angle scattering is indeed contributed by the fluctuation, it should wane out as the system moves out of the lamellar region. At high water concentration the system is close to the lamellar boundary, and the observed peak intensity is significantly suppressed. The intensity monotonically decreases as the system gets close to the next phase, consisting of the reversed cylindrical micelles and the bicontinuous phase. It may be a L3-phase region. The bending rigidity was computed through the average fluctuating mode, *i.e.* the average wave number of the fluctuation. Using this average fluctuating mode as the mean persistence length, the bending rigidity was calculated using the de Gennes-Taupin relation[1]. The values obtained spanned from 0.3 kT to about 1.5 kT, depending on the water content.

[1] P.G. de Gennes, and C. J. Taupin, (1982). J. Phys. Chem. **86**, 2294.

1.101 Observation of a Rod-to-sphere-to-rod Transition in SDS Micelles upon Addition of Cosurfactants

J. Samseth, *Institutt for Energiteknikk, Kjeller, Norway*, G. Førland, H. Høiland *Chemical Institute, University of Bergen, Norway*, K. Mortensen *Department of Solid State Physics, Risø National Laboratory, Denmark*, and E. Sheu, *Department of Pharmaseutics, University of Oklahoma, USA*

Small angle neutron scattering studies have been performed on micellar solutions of the surfactant sodium dodecyl sulfate (SDS) in D_2O. In order to screen the charges on the micellar surface NaCl was added. As cosurfactant n-butanol was used.

The SANS measurements were performed on samples with increasing cosurfactant content. The spectra were fitted to models of polydisperse spheres, rods and ellipsoids. The models for rods did not fit as well as for ellipsoids. The result shows that when butanol is added, a sudden increase in the axial ratio of the prolate ellipsoid occur. However, it soon decreases and reaches a minimum where the micelles can be considered as polydisperse spheres. Upon further addition of butanol the axial ratio starts to increase again. The SANS measurements have been complemented with light scattering and viscosity measurements which support the SANS results.

1.102 Studies of 1-C_{16}-2-C_6-PC Rod-like Micelles by Small-angle Neutron Scattering

T.L. Lin, Y. Hu, *Department of Nuclear Engineering, National Tsing-Hua University, Hsin-Chu, Taiwan*, S.-H. Chen, *Department of Nuclear Engineering, Massachusetts Institute of Technology, Cambridge, USA*, M.F. Roberts, *Deptartment of Chemistry, Boston College, Chestnut Hill, Massachusetts, USA*, J. Samseth, *Institutt for energiteknikk, Kjeller, Norway*, and K. Mortensen, *Department of Solid State Physics, Risø National Laboratory, Danmark*

Small-angle neutron scattering studies have been made in order to determine the structure of the 1-hexadecanoyl-2-hexanoyl-phosphatidylcholine (1-C_{16}-2-C_6-PC) and the 1-hexanoyl-2-hexadecanoyl-phosphatidylcholine (1-C_6-2-C_{16}-PC) lecithin micelles in aqueous solutions. The investigated concentrations are from 1 mM to 30 mM for 1-C_{16}-2-C_6-PC, and from 0.2 mM to 3 mM for 1-C_6-2-C_{16}-PC. Both the two isomeric synthetic lecithins have one long hydrocarbon chain and one short hydrocarbon chain. The $\ln(I(q)q^2)$ versus q^2 plots show that both lecithins form very large rodlike micelles even at very low concentrations. The radius of gyration of the cross section of these rodlike micelles, R_c, is found to be 18.5 ± 0.2 Å for 1-C_{16}-C_6-PC, and 19.9±0.8 Å 1-C_6-2-C_{16}. These two cross sectional radii of gyration are much larger than that for short-chain (with 6-8 carbons on each hydrocarbon chain) lecithin rodlike micelles. The aggregation number per unit rod length are determined to be 2.74±0.34 $Å^{-1}$ for 1-C_{16}-2-C_6-PC, and 2.56±0.46 $Å^{-1}$ for 1-C_6-2-C_{16}-PC. Each lecithin molecule in the straigth section of these rodlike micelles occupies about 53 $Å^2$ at the surface of the hydrocarbon core. The low value of the surface area occupied by each lecithin molecule indicates that the wedge shaped hydrophobic parts of the 1-C_{16}-2-C_6-PC and 1-C_6-2-C_{16}-PC molecules conform very well in the rodlike structure. The scattering intensities are found to increase faster than $1/q$ with decreasing q in the very low-q region for higher concentration samples. There must be strong attractive interactions between these rodlike micelles at high concentrations or these rodlike micelles may be flexible and entangle with each other at high concentrations. The weight averaged length of the polydispersed rodlike micelle formed by 1-C_6-2-C_{16}-PC at dilute concentrations of 0.2 mM and 0.4 mM are respectively determined to be 317 Å and 383 Å. The size distributions of these two low concentration micellar solutions are also obtained by using the indirect Fourier transformation method.

1.103 Swelling of Multi-lammellar Membrane Systems Induced by the Main Phase Transition

T. Hønger, J.H. Ipsen, J. Lemmich, O.G. Mouritsen *Department of Physical Chemistry, The Technical University,Denmark*, K. Mortensen, *Department of Solid State Physics, Risø National Laboratory, Denmark*, and R. Bauer, *Department of Mathematics and Physics, The Royal Veterinary and Agricultural University, Denmark*

Fluid, lipid bilayer membranes can at length scale much larger that the membrane thickness ($\sim$ 3 nm) be considered as a simple fluctuating surface with conformation properties determined by mechanical quantities like bending and splay rigidities, while surface tension is vanishing. However, the complex molecular microscopic structure of the membrane and in-plane cooperative phenomena is in general expected to modify the large-scale thermodynamic properties of the membrane. This seems to play a role in a range of biologically relavant membrane processes. A simple model system to investigate this coupling is the synthetic single-component phospolipid membranes, which display a first-order melting transition involving a disordering of the acyl chains and melting of the two-dimentional crystalline arrangement of the lipid molecules. As the acyl-chain length is shortened the transition becomes pseudo-critical with associated meso-length-scale density fluctuations in the transition region The effect of these in-plane fluctuations on the bending rigidity is reflected in conformational fluctuations of the membrane and the conformational entropy-driven repulsion between membranes in a multi-lamellar system. By small-angle neutron scattering of multi-lammellar dispersions of DMPC and DPPC vesicles it has been demonstrated that intermembrane repulsion is increased dramatically in the phase-transition region (Fig. 1). This observation indicates that the membrane bending rigidity is reduced significantly in the main phase transition region. Further, it has been demonstrated that a membrane protein, Grammicidin A, removes this swelling of the membranes around the transition temperature, in agreement with the expectation that this protein reduces the density fluctuations in the transition region.

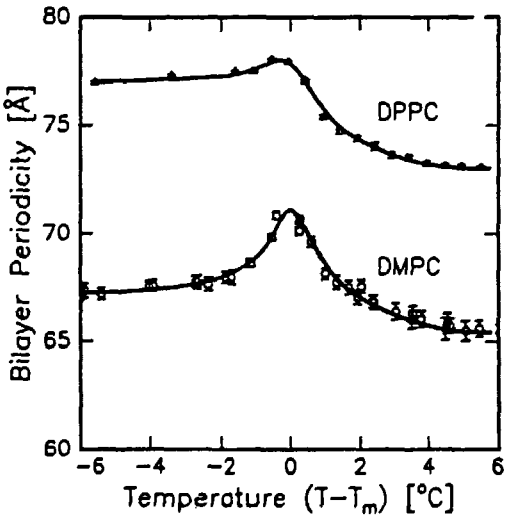

Fig. 1. Lamellar repeat distance for multilamellar bilayers of DMPC-d_{54} and DPPC-d_{62} plotted as a function of $T-T_m$, where T_m is the main transition temperature.

1.104 The Conformation of the Inositol Headgroup in Biological Membranes

J.P. Bradshaw, *University of Edinburgh, Scotland, UK*, R. Bushby, C. Giles, *University of Leeds, England, UK*, and J. Skov Pedersen, *Department of Solid State Physics, Risø National Laboratory, Denmark*

Phosphatidyl inositol is perhaps the most interesting of the phospholipids; it is the ultimate source of the second messengers inositol 1,4,5-trisphosphate and diacylglycerol and provides a covalent anchor for some important membrane proteins. However, experimental data on its headgroup orientation in biomembranes is limited to our own 1H-NMR and 2H-NMR spectroscopic measurements which indicate some ordering of the headgroup.

We have developed a synthesis procedure for DMPI and have produced it in five different forms: one undeuterated, and others specifically deuterated at either the sn3 position, carbon 2 of the inositol ring, carbons 4 and 6, or at all six carbons of the head group. Considerable time and effort has been expended in characterising the phase behaviour of DMPI, using X-ray diffraction and NMR. Unlike most other biological phospholipids, DMPI will not take up water from a humid atmosphere at normal temperatures, precluding its use in multi-bilayer stack diffraction experiments. However, it does order extremely well, producing highly aligned bilayers even when they are separated by 200 Å or more. For the SANS experiments the samples were prepared in specially manufactured cylindrical aluminium vials, where the DMPI oriented itself in concentric cylinders around the walls of the vessel. Two different levels of hydration were used and four different H_2O:D_2O ratios. Up to three orders of diffraction were obtained from all of the samples measured. The peaks were integrated after radial summing and background subtraction by curve fitting.

With only three orders of diffraction it is difficult to analyse the results in terms of Fourier inversions to produce neutron scattering profiles of the unit repeat. However, since the different deuterium labels approximate to Gaussian distributions in the difference profiles, analysis may proceed by fitting Fourier transforms of Gaussian models to the difference stucture factors. This is the approach we are currently employing, with additional information to aid this process coming from our recent neutron work on DMPC/DMPI mixtures, at much smaller repeats, using the same deuterated analogues, where eight orders of diffraction are available. Together, the two sets of data complement each other to give a much more comprehensive picture of the conformation and interactions of this most peculiar lipid.

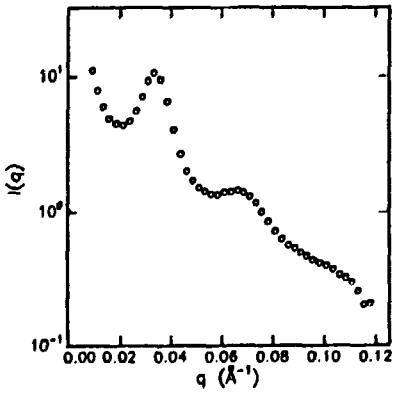

Fig. 1. The diffraction data set for perdeuterated DMPI in 100% D_2O recorded by the small-angle scattering instrument.

1.105 Structural Changes in Casein Micelles Studied by SANS

S. Hansen, R. Bauer, *Department of Mathematics and Physics, Royal Veterinary and Agricultural University, Denmark*, S. Lomholt, K. Quist, *Department of Dairy Research, Royal Veterinary and Agricultural University, Denmark*, G. Jones, M. Samsò, *Biology Support Laboratory, Daresbury Laboratory, UK*, J. Skov Pedersen, and K. Mortensen, *Department of Solid State Physics, Risø National Laboratory, Denmark*

The major part of the protein in cow's milk is present in the form of casein micelles. These micelles have an overall size of up to about 300 nm and consist of spherical submicelles of diameters of about 10-20 nm. The submicelles are connected by calcium phosphate in a concentration of 8 g per 100 g casein.

Upon addition of the enzyme chymosin the casein micelles start to clot. This is due to chymosin splitting off a negatively charged fraction of κ-casein on the surface of the micelles, and by this reducing the repulsion between the micelles. This is the core of the process responsible for the making of cheese from milk.

We have studied the structural changes in the casein micelles upon the aggregation initiated by the addition of chymosin and for this purpose we have used small-angle light X-ray and neutron scattering. The light scattering has been performed at the Royal Veterinary and Agricultural University, Copenhagen, the X-ray scattering at Daresbury Laboratory, UK, and the neutron scattering at Risø National Laboratory. The combination of the three different techniques allows a broad range of length scales to be investigated by the complementary q-ranges and scattering lengths involved. At SANS at Risø, changes on a length scale from 1 to 100 nm can be studied, which is appropriate for the study of the submicellar structure.

One set of results of the small-angle scattering studies on casein using neutron as well as light scattering is shown in the figure below. One immediate result of the experiments done, is that no major change in submicellar structure appears to take place upon addition of chymosin. This demonstrates that the structure of the submicelles is conserved when milk is changed into cheese. The further interpretation of the scattering results will be done through indirect Fourier transformation and model fitting.

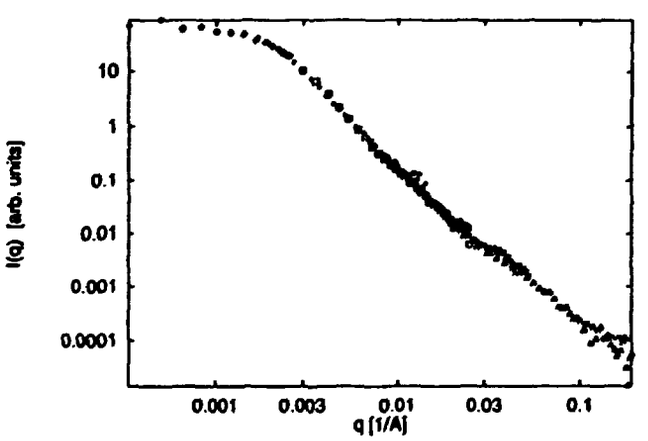

Fig. 1. The combined small-angle scattering data from light and neutron scattering.

1.106 Structure of the 50S Subunit of E. Coli Ribosomes from X-ray and Neutron Contrast Variation

D.I. Svergun, P. Brouillon, M.H.J. Koch, *EMBL, Hamburg Outstation, Germany*, J. Skov Pedersen, *Department of Solid State Physics, Risø National Laboratory, Denmark*, and I.N. Serdyuk, *Institute of Protein Research, Russian Academy of Sciences, Poustchino, Russia*

New methods of small-angle scattering data analysis were applied to a contrast variation study of the 50S ribosomal subunit of Escherichia Coli in solution. A preliminary model was obtained based on synchrotron radiation scattering data in sucrose solutions collected at the X33 camera of the EMBL in HASYLAB (DESY, Hamburg). The shape scattering from the 50S as well as the scattering curves from the RNA and protein component were evaluated. From these the shape of the particle volume inaccessible to sucrose and that of the RNA were determined. The two shapes were positioned so that their difference, which corresponded to the volume occupied by the proteins, produced a scattering curve which was in a good agreement with the experimentally determined scattering from the proteins. Further refinement was done in the frame of the advanced two-phase model[1] described by the shapes of the 50S subunit and its RNA taking into account density fluctuations inside the RNA and the protein moiety. Neutron contrast variation data collected at the SANS facility of Risø were fitted simultaneously with the X-xay curve in water. The shapes of the envelope of the 50S subunit and the RNA core inside it were evaluated with a resolution of about 4 nm (Fig. 1). The shape of the envelope is in good agreement with the models of the 50S subunit obtained by electron microscopy on isolated particles[2,3]. The shape of the RNA core correlates well with the model of the entire particle determined by crystalline diffraction from ordered sheets[4]. We conclude that the interpretation of the diffraction data which is based on the subjective contouring of density maps is strongly biased towards the RNA.

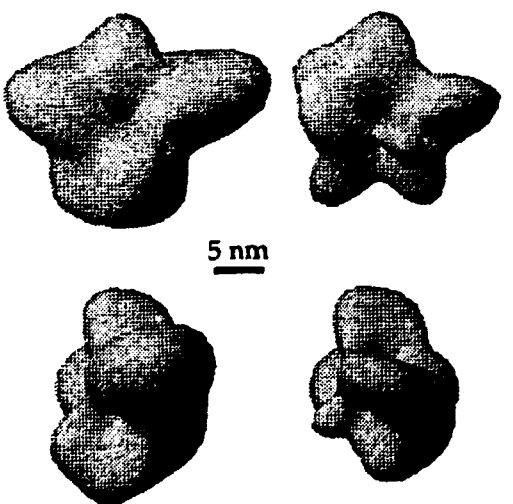

Fig. 1. Solid models of the 50S subunit (left) and its RNA (right). Top row: Crown view. Bottom row: Kidney view.

[1] D.I. Svergun, (1994). Acta Cryst. **A50**, *in press.*
[2] J.A. Lake, (1985). Ann. Rev. Biochem. **54**, 507.
[3] M. Rademacher, T. Wagenknecht, A. Verschoor, and J. Frank, (1987). EMBO Journal **6**, 1107.
[4] A. Yonath, K.R. Leonard, and H.G. Wittmann, (1987). Science **236**, 813.

1.107 Investigation of Moderately or Highly Concentrated Solutions of Colloidal Particles

B. Sjöberg, *Department of Medical Biochemistry, University of Göteborg, Sweden*, and
K. Mortensen, *Department of Solid State Physics, Risø National Laboratory, Denmark*

Moderately or highly concentrated solutions of colloidal particles are very complicated systems to understand both from the thermodynamic and structural point of view. This is mainly due to the fact that the non-ideality caused by the interparticle interaction potential arising from the surface charge, as well as from the ionic properties of the solvent, is very difficult to deal with theoretically.

Since most real systems, like biological fluids, solutions in technical processes, surfactants, lubricants, emulsifiers, *etc.*, deviate strongly from ideality, it is desirable to develop both experimental and theoretical methods for the exploration of the forces between colloidal particles. Especially in biochemistry it is very important to understand the behavior of highly non-ideal media. As an example: the thermodynamic activity of hemoglobin with the concentration; at the *in vivo* concentration of hemoglobin within the erythrocytes (about 35%) the activity is approximately 100 times its concentration, which clearly demonstrates the errors introduced when neglecting activity factors.

In this work we have used the SANS method to study the interactions and interparticle structure in solutions of human serum albumin (HSA) at varying concentration of NaCl. In order to obtain a model for the interactions, we have combined the SANS data with results obtained by Monte Carlo simulations, where we calculate the structure factor $S(Q)$ and the pair correlation function $g(r)$. The advantage of using the Monte Carlo method is that completely general models for the particle shape and the interactions can be considered. It is found that the SANS data can be explained by a model where the shape of the HSA molecule is approximated by an ellipsoid of revolution with semiaxes $a = 6.8$ nm and $b = 1.9$ nm (Fig. 1). The interaction potential between the HSA molecules consists of two parts originating from the properties: (a) the molecules are hard and impenetrable and (b) the molecules are surrounded by a spherically symmetric repulsive potential which can be expressed by a simple empirical formula. As expected the repulsive potential is more dominant at lower ionic strengths. Knowledge of the interaction potential opens the possibility to simulate other properties of the system, *e.g.* properties which are not directly attainable by experiments.

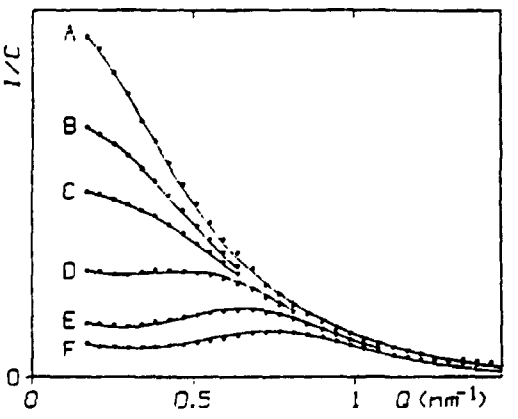

Fig. 1. Example of a data set obtained in 1.08 M NaCl and HSA concentrations from 0.0048 g/cm^3 (A) to 0.26 g/cm^3 (F). The points are the experimental SANS data and the curves represent the intensities calculated from the structure factor $S(Q)$, obtained by Monte Carlo simulation.

1.108 Structure and Reactions of the Humic Acids

R. Österberg, *The Swedish University of Agricultural Science, Uppsala, Sweden*, and K. Mortensen, *Department of Solid State Physics, Risø National Laboratory, Denmark.*

Humic acids, which are the main organic components present in soil and natural water systems, have been considered as a complex, highly disordered and polydispersed system for a long time. However, thanks to new structural studies using SANS, it has now been possible to characterize humic acids in physical terms: the scattering intensity from humic acids obeys a power law almost over two orders of magnitude in length scale of the scattering vector, Q, indicating that the structure is fractal (Fig. 1). The upper cut-off length of the fractal clusters vary in the range 200 to 700 Å, depending on method of preparation and composition[1,2]. However, the fractal dimension is essentially constant at 2.3±0.1. The autocatalytic polymerization of humic acids at pH 5 shows several criterions of kinetic growth. In agreement with the Smoluchowski equation, it depends on time and temperature but it is virtually independent of concentration. For instance, in the range 0.05 mg/ml to 2.5 mg/ml, SANS spectra from humic acid solutions yields in a log I versus log Q plot a set of parallel data, which collapse on a master curve. In addition, time-resolved electromotive force data of humic acids show no indication of equilibria. The temperature dependence is indicated by a restructuring of humic acids which occurs when the temperature is raised from 4° to 20°C. Then SANS data shows a change in fractal dimension from 1.85 to 2.5, which is complete within 35-40 hours. Simultaneously, electromotive force data show a flux of protons: an initial fast release of protons from the humic acids is followed by a slow uptake. The latter relaxes with a time constant of 22 hours, which is in good agreement with the SANS data[3].

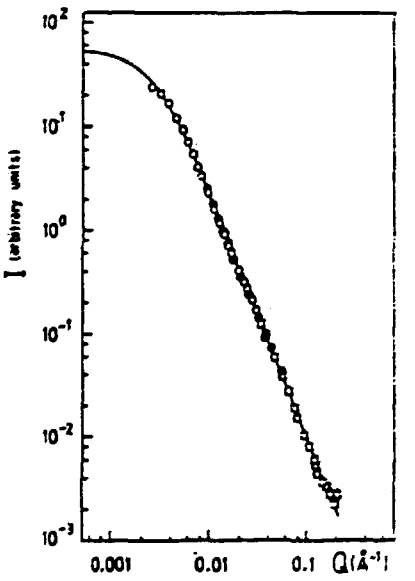

Fig. 1. SANS data, log(I) versus log(Q), from humic acids in a D_2O buffer.

[1] R. Österberg and K. Mortensen, (1992). Eur. Biophys. J. **21**, 163.
[2] R. Österberg, I. Lindqvist, and K. Mortensen, (1992). Soil. Sci. Coc. Am. J. **57**, 283.
[3] R. Österberg, L. Szajdak, and K. Mortensen (1994), Enviromen. Int. **20**, 77.

1.109 Solution Conformation of a Coiled-coil Protein from Salmonella Typhimurium

K. Österlund, R. Hurme, P. Koski, M. Rhen, M. Torkkeli, *Departments of Biochemistry and Physics, University of Helsinki, Finland*, B. Sjöberg, *Department of Medical Biochemistry, University of Göteborg, Sweden*, and K. Mortensen, *Department of Solid State Physics, Risø National Laboratory, Denmark*

A very specialized class of fibrous proteins consists of the double alpha helical coiled-coil proteins, exemplified by the abundant muscular proteins myosin and tropomyosin[1]. The general understanding of the remarkable capacity of the musculoskeletal system to perform lokomotion, deriving the required energy from ATP, is currently emerging, although the precise details as to the small movements at a molecular level have still to be worked out. Recently extensions to this family of proteins are the so-called leucine zippers, with the capacity to bind DNA, and, from the prokaryotic world, M6 from Streptococcus pyogenes[2]. This latter protein was soon found to play a role enabling this bacterium to evade attention of the immune system of the human host, ultimately leading to symptoms of streptococcus infection.

A related protein is the recently discovered[3] tropomyosin-like coiled-coil protein TlPA from Salmonella typhimurium. The amino acid sequence and secondary structure were worked out[3], and were found to be based on the same heptad repeat principle found in previous coiled-coil protein chains. There are, on the other hand, distinct differencies in the sequence, suggesting that the function in this case is based on different molecular mechanisms.

To understand the conduit of TlPA, especially the tendency to dimerize and multimerize, a series of experiments based on the small-angle neutron scattering technique have been initiated. The results obtained so far indicate that TlPA has a pronounced tendency to form long aggregates in solution. At present we investigate the effects of different chemical parameters upon this aggregation, hopefully the basis for a physico-chemical understanding of the behavior of TlPA in physiological milieu should be laid, eventually forwarding the understanding of the possible role of this coiled-coil variant from Salmonella.

[1] C. Cohen and B.A.D. Parry, (1990). Proteins: structure, function and getetics 7, 1.
[2] V.A. Fischetti, (1991). Sci. Am. **264:6**, 32.
[3] P. Koski, H. Saarilahti, S. Sukupolvi, S. Taira, P. Riikonen, K. Österlund, R. Hurme, and M. Rhen, (1992). J. Biol. Chem. **267**, 12258.

1.110 New Stretching Cell for Structural Studies of Elastomers and Swollen Gels

A.N. Falcão, J. Skov Pedersen, and K. Mortensen, *Department of Solid State Physics, Risø National Laboratory, Denmark*

A stretching cell is now available at the Risø small-angle neutron scattering facility (see Fig. 1). It was developed to enable structural studies on uniaxially stretched elastomers and swollen gels. The samples to be used in the experiments must have rectangular shape. Parallel to the stretching direction a minimum length of 35 mm is required, and in the perpendicular direction a maximum width of 12 mm is possible. The samples cannot have a thickness larger than 2.5 mm before stretching. The samples are clamped to two collinear axis, each of them connected to a micrometer. The maximum extension ratio, λ, permitted in the present version, is 2.0. The cell is equipped with quartz windows and is vacuum tight. The apparatus was used in studies of uniaxially stretched, swollen polydimethylsiloxane (PDMS) networks produced by electron irradiation. Samples with four different linking densities were measured, each of them at different extension ratios. The isointensity contour of Fig. 2 shows a typical result obtained. In the low scattering vector region, the characteristic butterfly pattern is observed. At high q the contours show a classical elliptical shape alongated in the direction perpendicular to the stretching. For all the samples measured there is an intermediate q value for which the contour is circular. This particular q value varies from sample to sample (obeying a scaling relation with the cross-linking density) and is, within experimental accuracy, independent of λ for each sample.

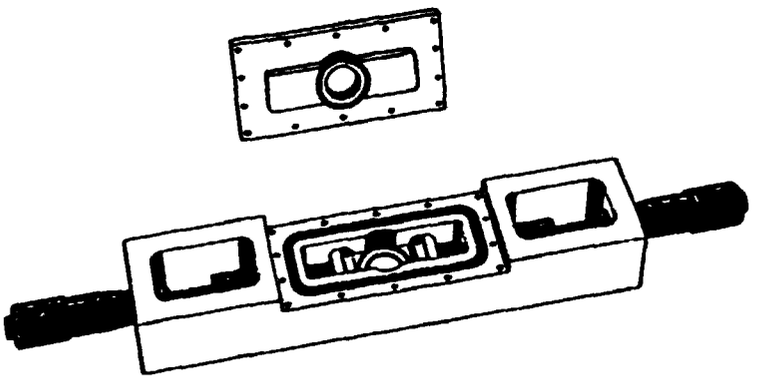

Fig. 1. Perspective view of the stretching cell.

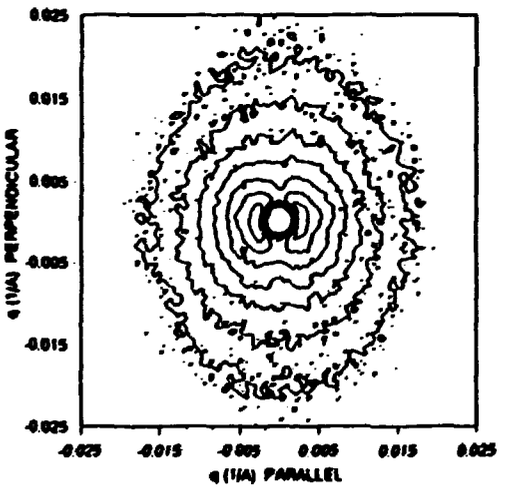

Fig. 2. Isointensity contour plot obtained from a PDMS network swollen in fully deuterated p-xylene and stretched to an extension ratio $\lambda = 1.9$.

1.111 Polarized Neutrons for Reflectometry

M.C. Gerstenberg and K.N. Clausen *Department of Solid State Physics, Risø National Laboratory, Denmark*

In reflectometry only a narrow neutron beam is used ($\leq$ 2 mm), and it is possible to design a transmission polarizing device for cold neutrons using a simple arrangement of supermirrors (SM), allowing transmission of only one spin state in a region up to six times the critical angle of Si. The SM consists of thin Si wafers which have been coated by a sequence of Fe-Si bilayers. The bilayer sequence is determined by Hayter's algorithm[1] and varies from 450 Å to 102 Å with a thickness ratio of Fe to the total thickness of 0.55.

The overall performance of the device is limited by the individual supermirror (SM), which therefore was investigated by reflectometry with polarized and un-polarized neutrons. A theoretical prediction, supplied by the manufacturer Ovonic Synthetics, estimated the region of acceptance to lie between a momentum transfer of 1.02×10^{-2} Å^{-1} and 6.20×10^{-2} Å^{-1}. This was verified experimentally.

Due to the warping of the thin SM's, stacks had to be used to improve the rigidity. It was found that the polarizing efficiency increase with better collimation of the incident beam and decrease with the number of SM's in the stack. The latter effect was explained by internal multiple reflections between the SM's in the stack, which direct the multiple reflected beam in the direction of the transmitted. Six stacks of five SM's were arranged in two rows with "accordion" geometry to compromise between rigidity and flatness of the mirrors and multiple scattering. The primary design parameter is the angle of incidence of the neutrons on the SM's, which was chosen to 0.8° corresponding to a working point in the mid-acceptance range for neutrons of wavelength 4.75 Å. The flipping ratio of this device is slightly above 20 for a beam width up to 2 mm. This is a minimum value due to the finite efficiency of the different parts of the experimental set-up (*e.g.* the Heusler alloy and the Mezei flipper).

The magnetism of the Fe-layer in a 202 Å MgO/ 402 Å Fe/ (100)MgO epitaxially grown film was investigated by the neutrons polarized by the device[2].

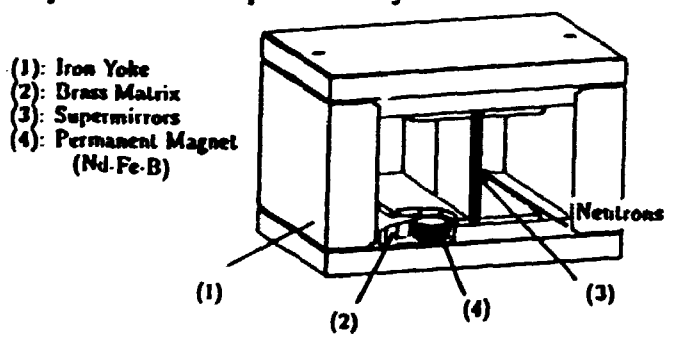

Fig. 1. The device (120 x 180 x 117 mm^3). Inside each brass matrix 15 permanent magnets ensure a minimum field of 0.06 T in the center of the gab sufficient for saturation of the supermirrors.

[1] J.B. Hayter and H. A. Mook, (1989). J. Appl. Cryst. 22, 35.
[2] Contribution 1.22 in this report.

1.112 Software for Analyzing Image-plate Data

A.R. Sandy, J. Bohr, *Department of Solid State Physics, Risø National Laboratory, Denmark*, and M.L. Petersen, *Department of Physics, Odense University, Denmark*

An image plate is a flat storage-phosphor screen. Image plates have a wide dynamic range ($\approx 10^5$), a large (20×25 cm^2) collection area, fine spatial resolution (≈ 100 μm), and high photon detection efficiency at typical X-ray-scattering energies. We conclude that the image plate is an ideal detector for many X-ray-scattering experiments. Risø recently purchased an image-plate system. A major weakness, however, of the as-supplied system is the lack of suitable software for analyzing the image-plate data. Specifically, software that can perform azimuthal integrations around Debye-Scherrer powder-diffraction rings recorded on the image plate. The azimuthal integrations must be performed as a function of radius (directly related to the scattering angle $\equiv 2\theta$) about a center position on the image plate. The two-dimensional image-plate data can thus be reduced to a more conventional one-dimensional form - scattered intensity versus 2θ - suitable for ordinary Rietvald analysis, but with the considerably enhanced signal obtained from using an area detector. These capabilities require, in turn, software that optimizes, via a greatest-squares criterion[1], the parameters that define the integration. These considerations motivated us to write our own software, the use of which is illustrated below. Figure 1 is a grey-scale representation of the scattering from a 10 μm thick Ni foil recorded by an image plate. The white irregular region near the center of the image is the shadow of the direct-beam stop. The ellipses surrounding it are the (111) (darker ellipse) and the (200) (lighter ellipse) Debye-Scherrer rings. The incident X-ray beam was graphite monochromatized radiation from a Cu-target rotating anode. For demonstration purposes, the image plate was intentionally skewed with respect to the incident X-ray beam. Figure 2 shows the resulting intensity versus 2θ profile obtained via integration using the optimized parameters. Evidently, we can successfully reduce data from the image plate to one-dimensional form. Before the image plate finds routine use however, it remains to measure and correct the spatial distortion of the image induced by the scanner.

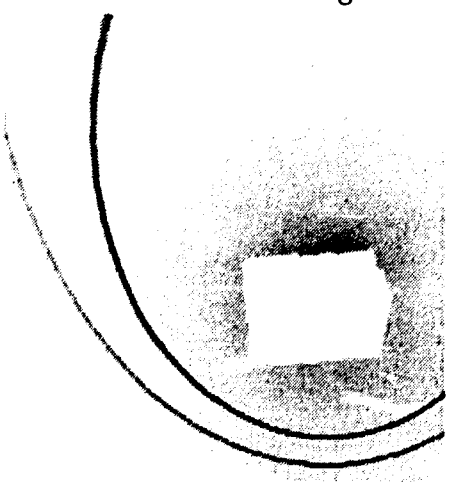

Fig. 1. Ni foil scattering recorded by the image plate.

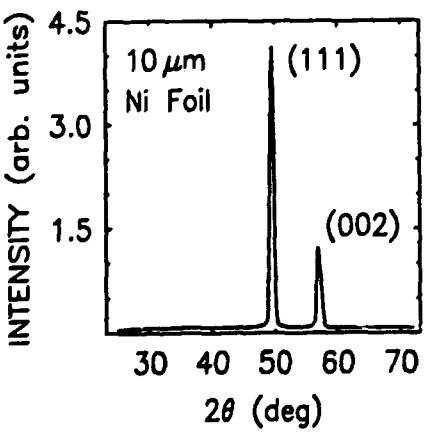

Fig. 2. Intensity versus 2θ for the Ni foil.

[1] R. O. Piltz, M.I. McMahon, J. Crain, P.D. Hatton, R.J. Nelmes, R.J. Cernik, and. G. Bushnell-Wye, (1992). Rev. Sci. Instrum. **63**, 700.

1.113 An Image-plate Camera for X-ray-Scattering Measurements of Freely Suspended Clusters

A.R. Sandy and J. Bohr, *Department of Solid State Physics, Risø National Laboratory, Denmark*

Experimental determination of the geometric structure of freely suspended clusters is a fundamental problem in cluster research. Given its success in determining bulk and surface structures, X-ray scattering seems an obvious choice for determining cluster structures. One reason for this success is that X-rays interact weakly with matter so the scattering cross section can be reliably calculated using only the first Born approximation. But, on account of their low number density, this is also why it has not been possible to study free clusters using X-rays.

Two recent developments have, however, made X-ray-scattering studies of free clusters more feasible. The first is the high incident X-ray intensities available from a third-generation X-ray source like the ESRF in Grenoble. Even at the ESRF, however, the expected scattering is still very weak. We can hope to overcome this by integrating the scattered signal over a large solid angle using an image plate[1)]. To be effective though, the image plate must be isolated from all sources of background, for example, air scattering and scattering from the incident X-ray-beam collimating slits. These considerations motivated us to design and construct a special image-plate camera.

A schematic cross section through the image-plate camera is shown in Fig. 1. The wedge-shaped chamber on the right holds the image plate. The flange on the bottom couples to the last differentially-pumped stage of a cluster source. A crystal oscillator for measuring mass deposition is attached to the top flange. The long arm to the left (the collimating arm) has motorized slit systems at either end. They collimate the incident X-ray beam and remove any stray scattering. During operation, the entire assembly is under a common vacuum - except for the X-ray entrance on the left, there are no windows in the system that contribute to background. Another feature is stainless steel tubes passing the length of the collimating arm; they shield the image plate from stray radiation.

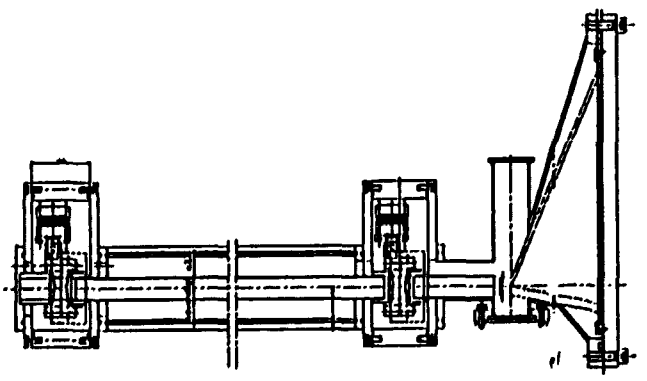

Fig. 1. Cross section of the image-plate camera.

[1)] Contribution 1.111 in this report.

1.114 Double Focussing Laue-Bragg Monochromator at Troika Beamline in ESRF

J. Als-Nielsen, A. Freund, G. Grubel, *ESRF, Grenoble, France*, and M. Nielsen, *Department of Solid State Physics, Risø National Laboratory, Denmark*

The Troika beamline at ESRF is an undulator line, where the principle of simultaneous use of an X-ray beam by several measuring stations has been implemented. Each station uses a monochromator crystal in Laue-geometry (transmission) to extract a narrow energy band (relative energy resolution of 10^{-4}). In order to further exploit the radiation from the undulator a new beamline geometry has been tested in a preliminary experimental set-up. The measuring stations of the existing Troika line are located 42 m from the undulator source and outwards. In front of the experimental hutch at a distance of 27 m from the source a new monochromator box was inserted in the beamline and from here a monochromatic beam could be extracted with the help of a diamond crystal in Laue-geometry. A second crystal, Ge(220), reflects the monochromatic beam to be almost parallel to the existing beamline, but displaced from this about 0.5 m. Different principles for focusing in both horizontal and vertical direction can be realized and the techniques were investigated in the new set-up. Horizontal focusing was studied for an asymmetric Laue monochromator using the (111) reflection of a diamond crystal with (100) faces. Vertical focussing is obtained by sagittally bending the Ge (220) crystal, and for the latter the figure below illustrate the results.

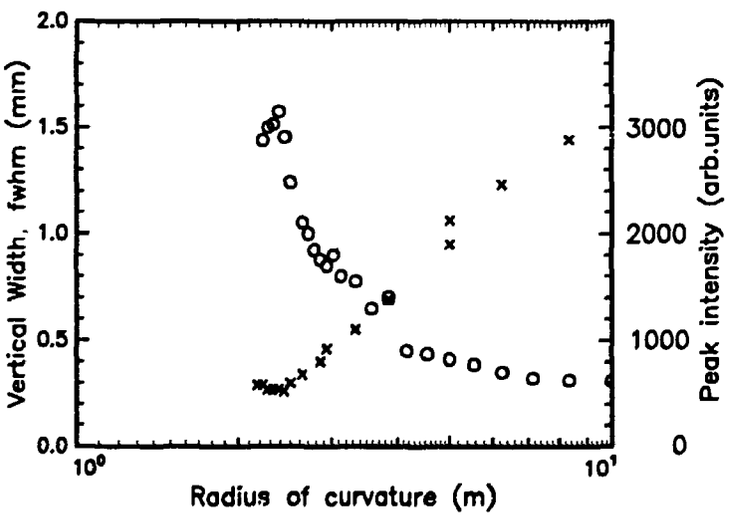

Fig. 1. The vertical width (x) and the peak intensity (o) of the X-ray beam 10 m from the Ge crystal and 38 m from undulator.

1.115 LIP - CEC Large Installation Programme at Risø

K. N. Clausen, *Department of Solid State Physics, Risø National Laboratory, Denmark,*
A.R. Mackintosh, *Niels Bohr Institute, Ørsted Laboratory, University of Copenhagen, Denmark*

The CEC Large Installation Programme was initiated in order to make large national facilities available to users from the whole EC, to promote European collaboration and to make more facilities available to the less favoured regions in the EC.

The cold neutron facilities at DR3 were included in this programme from early 1992. Risø receives funds from the CEC to cover the marginal expenses in connection with neutron scattering experiments. The programme covers (1) Travel and subsistence for the users, (2) Salaries to staff employed to run the user programme, (3) Running expenses (consumable), (4) Purchase of auxiliary equipment requested by the users, and (5) A contribution to the continued modernization and upgrading of the facilities.

The programme is managed by a programme director (A.R. Mackintosh) representing the users and a project leader (K.N. Clausen) responsible for the facilities and the practical arrangements in connection with the experiments.

Proposals for experiments are refereed by a group of four international experts, in collaboration with the programme director. Beam time is allocated four times a year, and amounts to 79 instrument weeks per year, approximately 30% of the available resources. Experiments are generally collaborative efforts between the user and Risø via the local contact. The duration of a single experiment is from 1/2 - 3 weeks, and both junior and senior visiting scientists participate in the experiment. In total approximately 110 EEC-scientist have spent up to three weeks at Risø during 1993 in connection with LIP experiments.

During 1993 an orange cryostat and a 9 T vertical field magnet has been aquired for the programme. The slit system for the reflectometer set-up on TAS8 has been motorized, a new analyzer for TAS7, and an improved focussing PG-002 monochromator has been installed on TAS3. All instruments have now been converted to the new motor drive system with up to 24 motors per spectrometer.

Below is a list of the titles of the LIP experiments performed in 1993. The column "Proposer" contains the first name on the proposal. The local contact at Risø is shown by initials (**NHA:** N.H. Andersen, **KNC:** K.N. Clausen, **DJJ:** D.J. Jensen, **KK:** K. Kjær, **BL:** B. Lebech, **TL:** T. Lorentzen, **TM:** T. Mason, **DFM:** D.F. McMorrow, **KM:** K. Mortensen **JSP:** J. Skov Pedersen). Reports on the experiments below will be published in the annual LIP report.

Proposer	Local contact	Title
M. Alba	TM	Mode Coupling Theory and Critical Dynamics of Disordered Ferromagents
J. Bradshaw	JSP	The Conformation of the Inositol Headgroup in Biological Membranes
E. Brecht	NHA	Location of Excess Oxygen in Al-doped Tetragonal $YBa_2Cu_{3-x}Al_xO_{7-y}$, $x = 0.18$
E. Brecht	NHA	Magnetic Structure of Oxygen Deficient Al Doped $YBa_2Cu_{3-x}Al_xO_{7-y}$ Single Crystals (x=0.19)
E. Brecht	NHA	Change of the Crystal Structure of Heat and Stress Treated, Al Doped $YBa_2Cu_{3-x}Al_x0_{7-y}$, x=0.18, Single Crystals
G. Caglioti	TL	Residual Strain Measurement of Highly Deformed Al Alloys
R.D. Cannon	BL	Crystal Structure of $[Cr_3O(OOCCH_3)6(OH_2)3]$-Cl_6H_2O
C. Cavaco	JSP	Flexibility and Local Structure of Polymerlike Reverse Micelles
M.M.R.R. da Costa	BL	Antiferromagnetism in the Cr-Ga System
R.A. Cowley	DFM	Trigonal Magnetic Interactions in Holmium
R.A. Cowley	TM	Spin Waves and Critical Scattering in $KFeF_4$
R.A. Cowley	KNC	Magnetic Structure of Rare Earth Multilayers
E.M. Forgan	KM	Flux Lattice Structures in Superconductors
E.M. Forgan	BL	Critical Scattering in $CeAl_2$
C. Greaves	BL	Magnetic Order in $YCa_2Fe_4SbO_{12}$
I.W. Hamley	JSP	Orientational Order in Thermotropic Liquid Crystals by Isotope Labelling Neutron Diffraction Experiments
M.J. Harris	KNC	Diffuse Magnetic Scattering From a Frustrated Pyrochlore
S.M. Hayden	BL	A study of the Ordered Moment and Antiferromagnetic Correlation Length in UPt_3
M. Garcia-Hernandez	TM	Low Frequency Dynamics of Liquid and Glassy Selenium
J.S. Higgins	KM	Model Ionomer Associations in Non-Polar Solvent under Shear Flow
J.S. Higgins	KM	Polyofin blends: LLDPE/PP study

H. Hoffmann	KM	The Influence of Ionic Surfactants on the Structural Properties of Micellar Aggregates of PEO-PPO-PEO Triblockcopolymers of a Thermal Dyotropomer
P. Van Houtte	DJJ	Texture Analysis during the Phase Transformation of Low Carbon Steel
J.A.K. Howard	BL	Single Crystal Neutron Diffraction Study of a Thermal Dyotropomer
M.T. Hutchings	NHA	Nuclear Diffuse Scattering From Atomic Disorder in a $La_{2-x}Sr_xCuO_{4+x}$ Single Crystal
W.H. de Jeu	KK	Neutron Reflectivity of Lamellar Triblock Copolymer Films
A. Lied	KK	Neutron Reflectometer Study of Premelting Effects at the Ice-Si interface
P. Lindner	KM	Polymer Solutions under Shear close to the Theta Point
M. Loewenhaupt	BL	Magnons in the Different Phases of $NdCu_2$
M. Lösche	KK	Investigation of the Internal Order of Ultrathin Polymer Films Grown by Incremental Deposition of Polyeletrolytes
K.A. McEwen	KNC	Magnetic Field Dependence of the Magnetic Excitations in Praseodymium
D. McMorrow	KNC	Magnetic Structure of Rare-Earth Superlattices (Ho-Lu)
P. W. Mitchell	BL	Diffraction Studies of Antiferromagnetic Ordering in α-titanium; Ordering Wavevector and Temperature Dependence
P. Müller	KNC	Spin Structure Determination of new Ternary Pnictides
J.A. de Carvalho Paixao	BL	Refinement of the Crystal Structure of UFe_4Al_8 (Single Crystal)
J. Pohl	KNC	Structure and Magnetism of Cr/δ-Mn and Fe/δ-Mn-superlattices
P.B. Prangnell	TL	The Development of Internal Stresses During Forward and Reverse Loading of Plastically Inhomogeneous Metallic based Materials
V. Randle	DJJ	Comparison Between Microtexture and Macrotexture in Hot Rolled Steel
H. Reynaers	KM	SANS of ABA Triblock Copolymer Gel Networks and the Investigation of Their Supermolecular Structure

S.J. Roser	KNC	Neutron Reflection From Biosensors
M. Stamm	KM	Conformation and Morphology of Block Copolymers near the Microphase Seperation Temperature
D. Schwahn	KM	Study of the Pressure and Temperature Dependence of the Flory-Huggins Interaction Parameter in Polymers Blends
U. Steigenberger	KNC	Magnetic Field Dependence of the Magnetic Structures and excitations in UPd_3
W.G. Stirling	KNC	Phonon Temperature-Dependence in Superfluid ^{4}He at $p = 20$ bar
G. Strobl	NHA	Analysis of the "Cage-Motion" in Polyethylene by Coherent Quasielastic Neutron Scattering
R. Strauss	BL	Neutron Diffraction on Single Crystals of $[(CD3)_3$-Sn]$2XO_{4.2}D_2O$, X = S, Se as a basis for Quatitative Interpretation of Tundel Spectra
B. Stühn	NHA	Concentration Fluctuations and Glass Transition in Block Copolymers
G. Swallowe	TL	Physics of Strain Measurements Using Neutrons
D.E.J. Talbot	JSP	SANS Investigation to Determine the Influence of Hydrogen on the Response of an Aluminium-Lithium Alloy of a Commercial Specification to Age-hardening
D. Tsipas	DJJ	Determination of Plastic Yielding in Anisotropic Metals (Zirckalloy-2)
V. Urban	KM	SANS Investigation of Tube Constraints and Microscopic Deformation in Elastomeric Networks
M.R. Wells	TM	Magnetic Order in $BaHo_2F_8$ and $BaEr_2F_8$

2 PARTICIPANTS IN THE WORK IN THE DEPARTMENT

Scientific Staff

Almdal, Kristoffer (From April 1)
Als-Nielsen, Jens (Stationed at ESRF, Grenoble, France)
Andersen, Niels Hessel
Bechgaard, Klaus (Head from August 1)
Berg, Rolf H. (From April 1)
Bohr, Jakob
Buras, Bronislaw (Part time consultant)
Clausen, Kurt Nørgaard
Feidenhans'l, Robert
Grey, Francois (Until March 31)
Hvilsted, Søren (From April 1)
Kjær, Kristian
Lebech, Bente
Lebech, Jens
Lindgård, Per-Anker
Mackintosh, Allan R. (Part time consultant)
Mason, Thomas E. (Until June 30)
McMorrow, Des (From October 1)
Mortensen, Kell
Nielsen, Mourits
Pedersen, Jan Skov
Pedersen, Walther Batsberg (From April 1)
Schou, Jørgen
Sørensen, Gunnar (From April 1 to June 30)

Ph.D. Students and Students

Christensen, Morten Jagd (From April 1)
Falcão, Antonio
Fiig, Thomas
Findeisen, Eberhard
Foss, Morten (Also at the Institute of Physics and Astronomy, Aarhus University)
Gerstenberg, Michael Christian
Hadfield, Richard (From October 1)
Harris, Pernille
Jensen, Carsten Povl (Until August 31)
Lefmann, Kim
Nielsen, Birgitte Thestrup (From February 1)
Pedersen, Marianne (From June 1)
Petersen, Thomas
Svendsen, Winnie (From February 1)
Sørensen, Steen Aagaard (From February 15)

Thoft, Nina Bjørn
Vigild, Martin
Winther, Lars (From April 1)

Temporary Student Assistants

Astradsson, Martin
Kmit, Maryanne
Madsen, Jesper
Oddershede, Lene
Petersen, Morten Lind
Sørensen, Alexis Hammer

Technical Staff

Bang, Steen
Berentsen, Allan (Temporary assistant)
Breiting, Bjarne (From October 1)
Børgesen, Knud-Edward (Temporary assistant)
Christensen, Kaj (On leave until December 31)
Eiby, Jan (Temporary assistant)
Hansen, Christina Fog (Temporary assistant)
Hansen, Lotte (From April 1)
Hubert, Lene (from April 1)
Kjær, Torben
Ladefoged, Tine (Apprentice from November 1)
Linderholm, Jens (Stationed at ESRF, Grenoble, France)
Lund, Morits
Nielsen, Anne Bønke (From April 1)
Nielsen, Steen
Nordskov, Arne
Pedersen, Dorte Juul (Apprentice from November 1)
Petersen, Henrik (Temporary assistant)
Rasmussen, Ove
Saxild, Finn B.
Stahl, Kim
Theodor, Keld
Wichmann, Poul E. (Temporary assistant)

Secretaries

Becker, Helle (Apprentice from September 1)
Frederiksen, Lajla
Kloster, Margit (Until October 31)
Studinski, Ca Thi

Guest Scientists, Long Time Visitors and Post Docs

Bouwman, Wim G.	
Casalta, Helene	
Nishikawa, Hiroyuki	
Montfrooij, Wouter	
Pengra, David (Until July 31)	
Pershan, Peter (Until July 1)	Harvard University, Cambridge, USA
Sandy, Alec R.	
Schleger, Paul	University of British Columbia, Vancouver
Shim, Hae Seop	Korea Atomic Research Institute, Seoul, Korea

Awards and Degrees

Bohr, Jakob, The 1993 Villum Kann Rasmussens Award for Technical Research

Hansen, Lotte and Almdal, Kristoffer, The Martin Marietta Energy Systems Awards Night Achievement for the paper "Molecular Weight Scaling in Critical Polymer Mixtures." by M.D. Gehlsen, J.H. Rosedale, F.S. Bates, G.D. Wignall, L. Hansen, and K. Almdal, (1992). Phys. Rev. Lett. **68**, 2452-2455.

Short Time Visitors (one week or more)

Aeppli, G.	AT&T Bell Laboratories, Murray Hill, New Jersey, USA
Azuah, R.	University of Keele, Staffordshire, UK
Bates, F.S.	University of Minnesota, USA
Bauer, R.	Royal Veterinary and Agricultural University, Denmark
Bertolus, J.	University of Bordeaux, France
Bishop, D.	AT&T Bell Laboratories, Murray Hill, New Jersey, USA
Broholm, C.	The Johns Hopkins University, Baltimore, USA
Brooks, R.L.	University of Guelph, Canada
Buyers, W.J.L.	AECL, Chalk River, Canada
Chen, S.H.	Massachusetts Institute of Technology, USA
Christensen, A. Nørlund	University of Aarhus, Denmark
Dender, D.	The Johns Hopkins University, Baltimore, USA
Dutkiewicz, L.	Jagellonian University, Cracow, Poland
Erikson, S.	Chalmers University of Technology, Gothenburg, Sweden
Fjellvåg, H.	University of Oslo, Norway
Frost, C.	University of Cambridge, UK
Förland, G.	University of Bergen, Norway
Gammel, P.	AT&T Bell Laboratories, Murray Hill, New Jersey, USA
Gehlsen, M.	University of Minnesota, USA
Greedan, J.	McMaster University, Hamilton, Canada
Göthelid, M.	Royal Institute of Technology, Stockholm, Sweden
Hasegawa, H.	University of Kyoto, Japan
Hauback, B.	Institute for Energy Technology, Kjeller, Norway
Hendann, C.	University of Essen, Germany
Huse, D.	AT&T Bell Laboratories, Murray Hill, New Jersey, USA
Hønger, T.	Technical University of Denmark, Lyngby, Denmark
Jünging, Z.	University of Kyoto, Japan
Jørgensen, H.	University of Lund, Sweden
Kawano, S.	University of Kyoto, Japan
Koppi, K.A.	University of Florida, USA
Kulinna, C.	University of Essen, Germany
Lupez, F.	University of Bordeaux, France
Leaver, M.	University of Lund, Sweden
Lottermoser, L.	University of Hamburg, Germany
Lucas, C.	Lawrence Berkeley Laboratory, USA
McEwen, K.	Birkbeck College, University of London, UK
Moiseev, I.	Russian Academy of Sciences, Moscow, Russia
Molinas-Mata, P.	Max Planck Institute, Stuttgart, Germany
Mook, A. H.	Oak Ridge National Laboratory, USA
Moze, O.	Universita Degli Studi di Parma, Italy
Nishikawa, H.	University of Kyoto, Japan
Nordén, B.	Chalmers University, Gothenburg, Sweden

Olsson, U.	University of Lund, Sweden
Reich, D.	The Johns Hopkins University, Baltimore, USA
Rial, C.	Universidad Compultense de Madrid, Spain
Robinson, R.A.	Los Alamos National Laboratory, New Mexico, USA
Sakai, N.	University of Oslo, Norway
Samseth, J.	Institute for Energy Technology, Kjeller, Norway
Scherrenberg. R.	DSM-Research, Geleen, The Netherlands
Schulz, M.F.	University of Minnesota, USA
Schurtenberger, P.	ETH Zürich, Switzerland
Sjöberg, B.	University of Gothenburg, Sweden
Squires, G.	Cavendish Laboratories, University of Cambridge, UK
Takahashi, M.	CNRS, Strasbourg, France
Tishin, A.	Moscow State University, Moscow, Russia
Vaknin, D.	Iowa State University, Ames, Iowa, USA
Wolny, J.	Institute of Mining and Metallurgy, Cracow, Poland
Yaron, U.	AT&T Bell Laboratories, Murray Hill, New Jersey, USA
Yethiraj, M	Oak Ridge National Laboratory, USA
Zebger, I.	University of Essen, Germany
Österberg, R.	Agricultural University of Sweden, Uppsala, Sweden

Visitors under the CEC Large Installation Program (one week or more)

Abetz, V.	Max Planck Institute, Mainz, Germany
Alba, M.	Institute Laue-Langevin, Grenoble, France
Al-Kanini, H.J.	University of Salford, UK
Allibon, J.R.	European Molecular Brology Laboratory, Grenoble, France
Amador, U.	Universidad Compultense de Madrid, Spain
Bartels, V.	Max Planck Institute, Mainz, Germany
Booth, J.G.	University of Salford, UK
Boothroyd, A.	Clarendon Laboratory, Oxford University, UK
Boué, F.	Léon Brillouin Laboratory, Saclay, France
Bourke, J.P.	University of East Anglia, Norwich, UK
Bradshaw, J.	University of Edinburgh, UK
Brecht, E.	Technical University, Darmstadt, Germany
Cannon, R.D.	University of East Anglia, Norwich, UK
Caruana, D.	University of Bath, UK
Cavaco, C.	ETH Zürich, Switzerland
Clock, V.	Imperial College, London, UK
Copley, R.	University of Durham, UK
Cowley, R.A.	Clarendon Laboratory, Oxford University, UK
Cubitt, R.	University of Birmingham, UK
Costa, M.M.R.R.	University of Coimbra, Portugal
Desert, A.	University of Le Mans, France
Dosch, H.	University of Munich, Germany
Downes, T.	Cavendish Laboratories, University of Cambridge, UK
Enderlee, M.	University of Mainz, Germany
Forgan, E.M.	University of Birmingham, UK
Garcia-Hernandez, M.	Instituto de Estructura de la Materia, Madrid, Spain
Geselle, M.	Technical University of Darmstadt, Germany
Gibbs, M.	University of Keele, Staffordshire, UK
Giles, C.	University of Leeds, UK
Goncalves, A.	LNETI/ICEN Sacavém, Lisbon, Portugal
Gradzielski, M	University of Bayreuth, Germany
Greaves, C.	University of Birmingham, UK
Grünewald, T.	University of Mainz, Germany
Hansen, C.	University of Freiburg, Germany
Harris, M.	Clarendon Laboratory, Oxford University, UK
Hayden, S.	University of Bristol, UK
Henry, D.	University of Brunel, Uxbridge, UK
Holzer, B.	University of Freiburg, Germany
Hutchings, M.T.	AEA Industrial Technology, Oxford,UK
James, H.	Imperial College, London, UK
Janssen, S.	IFA-KFA Jülich, Germany
de Jeu, W.	FOM-Institute for Atomic & Molecular Physics, The Netherlands

Jayasooriya, U.A.	University of East Anglia, Norwich, UK
Jehan, D.	Clarendon Laboratory, Oxford University, UK
Jeremy, M.	University of Birmingham, UK
Kimmig, M.	University of Freiburg, Germany
Langridge, S.	University of Keele, Staffordshire, UK
Larkman, D.	University of Manchester, UK
Leask, M.	Clarendon Laboratory, Oxford University, UK
Lee, S.L.	University of Birmingham, UK
Lied, A.	Institute Laue-Langevin, Grenoble, France
Lindner, P.	Institute Laue-Langevin, Grenoble, France
Loewenhaupt, M.	IFA-KFA Jülich, German
Longmore, A.	Clarendon Laboratory, Oxford University, UK
Lowden, J.	University of Manchester, UK
Lösche, M.	University of Mainz, Germany
Mason, S.	Institute Laue-Langevin, Grenoble, France
Martinez, J.L.	Instituto de Estructura de la Materia, Madrid, Spain
McEwen, K.	Birkbeck College, University of London, UK
McGreevy, R.L.	Clarendon Laboratory, University of Oxford, UK
McMorrow, D.	Clarendon Laboratory, University of Oxford, UK
Mischenko, N.	Catholic University of Leuven, Belgium
Mitchell, P.	University of Manchester, UK
Mol, L.	FOM-Institute, Amsterdam, The Netherlands
Müller, P.	University of Aachen, Germany
Nutley, M.	Institute Laue-Langevin, Grenoble, France
Oiarzabal, L.	Imperial College, London, UK
Osborne, J.	Laughborough University of Technology, UK
Paixão, J. A.	European Institute for Transuranium Elements, Karlsruhe, Germany
Paul, D. McKenzie	University of Warwick, UK
Pohl, J.	University of Konstanz, Germany
Pragnell, P.	Cavendish Laboratories, University of Cambridge, UK
Pyckhout-Hintzen, W.	IFA-KFA Jülich, Germany
Rainford, B.	Southampton University, UK
Randle, V.	University College Swansea, UK
Reif, T.	IFA-KFA Jülich, Germany
Reynders, K.	Catholic University of Leuven, Belgium
Richardson, R.M.	University of Bristol, UK
Ricketts, J.	University of Birmingham, UK
Roser, S.	University of Bath, UK
Schneiders, D	IFA-KFA Jülich, Germany
Schmitt, J.	University of Mainz, Germany
Schouwenaars, R.	University of Leuven, Belgien
Schwahn, D.	IFA-KFA Jülich, Germany
Seddon, J.	Imperial College, London, UK
Shaikh, S.J.	University of Birmingham, UK
Simpson, A.	Clarendon Laboratory, Oxford University, UK
Skoliaros, S.	Aristotle University, Thessalonike, Greece
Slater, P.	University of Birmingham, UK

Schmitt, J.	University of Mainz, Germany
Stamm, M.	Max Planck Institute, Mainz, Germany
Steigenberger, U.	Rutherford Laboratory, UK
Strauss, R.	Technical University, Darmstadt, Germany
Stirling, W.G.	University of Keele, Staffordshire, UK
Sulton, S.	Clarendon Laboratory, Oxford University, UK
Swaddling, P.	Clarendon Laboratory, Oxford University, UK
Timbo, A.	Imperial College, London, UK
Tomka, G.	University of Southampton, UK
Urban, V.	IFA-KFA Jülich, Germany
Viviani, L.	Dipartimeto di Ingegneria Nucleare, Milan, Italy
Wells, M.	Clarendon Laboratory, Oxford University, UK
de Wijn, H.W.	University of Utrecht, The Netherlands
Wilson, C.	University of Durham, UK
Withers, P.	Cavendish Laboratories, University of Cambridge, UK
Wylie, M.	University of Birmingham, UK
Zinkin, M.	Clarendon Laboratory, Oxford University, UK

3 PUBLICATIONS AND EDUCATIONAL ACTIVITIES IN THE DEPARTMENT

3.1 Publications

ABERNATHY, D.L., GIBBS, D., GRÜBEL, G., HUANG, K.G., MOCHRIE, S.G., SANDY, A.R., and ZEHNER, D.M. (1993). Reconstruction of the (111) and (001) Surface Science of Au and Pt: Thermal Behavior. Surface Science **283**, 260-276.

AEPPLI, G., HAYDEN, S.M., MOOK, H.A., MASON, T.E., TAYLOR, A.D., CLAUSEN, K.N., PERRING, T.G., CHEONG, S.-W., FISK, Z., and RYTZ, D. (1993). From Insulator to Metal with Hot and Cold Neutrons. Physica B **192**, 103-108.

ALMDAL, K., KOPPI, K.A., and BATES, F.S. (1993). Dynamically Sheared BCC Ordered Diblock Copolymer Melts. Macromolecules **26**, 4058-4060.

ALMDAL, K., DYRE, J., HVIDT, S., and KRAMER, O. (1993). Towards a Phenomenological Definition of the Term 'Gel'. Polymer Gels and Networks **1**, 5-17.

ALS-NIELSEN, J., FREUND, A., and GRÜBEL, G. (1993). Diamond Crystal Monochromator Performance under Full Heat Load from ESRF Undulator. ESRF Newsletter **16**, 9-10.

ALS-NIELSEN, J., BRAMWELL, S.T., HUTCHINGS, M.T., MCINTYRE, G.J., and VISSER, D. (1993). Neutron Scattering Investigation of the Static Critical Properties of Rb_2CrCl_4. J. Phys.: Cond. Matter **5**, 7871-7892.

ANDERSEN, J.V., ANDERSEN, N.H., MOURITSEN, O.G., and POULSEN, H.F. (1993). Effects of Co, Fe, and Al Doping on the Oxygen Disordering and Superconducting Transition Temperature of $YBa_2Cu_3O_{6+x}$. Physica C **214**, 143-152.

ANDERSEN, N.H., ANDERSEN, J.V., BÖRJESSON, L., HADFIELD, R., KAKIHANA, M., MCGREEVY, R., MOURITSEN, O.G., and POULSEN, H.F. (1993). Structure and Superconductivity in Co Doped $YBa_2Cu_3O_{6+x}$. J. Alloys Comp. **195**, 327-330.

ANDERSEN, N.H. (1993). Udvikling af keramiske superledere. (Development of Ceramic Superconductors). Risø-R-648(DA), p. 20.

ANDERSEN, N.H. (1993). Strukturelle studier af keramiske superledere. (Structural Studies of Ceramic Superconductors). Risø-R-649(DA), p. 18.

ANDERSEN, N.H. (1993). Defektstrukturer i keramiske superledere. (Defect Structures in Ceramic Superconductors). Risø-R-710(DA), p. 20.

BADDORF, A.P., ZEHNER, D.M., HELGESEN, G., GIBBS, D., SANDY, A.R., and MOCHRIE, S.G.J. (1993). X-ray-sattering Determination of the Cu(110)-(2×3)N Struc-

ture. Phys. Rev. **B 48**, 9013-9020.

BERG, R.H., ALMDAL, K., BATSBERG PEDERSEN, W., HOLM, A., TAM, J.P., and MERRIFIELD, R.B. (1993). Peptide Synthesis Method and Solid Support for Use in the Method. US Patent 5258454 A.

BERG, R.H., NIELSEN, P.E., BUCHARDT, O., and EGHOLM, M. (1993). Peptide Nucleic Acids (PNA). A New Strategy Toward the Rational Design of DNA Mimics. In: Peptides 1992, C. H. Schneider and A. N. Eberle (eds), (Escom, Leiden), 152-153.

BERG, R.H., ALMDAL, K., BATSBERG PEDERSEN, W., and WINTHER, L. (1993). Solid Supports for Use in Peptide Synthesis and Assays. DK Patent 930724 A (18 June 1993).

BOHR, J., BOHR, H., BRUNAK, S., COTTERILL, R.M.J., FREDHOLM, H., LAUTRUP, B., and PETERSEN, S.B. (1993). Protein Structures from Distance Inequalities. J. Mol. Biol. **231**, 861-869.

BRULS, G., WEBER, D., KOUROUDIS, I., WEINFURTER, H., CLAUSEN, K.N., YOSHIZAWA, M., LUTHI, B., and BUCHER, E. (1993). Ultrasound Effects and Neutron Scattering in UPt_3. Physica B **188**, 258-260.

BUCHARDT, O., EGHOLM, M., BERG, R.H., and NIELSEN, P.E. (1993). Peptide Nucleic Acids and Their Potential Applications in Biotechnology. Trends Biotechnol. **11**, 384-386.

BURAS, B., and GERWARD, L. (1992). X-ray Energy Dispersive Diffraction. International Tables for Crystallography. (Edited by A.J.C. Wilson), **Vol. C**, 84-87.

BURAS, B., and GERWARD, L. (1992). Energy-dispersive Detectors. International Tables for Crystallography. (Edited by A.J.C. Wilson), **Vol. C**, 542-543.

BÖHM, C., MÖHWALD, H., LEISEROWITZ, L., ALS-NIELSEN, J., and KJÆR, K. (1993). Influence of Chirality on the Structure of Phospholipid Monolayers. Biophys. J. **64**, 553-559.

CHERNY, D.Y., BELOTSERKOVSKII, B.P., FRANK-KAMENETSKII, M.D., EGHOLM, M., BUCHARDT, O., BERG, R.H., and NIELSEN, P.E. (1993). DNA Unwinding upon Strand-displacement Binding of a Thymine-substituted Polyamide to Double-stranded DNA. Proc. Nat. Acad. Sci. USA **90**, 1667-1670.

CLAUSEN, K.N. (1993). Nye Neutronlederør øger mulighederne for at forstå og forbedre fremtidens Materialer. (New Neutron Guide Enhances the Posibilities for Understanding and Improving Future Materials). Risønyt (no.1), 8-9.

EGHOLM, M., BUCHARDT, O., CHRISTENSEN, L., BEHRENS, C., FREIER, S.M., DRIVER, D.A., BERG, R.H., KIM, S.K., NORDÉN, B., and NIELSEN, P.E. (1993). PNA Hybridizes to Complementary Oligonucleotides Obeying the Watson-Crick Hydrogen-

bonding Rules. Nature **365**, 566-568.

EGHOLM, M., BEHRENS, C., CHRISTENSEN, L., BERG, R.H., NIELSEN, P.E., and BUCHARDT, O. (1993). Peptide Nucleic Acids Containing Adenine or Guanine Recognize Thymine and Cytosine in Complementary DNA Sequences. J. Chem. Soc. Chem. Commun, 800-801

ELLEGAARD, O., SCHOU, J., SØRENSEN, H., PEDRYS, R., and WARCZAK, B. (1993). Sputtering of Solid Nitrogen by keV Helium Ions. Nucl. Instrum. Methods Phys. Res. B **78**, 192-197.

FALÇAO, A.N., PEDERSEN, J. SKOV, and MORTENSEN, K. (1993). Structure of Randomly Cross-linked Poly(dimethylsiloxane) Networks Produced by Electron Irradiation. Macromolecules **26**, 5350-5364.

FIIG, T., and JENSEN, H.J. (1993). Diffusive Description of Lattice Gas Models. J. Stat. Phys. **71**, 667.

FIIG, T., ANDERSEN, J.V., ANDERSEN, N.H., LINDGÅRD, P.-A., MOURITSEN, O.G., and POULSEN, H.F. (1993). Oxygen Ordering Phenomena in $YBa_2Cu_3O_{6+x}$ Studied by Monte Carlo Simulation. Phase Diagram, Structure Factor and Oxygen Equilibrium Pressure. Physica C **217**, 34-52.

FINDEISEN, E., BRÜGEMANN, L., STETTUER, J., and TOLAN, M. (1993). X-ray Grazing Incidence Diffraction from Polycrystalline Sb Films on Single-crystal Substrates. J. Phys: Cond. Matter **5**, 8149-8158.

FORGAN, E.M., CUBITT, R., LEE, S.L., McK PAUL, D., MOOK, H.A., YETHIRAJ, M., KES, P.H., LI, T.W., MENOVSKY, A.A., TARNAWSKI, Z., and MORTENSEN, K. (1993). Direct Observation of Magnetic Flux Lattice Melting and Decomposition in the High T_c Superconductor $Bi_2Sr_2CaCu_2O_8$ Nature **365**, 407-411.

FOSS, M., FEIDENHANS'L, R., NIELSEN, M., FINDEISEN, E., BUSLAPS, T., JOHNSON, R.L., BESENBACHER, F., and STENSGAARD, I. (1993). X-ray Diffraction Investigation of the Sulphur Inducel 4×1 Reconstruction of Ni (110). Surface Science **296**, 283-290.

GREEDAN, J.E., MAIGNAN, A., SIMON, C., RAVEAU, B., PEDERSEN, J. SKOV, and SUBRAMANIAN, M.A. (1993). Re-entrant Spin-Glass Behavior in the Frustrated Pyrochlore $Y_2Mn_2O_7$. J. Appl. Phys. **73**, 5659.

GREY, F., and BOHR, J. (1993). An Alternative Explanation for Epitaxial Growth: The Case of fcc(111) on bcc(110). Applied Surface Science **65/66**, 35.

GRÜBEL, G., GIBBS, D., ZEHNER, D.M., ABERNATHY, D.L., SANDY, A.R., and MOCHRIE, S.G.J. (1993). Phase Behavior of Au and Pt Surfaces. Surface Science **287/288**, 842-845.

GRÜBEL, G., HUANG, K.G., GIBBS, D., SANDY, A.R., and MOCHRIE, S.G.J. (1993). Phasce Behavior of the Pt(111) surfasce: X-ray Scattering Measurements. Rev. **B 48** 18119-18139.

HAMLEY, I.W., KOPPI, K.A., ROSEDALE, J.H., BATES, F.S., ALMDAL, K., and MORTENSEN, K. (1993). Hexagonal Mesophases Between Lammellae and Cylinders in a Diblock Copolymer Melt. Macromolecules **26**, 5959-5970.

HARRIS, P., LEBECH, B., BERNHARD, J., HIGASHI, I., SHISHIDO, I., FUKUDA, T., and TAKEI, H. (1993). Crystal and Magnetic Structure of $ErRh_3B_2$ Studied by Neutron Diffraction. Proceedings of the 11th International Symposium on Boron, Borides, and Related Compounds. 54-56.

HENDRIKSEN, P.V., LINDEROTH, S., and LINDGÅRD, P.A. (1993). Finite-size Modifications of the Magnetic Properties of Clusters. Phys. Rev. B **48**, 7259-7273.

HENDRIKSEN, P.V., LINDEROTH, S., and LINDGÅRD, P.A. (1993). Magnetic Properties of Heisenberg Clusters. J. Phys: Cond. Matter **5**, 5675-5684.

HVILSTED, S., and RAMANUJAM, P.S. (1993). Nye Materialer husker med Laserlys. (New Materials Remember by Laser Light). Risønyt (no.1), 12-13.

HVILSTED, S., and RAMANUJAM, P.S. (1993). Nye Materialer husker med Laserlys. (New Materials Remember by Laser Light). PC World (no.6), 36-38.

HVILSTED, S., and RAMANUJAM, P.S. (1993). 60.000 A4-sider på en kvadratcentimeter. (60.000 A4 Pages on one Square Centimeter), Elteknik **10** (6/7), 8-9.

HVILSTED, S., and RAMANUJAM, P.S. (1993). Nye polymermaterialer til optisk hukommelse. (New Polymer Materials for Optical Storage). DOPS-Nyt **8**, 19-20.

HYRUP, B., EGHOLM, M., ROLLAND, M., NIELSEN, P.E., BERG, R.H., and BUCHARDT, O. (1993). Modifacation of the Binding Affinity of Peptide Nucleic Acids (PNA)-PNA with Exended Backbones Consisting of 2-Aminoehyl-Beta-Alanine or 3-Aminopropylglycine Units. J. Chem. Soc. Chem. Commun. 518-519.

JANSSEN, S., SCHWAHN, D., MORTENSEN, K., and SPRINGER, T. (1993). Pressure Dependence of the Flory-Huggins Interaction Parameter in Polymer Blends: a SANS Study and a Comparison to the Flory-Orwoll-Vrij Equation of States. Macromolecules **26**, 5587-5591.

JEHAN, D.A., MCMORROW, D.F., COWLEY, R.A., WARD, R.C.C., WELLS, M.R., and CLAUSEN, K.N. (1993). The Magnetic Structure of Ho/Y Superlattices. Phys. Rev. B **48**, 5594-5606.

de JEU, W.H., LAMBOOY, P., HAMLEY, I.W., VAKNIN, D., PEDERSEN, J SKOV., KJÆR, K., SEYGER, R., HUTTEN, P. van, and HADZIIOANNOU, G. (1993). On the

Morphology of a Lamellar Triblock Copolymer film. J. Phys. II France **3**, 139-146.

JOHNSON, R.E. and SCHOU, J. (1993). Sputtering of Inorganic Insulators. Mat. Fys. Medd. Kgl. Vid. Selsk. **43**, 403-493.

JUUL JENSEN, D., LORENTZEN, T., and PEDERSEN, J. SKOV (1993). Neutronspredning - et vigtigt værktøj i materialeforskningen. (Neutron Scatting - an Important Tool in Material Rescarch. Risønyt (no.1), 10-11.

JØRGENSEN, J.-E. and ANDERSEN, N.H. (1993). Crystal Structure and Charge Localization in $Pb_2Sr_2Y_{1-x}Ca_xCu_3O_8$ for $x = 0.0$–0.5. Physica C **218**, 43-50.

KAWANO, S., LEBECH, B., and ACHIWA, N. (1993). Magnetic Structures of Erbium under High Pressure. J. Phys: Cond. Matter **5**, 1535-1546.

KAWANO, S., ACHIWA, N., ONODERA, A., NAKAI, Y., and LEBECH, B. (1993). High Pressure "Neutron Diffraction studios of the Magnetic structures of Tb, Ho and Er. Proceedings of Neutrons as Microscopic Probe", Mito, Japan, 492-498.

KIM, S.K., NIELSEN, P.E., EGHOLM, M., BUCHARDT, O., BERG, R.H., and NORDÉN, B. (1993). Right-handed Triplex Formed between Peptide Nucleic Acid PNA-T8 and Poly(dA) Shown by Linear and Circular Dichroism Spectroscopy. J. Am. Chem. Soc. **115**, 6477-6481.

KOPPI, K.A., TIRELL, M., BATES, F.S., ALMDAL, K., and COLBY, R.H. (1993). Lammmellae Orientation in Dynamically Sheared Diblock Copymer Melts. J. Phys. France II **2**, 1941-1959.

KROMANN, R., KINGSTON, J.J., MIKLICH, A.H., SAGDAHL, L.T., and CLARKE, J. (1993). Integrated High-transition Temperature Magnetometer with Only Two Superconducting Layers. Appl. Phys. Lett. **63**, 559-561.

LEBECH, B. (1993). Magnetic Ordering in Nearly Ferromagnetic Antiferromagnetic Helices. In: Recent Advances in Magentism of Transition Metal Compounds. Festschrift in honour of professor K. Motizuki. A. Kotani and N. Suzuki (eds.), (World Scientific, Singapore), 167-178.

LEBECH, B. (1993). Major Increase in the Cold Neutron Flux at DR3, Risø National Laboratory, Denmark. Neutron News **4**, 31.

LEBECH, B., and RISTE, T. (1993). International Review of Neutron Research at Studsvik. Swedish Natural Science Research Council, Stockholm, Sweden, p. 12.

LINDGÅRD, P.A., and SCHMID, B. (1993). Theory of Singlet-gound-state Magnetism: Application to Field-induced Transitions in $CsFeCl_3$ and $CsFeBr_3$. Phys. Rev. B **48**, 13636-13646.

LÖSCHE, M., PIEPENSTOCK, M., DIEDERICH, A., GRÜNEWALD, T., KJÆR, K.,

and VALKIN, D. (1993). Influence of Surface Chemistry on the Structural Organization of Monomolecular Protein Layers Adsorbed to Functionalized Aqueous Interfaces. Biophys. J. **65**, 2160-2177.

MASON, T.E., AEPPLI, G., HAYDEN, S.M., RAMIREZ, A.P., and MOOK, H.A. (1993). Low Energy Excitations in Superconducting $La_{1.86}Sr_{0.14}CuO_4$. Phys. Rev. Lett. **71**, 919-922.

MCMORROW, D.F., JEHAN, D.A., SWADDLING, P.P., COWLEY, R.A., WARD, R.C.C., WELLS, M.R., and CLAUSEN, K.N. (1993). The Chemical and Magnetic Structures of Holmium-Yttrium and Holmium-Lutetium Superlattices. Physica B **192**, 150-162.

MCMORROW, D.F., JEHAN, D.A., COWLEY, R.A., SWADDLING, P.P., WARD, R.C.C., WELLS, M.R., HAGMANN, N., and CLAUSEN K.N. (1993). Helical Magnetic Order and Spin Slips in Holmium-Yttrium Superlattices. Europhys. Lett. **23**, 523-528.

MEIER, G., SCHWAHN, D., MORTENSEN, K., and JANSSEN, S. (1993). On the Crossover from Ising to Mean-field Behaviour in Compatible Binary-polymer Blends. Europhys. Lett. **22**, 577-583.

MIKLICH, A.H., KOELLE, D., DANTSKER, E., NEMETH, D.T., KINGSTON, J.J., KROMANN, R.F., and CLARKE, J. (1993). Biocrystal YBCO DC Squids with Low Noise. IEEE Trans. Appl. Superconduct. **3**, 2434.

MORTENSEN, K. (1993). PEO-PPO-PEO Block Polymer in Aqueous Solution: Micelle Formation and Crystallization. Progr. Colloid Polym. Sci. **91**, 69-71.

MORTENSEN, K. (1993). Block Copolymer in Aqueous Solution: Micelle Formation and Hard-sphere Crystallization. Progr. Colloid. Polym. Sci. **93**, 72-75.

MORTENSEN, K., and BROWN, W. (1993). Poly(ethylene oxide)-Poly(propylene oxide)-Poly(ethylene oxide) Triblock Copolymers in Aqueous Solution. The Influence of Relative Block size. Macromolecules **26**, 4128-4135.

MORTENSEN, K., and PEDERSEN, J. SKOV (1993). Structural Study on the Micelle Formation of Poly(ethylene oxide)-Poly(propylene oxide)-Poly(ethylene oxide) Triblock Copolymer in Aqueous Solution. Macromolecules **26**, 805-812.

MORTENSEN, K., SCHWAHN, D., and JANSSEN, S. (1993). Pressure Induced Melting of Micellar Crystal. Phys. Rev. Lett. **71**, 1728-1893.

NIELSEN, P.E., EGHOLM, M., BERG, R.H., and BUCHARDT, O. (1993). Peptide Nucleic Acids (PNA): Oligonucleotide analogs with a Polyamide Backbone. In: Antisense research and applications. S.T. Crooke and B. Lebleu, (eds.), (CRC Press, Boca Raton, Florida, USA), 363-373.

NIELSEN, P.E., EGHOLM, M., BERG, R.H., and BUCHARDT, O. (1993). Peptide

Nucleic Acids (PNAs): Potential Anti-sense and Anti-gene Agents. Anti-Cancer Drug Design 8, 53-63.

NIELSEN, P.E., EGHOLM, M., BERG, R.H., and BUCHARDT, O. (1993). Sequence Specific Inhibition of DNA Restriction Enzyme Cleavage by PNA. Nucleic Acids Res. 21, 197-200.

NIELSEN, P.E. EGHOLM, M., BERG, R.H., and BUCHARDT, O. (1993). Sequence Selective Recognition of DNA by Peptide Nucleic Acid Chimerae (PNA). In: Proceedings at the International Conference on Nucleic Acid Medical Applications. Vol. 1, 21-23.

NIELSEN, P.E., EGHOLM, M., BERG, R.H., and BUCHARDT, O. (1993). Sequence-Selective Recognition of DNA by Peptide Nucleic Acid Chimerae (PNA). Clin. Chem. 39, 715.

ODDERSHEDE, L., DIMON, P., and BOHR, J. (1993). Self-organized Criticality in Fragmenting. Phys. Rev. Lett. 71, 3107-3110.

PEDERSEN, J. SKOV (1993). Small-angle Scattering from Precipitates: Analysis by Use of a Polydisperse Hard-sphere model. Phys. Rev. B 47, 657-665.

PEDERSEN, J. SKOV (1993). Structure of Clathrin-coated Vesicles from Small-angle Scattering Experiments. Eur. Biophys. J. 22, 79-95.

PEDERSEN, J. SKOV (1993). Structure of Clathrin-coated Vesicles from Contrast-variation Small-angle Neutron Scattering Data. Progr. Colloid. Polym. Sci. 93, 33-36.

RAMANUJAM, P.S., HVILSTED, S., and ANDRUZZI, F. (1993). Novel Biphotonic Holographic Storage in a Side-chain Liquid Crystalline Polyester. Appl. Phys. Lett. 62, 1041-1043.

RAMANUJAM, P.S., HVILSTED, S., ANDRUZZI, F., KULINNA, C., and SIESLER, H.W. (1993). Side-chain Liquid Crystalline Polyesters with Unusual Optical Information Storage Properties. In: Organic Thin films for Photonic Applications. Conference Edition. (Technical Digest Series, Optical Society of America, Washington DC, 17, 244-247.

SAMSETH, J., SPONTAK, R.J., and MORTENSEN, K. (1993). The Response of Microstructure to Processing in a Series of Poly(siloxaneimide) Copolymers. J. Polym. Sci. B: Polym. Phys. 31, 467-474.

SANDY, A.R., MOCHRIE, S.G.J., ZEHNER, D.M., GRÜBEL, G., HUANG, K.G., and GIBBS, D. (1993). Au and Pt(111) Surface Phase Behavior. Surface Science 287/288, 321-324.

SCHERRENBERG, R., REYNAERS, H., MORTENSEN, K., VLAK, W., and GONDARD, C. (1993). Structural Aspects of Suspension Poly(Vinyl Chloride). Small-angle Neutron Scattering of Rigid and Plasticized Suspension PVC. Macromolecules 26, 3205-

3211.

SCHMITT, J., GRÜNEWALD, T., DECHER, G., PERSHAN, P., KJÆR, K., and LÖSCHE, M. (1993). The Internal Structure of Layer-by-layer Adsorbed Polyelectrolyte Films: A Neutron and X-ray Reflectivity Study. Macromolecules **26**, 7058-7063.

SCHOU, J., and ELLEGAARD, O. (1993). UV Laser Irradiation of Thin Films of Silver and Solid Nitrogen. Laser Ablation Mechanisms and Applications - II. J.C. Miller and D.B. Geohegan, (eds.), (New York, AIP) Con. Proc. **288**, 64-69.

SCHOU, J. (1993). Secondary Electron Emission from Insulators. In: Ionization of Solids by Heavy Particles. NATO Advanced Research Workshop on Ionization of Solids by heavy Particles. R.A. Baragiola, (ed.), (Plenum Press, New York), NATO Advanced Science Institutes Series B: Physics **306**, 351-358.

SCHOU, J.(1993). Laserablation fra faste stoffer. Et område i rivende udvikling. (Laser Ablation of Solid Materials. An Area in Fast Development). DOPS-Nyt **8**, 6-9.

SETO, H., SCHWAHN, D., MORTENSEN, K., and KOMURA, S. (1993). A Small Angle Neutron Scattering Syudy of Density Fluctuations at Near-critical Region and a van der Waals Model in a 3-Component Microemulsion. J. Chem. Phys. **99**, 5512-5519.

STENUM, B., SCHOU, J., SØRENSEN, H., and GÜRTLER, P. (1993). Luminescence from Pure and Doped Solid Deuterium Irradiated by keV Electrons. J. Chem. Phys. **98**, 126-134. -

SWADDLING, P.P., MCMORROW, D.F., SIMPSON, J.A., WELLS, M.R., WARD, R.C.C., and CLAUSEN, K.N. (1993). Observation of Novel Ferromagnetic Phase of $Ho^{(3+)}$ in Ho/Lu Superlattices. J. Phys. Cond. Matter **5**, L481-L486.

VAKNIN, D., KJÆR, K., RING, M., DORF, H., BLANKENBURG, R., PIEPENSTOCK, M., DIEDERICH, A., and LÖSCHE. (1993). X-ray and Neutron Reflectivity of a Protein Monolayer Adsorbed to a Functionnalized Aqueous Surface. Langmuir **9**, 1171-1174.

VIVES, E., and LINDGÅRD, P.A. (1993). Theory and Monte Carlo Simulation of Adsorbates on Corrugated Surfaces. Surface Science **248**, L449-L454.

VIVES, E., and LINDGÅRD, P.A. (1993). Theory and Simulation of Epitaxial: Rotation Light Particles Adsorbed on Graphite. Phys. Rev. B. **47** 7431-7445.

WEINBACK, S.P., JACQUEMAIN, D., LEVEILLER, F., KJÆR, K., ALS-NIELSEN, J., and LEISEROWITZ, L. (1993). The Effect of Cosolvent on the Lateral Order of Spontaneously Formed Amphiphilic Amide Two-dimensional Crystallites at the Air-liquid Interface. J. Am. Chem. Soc. **115**, 11110-11118.

WEINBACH, S.P., KJÆR, K., ALS-NIELSEN, J., LAHAV, M., and LEISEROWITZ, L. (1993). Self-assembled Monolayers and Trilayers at the Air-formamide Interface. J. Phys. Chem. **97**, 5200-5203.

WEISSBUCH, I., MAJEWSKI, J., KJÆR, K., ALS-NIELSEN, J., LAHAV, M., and LEISEROWITZ, L. (1993). Mixed Monolayers for the Design of Structured Surfaces to Induce Oriented 3-D Crystallization. J. Phys. Chem. **97**, 12848-12857.

WEISSBUCH, I., LEVEILLER, F., JACQUEMAIN, D., KJÆR, K., ALS-NIELSEN, J., and LEISEROWITZ, L. (1993). Crystalline Structures of Monolayers on Water Surfaces as Determined by Grazing Incidence X-ray Diffraction: N-(eicosanoyl)-3-Aminopropionic Acid and Its Mixtures with Eicosanoamide. J. Phys. Chem. **97**, 12858-12861.

ØRUM, H., NIELSEN, P.E., EGHOLM, M., BERG, R.H., BUCHARDT, O., and STANLEY, C. (1993). Single Base Pair Mutation Analysis by PNA Directed PCR clamping. Nucleic Acids Res. **21**, 5332-5336.

ÖSTERBERG, R., LINDQVIST, I., and MORTENSEN, K. (1993). Particle Size of Humic Acid. Soil Sci. Soc. Am. J. **57**, 283-285.

3.2 Conferences

ALMDAL, K., and MORTENSEN, K., The Response of Block Copolymer Melts to Large Strain Dynamic Shear. Optics and Dynamics of Polymers. 1993 Prague Meetings on Macromolecules. 33. Microsymposium, Prague, The Chech Republic, (July).

ALMDAL, K., MORTENSEN, K., BATES, F.S., TIRRELL, M., and KOPPI, K.A., Large Strain Dynamic Shear of Block Copolymer Melts. Danish Physical Society, Spring Meeting, Rødby, Denmark, (May).

ALMDAL, K., and MORTENSEN, K., The Effect of Conformational Asymmetry on Block Co-polymer Phase Behavior. Mini-workshop on Polymer Science, Technical University, Denmark, (October).

ALS-NIELSEN, J., 3rd Generation X-ray Synchrotrons - First Experiments from ESRF TROIKA Beamline. XVI International Conference on Crystallography, Beijing, China, (August).

ALS-NIELSEN, J., Neutron and X-ray Reflectrometry. IUCr XVI Satellite Meeting on Neutron Scattering, Beidahe, China, (August).

ALS-NIELSEN, J., Synchrotron Studies of Amphiphilic Monolayers. Surface and Colloid Science Symposium, Chemical Center, Lund, Sweden, (October).

ALS-NIELSEN, J., Two-dimensional Soft Condensed Matter - Structure and Function Studied by X-ray Synchrotron Diffraction. Trends in Physics, EPS Conference, Firenze, Italy, (September).

ANDERSEN, N.H., ANDERSEN, J.V., BÖRJESSON, L., FIIG, T., HADFIELD, R., KAKIHANA, M., LINDGÅRD, P.-A., MCGREEVY, R., MOURITSEN, O.G., and POULSEN, H.F., Structure and Thermodynamics of Oxygen Ordering in Pure and M-doped $YBa_2Cu_{3-y}M_yO_{6+x}$. 2nd Workshop on: The Influence of the Local Structure on the Superconducting Properties for Samples in the Y-Ba-Cu-O and Related Systems. Porta Hydra, Greece, (May).

BATES, F.S., KOPPI, K.A., HAMLEY, I.W., TIRRELL, M., ALMDAL, K., and MORTENSEN, K., Shear-induced Order and Orientation in Diblock Copolymer Melts. Danish Physical Society, Spring Meeting, Rødby, Denmark, (May).

BERG, R.H., NIELSEN, P.E., BUCHARDT, O., and EGHOLM, M., Design, Properties and Potential of Peptide Nucleic Acids (PNA). Third International Symposium on Innovations and Perspectives in Solid Phase Synthesis, Oxford, UK, (August).

BOHR, J., Carbon-60, and Epitaxial Rotations. Current Problems in Condensed Matter Research. 7th Summer School, Bialowieza, Polen, (June).

BOHR, J., Fragmentations of Macroscopic Systems. Multifragmentation of Heavy Nuclei.

Copenhagen, Denmark, (September).

BOUWMAN, W.G., KJÆR, K., ALS-NIELSEN, J., and VAKNIN, D., The Liquid Surfasce Reflectometer at Risø. New Horizons: A Workshop on the State of Art in Neutron Reflectivity, Gaithersburg, Maryland, USA, (December).

BUYERS, W.J.L., TUN, Z., PETERSEN, T., MASON, T.E., LUSSSIER, J.-G., GAULIN, B.D., and MENOVSKY, A.A., Spin Wave Collapse, Magnetic Divergence, and Incommensurate Fluctuations in URu_2Si_2. International Conference on Strongly Correlated Electron Systems, San Diego, USA, (August).

CASALTA, H., ALLOUL, H., and MARUCCO, J.F., Experimental Determination of the Magnetic Phase Diagram of the $Y_{1-y}Ca_yBa_2Cu_3O_6$ System. 2nd Workshop on: The Influence of the Local Structure on the Superconducting Properties for Samples in the Y-Ba-Cu-O and Related Systems, Porta Hydra, Greece (May).

CLAUSEN, K.N., Magnetic Excitons and Stoner Excitations in Pr. Danish Physical Society, Spring Meeting, Rødby, Denmark, (May).

EGHOLM, M., BUCHARDT, O., NIELSEN, P.E., and BERG, R.H., Peptide Nucleic Acids (PNA). DNA Analogues with a Peptide Backbone. Thirteenth American Peptide Symposium, Edmonton, Canada, (June).

FIIG, T., Monte Carlo Simulation of Oxygen Ording in YBaCuO. 1993 March Meeting of American Physical Society, Seattle, USA, (March).

FIIG, T., Oxygen Ordering Phenomena in YBaCuO, Studied by Monte Carlo Simulation. Statistical Meeting at Rutgers University, New Jersey, USA, (May).

FOSS, M., FEIDENHANS'L, R., NIELSEN, M., FINDEISEN, E., BUSLAPS, T., JOHNSON, R.L., BESENBACHER, F., and STENSGAARD, I., X-ray Diffraction Investigation of the Sulphur Induced 4×1 Reconstruction of Ni(110). HERCULES Course, Grenoble, France, (March)

FOSS, M., FEIDENHANS'L, R., NIELSEN, M., FINDEISEN, E., BUSLAPS, T., JONNSON, R.L., BESENBACHER, F., and STENSGAARD, I., X-ray Diffraction Investigation of the Sulphur Induced 4×1 Reconstruction of Ni(110). Danish Physical Society, Spring Meeting, Rødby, Denmark, (May).

FOSS, M., FEIDENHANS'L, R., NIELSEN, M., FINDEISEN, E., BUSLAPS, T., JOHNSON, R.L., BESENBACHER, F., and STENSGAARD, I., X-ray Diffranction Investigation of the Sulphur Induced 4×1 Reconstruction of Ni(110). European Conference on Surface Crystallopraphy, Århus, Denmark, (May).

FOSS, M., FEIDENHANS'L, R., NIELSEN, M., FINDEISEN, E., BUSLAPS, T., JOHNSON, R.L., BESENBACHER, F., and STENSGAARD, I., X-ray Diffranction Investigation of the Sulphur Induced 4×1 Reconstruction of Ni(110). European Conference on Surface Science, Warwick, UK, (August).

FINDEISEN, E., FEIDENHANS'L, R., and NIELSEN, M., Radial Distribution Function of Amorphous Diamond-like Carbon Obtained by X-ray Scattering. Danish Physical Society, Spring Meeting. Rødby, Denmark, (May).

GERSTENBERG, M.C., CLAUSEN, K.N., MCMORROW, D.F. JEHAN, D.A., SWADDLING, P.P., The Magnetic Structure of Ho-Y and Ho-Lu Superlattices. Danish Physical Society, Spring Meeting, Rødby, Denmark, (May).

HAMLEY, I.W., KOPPI, K.A., ROSEDALE, J.H., BATES, F.S., ALMDAL, K., and MORTENSEN, K., Fluctuation Induced Phase Transitions in an Ordered Block Copolymer Melt. 1993 March Meeting of the American Physical Society, Seattle, USA, (March).

HAMLEY, I.W., KOPPI, K.A., ROSEDALE, J.H., BATES, F.S., ALMDAL, K., and MORTENSEN, K., SANS Studies of Diblock Copolymers Near the Order-disorder Transition. 9. International Conference on Small Angle Scattering, Saclay, France, (April).

HARRIS, P., and LEBECH, B., Magnetic Structures of Cubic FeGe. Neutrons and X-rays in Magnetism, Grenoble, France, (January).

HARRIS, P., LEBECH, B., and BERNHARD, J., Diffraction Study of the Crystal Structure of $ErRh_3B_2$. Danish Physical Society, Spring Meeting, Rødby, Denmark, (May).

HARRIS, P., LEBECH, B., ACHIWA, N., and LARSEN, F.K., Crystalline and Magnetic Ordering in the Monoclinic Phase of the Layered Perovskite PAMC. XVI Congress and General Assembly of the International Union of Crystallography, Beijing, China, (August).

HARRIS, P., LEBECH, B., BERNHARD, J., HIGASHI, I., SHISHIDO, T., FUKUDA, T., and TAKEI, H., Crystal and Magnetic Structure of $ErRh_3B_2$ Studied by Neutron Diffraction. 11th International Symposium on Boron, Borides and Related Compounds (ISBB'93), Japan, (August).

HARRIS, P., PEDERSEN, J. SKOV, and LEBECH, B., The 3-dimensional Resolution Function for Small-angle Scattering Set-ups: Analysis of the Magnetic Structure in FeGe and MnSi. IUCr XVI Satellite Meeting on Neutron Scattering, Beidaihe, China, (August).

HVILSTED, S., RAMANUJAM, P.S., and ANDRUZZI, F., Influence of New Architecture for Side-chain Liquid Crystalline Polyesters on Holographic Behaviour. Molecular Engineering of Side Chain Liquid Crystalline Polymers, European Polymer Federation Workshop, Yverdon-les-Bains, Switzerland, (June).

HVILSTED, S., RAMANUJAM, P.S., and ANDRUZZI, F., New Side-chain Liquid Crystalline Polyester Arhitecture for Erasable Optical Information Storage. Chemistry for 21st Century - the Central Science. 34. IUPAC Congress, Beijing, China, (August).

HØNGER, T., LEMMICH, J., IPSEN, J.H., MOURITSEN, O.G., MORTENSEN, K., and BAUER, R., Phase Behaviour of Gramicidin-Phosphatidylcholine Mixtures. NATO Advanced Science Institute Conference on Structure and Dynamics of Biological Mem-

branes, Corsica, France, (June).

JANSSEN, S., SCHWAHN, D., MORTENSEN, K., and SPRINGER, T., Pressure Dependence of the Flory-Huggins Interaction Parameter in Polymer Blends. 1993 March Meeting of the American Physical Society, Seattle, USA, (March).

JANSSEN, S., SCHWAHN, D., MORTENSEN, K., and SPRINGER, T., Pressure Dependence of the Flory-Huggins Interaction Parameter in Polymer Blends Studied by SANS and by Discussing the FOV Equation of State. 9. International Conference on Small Angle Scattering, Saclay, France, (April).

JANSSEN, S,. SCHWAHN, D., MORTENSEN, K., and SPRINGER, T., Pressure Dependence of the Flory-Huggins Interaction Parameter in Polymer Blemds. 13th General Conference, European Physical Society, Regensburg, (March).

JENSEN, C.P., and FEIDENHANS'L, R., Diffuse Scattering of X-rays from MgO and Metal Surfaces. Danish Physical Society, Spring Meeting, Rødby, Denmark, (May).

JOHNSON, E., JOHANSEN, A., THOFT, N.B., ANDERSEN, H.H., and SARHOLT-KRISTENSEN, L., Nanosize fcc Thallium in Aluminium. Danish Physical Society, Spring Meeting, Rødby, Denmark, (May).

KAWANO, S., LEBECH, B., and ACHIWA, N., Magnetic Structures of Erbium under High Pressure. Scientific Meeting of the Research Reactor Institute, Kyoto, Japan, (February).

KAWANO, S., ACHIWA, N., ONODERA, A. NAKAI, Y., and LEBECH, B., High Pressure Diffraction Studies of the Magnetic Structures of Tb, Ho and Er. Neutrons as Microscopic Probes, Mito, Japan, (March).

KLEIMAN, R.N., GAMMEL, P.L., BISHOP, D.J., YETHIRAJ, M., MOOK, H.A., ARMSTRONG, T., LEE, S.L., FORGAN, E.M., PAUL, D.M., and MORTENSEN, K., Neutron Diffraction from Vortex Structures in $YBa_2Cu_3O_7$. 1993 March Meeting of the American Physical Society, Seattle, USA, (March).

KOPPI, K.A., BATES, F.S., ALMDAL, K., and MORTENSEN, K., Dynamic Shear of a Spherical Diblock Copolymer Melt. 1993 March Meeting of the American Physical Society, Seattle, USA, (March).

KJÆR, K., X-ray and Neutron Studies of Thin Surfactant Layers. 3rd International Conference on Surface X-ray and Neutron Scattering, Dubna, Russia, (June).

KULINNA, C., ZEBGER, I., SIESLER, H.W., HVILSTED, S., and RAMANUJAM, P.S., Characterization of the Orientational Behaviour of Liquid-crystalline Side-chain Polymers for Reversible Optical Data Storage by Fourier-transform IR-Spectroscopy, 9. International Conference on Fourier Transform Spectroscopy, Calgary, Canada, (August).

KULINNA, C., ZEBGER, I., SIESLER, H.W., HVILSTED, S., and RAMANUJAM,

P.S., Characterization of Segmental Mobility in Liquid-crystalline Polymers by Fourier-Transform Infrared Spectroscopy, International Conference on Advanced Polymer Materials, Dresden, Germany, (September).

LEBECH, B., SUNDBERG, M., and FJELLVÅG, H., Powder Diffraction and Electron Microscopy - a Combination? Nordic Workshop on Quantitative Electron Microscopy and Diffraction, Oslo, Norway, (June).

LEFMANN, K., and HEDEGÅRD, P., Theory of the Frustrated S=1/2 Quantum Antiferromagmet on a 2D Triangular Lattice. Danish Physical Society, Spring Meeting, Rødby, Denmark, (May).

LINDGÅRD, P.A., Transitions Between Ordered Phases. Workshop on Spinodal Decomposition, Technical University, Denmark, (June).

LINDGÅRD, P.A., Thermal Properties Magnetic Clusters. 2nd Latin-American Workshop on Magnetism, Guanjuato, Mexico, (August).

MACKINTOSH, R.A., A new mode of Magnetic Excitation in Praseodymium. Conference on Strongly Correlated Electron Systems, San Diego, USA, (August).

MANNSTEADT, S., FIIG, T., MOURITSEN, O.G., LINDGÅRD, P.A., and ANDERSEN, N.H., Using CM-200 to Study High-temperature Superconductors. Second European Connection Machine Meeting, Observatoire de Meudon, Paris, France, (October).

MASON, T.E., PETERSEN, T., AEPPLI, G., RAMIREZ, A.P., BÜCHER, E., and HUFNAGL, J., Magnetic Fluctuations in the Heavy Fermion Superconductor UPd_2Al_3. Danish Physical Society, Spring Meeting, Rødby, Denmark, (May).

MASON, T.E., Spin Gap Formation in the Kondo Insulator CeNiSn. Adriatico Research Conference on Strong Correlations at Low Carrier Densities, International Centre for Theoretical Physics, Trieste, Italy, (June).

MASON, T.E., AEPPLI, G., HAYDEN, S.M., RAMIREZ, A.P., and MOOK, H.A., Magnetic Fluctuations in Superconducting $La_{2-x}Sr_xCuO_4$. International Conference on Strongly Correlated Electron Systems, San Diego, USA, (August).

MEIER, G., SCHWAHN, D., MORTENSEN, K., and JANSSEN, S., On the Crossover from Ising to Mean Field Behavior in Compatible Binary Polymer Blends. 9. International Conference on Small Angle Scattering, Saclay, France, (April).

MISCHENKO, N., REYNDERS, K., MORTENSEN, M., FONTAINE, F., GRAULUS, R., and REYNAERS, H., Investigation of 3-dimensional Domain Network in Triblok Copolymer Gels. Joint Symposium on Polymer Gels and Networks, Tsukaba, Japan, (August).

MONTFROOIJ, W,. MCGREEVY, R., and ANDERSEN, N.H., Reverse Monte Carlo as a Tool for Studying Defect Structures. 2nd Workshop on: The Influence of the Local Structure on the Superconducting Properties for Samples in the Y-Ba-Cu-O and Related

Systems. Porta Hydra, Greece (May).

MONTFROOIJ, W., and SVENSON, E.C., Evidence for Soft Mode Behavior of the Roton at High Density. XX International Conference on Low Temperature Physics, Eugene, Oregon, USA, (August).

MORTENSEN, K., SCHWAHN, D., and JANSSEN, S., Concentration Fluctuations in Aqueous Solutions of PEO, PPO, and Self-Assembling PEO-PPO-PEO. Effect of Hydrostatic Pressure. 9. International Conference on Small Angle Scattering, Saclay, France, (April).

MORTENSEN, K., Self-assembling Macromolecules: Micelle Formation, Micellar Form Transformation, and Hard-sphere Crystallization. 9. International Conference on Small Angle scattering, Saclay, France, (April).

MORTENSEN, K., SCHWAHN, D., and JANSSEN, S., Pressure Induced Melting of Micellar Crystal. Danish Physical Society, Spring Meeting, Rødby, Denmark, (May).

MORTENSEN, K., SCHWAHN, D., JANSSEN, S., and MEIER, G., Cross-over from Ising to Mean-field Behavior in Compatible Polymer Blends. Workshop on Spinodal Decomposition, Technical University, Denmark, (June).

MORTENSEN, K., Small-angle Scattering on Dispersed Systems. Polymers, Colloids and Factals. International School and Symposium on Physics in Material Science, Jaszowiec, Poland, (September).

MORTENSEN, K., PEO-PPO-PEO Triblok Copolymers in Aqueous Solution. Micelle Formation, Micellar Form Transformation and Hard-sphere Crystallization. 2nd European Gordon Conference on Complex Fluids, Irsee, Germany, (September).

MORTENSEN, K., SCHWAHN, D., and JANSSEN, S., Pressure Induced Melting of Micellar Crystal. 1993-Fall Meeting of the Material Research Society. Symposium on Complex Fluids, Boston, (November).

ODDERSHEDE, L., DIMON, P., and BOHR, J., Self-organized Criticality in Fragmenting. Danish Physical Society, Spring Meeting, Rødby, Denmark, (May).

PEDERSEN, J. SKOV, Structure of Clathrin-coated Versicles from Small-angle Scattering Experiments. 9. International Conference on Small Angle Scattering, Saclay, France, (April).

PEDERSEN, J. SKOV, Structure of Clathrin-coated Vesicles from Small-angle Scattering Experiments. International Workshop on Membrane Strueture, Dynamics and Interractions via Neutron and X-ray Scattering, Saclay, France, (April).

PEDERSEN, J. SKOV, Small-angle Scattering from Precipritates : Analysis by Use of a Polydisperse Hard-sphere Model. 9. International Conference on Small Angle Scattering, Saclay, France, (April).

PEDERSEN, J. SKOV, Resolution Effects and Analysis of Small-angle Neutron Scattering Data. 9. International Conference on Small Angle Scattering, Saclay, France, (April).

PEDERSEN, J. SKOV, and HAMLEY, I.W., Analysis of Neutron and X-ray Reflectivity Data by Constrained Least-squares Methods. 9. International Conference on Small Angle Scattering, Saclay, France, (April).

PEDERSEN, J. SKOV, Instrumentation for Small-angle Scattering. NATO Advanced Study Institute on Modern Aspects of Small-angle Scattering, Como, Italy, (May).

PEDERSEN, J. SKOV, and HAMLEY, I.W., Analysis of Neutron and X-ray Reflectivity data by Constrained Least-squares Methods. 3rd International Conference on Surface X-ray and Neutron Scattering, Dubna, Russia, (June).

PEDERSEN, J. SKOV, and HAMLEY, I.W., Analysis of Neutron and X-ray Reflectivity Data by Constrained Least-squares Methods. New Horizoins: A Workshop on the State of the Art in Neutron Reflectivity, Gaithersburg, Maryland, USA, (December).

PETERSEN, T., MASON, T.E., AEPPLI, G., RAMIREZ, A.P., BUCHER, E., and KLEIMAN, R.N., Magnetic Fluctuations and Superconductivity in UPd_2Al_3. International Conference on Strongly Correlated Electron Systems, San Diego, USA, (August).

PENGRA, D.B., THOFT, N.B., FEIDENHANS'L, R., BOHR, J., and WULFF, M., Neutron and X-ray Diffraction from a HoEr Random Alloy. Danish Physical Society, Spring Meeting, Rødby, Denmark, (May).

POSSELT, D., DEGN EGEBERG, E., PEDERSEN, J. SKOV, and MORTENSEN, K., Small-angle Scattering Studies of Freeze Dried and Super-critically Dried Silica Gels. 9. International Conference on Small Angle Scattering, Saclay, France, (April).

RANLØV, J., LEBECH, B., and NIELSEN, K., On the Crystal Strucutures of $SrCeO_3$ and $SrCe_{1-x}M_xO_{3-\alpha}$ (M = Al, In, Gd, Er, Yb). Annual Meeting of the American Crystallographic Association, Alberqueqe, New Mexico, USA, (May).

REYNDERS, K., MORTENSEN, K., MISCHENKO, N., FONTAINE, F., and REYNAERS, H., SAXS Investigations of a Triblock Copolymer Gel. 9. International Conference on Small Angle Scattering, Saclay, France, (April).

ROSEDALE, J.H., SCHULZ, M.F., KOPPI, K.A., HAMLEY, I.W., BATES, F.S., ALMDAL, K., and MORTENSEN, K., The Role of Conformational Asymmetry on Ordered Diblock Copolymers. 1993 March Meeting of the American Physical Society, Seattle, USA, (March).

SAMSETH, J., FØRLAND, G.M., MORTENSEN, K., SHEU, E., and HØILAND, H., The Structural Evolution of SDS Micelles in Brine Solutions upon Addition of Medium Chain Alcohols. 9. International Conference on Small Angle Scattering, Saclay, France, (April).

SAMSETH, J., SPONTAK, R.J., SMITH, S.D., and MORTENSEN, K., Microstructural Characteristics of Microphase-separated Tapered Block Copolymers. 9. International Conference on Small Angle Scattering, Saclay, France, (April).

SANDY, A.R., FINDEISEN, E., NIELSEN, M., BOHR, J., SPANNINGA, W.G., and NIELSEN, L., Structural Phase Transition in a $CoSi_2$ Buried Layer at Low Temperatures. Danish Physical Society, Spring Meeting, Rødby, Denmark, (May).

SCHERRENBERG, R., REYNAERS, H., MORTENSEN, K., VLAK, W., and GON - DARD, C., Small-angle Neutron Scattering of Plasticized PVC. 9. International Conference on Small Angle Scattering, Saclay, France, (April).

SCHLEGER, P., HARDY, W., CASALTA, H., and ANDERSEN, N.H., Model for High Temperature Oxygen Ordering in $YBa_2Cu_3O_{6+x}$: Inclusion of Spin and Charge Degrees of Freedom. 2nd Workshop on: The Influence of the Local Structure on the Superconducting Properties for Samples in the Y-Ba-Cu-O and Related Systems, Porta Hydra, Greece, (May).

SCHLEGER, P., HARDY, W., CASALTA, H., and ANDERSEN, N.H., Model for High Temperature Oxygen Ordering in $YBa_2Cu_3O_{6+x}$: Inclusion of Spin and Charge Degrees of Freedom. NATO Advanced Study Institute on: Materials and Crystallographic Aspects of High T_c Superconductivity, Erice, Italy, (May).

SCHOU, J., and ELLEGAARD, O., UV-Laser Irradiation of Thin Films of Silver and Solid Nitrogen. 2nd International Conference on Laser Ablation, Knoxville, USA, (April).

SCHULZ, M.F., ROSEDALE, J.H., FÖRSTER, S., BATES, F.S., ALMDAL, K., and MORTENSEN, K., Order-order Transitions in PE-PEE Diblock Copolymers. 1993 March meeting of the American Physical Society, Seattle, USA, (March).

SCHWAHN, D., JANSSEN, S., and MORTENSEN, K., Pressure Dependence on the Flory Huggins Interaction Parameter in Polymer Blends. Fourth European Confereence on Polymer Blends, Capri, Italy (May).

SETO, H., YOKOI, E., KOMURA, S., SCHWAHN, D., MORTENSEN, K., SUZUKI, J., FUNAHASHI, S., and ITO, Y., Small Angle Neutron Scattering Study on a Phase Separation in a 3-Component Microemulsion System. Neutrons as Microscopic Probe, Mito, Japan, (March).

SETO, H., SCHWAHN, D., MORTENSEN, K., YOKOI, E., KOMURA, S., SUZUKI, J., FUNAHASHI, S., and ITO, Y., Small Angle Neutron Scattering Study on a Phase Separation in a 3-Component Microemulsion System. 9. International Conference on Small Angle Scattering, Saclay, France, (April).

SEQUEIRA, A.D., CALDERON, H.A., PEDERSEN, J. SKOV, and KOSTORZ, G., Determination of γ' Size Distributions in Ni-Al-Mo Alloys by SANS and TEM. 9. International Conference on Small-angle Scattering, Saclay, France, (April).

SVENDSEN, W., and O'SULLIVAN, G., $4d^N$-$4d^{N-1}$ (5f+6p) Transitions in the Spectra of Ionised Tin, Antimony, Tellerium and Iodine. European Group for Atomic Spectroscopy, 25th EGAS, Caen France, (June).

THESTRUP, B., SVENDSEN, W., and SCHOU, J., Sputtering of Solid Deuterium by keV Electrons. Danish Physical Society, Spring Meeting, Rødby, Denmark, (May).

THOFT, N.B., PENGRA, D., BOHR, J., HELGESSON, G., and GIBBS, D., Anomalous X-ray Diffranction Study of Ho-Y Multilayers. Neutrons and X-rays in Magnetism, Grenoble, France, (January).

VICKERS, T.A., FREIER, S.M., ECKER, D.J., BERG, R.H., EGHOLM, M., NIELSEN, P.E., and BUCHARDT, O., Site Specific Termination of Transcription in Eukaryotic Cell Extracts by Peptide Nucleic Acid (PNA) Oligomers. Keystone Symposia on Antisense and Gene Therapy, Bolder, Colorado, USA, (March).

VIGILD, M.E., FINDEISEN, E., FEIDENHANS'L, R., CLAUSEN, K.N., BARHOLM-HANSEN, C., and BENTZON, M.D., Diamond-like Carbon Films Investigated with Neutron- and X-ray Reflectivity. Danish Physical Society, Spring Meeting, Rødby, Denmark, (May).

VYSKOCIL, P., SCHÖNFELD, B., PEDERSEN, J. SKOV, and KOSTORZ, G., Decomposition and Coarsening Study in Ni-11at.%-Ti. 9. International Conference on Small-angle Scattering, Saclay, France, (April).

WINTHER, L., ALMDAL, K., BATSBERG PEDERSEN, W., KOPS, J., and BERG, R.H., Film Supports with Hydrophilic Properties. Thirteenth American Peptide Symposium, Edmonton, Canada, (June).

WINTHER, L., ALMDAL, K., BATSBERG PEDERSEN, W., KOPS, J., and BERG, R.H., Hydrophilic Film Supports for Use in Peptide Synthesis and Assays. Third International Symposium on Innovations and Perspectives in Solid Phase Synthesis, Oxford, UK, (August).

ØRUM, H., NIELSEN, P.E., EGHOLM, M., BERG, R.H., BUCHARDT, O., and STANLEY, C., Single Base Pair Mutation Analysis by PNA Directed PCR Clamping. International Conference on DNA Recognition, Snekkersten, Denmark, (August).

3.3 Lectures

ALMDAL, K., Experimental Observations Relating to the Applicability and Short-comings of the Flory-Huggins Theory. Rheologby Group Semiar, Risø National Laboratory, Denmark, (March).

ALMDAL, K., Dynamically Sheared BCC Ordered Diblock Copolymer Melt. Rheology Group Seminar, Risø National Laboratory, Denmark, (November).

ALS-NIELSEN, J., Introductory Lectures on X-ray and Neutron Scattering. The European Course HERCULES 1993, Grenoble, France, (February).

ALS-NIELSEN, J., Two-Dimensional Soft Condensed Matter - Structure and Function Studied by X-Ray Synchrotron Diffraction. Institute of Physics, Aarhus University, Denmark, (May).

ALS-NIELSEN, J., Introductory Lectures on Synchrotron Radiation. Nordic School on the Application of Synchrotron Radiation in Chemistry, Biology, and Physics, Aarhus University, Denmark, (June).

ALS-NIELSEN, J., Synchrotron Studies of Amphiphilic Monolayers. European Synchrotron Radiation Society, Grenoble, France, (September).

ALS-NIELSEN, J., Hard X-ray Undulator Bemaline Experience at TROIKA, ESRF. HASYLAB, DESY, Hamburg, Germany (December).

ANDERSEN, N.H., Superledning ved høje temperaturer (Superconductivity at High Temperatures). High School Summer Course on Physics, Sorø, Denmark, (June).

ANDERSEN, N.H., Højtemperatur superledning (High Temperature Superconductivity). Topical Day at the Museum on the History of Electricity, Bjerringbro, Denmark, (October).

BERG, R.H., Peptide Nucleic Acids (PNA): DNA Analogs with a Peptide Bacbone. MODECS Meeting on Molecular Recognition and Self-Organization, Hotel Frederiksdal, Lyngby, Denmark, (October).

BOHR, J., Magnetic X-ray Scattering. Nordic School on the Application of Synchrotron Radiation in Chemistry, Biology, and Physics, Sandbjerg, Denmark, (June).

BOHR, J., A Simpel Fragmentation Process. The Technical University, Denmark, (October).

BOHR, J., Epitaxial Rotations, Odense University, Denmark, (December).

CLAUSEN, K.N., Anvendelse af Neutronstråling til Materialeforskning (Application of Neutron Radiation for Material Research). Folkeuniversitetet i Roskilde (University Ex-

tension Services, Roskilde), Risø National Laboratory, Denmark, (October).

FEIDENHANS'L, R., Surface X-ray Diffraction. Nordic Research Course. Synchrotron Radiation: Techniques and Applications, Jäaravallen, Sweden, (June).

FEIDENHANS'L, R., Surface X-ray Diffraction. Nordic School on The Application of Synchrotron Radiation in Chemistry, Biology, and Physics, Sandbjerg, Denmark, (June).

FEIDENHANS'L, R., Structural Investigations of Surfaces by X-ray Diffraction. University of Kiel, Kiel, Germany, (December).

FEIDENHANS'L, R., Nye Materialer på Nanometerskala (New Materials on Nanometer Scale), Folkeuniversitetet i Roskilde (University Extension Services, Roskilde), Risø National Laboratory, Denmark, (December).

HVILSTED, S., Novel Side-chain Liquid Crystalline Polyester Architecture for Optical Storage. Materials Department, Risø National Laboratory, Denmark, (April).

HVILSTED, S., and RAMANUJAM, P.S., Optisk Informationslagring (Optical Information Storage). Polymerteknisk Selskab (Polymer Technical Society), Copenhagen, Denmark, (October).

LEBECH, B., Effects of Hydrostatic Pressure on the Magnetic Structure of Erbium Metal. Institut for Energiteknik, Kjeller, Norway, (June).

LEBECH, B., Magnetic Ordering in Nearly Ferromagnetic Antiferromagnetic Spirals.
University of Copenhagen, Denmark, (August).
Institute of Mining and Metallurgy, Cracow, Poland, (September).

LEFMANN, K., Experimenter ved nK temperatur (Experiments at nK Temperatures). Universiteternes vinterskole i fysik (University Winterscool in Physics), Sandbjerg, Denmark, (January).

LINDGÅRD, P.A., Calculation of Magnetic Properties of Small Clusters. NORDITA, Copenhagen, Denmark, (June).

LINDGÅRD, P.A., Effect of Electronic and Structural Behaviour on the Thermel Magnetic Properties of Clusters. Womens University of Nora, Japan, (September).

MASON, T.E., Making Maps in Reciprocal Space: Neutrons as a Probe of Condensed Matter. University of Toronto, Canada, (December).

MASON, T.E., Low Energy Magnetic Excitations in Superconducting $La_{1.86}Sr_{0.14}CuO_4$. McMaster University, Canada, (December).

MCMORROW, D., Recent Advances in Rare-earth Magnetism from Spin-slips to Superlattices. University of Florida, USA, (October).

MORTENSEN, K., Neutron Scattering on Biological System. Kursus i biologisk systemers fysik (Course on the Physics af Biological Systems). The Technical University, Denmark, (January).

MORTENSEN, K., SANS Measurements on Block Copolymers. Universität Bayreuth, Bayreuth, Germany, (March).

MORTENSEN, K., Block Copolymers in Aqueous Solution: Micelle Formation and Hard-sphere Crystallization. Forschungszentrum Jülich, Germany, (June).

MORTENSEN, K., Block Copolymers in Aqueous Solution. Dependence on Shear, Temperature and Pressure. Massachusetts Institute of Technology, Boston, USA, (December).

NIELSEN, M., Synchrotron X-ray Radiation and Solid State Physics. Århus University in a series of lectures on Large Facilities in Physics, Denmark, (March).

PEDERSEN, J. SKOV, Resolution Effect and Analysis of Small-angle Neutron Scattering Data. Forschungzentrum Jülich, Germany, (October).

RAMANUJAM, P.S., HVILSTED, S., Optisk Informationslagring (Optical Information Storage). Folkeuniversitetet i Roskilde (University Extension Services, Roskilde), Risø National Laboratory, Denmark, (November).

SANDY, A.R., X-Ray Diffraction from Freely Suspended Clusters. Materials Department, Risø National Laboratory, Roskilde, Denmark, (May).

SANDY, A.R., Phase Behavior of the Au and Pt, (111) Surfaces.
University of Konstanz, Konstanz, Germany, (February).
European Synchrotron Radiation Facility, Grenoble, France, (February).
Ecole Polytechnique Fédérale de Lausanne, Lausanne, Switzerland, (March).
University of Munich, Munich, Germany, (November).
Advanced Photon Source, Argonne, USA, (December).

SCHOU, J., Laser Ablation from Solids.
Optics and Fluid Dynamics Department, Risø National Laboratory, Denmark, (February).
Ørsted Laboratory, University of Copenhagen, Denmark, (March).
NBI Tandem, University of Copenhagen, Denmark, (November).
Institute of Physics, Jagellonian University, Krakow, Poland, (November).

MACKINTOSH, A.R., A New Mode of Magnetic Excitation in Praseodymium.
University of California, Berkeley, USA, (September).
Max-Planck Institut für Festkörperforschung, Stuttgart, Germany, (October).
Niels Bohr Institute, University of Copenhagen, Denmark, (November).

3.4 Organizations of Conferences, Schools

LIP USERS' MEETING

8-9 January, Risø National Laboratory, Denmark

The first annual user meeting of the LIP programme was attended by 68 scientists from the EU member states. The programme consisted of 9 plenary lectures listed below and a poster session with 35 contributions.

Organization

CLAUSEN, K.N., Risø National Laboratory, Denmark
MACKINTOSH, A.R., Niels Bohr Institute, Denmark

Programme

MASON, T., *Risø National Laboratory, Denmark*
"Tutorial Session - The Theory of Neutron Scattering"

CLAUSEN, K.N., *Risø National Laboratory, Denmark*
"Tutorial Session - The Neutron Scattering Spectrometers at Risø "

WITHERS, P., *University of Cambridge, UK*
"Internal Stresses by Neutron Diffraction"

SCHWAHN, D., *Forschungszentrum Jülich, Germany*
"Critical Scattering from Polymer Blends"

SVERGUN, D., *EMBL, c/o DESY, Germany*
"Solution Scattering Studies of Biological Macromolecules"

FORGAN, E., *University of Birmingham, UK*
"Neutron Diffraction and Flux Lines in Superconductors"

BOOTHROYD, A., *Clarendon Laboratory, UK*
"Magnetic Ordering in High-Tc Superconductors"

McEWEN, K., *Birkbeck College, UK*
"Neutron Scattering and the Magnetism of Lanthanides and Actinides"

WELLS, M., and SWADDLING, P., *Clarendon Laboratory, UK*
"Rare Earth Superlattice; Growth and Magnetism"

RISØ-MAG '93: WORKSHOP ON MAGNETISM

12 March, Risø National Laboratory, Denmark

Organization

BOHR, J., Risø National Laboratory, Denmark
LEBECH, B., Risø National Laboratory, Denmark
PENGRA, D., Risø National Laboratory, Denmark

Programme

TISHIN, A., *Moscow State University, Russia*
"Magnetic Phase Transitions in Rare Earth Metals"

KAWANO, S., *Kyoto University, Japan*
"Magnetic Sructures and Magnetic Phase Diagrams of hcp Er-Y-La Alloys"

MOZE, O., *University of Parma, Italy*
"Magnetism in Disordered fcc Alloys"

McMORROW, D. F., *University of Oxford, U.K.*
"Structure and Magnetic Properties of Rare Earth Superlattices"

WOLNY, J., *Institute of Mining and Metallurgy, Cracow, Poland*
"Commensurate - Incommensurate Magnetic Structures in Neodymium – Model and Experimental Results"

PENGRA, D., *Risø National Laboratory, Denmark*
"Neutron and X-ray Diffraction from a HoEr Random Alloy"

LEBECH, B., *Risø National Laboratory, Denmark*
"Magnetic Ordering and Phase Transitions in Dzyaloshiinski Helices"

CLAUSEN, K. N., *Risø National Laboratory, Denmark*
"Magnetic Excitons and Stoner Excitations in Pr"

NORDIC SCHOOL ON THE APPLICATION OF SYNCHROTRON RADIATION IN CHEMISTRY, BIOLOGI, AND PHYSICS

25 June - 3 July at University of Århus, Denmark, and at Sandbjerg Castle, Denmark

The summer school consisted of about 25 lectures and exercises, and was concentrated on the use of synchrotron radiation in biologi, chemistry and physics, with a special emphasis on the ESRF.

The school was held at the Institute of Chemistry, University of Århus 25-26 June and then transferred to Sandbjerg Castle. There were 37 participants and 17 lectures.

Organization:

KREBS LARSEN, F., Institute of Chemistry, University of Århus, Denmark
NØRLUND CHRISTENSEN, A., Institute of Chemistry, University of Århus, Denmark
FEIDENHANS'L, R., Risø National Laboratory, Denmark

INTERDISCIPLINARY WORKSHOP ON PROPERTIES OF NOVEL STRUCTURES

20 July, Risø National Laboratory, Denmark

Organization

BOHR, J., Risø National Laboratory, Denmark
SANDY, A.R., Risø National Laboratory, Denmark
THOFT, N.B., Risø National Laboratory, Denmark

Programme

SCHMID, G., *Universität Essen, Germany*
"The Beginning and the End of the Metallic State"

BERG, R., *Risø National Laboratory, Roskilde, Denmark*
"Peptide Nucleic Acids: A Backbone Replacement for DNA"

TEMPLIER, C., *Université de Poitiers, Poitiers, France*
"Fluid Rare Gas Bubbles in Copper: Influence of Gas Pressure on Bubble Shape"

WORKSHOP ON RITA: THE RE-INVENTED TRIPLE-AXIS SPECTROMETER

28 August, Risø National Laboratory, Denmark

Redesigning the triple-axis spectrometer using state of the art optic and mechanical components plus workstations with modern control and visualization software was discussed at the workshop. The participants (25 in total) came from leading neutron scattering centres in North America, Japan and Europe. The discussions were stimulated by six oral contributions.

Organization

CLAUSEN, K.N., Risø National Laboratory, Denmark
MASON, T.A., Risø National Laboratory, Denmark

COURSE IN SURFACE SCIENCE

R. FEIDENHANS'L together with I. Chorkendorff from the Laboratory of Applied Physics, the Technical University (DtH) of Denmark, gave a course in Surface Physics at the DtH. The course consisted of two lectures of 2x35 minutes duration every week together with exercises. R. Feidenhans'l was lecturing in total eight lectures about Surface Crystallography, Phase Transitions at Surfaces and Epitaxy and Growth.

BOUWMAN, W.G., *FOM-Institute, The Netherlands.* Critical Behaviour of the Nematic to Smetic A Phase Transition. A High Resolution X-ray Study. (January).

MIKEEV, L., *NORDITA, Denmark.* Topics in Roughening: Surfaces of Liquids, Melted and Growing Crystals. (Januray).

MØLLER, S.P., *ISA, Århus, Denmark.* The Århus Storage Ring Project ASTRID. (January).

SKRIVER, H., *Technical University, Denmark.* Surface Energies and Magnetic Multilayers. (January).

VARDAPETIAN, R., *Technical University, Physics Laboratory 3, Denmark.* Mößbauer and Magnetic Susceptibility Study of Semimagnetic Semiconductor $Cd_{1-x}Fe_xSe$ (x = 0.006, 0.01 and 0.02). (January).

GLATTER, O., *University of Graz, Austria.* Characterization of the Triblock Copolymer P-85 in Aqueous Solution by Small-angle X-ray Scattering and Complementary Methods. (February).

LÖSCHE, M., *Mainz University, Germany.* Control of the Structural Organization of Monomolecular Protein Layers Adsorbed to Functionalized Aqueous Surfaces. (February).

PERSHAN, P., *Harvard University, USA.* X-ray Studies of Liquid Surfaces. (February).

SCHURTENBERGER, P., *ETH Zürich, Switzerland.* On the Application of Polymer Theory to Viscoelastic Lecithin Microemulsions. (February).

SNEPPEN, K., *Niels Bohr Institute, University of Copenhagen, Denmark.* Self-organized Pinning and Interface Growth in Random Media. (February).

LARADJI, M., *McGill University, USA.* Ternary Mixtures of Water, Oil, and Surfactants. (March).

MORTENSEN, K., *Risø National Laboratory Denmark.* Block Copolymers in Aqueous Solution: Micelle Formation and Hard-sphere Crystallization. (March).

MOLINAS-MATA, P., *Max Planck Institut für Festkörperforschung, Stuttgart, Germany.* Ga-induced Reconstructions on Ge(111): an STM Study. (March).

ZIA, R., *West Virginia University, USA.* Generically Singular Structure Factors and Correlations in a Driven System. (March).

BAHR, D., *Institut für Experimentalphysics der Universität Kiel, Germany.* Diffuse Scattering from Rough Interfaces and Defects - Thin Films of Silicon and Silicide. (April).

BROOKS, R.L., *University of Guelph, Canada.* Proton-beam Irradiation of Solid Hydrogens. (April).

GIEBULTOWICZ, T., *National Institute of Science and Technology, Washington DC, USA.* Neutron Diffraction Studies of Frustrated Antiferromagnetic Layers With Built-in Strain. (April).

CHRISTENSEN, F., *Danish Space Research Institute, Denmark.* Studies of X-ray Optics for X-ray Astronomy. (May).

HAGLUND, R.F., *Vanderbilt University, Nashville, USA.* Nonlinear Optical Physics of a Metal "Particel in a Box". (May).

SCHNEIDER, J., *HASYLAB, Hamburg, Germany.* New Possibilities for Hard X-ray Measurements at DESY. (May).

TAUB, H., *University of Missouri, USA.* Structure and Multilayer Growth of Xe on Ag(111). (August).

TANOVIC, N., *Niels Bohr Institutet, University of Copenhagen, Denmark.* Ion Bombardment Induced Self-organization in the Surface Topography of Metals. (September).

ZALIZNYAK, A., *Kapitza Institute for Physical Problems, Moscow, Russia.* Neutron Scattering Studies of a $S = 1$ Quasi 1-D Antiferromagnet. (September).

MOISEEV, I., *Russian Academy of Sciences, Russia.* Palladium Giant Clusters: Synthesis, Characterization and Catalysis. (October).

RASMUSSEN, K.L., *Odense Univesity, Denmark.* Chalk and Clay. (October).

JÜNGING, Z., *University of Florida, USA.* Induced Disordering of the Charge Density-waves in $K_{0.3}MoO_3$. (November.)

LUCAS, C., *Lawrence Berkeley Laboratory, USA.* The Structure and Growth of CaF_2/Si(111): a ionic/covalent System. (November).

UIMIN, G., *Landau Institute for Theoretical Physics, Russia.* Cu-chain Fragments in Oxygen Deficient Plans: Superstructures, Charge Transfer Mechanisms, and Order/disorder Phenomena. (November).

ZHAO, J., *GKSS Forschungzentrum, Germany.* In Situ Structure of L3 and L4 of the Large Ribosomal Subunit from Nuclea Spin Contrast Variation. (November).

AKSENOV, V.L., *Frank Laboratory of Physics, Joint Institute for Nuclear Research, Russia.* Neutron Investigations of High Temperature Superconductors in a Mixed State. (December).

BOUÉ, F., *Laboratoire Léon Brillouin, Saclay, France.* Stretched Polymer Gels and Melts. (December).

FEAST, W.J., *University of Durham, UK.* Precision and Control in Polymer Synthesis as Exemplified in ROMP. Why it is an Interesting Objective for Polymer Chemists with Important Consequences for the Physics of Materials. (December).

GABRIEL, J.C., *Université Paris-Sud, Laboratoire de Physique des Solides, France.* Molecular Chemistry of Octahedral Mineral Cluster of Rhenium and Molybdenum. Associated Organic-mineral Materials. (December)

LINDNER, P., *Institute Laue-Langevin, Grenoble, France.* Dilute and Semidilute Polymer Solutions under Shear. (December).

MONCTON, D., *APS, Argonne National Laboratory, USA.* The Status of the Advanced Photon Source. (December).

SMILGIES, D., *Rutgers Univesity, USA.* Structure of Surfaces and Interfaces Studied with Synchrotron X-ray Diffraction. (December).

SÜSSENBACH, J., *Institut für Experimentalphysik, Christian-Albrechts-Universität Kiel, Germany.* Neutron- and X-ray Diffraction on Low-dimensional $Me(CH_3)_4$ Physisorbed on Graphite, Me = Si, Ge, Sn, Pb. (December).

Bibliographic Data Sheet **Risø–R–725(EN)**

Title and author(s)

Annual Progress Report of the of Department of Solid State Physics
1 January - 31 December 1993

J. Skov Pedersen, K. Almdal, R. Feidenhans'l, K.N. Clausen, and K. Bechgaard (eds.)

ISBN	ISSN
87-550-1947-1	0106-2840 0907-0249

Dept. or group	Date
Department of Solid State Physics	January 1994

Groups own reg. number(s)	Project/contract no.
-	-

Pages	Tables	Illustrations	References
164	4	109	168

Abstract (Max. 2000 char.)

Research in the department is concerned with "Materials with Distinct Physical and Chemical Properties". The principal activities of the department in the period from 1 January, to 31 December, 1993, are presented in this Progress Report.

Neutrons and X-ray diffraction techniques are used to study a wide variety of problems in condensed matter physics and include: two- and three-dimensional structures, magnetic ordering, heavy fermions, high T_c superconductivity, phase transitions in model systems, precipitation phenomena, and nano-scale structures in various materials. The research in chemistry includes chemical synthesis and physico-chemical investigations of small molecules and polymers, with emphasis on polymers with new optical properties, block copolymers, surface modified polymers, and supramolecular structures.

This report is organized in 13 categories with the following headings:

- Theory, Monte Carlo simulations, and methods of data analysis
- Magnetic structures, magnetic phase transitions, and spin dynamics
- High T_C superconductivity
- Structures and structural phase transitions
- Inclusions and precipitates in alloys and metals
- Interaction of particles and photons with surfaces
- Surfaces, interfaces, and amorphous structures
- Langmuir films
- Polymers
- Molecular science
- Microemulsions and biological systems
- Instrument developments
- Other activities

Descriptors INIS/EDB

MAGNETISM; PROGRESS REPORT; RESEARCH PROGRAMS; RISOE NATIONAL LABORATORY; SOLID STATE PHYSICS; SUPERCONDUCTIVITY

Available on exchange or request from:
Risø Library, Risø National Laboratory (Risø Bibliotek, Forskningscenter Risø)
P.O. Box 49, DK-4000 Roskilde, Denmark
Phone (+45) 46 77 46 77, ext. 4004/4005 · Telex 43 116 · Telefax (+45) 46 75 56 27

RISØ

OBJECTIVE

The objective of Risø National Laboratory is to further technological development in three main areas: energy, environment and materials.

USERS

Risø's scientific results are widely applied in industry, agriculture and public services. Risø contributes its share of new knowledge to the global research community.

RESEARCH PROFILE

Risø emphasises long-term and strategic research providing a solid scientific foundation for the technological development of society.

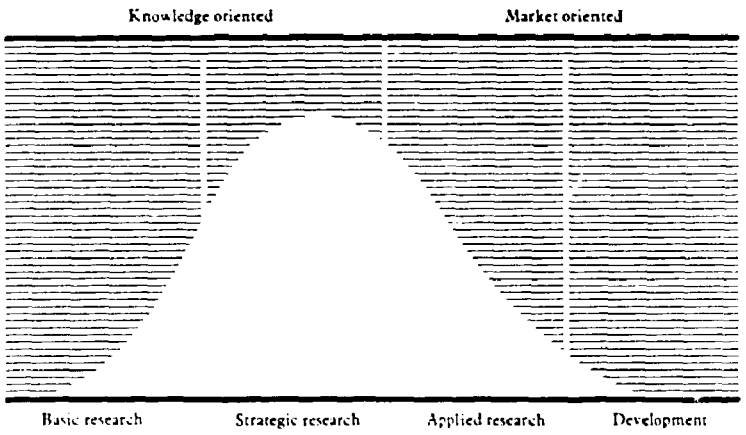

PRIORITY AREAS

- **Combustion and gasification**
- **Wind energy**
- **Energy materials**
- **Energy and environmental planning**
- **Assessment of environmental loads**
- **Reduction of environmental loads**
- **Safety and reliability of technical systems**
- **Nuclear safety**
- **Atomic structure and properties of materials**
- **Advanced materials and materials technologies**
- **Optics and fluid dynamics**

Risø-R-725(EN)
ISBN 87-550-1947-1
ISSN 0106-2840
ISSN 0907-0249

Available on request from:
Risø Library
Risø National Laboratory
P.O. Box 49, DK-4000 Roskilde, Denmark
Phone +45 46 77 46 77, ext. 4004/4005
Telex 43116, Telefax 46 75 56 27